THE ASTROPHYSICAL JOURNAL

An International Review of Spectroscopy and Astronomical Physics

FOUNDED IN 1895 BY GEORGE E. HALE AND JAMES E. KEELER

EDITORS

PAUL W. MERRILL
Mount Wilson Observatory of the Carnegie Institution of Washington

HARLOW SHAPLEY
Harvard College Observatory
Cambridge, Massachusetts

OTTO STRUVE
Yerkes Observatory of the University of Chicago

COLLABORATORS

WALTER S. ADAMS, *Mount Wilson Observatory;* JOSEPH S. AMES, *Johns Hopkins University;* HENRY CREW, *Northwestern University;* CHARLES FABRY, *Université de Paris;* EDWIN HUBBLE, *Mount Wilson Observatory;* ROBERT A. MILLIKAN, *Institute of Technology, Pasadena;* HUGH F. NEWALL, *Cambridge University;* FRIEDRICH PASCHEN, *Reichsanstalt, Charlottenburg;* C. H. PAYNE-GAPOSCHKIN, *Harvard College Observatory;* HENRY N. RUSSELL, *Princeton University;* FRANK SCHLESINGER, *Yale Observatory;* FREDERICK H. SEARES, *Mount Wilson Observatory* F. J. M. STRATTON, *Cambridge University*

VOLUME 93

JANUARY–MAY, 1941

THE UNIVERSITY OF CHICAGO PRESS
CHICAGO, ILLINOIS

THE CAMBRIDGE UNIVERSITY PRESS, LONDON
THE MARUZEN COMPANY LIMITED, TOKYO
THE COMMERCIAL PRESS LIMITED, SHANGHAI

PUBLISHED JANUARY, MARCH, MAY, 1941

COMPOSED AND PRINTED BY THE UNIVERSITY OF CHICAGO PRESS
CHICAGO, ILLINOIS, U.S.A.

Astron. Obs.

CONTENTS

NUMBER 1

PAGE

On the Atmospheric Structure of ζ Aurigae. F. E. Roach 1

Some Results with the Coudé Spectrograph of the Mount Wilson Observatory. Walter S. Adams 11

The Nature of Solar Hydrogen Vortices. R. S. Richardson 24

On the Determination of Mass Ratios of Spectroscopic Binaries. O. C. Wilson . 29

Systematic and Accidental Errors in the Spectroscopic Absolute Magnitudes of Dwarf Stars of Types F, Late K, and M. Gustaf Strömberg 33

Ultraviolet Emission Lines in the Spectra of Me Variables. Paul W. Merrill . . 40

The Continuous Spectrum of Stellar Atmospheres Consisting Only of Atoms and Negative Ions of Hydrogen. Rupert Wildt 47

RT Aurigae. Arthur L. Bennett 52

An Interpretation of Stellar Motions in Terms of a Nonsteady-State Model for the Galaxy. John Titus 57

Interstellar Absorption near the North Pole of Rotation. Philip C. Keenan and Horace W. Babcock 64

Diffuse Radiation in the Galaxy. L. G. Henyey and J. L. Greenstein 70

The Spectroscopic Binary 29 Canis Majoris. Otto Struve and Frances Sherman . 84

On the Nature of the System of β Lyrae. Zdeněk Kopal 92

The Spectrum of β Lyrae. Otto Struve 104

Some Line Intensities in β Lyrae. Jocelyn R. Gill 118

The Spectrum of β Lyrae in the Visual Region. J. L. Greenstein and T. L. Page . 128

On the Interpretation of β Lyrae and Other Close Binaries. Gerard P. Kuiper . 133

Physical Processes in Gaseous Nebulae. XI. G. H. Shortley, L. H. Aller, J. G. Baker, and D. H. Menzel 178

Physical Processes in Gaseous Nebulae. XII. Donald H. Menzel and Lawrence H. Aller 195

The Absolute Dimensions of a Wolf-Rayet Eclipsing Binary: HV 11111 = BD +38°4010 = HD 193576. Sergei Gaposchkin 202

Notes

Use of the Hale Spectrohelioscope for the Observation of Spectra of Chromospheric Eruptions. Helen W. Dodson 208

NUMBER 2

PAGE

FREDERICK EUGENE FOWLE. C. G. Abbot 209

THE LUMINOSITIES OF THE NONVARIABLE c STARS. Ralph E. Wilson 212

PHYSICAL PROCESSES IN GASEOUS NEBULAE. XIII. Donald H. Menzel, Lawrence H. Aller, and Malcolm H. Hebb 230

PHYSICAL PROCESSES IN GASEOUS NEBULAE. XIV. Lawrence H. Aller 236

PHYSICAL PROCESSES IN GASEOUS NEBULAE. XV. Leo Goldberg 244

THE STREAM-MOTIONS OF 92,656 STARS. W. J. Luyten 250

ON THE THEORY OF THE ORIGIN OF THE PLANETS. R. A. Lyttleton 267

INTERSTELLAR LINE INTENSITIES AND THE DISTANCES OF THE B STARS. John W. Evans 275

THE TIME OF RELAXATION OF STELLAR SYSTEMS. I. S. Chandrasekhar 285

THE TIME OF RELAXATION OF STELLAR SYSTEMS. II. Ralph E. Williamson and S. Chandrasekhar 305

THE TIME OF RELAXATION OF STELLAR SYSTEMS. III. S. Chandrasekhar 323

THE RATIO OF INTERSTELLAR ABSORPTION TO REDDENING. J. L. Greenstein and L. G. Henyey 327

THE RECENT SHELL SPECTRUM OF γ CASSIOPEIAE. Ralph B. Baldwin 333

THE SPECTRUM OF THE NIGHT SKY. C. T. Elvey, P. Swings, and Walter Linke . . . 337

THE SPECTRA OF TWO PECULIAR STARS: MWC 17 AND CD $-27°11944$. P. Swings and O. Struve 349

THE EVOLUTION OF A PECULIAR STELLAR SPECTRUM: Z ANDROMEDAE. P. Swings and O. Struve 356

REVIEWS 368

ERRATUM 368

NUMBER 3

THE DYNAMICS OF THE INTERSTELLAR MEDIUM. I. LOCAL EQUILIBRIUM. Lyman Spitzer, Jr. 369

DISPLACEMENTS OF LINES IN THE SPECTRA OF LONG-PERIOD VARIABLES. P. W. Merrill . 380

ABSORPTION SPECTRA OF GASES IN THE EXTREME ULTRAVIOLET. Toshio Takamine and Yoshio Tanaka 386

PLANETARY ATMOSPHERES AND WATER-CELL TEMPERATURES. Arthur Adel and C. O. Lampland 391

THE IMPORTANCE OF CERTAIN CARBON DIOXIDE BANDS IN THE TEMPERATURE RADIATION FROM VENUS. Arthur Adel 397

PAGE

On the Observable Radiation from the Carbon Dioxide in the Atmosphere of Venus. Comments on Dr. Adel's Paper. C. O. Lampland 401

The Reciprocity Principle in Lunar Photometry. M. Minnaert 403

Reynolds' Numbers for Extragalactic Nebulae. F. Zwicky 411

The Distances and Luminosities of Three Novae. Dean B. McLaughlin . . . 417

The 1914 Shell Spectrum of ζ Tauri. Ralph B. Baldwin 420

Intercomparison of Various Spectral Classifications of Faint Stars. Alexander N. Vyssotsky 425

The Light-Curve of the Eclipsing Variable, 29 Canis Majoris. Carl K. Seyfert . 442

The Spectrum of the Shell of Pleione. Otto Struve and P. Swings 446

The Visual Spectrum of Pleione. Jesse L. Greenstein 453

The Emission Lines in the Spectra of B 1985 and WY Geminorum. P. Swings and O. Struve 455

Studies of Faint B-Type Stars. Carl K. Seyfert and Daniel M. Popper 461

The Extension to the Supergiants of the Cyanogen Criterion of Stellar Luminosity. Philip C. Keenan 475

Radiation Pressure in the Convective Stellar Model. Louis R. Henrich . . . 483

Notes

The Resonance Bands of the *NH* Molecule in Spectra of Class R. Rupert Wildt 502

A Note on the Spectrum of 17 Leporis (BS 2148). Otto Struve 504

Temperature Variations of γ Cassiopeiae. W. Albert Hiltner 505

Photographs of the Milky Way in Cygnus and Scorpius. Harold A. Lower . . 506

Note on Eclipsing Variables. Newton L. Pierce 506

The Grating Infrared Solar Spectrum. I. Rotational Structure of Heavy Water (*HDO*) Band ν_2 at 7.12 μ. Arthur Adel 506

The Grating Infrared Solar Spectrum. II. Rotational Structure of the Nitrous Oxide (*NNO*) Band ν_1 at 7.37 μ. Arthur Adel 509

A Simple Demonstration of Star-Streaming. Ralph E. Williamson 511

Erratum 512

Reviews 513

Index 515

THE ASTROPHYSICAL JOURNAL

AN INTERNATIONAL REVIEW OF SPECTROSCOPY AND ASTRONOMICAL PHYSICS

VOLUME 93 JANUARY 1941 NUMBER 1

ON THE ATMOSPHERIC STRUCTURE OF ζ AURIGAE

F. E. ROACH

ABSTRACT

Photoelectric observations of ζ Aurigae made at the Steward Observatory during the ingress of its recent eclipse in December, 1939, together with those of Kron and of Guthnick and Schneller are interpreted according to two hypotheses; first, a geometrical eclipse the partial phase of which lasts 1.3 days and, second, the gradual extinction of the B star by the atmosphere of the K star.

In order to obtain a temperature for the B star consistent with its spectral class a central eclipse is not possible if the partial phase is due to a geometrical eclipse.

The extinction solution gives a good representation of the observations, especially when the points of Kron and of Guthnick and Schneller are corrected to the effective wave length of the Tucson observations. The consequences of the acceptance of extinction as the mechanism of obscuration are discussed.

Color observations both in and out of eclipse are recorded.

During the 1939–1940 eclipse of the system ζ Aurigae, conditions were particularly suitable for extended observations, since the meridian passage occurred near the middle of the night. Photometric skies in Tucson around the time of the ingress permitted photoelectric observations not only during the crucial night when the B star was being rapidly eclipsed, December 18, 1939, but also for several nights preceding and following this date. At the time of egress sky conditions were less favorable.

The comparison star was 2 Aurigae, and 133 magnitude determinations were made with a potassium hydride cell having an effective wave length of about 4500 A. They have been collected into 25 normal points in Table 1. Because of the intrinsic variability of the K component it is difficult to assign the proper values to the total light of the system as well as to the K star alone. For the purpose of discussing the observations, normal points 2, 3, and 4 have been taken for the light of the system, and points 16–20, inclusive, for the light of the K star alone. This gives outside eclipse $\Delta m(2 - \zeta) = 1.105$; during totality, $\Delta m = 0.633$. The depth of eclipse is, thus, 0.472 mag., which leads to $L_B = 0.353$, $L_K = 0.647$ in units of $L_B + L_K$ and $L_B/L_K = 0.545$. The entries of Table 2 follow, in which the second column records the fraction of eclipse and the third column the value of log $(m - m_0)$, referred to the B star, for the observations during the partial phase.

It is impossible for a single observer to cover the entire partial phase, and it is difficult to employ data from several eclipses because of the variability of the K star. It is desirable, therefore, to utilize observations made at various longitudes and combine them into a single light-curve. The practical difficulty encountered in doing this arises from the fact that the depth of eclipse depends on the effective wave length of the observations, and some adjustment must be made to bring all the data to the same scale. For example,

Kron[1] finds a depth of eclipse of 0.41 mag., as compared with 0.47 mag. of this paper. Both instruments employ Kunz potassium hydride cells, but Kron used the 36-inch Lick refractor, which may be expected to transmit a somewhat longer effective wave length than that produced by the Steward reflector. An examination of the dependence of depth of eclipse on wave length[2] reveals that the results by Kron and by the writer are consistent with the assumption that the effective wave lengths differ by 120 A.

TABLE 1

OBSERVATIONS OF ζ AURIGAE

No.	JD 2429000+	Δ Mag. (2−ζ)	Obs.	No.	JD 2429000+	Δ Mag. (2−ζ)	Obs.
1	606.820	1.068	2	14	617.920	0.873	3
2	13.725	1.109	8	15	17.956	0.847	4
3	14.686	1.098	4	16	18.609	0.642	8
4	15.695	1.104	4	17	18.684	0.621	8
5	16.687	1.096	14	18	18.794	0.622	8
6	16.914	1.088	13	19	18.882	0.636	4
7	17.589	1.018	3	20	19.621	0.647	8
8	17.624	1.000	4	21	28.644	0.627	8
9	17.693	0.985	4	22	50.676	0.703	4
10	17.726	0.972	4	23	53.597	0.667	1
11	17.778	0.956	2	24	54.619	0.700	4
12	17.846	0.914	3½*	25	657.699	1.199	4
13	617.885	0.898	2				

* One point with a high residual was given half weight.

TABLE 2

Normal Point	Fraction of Eclipse (f)	log ($m-m_0$)	Normal Point	Fraction of Eclipse (f)	log ($m-m_0$)
5	0.023	−1.59	13	0.492	−0.13
6	.044	1.32	14	0.545	− .07
7	.218	0.57	15	0.599	0.00
8	.261	0.48	16	0.983	.....
9	.296	0.42	17	1.018	.....
10	.326	0.37	18	1.017	.....
11	.363	0.31	19	0.993	.....
12	0.457	−0.18			

If the depth of eclipse is well known for a particular instrument, the results may be expressed as fractions of the eclipse, which may be presumed to be independent of the wave length if a geometrical eclipse is involved. Any error in the knowledge of the light intensity either outside eclipse or during totality will affect the results. For the 1939 eclipse three sets of data made with photoelectric photometers lend themselves to this treatment, namely, the observations of Kron,[1] of Guthnick and Schneller,[3] and of the writer. In Table 3 these additional observations are tabulated. For Kron's observations, $\Delta m(2-\zeta)$ outside eclipse was taken as 1.081, and during totality Δm was set equal to 0.669. The observations of Guthnick and Schneller were based on λ Aurigae as the comparison star. Outside eclipse they give $\Delta m\ (\zeta-\lambda) = -0.514$, and for totality Δm was

[1] *Pub. A.S.P.*, **52**, 124, 1940.

[2] *Ap. J.*, **90**, 317, 1939.

[3] *I.A.U. Circ.*, No. 808, 1940.

taken as −0.145 from the last three observations recorded by them. The discussion of these observations will consist of three separate solutions which we shall refer to as I, II, and III. The method employed in correcting the observations of Table 3 to 4520 A will be explained under solution III.

TABLE 3

PHOTOELECTRIC OBSERVATIONS BY KRON AND BY GUTHNICK AND SCHNELLER

JD 2429000+	No. of Obs.	Fraction of Eclipse (f)		log ($m-m_0$)	
		Uncorrected	Corrected to 4520 A	Uncorrected	Corrected to 4520 A
Kron:					
616.683	9	0.000	.....	.....	.....
6.803	9	0.002	0.002	−2.70	−2.62
6.937	10	0.025	0.030	−1.56	−1.48
7.690	6	0.266	0.308	−0.47	−0.39
7.733	6	0.294	0.340	−0.42	−0.34
7.862	2	0.427	0.485	−0.22	−0.14
8.652	7	0.997	.....	.....	.....
8.729	6	1.003	.....	.....	.....
618.875	5	1.010	.....	.....	.....
G and S:					
618.250	2	0.847	0.934	+0.31	+0.47
8.273	2	0.847	0.934	+0.31	+0.47
8.295	2	0.862	0.944	+0.33	+0.49
8.318	2	0.900	0.964	+0.40	+0.56
8.357	2	0.917	0.973	+0.43	+0.59
8.369	2	0.925	0.977	+0.45	+0.61
8.415	2	0.965	1.000	+0.56	+0.72
8.488	2	0.993	1.000	.....	.....
8.501	2	0.993	1.000	.....	.....
618.540	1	1.016	.....	.....	.....
Kron:					
656.634	4	0.177	0.208	−0.67	−0.59
656.775	4	0.111	0.131	−0.89	−0.81

SOLUTION I

It has been assumed in this case that the B star is a uniform disk eclipsed by a straight edge. A family of such curves was compared with the observations, and a graphical solution was obtained leading to a duration of partial phase of 1.3 days, as shown in Figure 1. From the two observations by Kron at egress (last two entries of Table 3) it is possible to determine the epoch of minimum as JD 2429637.10, which leads to the following tabulation:

	DAYS
Duration of eclipse	39.72
Duration of totality	37.12
Duration of partial phase	1.3

The calculation of the density and temperature of the B star depends on the assumed inclination of the orbit. In Table 4 are assembled figures for a number of different inclinations.

The B star has been classified by Kuiper[4] as B6. It is necessary to consider that the eclipse is far from central in order to obtain temperatures of the proper order of magnitude ($T \approx 15{,}000°$ K). However, even if the eclipse takes place at a latitude of 66° it can still be total, owing to the extreme difference in the sizes of the two stars. It is to be noted that the *shape* of the theoretical light-curve of a uniform disk occulted by a straight edge does not depend on the angle between the normal to the straight edge and the direction of motion of the disk. Hence, the solution plotted in Figure 1 applies to any case in Table 4, provided the appropriate deduction of the radius of the B star from the duration of the partial phase is made.

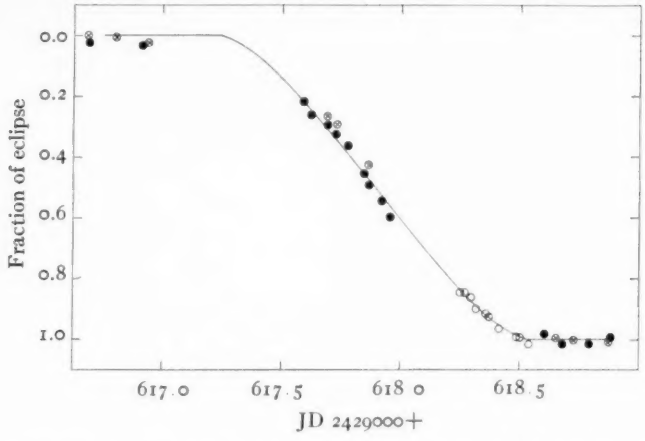

FIG. 1.—Solution I. Open circles, Guthnick and Schneller; closed circles, Roach; ⊗, Kron.

TABLE 4

TEMPERATURE AND DENSITY OF THE B STAR

Inclination	Latitude	R_B/R_K	R_B (Cm×10^{-11})	R_B (⊙)	ρ_B (⊙)	T_B (T_K=3200° K)
90°	0°	0.035	4.7	6.7	0.028	8,100° K
86.5	15	.034	4.6	6.5	.030	8,200
83.3	30	.030	4.0	5.8	.043	8,800
80.6	45	.025	3.3	4.8	.076	9,900
78.5	60	.018	2.3	3.4	.21	12,700
78	66	0.014	1.9	2.7	0.44	14,700

SOLUTION II

It is assumed that the obscuration of the light of the B star is an extinction phenomenon resulting from the opacity of the atmosphere of the K star. The presence of absorption lines originating in the outer atmosphere of K several days before (and after) totality suggests that this mechanism be considered. The problem was outlined by S. Gaposchkin,[5] and the appropriate equations were introduced by Menzel.[6] For this discussion a

[4] Unpublished material.

[5] *Harvard Bull.*, No. 900, 1935.

[6] *Harvard Circ.*, No. 417, 1936.

number of Menzel's equations will be reproduced. The optical depth, τ_ν, at frequency, ν, is given by

$$\left.\begin{aligned}\tau_\nu &= \frac{2.67 \times 10^{24} k}{\nu^3 T^{1/2}} (e^{h\nu/kT} - 1) \int N_i N_e ds \\ &= 4.90 \times 10^{-34} \int N_i N_e ds ,\end{aligned}\right\} \tag{1}$$

if $\lambda = 4520$ A and $T = 3200°$ K. The quantities N_i and N_e are the number of ions and electrons, respectively, per cubic centimeter. The ionic and electronic densities are taken to decrease exponentially with the radial distance from the photosphere, h, according to the equation

$$N_i = N_e = N_{0e} e^{-ah} . \tag{2}$$

For an isothermal atmosphere in hydrostatic equilibrium,

$$a = \frac{mGM}{R^2 kT} = \frac{mg}{kT} = 4.3 \times 10^{-11} \text{ cm}^{-1} , \tag{3}$$

for $T = 3200°$ K, $M = 3.04 \times 10^{34}$ g, $R_K = 1.34 \times 10^{13}$ cm, and $m = 1.6 \times 10^{-24}$ g (hydrogen). To a sufficient approximation

$$\int N_i N_e ds = N_{0e}^2 e^{-2ah_0} \left[\frac{\pi(R_K + h_0)}{a}\right]^{1/2} , \tag{4}$$

where h_0 is the projected distance from the B star to the K star's photosphere.

If $E_{0\nu} d\nu$ and $E_\nu d\nu$ are the energies per square centimeter falling on the earth from the B star outside of eclipse and during partial obscuration, respectively, then a pure absorption mechanism requires that

$$\frac{E_\nu}{E_{0\nu}} = 1 - f = e^{-\tau_\nu} , \tag{5}$$

where f is the fraction of the eclipse. Further, going to apparent magnitudes,

$$m - m_0 = -2.5 \log \frac{E_\nu}{E_{0\nu}} = 2.5 \, \tau_\nu \log e . \tag{6}$$

Finally, the appropriate integration leads to the following approximate equation in which all logarithms are to the base ten:

$$\log (m - m_0) = -26.5 + 2 \log N_{0e} - \tfrac{1}{2} \log a - (0.87a - 1.65 \times 10^{-14}) h_0 \tag{7}$$

for

$$T_K = 3200° \text{ K} , \qquad \lambda = 4520 \text{ A} , \qquad \text{and} \qquad R_K = 1.34 \times 10^{13} \text{ cm} .$$

Equation (7) shows that $\log (m - m_0)$ is linear with h_0 and hence with time. A necessary condition for the existence of the extinction mechanism is, therefore, that $\log (m - m_0)$ plotted against time give a straight line.

For solution II the values of $\log (m - m_0)$ from Table 2 (excluding the first two entries) and from the fifth column of Table 3 (excluding the last two entries) were plotted against time, and a least-squares solution was obtained. In Figure 2 the solid line repre-

sents this solution, in which the ordinate is the fraction of the eclipse, f, rather than log $(m - m_0)$. A comparison of Figures 1 and 2 indicates that each of the two solutions is fairly satisfactory. This is a consequence of the fact that from $f = 0.3$ to $f = 0.9$ the function representing straight-edge obscuration of a uniform disk, when plotted as log $(m - m_0)$, is practically linear with time. The two functions, however, are quite dissimilar from $f = 0$ to $f = 0.3$, the extinction function giving a slower increase of f. The critical observations are thus in the early stages. If the observations, made on JD 2429616 by Kron and the writer, are reliable in indicating a slight diminution of the light, the extinction hypothesis is favored. It should be remarked that the normal point in Table 3 for JD 616.937 was given by Kron as individual observations which were collected into a normal point by the writer. Kron observed that the differential extinction correction might account for the apparent weakening of the light. It is significant, however, that the observations made at Tucson also give the weakening, and the probability that the effect is real is thus enhanced.

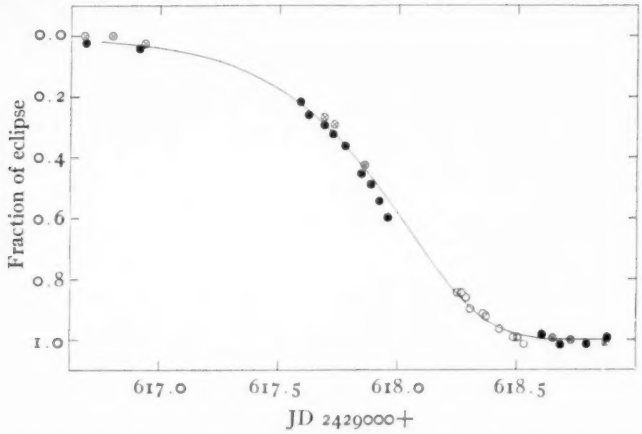

FIG. 2.—Solution II. Open circles, Guthnick and Schneller; closed circles, Roach; ⊗, Kron.

Observations were made by Brück and Green[7] between JD 617.459 and JD 617.585. Since they do not record the light of the system or of totality, it is impossible to include them in this discussion. It is worthy of note that their observations, made during the early stages of the partial phase, indicate a more rapid change in the brightness of the system than is consistent with either solution.

SOLUTION III

There are two criticisms of solution II. In the first place, Kron's observations are systematically above those of this paper. Secondly, the solution departs systematically from my last four observations. Both of these objections to the extinction solution are removed if we take account of the fact that the three sets of observations are not made at the same effective wave length, as evidenced by the observed depths of eclipse. From a plot of depth of eclipse against effective wave length[2] it is possible to determine the latter if the depth of eclipse is known. From equations (1) and (6) it is then feasible to adjust the observations of Kron and of Guthnick and Schneller to the effective wave length of this paper (4520 A). The results are summarized in Table 5 and in the fourth and sixth columns of Table 3. A plot of log $(m - m_0)$ against time, with these revised points, is shown in Figure 3, together with their least-squares solution. The three sets of observations are now seen to be consistent. In Figure 4 this solution is shown with f as ordinate.

[7] *I.A.U. Circ.*, No. 807, 1940.

TABLE 5

Observer	Depth of Eclipse	Effective λ (A)	Correction of log $(m-m_0)$ to 4520 A
Guthnick and Schneller	0.37	4780	+0.16
Kron	.41	4640	+0.08
Roach	0.47	4520	.....

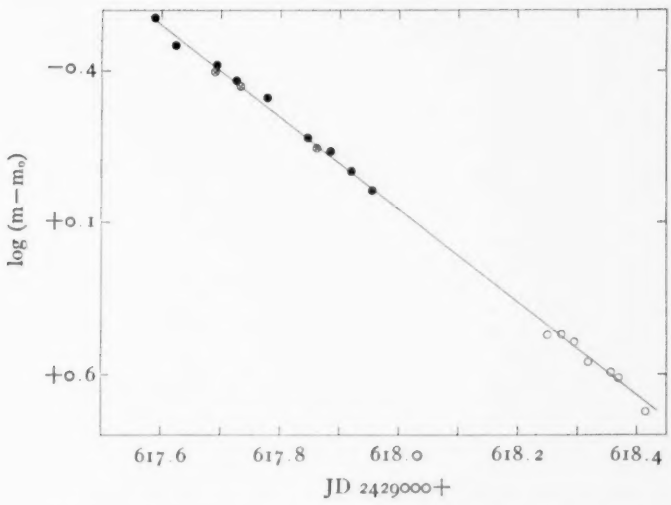

FIG. 3.—Solution III. Open circles, Guthnick and Schneller; closed circles, Roach; ⊗, Kron.

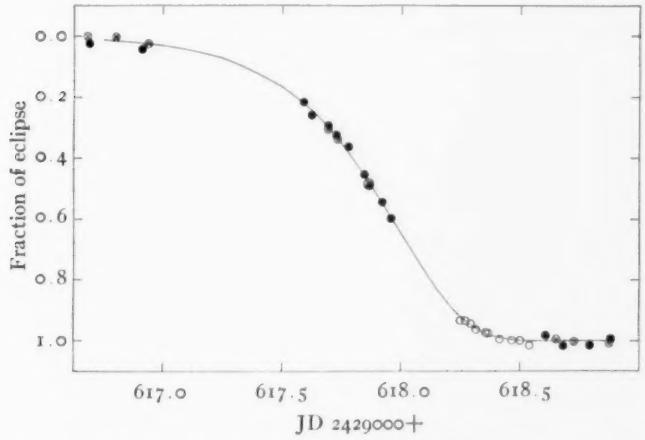

FIG. 4.—Solution III. Open circles, Guthnick and Schneller; closed circles, Roach; ⊗, Kron.

DISCUSSION OF EXTINCTION HYPOTHESIS

The success of the extinction mechanism in reproducing the details of the light-curve suggests that it deserves further consideration. If we again use the two points observed by Kron during egress we find that the epoch of principal minimum is the same as in the case of the eclipse solution I, namely, JD 2429637.10. The duration of totality becomes 37.18 days. If we assume that the eclipse is central, the radius of the K star, 1.34×10^{13} cm, gives the relationship between a given time interval and the distance traveled by the B star, namely, one day corresponds to 7.22×10^{11} cm. Now, in solution III, it was found that

$$\frac{\Delta \log (m - m_0)}{\Delta t} = + 1.524 ,$$

from which

$$\frac{\Delta \log (m - m_0)}{\Delta h_0} = - 2.11 \times 10^{-12} .$$

Equation (7) now gives $a = 2.40 \times 10^{-12}$ cm^{-1}. An extrapolation of the plot in Figure 3 to the photosphere gives $\log (m - m_0) = 0.74$, from which $\log N_{0e} = 10.715$ or $N_{0e} = 5.19 \times 10^{10}$ cm^{-3}, and $P_{0e} = 2.3 \times 10^{-2}$ dynes per square centimeter, or 2.3×10^{-8} atm. Equation (4) now gives

$$\int N_i N_e ds \approx 1.13 \times 10^{34} e^{-4.8 \times 10^{-12} h_0}$$

or, if $N_i = N_e$,

$$\int N_i ds = \int N_e ds \approx 3.07 \times 10^{23} e^{-2.4 \times 10^{-12} h_0}$$

and at the photosphere, $h_0 = 0$, which gives

$$\int N_i ds = \int N_e ds \approx 3.07 \times 10^{23} .$$

In all cases the integration is considered to be carried out over the entire path.

It is of interest to examine the published spectrographic data to determine whether the number of hydrogen atoms in the line of sight determined from the intensities of the hydrogen lines is of the correct order of magnitude to produce the observed general extinction. In Menzel's discussion of the work of Christie and Wilson[8] he finds that, unless there is a very high turbulent velocity, the intensity of $H\delta$, when $h_0 = 0$, leads to 1.4×10^{18} as the number of hydrogen atoms in the second level in the line of sight. Menzel's equation (21) may now be applied, and it is found that

$$\frac{\int N_i N_e ds}{\int N_2 ds} = 4.8 \times 10^{14} .$$

Thus, $\int N_i N_e ds = 6.7 \times 10^{32}$, which, combined with equation (1), gives $\tau_\nu = 0.33$. It thus appears that the spectrographic data are consistent with the extinction hypothesis.

The difference between the observed logarithmic decrement, a, and the gravitational value may be interpreted in a number of ways. In the gravitational problem in which hydrostatic equilibrium is assumed,

$$a = \frac{mg}{kT} . \tag{8}$$

[8] *Mt. W. Contr.*, No. 519; *Ap. J.*, **81**, 213, 1935.

Or, if it is desired to consider the effect of macroscopic turbulence,

$$a = \frac{mg}{kT + \frac{mc^2}{3}} \approx \frac{3g}{c^2}, \tag{9}$$

where c is the root-mean-square value of the turbulent velocity. The approximation in equation (9) is valid for high turbulent velocities. For a hydrogen atmosphere the numerical value of a of solution III applied to equation (8) gives $g = 0.635$ cm per sec², as compared with the dynamical value of 11.33 cm per sec². Pannekoek[9] has discussed similar discrepancies in supergiant atmospheres and has carried out an analysis in terms of radiation pressure.

Equation (9) yields a value of c if g is assumed. In Table 6 the value of the calculated turbulent velocity is recorded for values of g ranging from the dynamical, 11.33 cm per sec², to the extreme case for which $g = 0.635$. If the values of g lower than the dynamical are due to radiation pressure operating against gravity, it is possible to calculate the ratio of radiation pressure to gravity, the values of which have been entered in the third column of Table 6.

TABLE 6

g (Cm/Sec²)	c (Km/Sec)	Ratio: Radiation Pressure to Gravitation
11.33	37	0.00
4.00	21	.65
2.00	13	.82
0.635	0	0.94

It is instructive to compare the value of the logarithmic decrement obtained in this paper with the gradients observed spectrographically by Christie and Wilson[8] during the 1934 eclipse. From their Figure 10 the entries of Table 7 have been calculated. In no case does the spectrographic gradient exceed that which would occur in an isothermal atmosphere in hydrostatic equilibrium, and most of the gradients, excepting those for hydrogen and ionized calcium, are of the same order of magnitude as that deduced in solution III.

TABLE 7

Element	Gradient, a, $\times 10^{12}$	Element	Gradient, a, $\times 10^{12}$
Ions, electrons (solution III)	2.40	Ca^+ (h_0=0.05–0.20 R_K)	0.86
Pure gravitation (hydrogen)	43.0	Ti^+ { 3757–3761; h_0=0.10–0.20 R_K }	2.4
Neutral metals	4.6		
Hydrogen (to h_0=0.15 R_K)	0.17	Other Ti^+	1.7
Ca^+ (to h_0=0.05 R_K)	5.7	Mg	2.1

The evaluation of the radius of the B star is impossible in the case of the extinction solution. The fact that there is no observable departure from linearity of the points in Figure 3 indicates that the B star behaves as a point source. The condition for this is

$$aR_B < 1$$

[9] *B.A.N.*, **8**, 175, 1937.

or

$$R_B < \frac{1}{a} = 4.17 \times 10^{11} \text{ cm} ,$$

which leads to

$$\frac{R_B}{R_K} < 0.031 ,$$

a limitation which is consistent with the spectral class and probable temperature of the B star as discussed under solution I (cf. Table 4).

Photoelectric colors were observed on a number of nights with the same filters used in a previous investigation[10] and are given in Table 8. The mean color in eclipse is +1.25 mag. (yellow/blue = 3.16), and outside of eclipse +0.45 mag. (yellow/blue = 1.51).

TABLE 8

COLORS OF ζ AURIGAE

JD 2429000+	Color	JD 2429000+	Color
606.785	+0.46	614.665	+0.44
06.835	.45	15.662	0.45
13.645	.42	50.681	1.38
13.712	.44	54.656	1.12
13.778	.42	657.629	+0.53
613.845	+0.41		

Some of the expenses of this investigation were met by a grant-in-aid from the Society of the Sigma Xi. I wish to acknowledge the value of discussions of this problem with a number of the members of the Yerkes Observatory staff.

STEWARD OBSERVATORY
UNIVERSITY OF ARIZONA
July 1940

[10] *Ap. J.*, **89**, 669, 1939.

SOME RESULTS WITH THE COUDÉ SPECTROGRAPH OF THE MOUNT WILSON OBSERVATORY*

WALTER S. ADAMS

ABSTRACT

The development of the coudé spectrograph in use with the 100-inch telescope is traced through its successive stages to its present form. At present three Schmidt cameras with focal lengths of 32, 73, and 114 inches, respectively, may be used in conjunction with a concave off-axis collimating mirror and a Wood aluminium on pyrex-glass plane grating. The grating has great concentration of light in the red of the first order and the ultraviolet of the second. The linear scale of the 20-inch spectrograms in the second order of the 114-inch Schmidt camera is 2.9 A/mm.

Illustrations of the application of the spectrograph consist of five investigations. The first of these is a determination of the solar parallax from 37 spectrograms of α Boötis. The range among the observations is 0.398 km/sec, and the resulting parallax is $8''.805 \pm 0''.007$. The radial velocity of the star is -5.621 ± 0.005 km/sec.

Seven spectrograms of Mars in the region about λ 7000 have been used in a study of the water-vapor lines. Four of the spectrograms were taken when Mars was approaching the earth, and three when it was receding. Measurements of the wave lengths of the water-vapor lines show no certain displacements from their normal terrestrial positions and indicate an upper limit for the amount of water vapor in the equatorial regions of Mars certainly not exceeding 5 per cent of that in the earth's atmosphere.

A high-dispersion spectrogram of o Ceti taken about one month after maximum of light provides evidence that the multiple structure of at least some of the emission lines of hydrogen is due to superimposed absorption lines of other elements. Comparison of the displacements of a large number of absorption lines of different excitation levels indicates a small systematic difference with level, lines of the lowest excitation level showing the smallest positive displacement.

The doubling of a considerable number of lines in the spectra of supergiant M-type stars was discovered with the coudé spectrograph. The separation and the relative intensities of the two components vary greatly in different stars, the separation being largest and the difference of intensity greatest in α Orionis, and less in α Scorpii, α^1 Herculis, and o Ceti. All the double lines arise from near the ground state of the neutral or ionized atom, and the amount of widening of other lines appears to depend upon their excitation levels. The position of the mean of the two components agrees well with that of the normal line, but the effect can hardly be ascribed to reversal and is probably due to Doppler shifts in the extensive atmospheres of these stars, as has been suggested by Spitzer.

The original discovery with the coudé spectrograph of several previously unobserved sharp interstellar lines in the ultraviolet and violet spectra of some stars of early type has been supplemented by recent observations of the bright star ζ Ophiuchi with higher dispersion. A number of additional lines has been found; and the presence of several lines of *CH*, predicted by McKellar, has been established. The existence of molecules of *CH* in interstellar space, first suggested by Swings and Rosenfeld, and given much greater probability by the work of McKellar, and of *CN* as suggested by McKellar, now seems to be beyond reasonable doubt.

The spectrograph used at the coudé focus of the 100-inch telescope has undergone many modifications since it was first placed in operation. Originally designed as an autocollimating prismatic spectrograph with an aperture of 6 inches and a focal length of 15 feet, successive developments have included the addition of a smaller instrument 9 feet in focal length with an ultraviolet glass prism, a similar spectrograph with a crystalline quartz prism aluminized on its back surface, a plane-grating autocollimating spectrograph of 9 feet focal length, and a 15-foot concave-grating spectrograph. Some of these instruments were more or less experimental in character, while others were used over considerable periods of time. Since exposure times necessarily were long, an attempt to increase the light-efficiency of these spectrographs and the extent of spectrum in focus on the photographic plate was a primary consideration. Still more important were the factors of definition and resolving-power, stability and accurate temperature control.

* *Contributions from the Mount Wilson Observatory, Carnegie Institution of Washington*, No. 638.

The development of the Schmidt camera for spectrographic use and the remarkable success attained by Professor R. W. Wood in the ruling of diffraction gratings on aluminium surfaces with high concentration of light in the first or second orders led to a complete reconstruction of the spectrograph in 1935. A massive steel frame, resting on a three-point ball support and held at the proper angle by brackets attached to the side of the concrete pier, carries the optical parts of the spectrographs. Previously these had been attached directly to the pier and were affected by any strains or deflections in the pier itself. A structural-steel framework, triangular in shape, is attached to the I-beams of the main frame, the upper surface being horizontal. The whole structure forms approximately an inverted right triangle with the slit lying near the acute vertex and the hypothenuse parallel to the optical axis of the beam from the telescope. The horizontal base carries the various Schmidt cameras as well as a lens of 108 inches focal length. The light passing through the slit falls upon a concave collimating mirror corrected to operate off its axis. This mirror throws the parallel beam of light backward and slightly upward in the general direction of the slit to the plane grating placed just above the optical axis. By simple rotation of the grating the spectrum can be thrown, either horizontally into the Schmidt cameras and 9-foot lens camera, or downward nearly along the optical axis.

Two Schmidt cameras have been used, one with a focal length of 32 inches and the other of 73 inches. The correcting plates for these instruments and the lens of the 108-inch camera rest on a steel plate immediately in front of the grating and are readily interchangeable. The 32-inch camera and the plateholder frame for the 108-inch lens camera are mounted upon rails and can quickly be moved to one side when the 73-inch Schmidt camera is to be used. Since all the instruments are in adjustment, the change from one to the other in the course of the observations requires not more than 2 or 3 minutes. The steel frame carrying the spectrographs is completely inclosed in an insulated wooden house, and the temperature is controlled by a series of heating coils operated by an ether thermostat. Since the contacts in the thermostat are made in a hydrogen atmosphere, no oxidation occurs, and they have been used for several years without requiring attention. Stratification of air is prevented by fans placed within the wooden housing.

At the slit, provision is made for a comparison spectrum from an electric arc or vacuum tubes, a slotted diagonal prism allowing exposures to be made at any time without interrupting the exposure on the star. The optical projection system, including diffusion screen, projecting lens, and field lens over the slit, is made of quartz, so that the ultraviolet spectrum is transmitted freely. Calibration is afforded by a series of spectra from a step slit, the light from an incandescent lamp, adjustable in distance, passing through the spectrograph on either side of the comparison spectrum. A complete unit, consisting of a slit equipped with Bowen's "image-slicer" device, may be used in place of the regular slit, the change being made quickly and easily through the use of dowel pins which define the positions of both slits accurately. When the image-slicer is in use, cylindrical lenses attached to the various plateholder frames of the Schmidt cameras are brought into position in front of the photographic plate.

The most recent and an extremely valuable addition to the coudé spectrograph is the large Schmidt camera with a focal length of 114 inches. This instrument lies along the main structural frame of the spectrograph nearly in the optical axis of the telescope; and the mirror, 36 inches in diameter, is supported on a strong steel framework attached to the heavy I-beams. The mirror is the property of the Friends of Astrophysical Research and is loaned for use in this spectrograph. Its aperture permits a region of spectrum nearly 17 inches in length to receive full illumination at the plateholder, and the operating ratio of the camera is such that no correcting plate is required. As a result there is no glass or quartz in the entire optical system between the star and the photographic plate; and since all reflections are at aluminium surfaces, transmission in the ultraviolet

is exceptionally high. An important practical advantage is the possibility of using ultraviolet comparison lines of higher orders in regions of the spectrum where the normal iron lines are few in number. A comparison of spectra taken with the 108-inch lens camera and the 114-inch Schmidt camera shows essentially identical definition and resolving-power, but in the case of the Schmidt camera a reduction of roughly 50 per cent in exposure time in the blue, and, of course, far higher ultraviolet transmission.

The diffraction grating used almost entirely for these various instruments is a Wood aluminium on pyrex-glass grating with a ruled area of $4\frac{3}{8} \times 5\frac{1}{2}$ inches, 14,400 lines to the inch. It has excellent concentration of light in the red-infrared of the first order and similar concentration in the violet-blue of the second order. With the cameras used, the definition is excellent in the first, second, and third orders. An illustration of its resolving-power on emission lines is the complete photographic resolution even on fast plates of the components of the *Fe* line λ 3918 with a separation of 0.099 A. The only serious drawback of this grating is the presence of strong scattered light in the far ultraviolet, and below λ 3300 a diaphragm covering about one-half its surface must be used to insure the best results.

For convenience of reference the following table gives the linear dispersion of the spectra in angstroms per millimeter for the various instruments:

32-inch Schmidt, second order	1 mm	= 10.4 A
73-inch Schmidt, second order	1	= 4.5
108-inch lens, second order	1	= 3.1
114-inch Schmidt, second order	1	= 2.9

Because of the distribution of brightness in the grating, nearly all spectrograms in the blue and violet regions have been made in the second order, and those in the red and yellow in the first order. The linear scale in the first order is, of course, closely one-half that of the second.

Investigations carried on with the coudé spectrographs have naturally been limited to the brighter stars. The faintest star so far observed with the highest dispersion (114-inch Schmidt) is *o* Ceti when it had a photographic magnitude of about 6.0. The exposure time was $5\frac{1}{2}$ hours. With the 32-inch Schmidt camera stars of magnitude 7.0 have been observed frequently, and fainter stars to a less extent. In the yellow and red region of the spectrum, the number of reflections from aluminium surfaces (six including the telescope and spectrograph) results in a serious loss of light as compared with that from silver surfaces, and observations are necessarily limited to very bright stars or those of late spectral type.

The use of high resolving-power and large linear scale is most valuable for accurate determinations of radial velocity, the detection of differential displacements among lines of various elements, physical studies of line-structure and contours, and the discovery of faint lines and bands. Illustrations of some of these applications are contained in the remaining pages of this communication.

α BOÖTIS AND THE SOLAR PARALLAX

The lines in the spectrum of α Boötis remain sharp and narrow under the highest dispersion applied to the study of this star. Accordingly, it has been used frequently by astronomers as a star of standard velocity to serve as a control upon the adjustments and behavior of their spectrographs. Its brightness and convenient position have made it equally useful in connection with the coudé spectrograph; and during the past years many spectrograms have been obtained—37 of these since the grating came into regular use in the spectrograph. Since these spectrograms were taken under reasonably similar conditions, it seemed of interest to attempt a solution for the solar parallax with this comparatively limited material with a view to learning what degree of accuracy might be expected of the method in the future.

The spectrograms were all taken in the blue and violet region of the spectrum in the second order of the grating. The first 28 were with the 108-inch lens camera, and the last 9 with the 114-inch Schmidt. Since there seems to be no appreciable systematic difference between the results with the two cameras, all the material has been used. The plates are given equal weight and are used individually except that the two spectrograms, taken in immediate succession on March 2, 1939, are combined into a single value with unit weight. Cramer Hi-Speed Special plates were used for nearly all the spectrograms with exposure times of 30–40 minutes under average conditions of seeing.

A list of 25 suitable lines in the region between λ 4337 and λ 4466 was selected for measurement; and in so far as possible, the same lines were measured upon all the negatives. The wave lengths of the stellar lines were taken from the *Revised Rowland Table*, and those of the comparison lines from the measures of St. John and Babcock of the iron spectrum in the laboratory. Although the absolute radial velocity derived in this way will differ from that in which the same wave lengths are used for both stellar and comparison lines to the extent to which solar wave lengths differ systematically from terrestrial wave lengths, solar wave lengths have the advantage of being strictly homogeneous. In a differential comparison, like the present one, the system of wave lengths used is, of course, of no importance.

Table 1 contains the values for the individual spectrograms. The successive columns give the number of the plate; the date in Greenwich Civil Time; v_o, the correction due to the earth's orbital motion; v_d, the correction due to the earth's rotation; and V, the final radial velocity of the star. If v_m is the directly measured radial velocity, $V = v_m + v_o + v_d$.

The method for determining the solar parallax from measurements of the radial velocity of one or more stars at various epochs has been worked out in detail and applied by several observers[1] and hence does not require extended comment. For simplicity, a standard value of the parallax is assumed, and a correction $d\pi$ is derived by least squares from the equations of condition provided by the observations. In the present case there are 37 equations of condition of very simple form, since equal weights are assumed. The solution on the basis of an assumed parallax of $8''.80$ gives $d\pi = +0''.0054$. The final results, with their probable errors, are

$$\pi = 8''.805 \pm 0''.007\,, \qquad V = -5.621 \pm 0.005 \text{ km/sec}\,.$$

Although these results are fairly satisfactory in view of the relatively small amount of observational material, the probable error is larger than it should be, considering the small probable error of the determination of V from a single spectrogram. The extreme range in values of the 25 lines measured rarely exceeds 1.5 km/sec, and the probable error of the mean averages ±0.05 km/sec. The values of V given in Table 1 show larger differences among the separate plates than would be expected under these circumstances, and it is clear that slight systematic sources of error must be present. These are probably to be sought for in the character of the arc which produces the comparison spectrum and in the general system of temperature control throughout the spectrograph. These are, at present, under investigation. If the sources of systematic error can be removed or even considerably reduced, it is evident that a highly accurate value of the solar parallax can be derived at the cost of a small fraction of the labor required in observation and computation by the more usual methods.

The radial velocity of α Boötis derived from numerous sources and given in Moore's *Catalogue of Radial Velocities*[2] is −5.2 km/sec. Since most of the results were obtained with the use of the same wave lengths for comparison and stellar lines, it is necessary to make allowance for an average difference of +0.006 A (solar − comparison) in comparing the coudé results with previous determinations. This would give a value of −5.2 km/sec,

[1] Among others, H. Spencer Jones, *Annals Cape Obs.*, **10**, Part 8, 1928.

[2] *Pub. Lick. Obs.*, **18**, 1932.

PLATE I

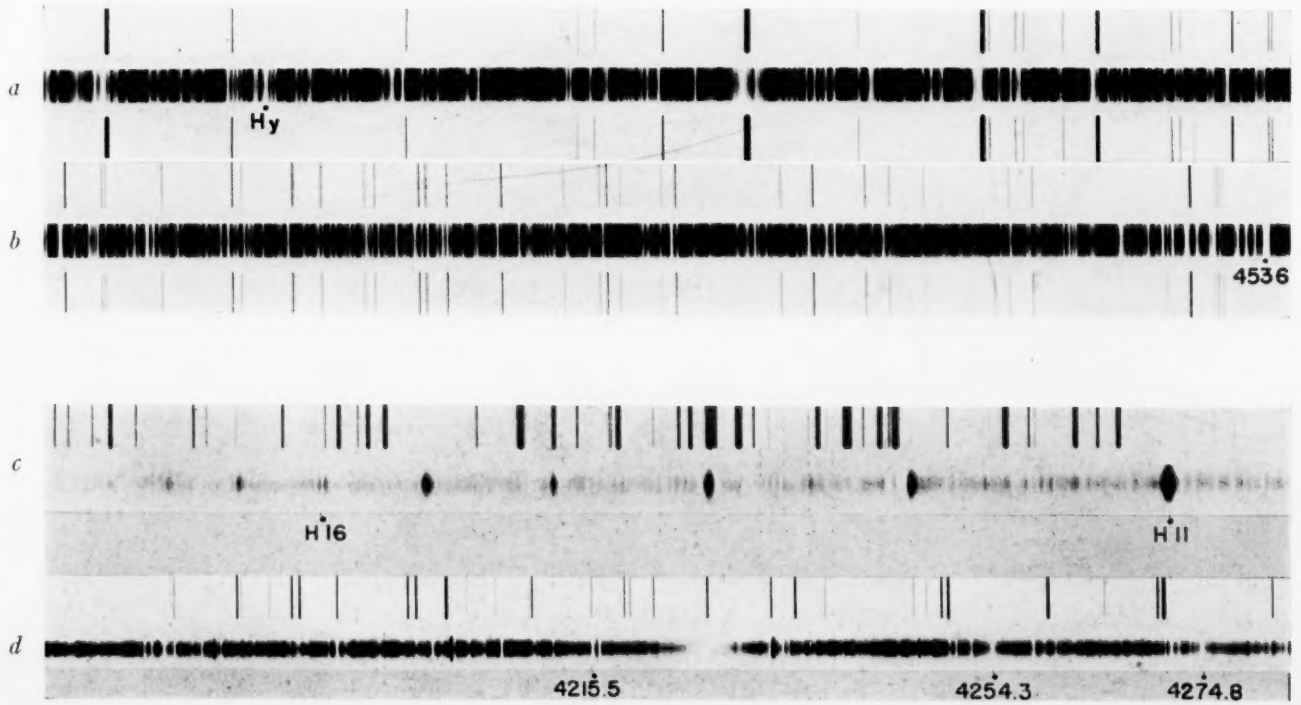

STELLAR SPECTRA WITH HIGH DISPERSION

a, *b*) α Boötis; *c*, *d*) ο Ceti. Note structure of *H*16 and doubling of λ 4254 and λ 4274

UNIV. OF WICH.

as against -5.2 for the mean of the collected results, or -5.4 for the Lick Observatory observations alone.

An interesting illustration of differences in wave length between solar and stellar lines is afforded by the *V* line λ 4428 in the spectrum of α Boötis. This is listed as

TABLE 1

RADIAL VELOCITIES OF α BOÖTIS

Plate No.	Date	v_0	v_d	*V*
		km/sec	km/sec	km/sec
1356	1937 Apr. 25.23	− 4.568	+0.125	−5.606
1360	26.25	− 5.004	+ .166	−5.532
1370	May 27.45	−16.806	− .353	−5.431
1371	28.18	−17.037	+ .122	−5.590
1375	29.17	−17.344	+ .137	−5.434
1399	June 27.16	−23.861	− .014	−5.554
1402	28.18	−23.994	− .063	−5.734
1405	29.15	−24.114	− .013	−5.782
1425	July 27.18	−24.736	− .238	−5.668
1596	Dec. 22.55	+23.944	+ .257	−5.667
1618	1938 Jan. 20.51	+25.830	+ .162	−5.570
1628	Mar. 15.48	+12.869	− .098	−5.663
1633	16.46	+12.486	− .057	−5.789
1635	16.51	+12.466	− .170	−5.828
1670	May 14.28	−12.153	− .008	−5.832
1894	1939 Jan. 10.53	+25.929	+ .197	−5.488
1897	11.50	+25.955	+ .237	−5.498
1901	30.51	+24.958	− .019	−5.519
1913	Mar. 1.50	+17.977	− .057	−5.436
1916–17	2.44	+17.660	+ .011	−5.591
1983	Apr. 8.36	+ 2.985	+ .038	−5.494
1984	8.41	+ 2.961	− .087	−5.776
1990	9.34	+ 2.557	+ .074	−5.829
1993	27.25	− 5.208	+ .156	−5.700
1996	28.28	− 5.644	+ .093	−5.818
2030	June 1.17	−18.099	+ .143	−5.429
2033	2.15	−18.387	+ .168	−5.763
2036	3.15	−18.674	+ .165	−5.510
2052	29.16	−24.054	− .013	−5.417
2056	30.15	−24.173	.000	−5.726
2060	July 1.15	−24.287	− .013	−5.777
2080	Aug. 24.18	−20.078	− .330	−5.490
2084	25.13	−19.830	− .271	−5.664
2224	Dec. 31.53	+25.182	+ .246	−5.464
2230	1940 Jan. 19.52	+25.898	+ .193	−5.796
2276	Mar. 20.37	+10.732	+ .130	−5.640
2281	21.49	+10.275	−0.154	−5.464

4428.551 *V—d?* in the *Rowland Table*. It is of excellent quality in α Boötis but gives a systematic difference of -2.0 km/sec from other stellar lines. Mr. Babcock made a special study of this line when it was called to his attention and found no less than three lines apparently involved in the solar wave length: 4428.51 *Cr*, 4428.52 *V*, and 4428.55

Fe predicted. On a photograph taken in the third order of the 75-foot spectrograph the last two lines were resolved, and their wave lengths measured as 4428.524 and 4428.578. It is clear that in α Boötis the *V* line is the effective one and that a wave length of 4428.524 gives good agreement with the results from other lines.

WATER-VAPOR LINES IN THE SPECTRUM OF MARS

Four spectrograms of Mars in the region covering the B band of oxygen and the water-vapor lines as far as λ 7300 were taken during February–April, 1937, and three during October–December, 1939. The first four photographs were taken on IIIN

TABLE 2

MEASUREMENTS OF SPECTROGRAMS OF MARS

Plate No.	Calc. *V*	Obs. *V*	Displacements (Rowland λ)		Displacements (Babcock λ)	
			A_{wv}	*A*	A_{wv}	*A*
	km/sec	km/sec	A	A	A	A
1329.....	−18.9	−19.4	+0.051(12)	+0.005 (9)	+0.022 (2)	+0.002(10)
1337.....	−18.7	−18.9	+ .005 (6)	+ .019(13)	+ .019 (6)	+ .020(12)
1338.....	−16.7	−17.7	+ .020(11)	− .012(12)	+ .023(11)	+ .003 (9)
1361.....	−11.5	−11.4	+ .011 (3)	+ .006 (9)	− .002 (3)	− .002(10)
2143.....	+12.9	+12.5	+ .012(13)		+ .027(14)	
2170.....	+15.1	+14.8	+ .008 (9)	+ .019 (9)	+ .017 (9)	+ .016(10)
2177.....	+15.5	+15.5	+0.026 (3)	+0.017(23)	+0.027 (3)	+0.018(27)

TABLE 3

MEAN DISPLACEMENTS

Plate Nos.	Rowland λ		Babcock λ	
	A_{wv}	*A*	A_{wv}	*A*
1329–61.....	+0.018 A	+0.005 A	+0.018 A	+0.007 A
2143–77.....	+0.012	+0.018	+0.024	+0.017

emulsions, one of the others on IS and the other two on IN. They were made in the first order of the 9-foot lens spectrograph and are of only fair quality, the aluminized surfaces of the mirrors in both telescope and spectrograph causing a serious loss of light in this region of the spectrum, as compared with silver surfaces. The coarseness of the grain of the IN emulsions is also a drawback to accurate measurement. The series of spectrograms, however, has the important advantage of having been taken in part when Mars was approaching the earth and in part when it was receding, so that Martian components of the water-vapor lines should lie on opposite sides of the terrestrial lines, and the problem of their detection by measurement becomes a differential one.

Since the comparison lines of iron in this region of the spectrum are, for the most part, faint and few in number, the sharp lines of oxygen in the B band have been used as standards for the wave lengths of the water-vapor lines. It has been shown previously[3]

[3] *Mt. W. Contr.*, No. 488; *Ap. J.*, **79**, 308, 1934.

that the amount of free oxygen in the atmosphere of Mars which could produce components of these lines must be extremely small, and the use of the terrestrial wave lengths of these lines will show whether or not the water-vapor lines behave similarly. A check on the procedure is also afforded by the displacements of the lines of solar origin, which should, of course, show displacements corresponding to the theoretical radial velocity of Mars with reference to the earth, i.e., the time-rate of change of the light-path sun to Mars to earth.

In Table 2 are given in successive columns the number of the spectrogram, the calculated radial velocity of Mars, the observed radial velocity based upon the wave lengths of the oxygen lines as standards, and the displacements in angstroms of two groups of lines designated in the *Revised Rowland Table* as A_{wv} and A, respectively. It seems very probable that both sets of lines are due to water vapor. Two sets of wave lengths are used for the solar, oxygen, and water-vapor lines—the first, those of the *Rowland Table*, and the second, more recent determinations by Babcock. The number of lines is given in parenthesis.

If the results for the first four spectrograms when Mars was approaching are compared with the last three when it was receding, the differences between calculated and observed velocity, -0.45 km/sec and -0.23 km/sec, differ so little from each other as to afford no evidence of change in the position of the oxygen lines upon which the determinations are based. In fact, the sign of the difference is in the wrong direction for the presence of a Martian component to the oxygen lines. Similar means for the groups of A_{wv} and A lines, weighted according to the number of lines, are given in Table 3.

The persistence of the positive sign in these differences is very marked. It may be due to a systematic difference in wave length between the oxygen and the water-vapor lines, which is not at all probable; or to the reduction of the wave lengths of the water-vapor lines on the spectrograms from the oxygen lines, which involves some extrapolation, although the attempt was made to allow for this factor. The important question, however, is that of the differences between the two groups of values in Table 3. When the results for the two sets of wave lengths are combined, the difference, Mars approaching *minus* Mars receding, is 0.000 for the A_{wv} lines, -0.012 for the A lines, or -0.006 A for the mean of the two. This quantity, although of the right sign to indicate the presence of Martian lines, is of little or no significance when the accidental error of measurement of these rather diffuse lines is considered. The general conclusion to be drawn from this investigation with rather limited material is that, if water-vapor lines are present in the spectrum of the equatorial areas of Mars, they cannot be more than 5 per cent as strong as in the earth's atmosphere and are probably very much less.

I am indebted to Dr. Dunham for some of the spectrograms used in this investigation.

THE SPECTRUM OF *o* CETI

A large-scale spectrogram of *o* Ceti with the 114-inch Schmidt camera was obtained on September 29, 1939, in the second order of the grating. The maximum of light had occurred in August, and the star's visual magnitude at the time of observation was about 4.2. The photograph covers the region λλ 3700–4900 and is of good quality to show the absorption spectrum and bands. The bright hydrogen lines $H\zeta$, $H\delta$, and $H\gamma$ are necessarily overexposed, but other fainter emission lines are well shown. The exposure time was $5\frac{1}{2}$ hours on a Cramer Hi-Speed Special plate.

The resolving-power of this spectrogram is such that the study of the molecular bands forms an extensive investigation in itself, which is being undertaken by Miss Dorothy N. Davis in connection with similar work on other M-type stars. Certain features of the atomic spectrum have also proved of sufficient interest to deserve comment.

A simple inspection of the spectrum shows that the cause producing great widening, and in numerous cases doubling, of lines in the spectra of α Orionis, α Scorpii, α Herculis,

and other M-type supergiants is present in *o* Ceti, although in less degree. The lines of the *Mn* I triplet near λ 4030 and λ 4275 of *Cr* I are resolved, and their separations have been measured, while the other two lines of the *Cr* I triplet, the lines of *Sr* II λ 4077 and λ 4215, and the *Ba* II line λ 4554 show great widening but are not resolved. *Ca* I 4227 is not measurable. All these lines arise from the ground level of the neutral or ionized atom. Measures of the separations in *o* Ceti are given in a later section of this communication where M-type stars are discussed. Many of the emission lines in this spectrum appear as bright wings on the violet side of the corresponding absorption lines. In a few cases there seems to be evidence of similar bright wings on the red side, but this is by no means conclusive. They may be portions of the continuous spectrum or close lines of other origin, but they usually appear only in connection with strong absorption lines. Illustrations are λλ 3893, 3907, 3956, and 3992. An interesting fact about the emission lines appearing on the violet side of absorption lines is that apparently they do not affect the wave lengths of the absorption lines. For example, the well-known *Fe* I lines λ 4202 and λ 4376 have strong emission components, but the absorption lines have the same displacements as other absorption lines unaccompanied by emission. Furthermore, the displacements of such emission lines correspond closely to those of emission lines unaccompanied by absorption, such as the hydrogen and silicon lines. These results argue strongly against reversal and for an independent spectrum of bright lines superimposed upon the absorption spectrum.

The behavior of the emission lines of hydrogen in the spectrum of *o* Ceti has always presented a remarkable problem. Many of the lines of the Balmer series are wide but single, while others, notably *Hγ*, *Hδ*, *Hζ*, *H*10, and *H*16, show two, three, or even more components. It is exceedingly difficult to ascribe such a diversity of behavior of the series lines of a single element to intrinsic causes alone, and Merrill has suggested that in the lines showing components the effect is merely an apparent one due to the superposition of absorption lines upon the broad emission lines, thus dividing them into what appear to be individual lines. That this occurs in *H*16 is quite certain. *H*16 is a double bright line with strong central absorption due to the *V* line λ 3703.59 of low excitation.[4] Its position agrees perfectly with that of other *V* lines of similar excitation in the general absorption spectrum. *H*10 appears on the high-dispersion spectrogram as a triplet with relatively faint absorption lines or spaces dividing the components. Measures of the positions of these absorption features show that they can be identified with the lines λ 3797.52 *Fe* 5, and λ 3797.72 *Cr* I of the solar spectrum. Their displacements agree closely with those of other absorption lines in their vicinity; and, although their identification is not so certain as that in the case of *H*16, it seems fairly probable.

The emission lines *Hζ*, *Hδ*, and *Hγ* are greatly overexposed upon the present spectrogram, but some details have been measured upon other spectrograms taken by Joy with less exposure. A faint absorption feature dividing *Hζ* into nearly equal parts agrees closely in wave length with λ 3888.83 *Fe* 2 in the solar spectrum, and a strong absorption line forming the violet edge of the strong emission is λ 3888.52 *Fe* 5. The *Hδ* line is characterized by an apparent emission component on the red side. Whether this is a portion of *Hδ* set off by absorption or is due to *V* 4102.17 is uncertain, since but few *V* lines appear in emission in the spectrum. The apparent absorption setting off this component may be λ 4101.68 *Fe* 3 in the solar spectrum, which is nearly coincident with the hazy hydrogen line itself. At *Hγ* a fairly strong emission line lies just to the red of the principal line. It almost certainly forms a part of *Hγ*, although it may be influenced by a possible violet component on the strong *V* line λ 4341. It is separated from the main *Hγ* line by an absorption feature which corresponds to no line of the *Rowland Table*. A spectrum of α Herculis, however, shows a maximum of absorption on the red edge of the wide hazy *Hγ*, which would coincide reasonably well with the absorption in *o* Ceti.

[4] C. D. Shane had previously suggested (*Lick Obs. Bull.*, **10**, 131, 1922) that this *V* line might be the cause of the abnormal faintness of *H*16.

UNIV. OF MICH.

PLATE II

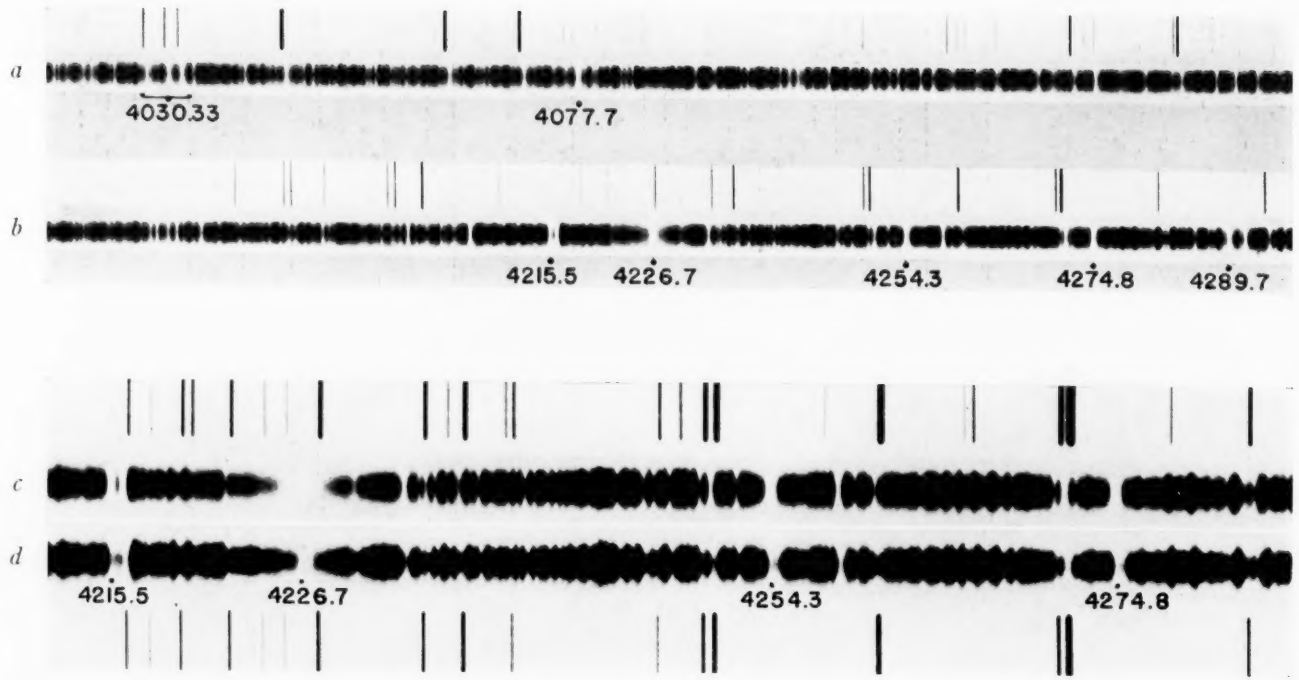

STELLAR SPECTRA WITH HIGH DISPERSION

a, *b*) α Orionis. Note doubling of λλ 4030–33, 4077, 4215, 4226, 4254, 4274, and 4289

c) α Herculis; *d*) α Scorpii

The general conclusion from these results is that, while superposed absorption lines may not account fully for the multiple character of several emission hydrogen lines in *o* Ceti, they must affect them greatly. In the case of *H*16 the evidence is conclusive and in that of *H*10 very probable. These results lend support to Merrill's view that the absorption spectrum in variable stars of this type is produced in a portion of the stellar atmosphere overlying that which gives rise to the emission lines.

Many absorption lines in the spectrum of *o* Ceti have been measured with a view to the study of possible differential displacements. If the lines are divided into groups according to their lower excitation potentials, a slight but systematic effect seems to be present. The results are given in Table 4. *V* is the mean velocity given by each group with its probable error. Although the differences are small, the quality of the lines and the size of the probable errors afford considerable evidence for the reality of the effect.

TABLE 4

DISPLACEMENTS OF LINES IN THE SPECTRUM OF *o* CETI

Low E.P.	Mean Low E.P.	No of Lines	*V*
			km/sec
0.00–0.19	0.04	51	+60.96±0.20
0.20–1.00	0.64	37	+62.59±0.22
1.01–1.99	1.45	34	+63.33±0.29
>2.00	2.43	32	+64.10±0.35

DOUBLE LINES IN M-TYPE STARS

The double character of numerous lines in the spectrum of α Orionis was first recognized on a spectrogram taken with the grating in December, 1936. Previously a marked asymmetry of these lines had been observed with the prismatic spectrograph, and an extensive investigation of the effect with the aid of the microphotometer has been completed and published by Dr. Lyman Spitzer.[5] Other supergiant stars of the M type showing doubling to some extent, but much less clearly than α Orionis, are α Scorpii and α^1 Herculis. Apparently ordinary giant M stars like β Andromedae, μ Geminorum, δ and ν Virginis, and σ Librae do not show the effect, all lines being sharp. The spectrogram of *o* Ceti taken about one month after maximum light, however, shows distinct doubling of the same lines as in α Orionis.

A simple examination of the spectrum of α Orionis shows that all lines are much widened when compared with the spectrum of such a star as α Boötis, for example. Some lines are much more widened than others, however, in many cases showing traces of doubling, and finally a group of lines is found which are fully resolved into two components. In α Orionis these components are of very unequal intensity, the violet member, which is sharp and strong, having several times the intensity of the diffuse red component. An interesting fact about these double lines is that all arise from very nearly the ground state of the neutral or ionized atom. The most widened lines which are not fully resolved arise from the next lowest level of excitation potential, while lines which arise from higher levels, although widened, show no evidence of doubling. Table 5 gives a list of the resolved doublets and of lines showing evidence of doubling, though not fully resolved, on a recent spectrogram in the region λλ 3750–4600.

The list of doublets not fully resolved is certainly incomplete, but enough are given to indicate the higher average excitation potential of the lower state from which they arise. The H and K lines of *Ca* II are not resolved merely because of the great intensity

[5] *Mt. W. Contr.*, No. 619; *Ap. J.*, **90**, 494, 1939.

and diffuseness of the components. Almost without exception the components of the resolved doublets have very unequal intensities with the violet component strong and sharp, while the components of the unresolved doublets are much more equal in intensity and more diffuse in appearance.

The separation of the components of the double lines has been measured on eight spectrograms of α Orionis, ranging in date from December, 1936, to January, 1940. The lines include most of the double lines listed in Table 5, especially the *Mn* I triplet near λ 4030, the *Sr* II pair λ 4077 and λ 4215, and the *Cr* I triplet λλ 4254, 4275, and 4289. Of the double lines in the spectrum, these are of the best quality for measurement.

TABLE 5

DOUBLE LINES IN THE SPECTRUM OF α ORIONIS

RESOLVED DOUBLETS

λ	Elem.	Low E.P.	λ	Elem.	Low E.P.
3759.30	*Ti* II	0.60	3981.78	*Ti* I	0.00
3761.32	*Ti* II	.57	3989.77	*Ti* I	.02
3824.45	*Fe* I	.00	3998.64	*Ti* I	.05
3856.38	*Fe* I	.05	4030.77	*Mn* I	.00
3859.92	*Fe* I	.00	4033.08	*Mn* I	.00
3886.30	*Fe* I	.05	4034.49	*Mn* I	.00
3895.67	*Fe* I	.11	4077.73	*Sr* II	.00
3899.72	*Fe* I	.09	4215.52	*Sr* II	.00
3920.27	*Fe* I	.12	4226.74	*Ca* I	.00
3922.92	*Fe* I	.05	4246.84	*Sc* II	.31
3927.94	*Fe* I	.11	4254.35	*Cr* I	.00
3930.31	*Fe* I	.09	4274.81	*Cr* I	.00
3944.02	*Al* I	.00	4289.73	*Cr* I	.00
3948.68	*Ti* I	.00	4554.04	*Ba* II	0.00
3961.54	*Al* I	0.00			

DOUBLETS NOT FULLY RESOLVED

λ	Elem.	Low E.P.	λ	Elem.	Low E.P.
3758.25	*Fe* I	0.95	3878.58	*Fe* I	0.95
3763.80	*Fe* I	0.99	3933.68	*Ca* II	0.00
3767.21	*Fe* I	1.01	3968.49	*Ca* II	0.00
3820.44	*Fe* I	0.86	4045.83	*Fe* I	1.48
3825.89	*Fe* I	0.91	4063.61	*Fe* I	1.55
3834.24	*Fe* I	0.95	4375.95	*Fe* I	0.00

Table 6 gives, in kilometers per second, the radial velocity from each component, the mean velocity, and the radial velocity of the star as determined from a list of selected single lines. The last two columns give the separations in kilometers per second, and in angstroms, respectively.

It is well known that the radial velocity of α Orionis is variable, and these results show that the mean of the velocities given by the two components of the doublets agrees fairly closely with the stellar velocity. The average difference of +1.4 km/sec is within the limits of error of measurement. The centers of these double lines, therefore, have very nearly their normal wave lengths. Whether the separation of the components varies on different spectrograms is uncertain; the range of nearly 7 km appears large, but the measurement of the diffuse second component is somewhat difficult.

The separations of the doublets agree with one another rather well except in the case

of *Ca* λ 4227. This line shows a separation larger by about 0.12 A, on the average, than the other doublets. A few measures on the incompletely resolved components of H and K also give larger separations.

In the spectra of α Herculis, α Scorpii, and ο Ceti a few of the doublets measured in α Orionis appear as double lines but only partially resolved. The most prominent of these are the *Mn* I, *Sr* II, and *Cr* I lines already mentioned. The relative intensities of the components, however, are much more nearly equal than in α Orionis, and this fact makes their resolution more difficult. The average separation of the components in these stars is: α Herculis, 0.27 A; α Scorpii, 0.28 A; ο Ceti, 0.19 A. These values are considerably smaller than in α Orionis.

The explanation of the doubling and great widening of numerous lines in the spectra of these M-type stars on the basis of motions in their extended atmospheres, a hypothesis discussed in detail by Spitzer, seems to be most nearly in accord with the facts of observation. No emission other than bright wings on H and K is present in the spectra of any

TABLE 6

VELOCITIES FROM DOUBLE LINES IN THE SPECTRUM OF α ORIONIS

Plate No.	Date	Comp. 1	Comp. 2	Mean	Stellar Velocity	Separation	
		km/sec	km/sec	km/sec	km/sec	km/sec	A
1289.....	1936, Dec. 23	+ 8.6	+35.5	+22.0	+22.2	26.9	0.369
1331.....	1937, Feb. 23	11.0	36.0	23.5	22.0	25.0	.342
1530.....	Oct. 21	11.5	33.4	22.4	19.9	21.9	.300
1594.....	Dec. 21	9.7	36.7	23.2	21.8	27.0	.370
1822.....	1938, Nov. 8	8.7	29.5	19.1	16.0	20.8	.285
1827.....	9	9.4	30.8	20.1	17.7	21.4	.293
1911.....	1939, Feb. 28	8.3	36.0	22.2	23.3	27.7	.379
2227.....	1940, Jan. 18	+14.3	+35.9	+25.1	+23.3	21.6	0.296

of these stars except ο Ceti. The great difference in the relative intensities of the components of the double lines in α Orionis is also opposed to the view that the doubling can be an effect of reversal. The hypothesis that the difference in displacement between emission and absorption lines in the spectra of Me variables is due to Doppler motion is rather generally accepted by astronomers, and the doubling and displacements of absorption lines in the spectra of the stars here considered may well be quite analogous in character.

INTERSTELLAR LINES

The discovery of several previously unobserved narrow interstellar lines was announced by Dunham and Adams in December, 1936,[6] and the identification of four lines in the far ultraviolet with ground-state lines of *Ti* II was established. In a later communication Dunham presented evidence for the presence of interstellar *Ca* I 4227 and *K* I 7699.[7] The principal stars observed were χ^2 Orionis, 55 Cygni, and ο Persei. Several prominent lines remained unidentified, notably three at λλ 3957.72, 4232.58, and 4300.33. Marked variations in the intensities of these lines relative to each other and especially to interstellar H and K were noted in different stars and have been commented upon by Dunham.

Observations of these stars were made almost wholly with the 32-inch Schmidt camera and fine-grained plates. Since the interstellar lines are extremely narrow, it

[6] *Pub. A.A.S.*, **9**, 5, 1937.

[7] *Pub. A.S.P.*, **49**, 26, 1937.

seemed desirable to use the greater photographic resolving-power and the larger linear scale of the 114-inch Schmidt camera, and a few bright stars of type approximating Bo were selected for observation. One of these, ζ Ophiuchi, of magnitude 2.7 and type Bon, has proved to be exceptionally favorable for a study of the unidentified lines. Although interstellar H and K and the D lines are of relatively moderate strength in the spectrum, the unidentified lines λλ 3957, 4232, and 4300 are very well marked. On a spectrogram taken on a coarse-grained plate these three lines, with H and K, are the principal features. In addition, a faint narrow line has been measured at λ 3874.6. On the other hand, λ 3934 and *Ca* I 4227 do not appear. This calcium line seems to be definitely correlated in intensity with H and K, and unless these are exceptionally strong, λ 4227 is not seen.

In 1937 Swings and Rosenfeld[8] offered the suggestion that the interstellar line λ 4300.3 might be due to *CH*, and recently McKellar has applied to molecular spectra the considerations derived from the study of the interstellar atomic lines of *Ti* II in the far

TABLE 7

INTERSTELLAR LINES OF *CH*

McKellar		ζ Ophiuchi		
λ	Intensity	λ	Intensity	Δλ
3878.8.....	1	3878.81.....	1	0.0
3886.39.....	3	3886.44.....	3	+ .05
3890.23.....	2	3890.25.....	2	+ .02
4300.29.....	>6	4300.34.....	8	+0.05

ultraviolet and has succeeded in identifying with considerable probability three of the lines with lines arising from common diatomic molecules.[9] These are: λ 4300.33 with *CH*, as already suggested by Swings and Rosenfeld; λ 3934.3 with *NaH;* and λ 3874.62 with *CN*. McKellar has made these provisional identifications on the basis of agreement of wave length through consideration of the few lines which would arise from the most probable transitions for molecules in the lowest rotational level of the zero vibrational level of the ground electronic state. As a result of this investigation McKellar could predict the presence of certain fainter interstellar lines in addition to those already identified, in case the identification were correct.

An examination of the available spectrograms did not show any of these additional lines with certainty; but since the visibility of faint, narrow lines depends greatly upon the contrast and grain of the photographic plate, the attempt was at once made to obtain a suitable spectrogram with the 114-inch Schmidt camera. A Cramer Contrast plate was used, and the star ζ Ophiuchi was selected because of its brightness and the intensity of several of its interstellar lines, including λ 4300. An exposure of nearly five hours gave a fully satisfactory plate in the region λλ 3700–4700.

Since the line at λ 3934.3 ascribed to *NaH* by McKellar does not appear to be present in the spectrum of ζ Ophiuchi, it is hardly to be expected that any of the other predicted lines of this molecule would appear. The line λ 3874 ascribed to *CN* is well marked, but the predicted line λ 3580 is outside the range of the spectrogram. The chief interest lies in the predicted lines of *CH*, the strongest line of which is at λ 4300. The three additional lines given by McKellar lie at λλ 3879, 3886, and 3890, with estimated intensities of 1, 3, and 2, respectively. Their combined intensity should be somewhat less than that of

[8] *Ap. J.*, **86**, 483, 1937. [9] *Pub. A.S.P.*, **52**, 187, 1940.

PLATE III

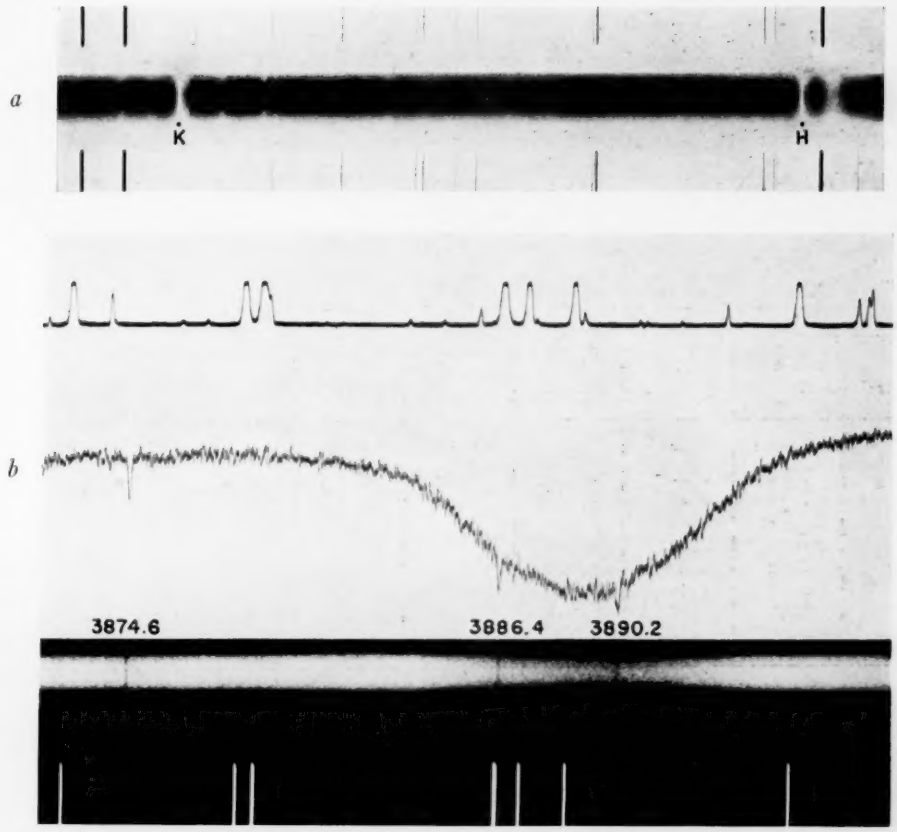

INTERSTELLAR LINES

a) α Cygni showing interstellar H and K superposed upon stellar lines; *b*) ζ Ophiuchi, positive reproduction of stellar and comparison spectra, with photometric tracings. Two lines of *CH* are shown, λ 3886 and λ 3890; also λ 3874.6 and a trace of λ 3874.0, both probably *CN*.

UNIV OF MIC

PLATE IV

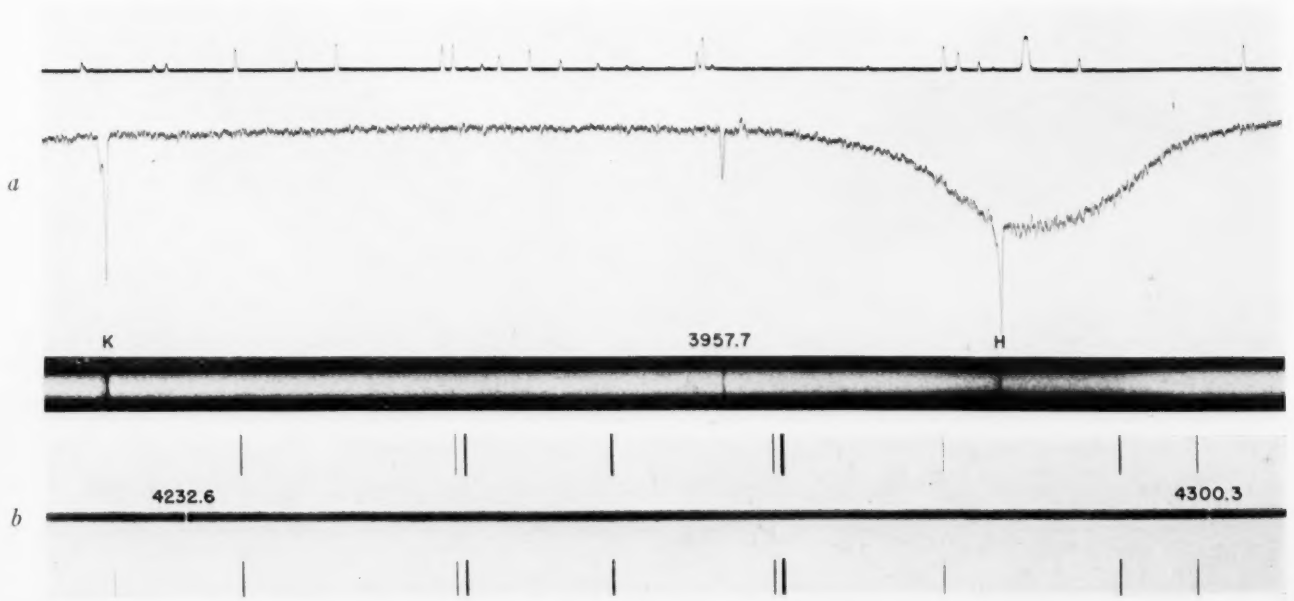

INTERSTELLAR LINES IN THE SPECTRUM OF ζ OPHIUCHI

a) Interstellar H and K (double) and λ 3957.7 (unidentified); *b*) λ 4232.6 (unidentified) and λ 4300.3 (*CH*)

UNIV. OF MICH.

λ 4300. An inspection of the stellar spectrogram shows three lines to be present near the predicted positions with relative intensities corresponding to the predicted values. Table 7 gives the results of measurement and a comparison with McKellar's recent values. The lines all belong to the 0, 0 band of *CH*. The measured wave lengths of the lines in ζ Ophiuchi have been corrected for the displacements of interstellar H and K.

The small systematic difference in wave length may readily be accounted for by a difference in the two systems of wave lengths or in the radial velocities of molecular *CH* and atomic *Ca* II. The evidence for the correctness of Dr. McKellar's identification is surprisingly strong and provides definite proof of the existence of interstellar lines arising from molecular transitions.

Assuming McKellar's identification for the lines λ 3874.62 with *CN* and λ 3934.3 with *NaH*, the only remaining narrow unidentified interstellar lines in the region λλ 3800–4700 are λ 3957.72 and λ 4232.58. Both are prominent in the spectrum of ζ Ophiuchi, λ 4232 having about the same intensity as interstellar *H*. Their identification should be greatly facilitated by the results already found.

Since the last paragraph was written, two recent spectrograms of ζ Ophiuchi extending farther to the violet show the presence of two lines not previously observed and one doubtfully suspected but now fully confirmed. These are λλ 3579.04, 3745.330, and 3874.018. The first of these, λ 3579, which is faint, lies nearly an angstrom to the violet of a line of *CN* predicted by McKellar and evidently cannot be identified with it. The line at λ 3745 is fairly prominent. Especial interest attaches to the line λ 3874.018, since this is almost certainly to be identified with λ 3874.00 of *CN* given by McKellar. It is the R(1) line, while the R(0) line is represented by the more conspicuous interstellar line λ 3874.62. The difference in rotational level, as McKellar states, is only 0.00047 volt. Although McKellar's predicted line of *CN* at λ 3579.98 has not as yet been observed with certainty, the close agreement of the two lines at λ 3874 with the two *CN* lines of very low rotational level makes the identification of *CN* in interstellar space highly probable.

I am indebted to Mr. Milton L. Humason both for some of the measures of the interstellar lines and for a careful study of the fainter details upon the spectrograms.

CARNEGIE INSTITUTION OF WASHINGTON
MOUNT WILSON OBSERVATORY
June 1940

THE NATURE OF SOLAR HYDROGEN VORTICES*

R. S. RICHARDSON

ABSTRACT

The hydrogen vortices surrounding spot-groups have been explained by the existence of magnetic fields produced by charged particles whirled around the spot at a low level, or as hydrodynamical vortices whose form depends upon how the gases are flowing into or out of the spot.

It is possible to test these ideas if we are allowed to assume that the charged particles in the low-level whirl always have the same sign. For then all spots with the same polarity must also have the same direction of whirl. Furthermore, when the reversal of polarity occurs at sunspot minimum, there should be a reversal in the direction of whirl.

Hale applied this test to the best hydrogen vortices observed from 1908 to 1924 and was unable to find any relationship between the polarity and the direction of whirl. But since about 80 per cent of the whirls were in the same direction as terrestrial cyclones, he concluded that the observations favored the hydrodynamical, rather than the electromagnetic, hypothesis.

This test has been repeated, using all the observations from 1908 to 1939, extending over four sunspot cycles. The results obtained agree closely with those of Hale. Evidently, the direction the vortex takes is determined primarily by the solar rotation.

Estimates were also made of the degree of curvature in the vortices. Closely wound spirals are rare; open ones, far more numerous.

Spectroheliograms taken in the center of the *Hα* line probably show the solar atmosphere at the highest level observable. On such exposures the chromosphere has a fine granular structure resembling the skin of an orange. Near large spot-groups, however, it is drawn out into long filaments, indicating the presence of an extensive field of force. Seen under the best conditions, these filaments remind one of petals or tendrils growing out of the sunspot penumbra and spreading over the hydrogen chromosphere. They are not only smaller and lighter than the prominences projected against the disk but are at a lower level and should not be confused with them, although in certain instances it might be difficult to distinguish between the two. Occasionally the filaments form a pattern similar to the arrangement of iron filings around a bar magnet or to the lines of flow in a vortex.

Two theories have been advanced to account for this pattern: first, that the forms of the filaments are due to magnetic fields produced by charged particles whirled around the spot at a low level; second, that they are hydrodynamical vortices whose form depends upon how the gases are flowing into or out of the spot.

The presence of magnetic fields of moderate intensity in sunspot umbrae distinctly favors the electromagnetic hypothesis. Carl Störmer[1] has developed this hypothesis on the assumption that the direction of curvature of the filaments (clockwise or counterclockwise) depends upon the flow of an electric current far below the surface layers. In this way he was able to account for many of the visible surface features.

Störmer's theory can be put to a rather crucial test if we are allowed to assume that the charged particles in the low-level current always have the same sign in single spots and in the preceding member of bipolar groups, for then all spots with the same polarity must also have the same direction of whirl. Furthermore, when the reversal of polarity in each hemisphere occurs at sunspot minimum, a reversal should also take place in the direction of whirl.

Hale[2] applied this test to the best hydrogen whirls he could find on the spectrohelio-

* *Contributions from the Mount Wilson Observatory, Carnegie Institution of Washington*, No. 639.

[1] *Mt. W. Contr.*, No. 109; *Ap. J.*, **43**, 347, 1916.

[2] *Mt. W. Comm.*, No. 95; *Proc. Nat. Acad. Sci.*, **11**, 691, 1925; *Nature*, **119**, 708, 1927.

grams taken at Mount Wilson from 1908 to 1924. Since more than 3000 spot-groups were recorded during this time, hydrogen spectroheliograms having been taken on every clear day, it might be supposed that hundreds of cases would be available for study. On the contrary, only 51 good examples were found. This circumstance may be explained partly by a variety of reasons, such as instrumental mishaps, the poor quality of the red-sensitive emulsions then available, the small size of many of the spots, but principally by the fact that well-marked whirls are exceedingly rare phenomena. Generally the filaments are so indefinite and so badly jumbled together that it is difficult not only to determine the direction of whirl but even to decide whether there is any whirl at all.

Hale was unable to discover a relationship between the polarities of the 51 selected whirls and their directions of rotation. That is, regardless of polarity, about as many spots whirled one way as the other. But when the spots are grouped according to hemisphere, the direction of whirl for slightly more than 80 per cent agreed with that in terrestrial cyclones. Thus, the observational evidence, although somewhat meager, appeared to favor the hydrodynamic, rather than the electromagnetic, hypothesis.

These results are of the greatest importance in the interpretation of solar phenomena. It seemed advisable, therefore, not only to make use of the material that has accumulated since Hale's investigation but also to re-examine the plates taken from 1908 to 1924. In this way the data would be as homogeneous as possible over the entire interval, 1908–1939, inclusive.

Two methods were tried. The first was the one adopted by Hale of using a few selected spots for which there could not be the slightest doubt concerning the direction of whirl. The only difference was that, while Hale used both single spots and the leading members of bipolar groups, the latter were excluded from the present investigation. In the second method *all* single spots with a well-marked filamentary structure were examined, and estimates were made of the percentage of filaments that were clockwise, counterclockwise, radial, and indeterminate. For example, 50 per cent of the filaments surrounding a certain spot might be clockwise, 20 per cent counterclockwise, and the remainder so scattered in direction as to be indeterminate. In making these estimates, the selected spots with definite directions of whirl used in the first method were necessarily included, since all available data were used. But the estimates were made entirely without reference to this previous work, in order to keep them as free from bias as possible. Thus, a spot listed "clockwise" in the first investigation might appear in the second as 80 per cent clockwise and 20 per cent radial.

The observations extend over the thirty-two years from 1908 to 1939, thus including portions of four sunspot cycles and three reversals of polarity at the minima of 1913, 1923, and 1933. The results of the first method are based on 141 definitely directed whirls, and those of the second on these same 141 plus 84 others whose direction of whirl is more or less indeterminate.

The results for the 141 selected spots are given in Tables 1 and 2. Table 1 shows these data arranged according to hemisphere. Throughout all four cycles the direction of rotation is predominantly the same as in terrestrial cyclones.

Table 2 contains the same data arranged according to magnetic polarity. Arranged in this way, the majority of vortices surrounding the spots appear to have opposite whirls in alternate cycles. Now the basic assumption of the electromagnetic hypothesis is that the direction in which the charged particles are whirling determines the polarity of the spot. Hence, if the direction of whirl changes but the polarity remains the same, we are forced to conclude that the sign of the charged particles must also have changed. Although such a possibility cannot be ruled out entirely, it seems so unlikely that we much prefer quite a different conclusion, namely, that there is no connection whatever between the direction of whirl shown by the hydrogen flocculi and the polarity of the spot.

Table 3 contains the results for all the material. Despite the fact that this includes the 141 selected examples for which the filaments had nearly 100 per cent clockwise or coun-

terclockwise curvature, the form of the majority of hydrogen flocculi was either radial or indeterminate. Of the filaments having a definite direction of whirl, the percentages clockwise and counterclockwise in the northern hemisphere are 29 and 71, respectively; in the southern hemisphere, 66 and 34. These values agree closely with those in Table 1.

TABLE 1

DIRECTION OF WHIRL IN EACH HEMPISHERE (141 SELECTED SPOTS)

Direction of Whirl	1901–1913		1913–1923		1923–1933		1933–1944		Total	
	No.	Per Cent	No.	Per Cent	No.	Per Cent	No.	Per Cent	No.	Per Cent
	Northern Hemisphere									
Clockwise	0	0	9	27	4	25	3	30	16	25
Counterclockwise	4	100	24	73	12	75	7	70	47	75
	Southern Hemisphere									
Clockwise	6	75	24	75	16	67	9	64	55	71
Counterclockwise	2	25	8	25	8	33	5	36	23	29

TABLE 2

DIRECTION OF WHIRL AND POLARITY (141 SELECTED SPOTS)

Direction of Whirl	1901–1913		1913–1923		1923–1933		1933–1934		Total	
	No.	Per Cent	No.	Per Cent	No.	Per Cent	No.	Per Cent	No	Per Cent
	Spots of Positive Polarity									
Clockwise	6	75	9	26	16	67	4	36	35	45
Counterclockwise	2	25	25	74	8	33	7	64	42	55
	Spots of Negative Polarity									
Clockwise	0	0	24	77	4	25	8	38	36	56
Counterclockwise	4	100	7	23	12	75	5	62	28	44

This persistence in the direction of whirl in hydrogen vortices in each hemisphere regardless of the polarity of the underlying spot strongly favors a hydrodynamical hypothesis. Apparently, the direction the vortex takes is determined largely by the solar rotation, just as the earth's rotation tends to establish a preferred direction of the circulation about terrestrial cy-

clones of the northern and southern hemispheres. On the sun, exceptions might arise from the slow change in the angular velocity of rotation with latitude or from violent turbulence in the formation of active spots.

TABLE 3

ESTIMATED DISTRIBUTION OF FILAMENTS FOR ALL SPOTS

DISTRIBUTION OF FILAMENTS	Northern Hemisphere (Per Cent)	Southern Hemisphere (Per Cent)
Clockwise	11.4	28.1
Counterclockwise	28.0	14.7
Radial	30.0	25.1
Indeterminate	30.6	32.1

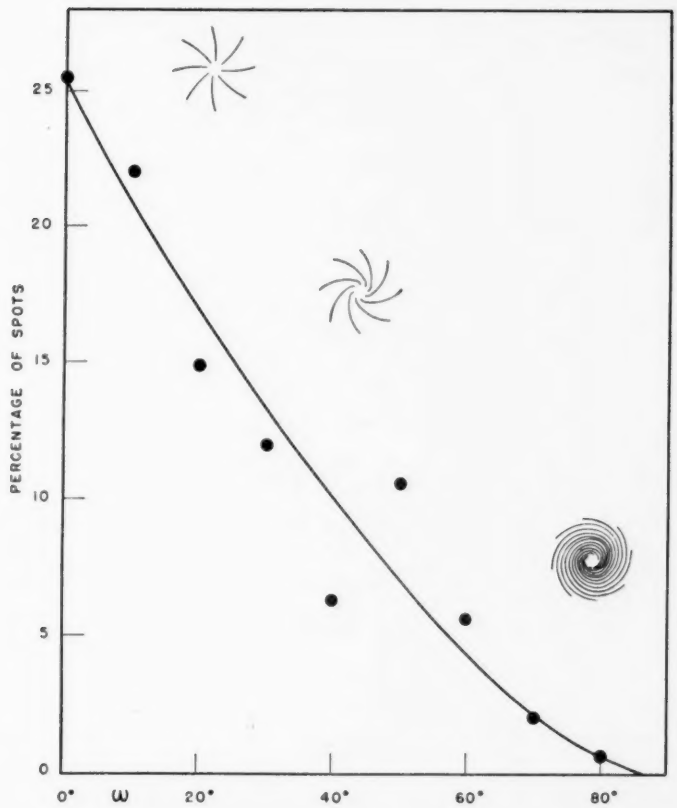

FIG. 1.—Frequency of various degrees of curvature in the hydrogen whirls surrounding 141 selected spots

A point which so far has received no attention is the percentage of whirls having different degrees of curvature. Clearly defined hydrogen whirls resemble logarithmic spirals so closely that they may be conveniently described by curves of this form. The shape

of the spiral is then determined by an angle, ω, defined as the constant angle between the tangent to the curve and the normal to the radius vector at that point, both reckoned in the direction of receding distance from the origin. For small values of ω the spiral is nearly radial, while closely wound spirals correspond to values of ω ranging from 60° to 90°. Using the 141 selected cases, this angle was estimated in steps of 10° by comparing the photographs with the diagrams in Störmer's paper. The results are shown graphically in Figure 1. Small values of ω predominate, 62 per cent of the forms being open spirals with values of ω 20° or less. Closely wound spirals occur but are very rare.

According to Störmer's theory, the strength of the magnetic field along the line of sight should be proportional to cosine ω. This component of the magnetic field can be measured from the displacement and relative intensity of the components of the spectral lines produced by the Zeeman effect. No evidence was found, however, to indicate a relationship between the form of the spiral and the field strength at the center of the spot.

Although only 141, or 2 per cent, of the 7500 spot-groups counted from 1908 to 1939 showed well-marked hydrogen whirls, the percentage for which whirls are *observable* is much larger. The average area of the 141 spot-groups—which in this particular investigation consisted almost wholly of single spots—was 250-millionths of the sun's visible hemisphere. It is doubtful if whirls can be detected around spots with mean areas of less than 200-millionths of the area, except under the finest observing conditions. If then we limit ourselves to spot-groups with mean areas greater than 200-millionths, we find that from 1916 to 1935[3] only 668 groups appeared large enough to show the vortex structure if it existed. Out of the 141 selected examples, 105 occurred during this interval; that is, vortices were actually observed around 16 per cent of those spot-groups sufficiently large to show them clearly. The percentage would probably be doubled if allowance could be made for defective plates and poor seeing. Thus, under perfect conditions about a third of all spots with areas greater than 200-millionths might be expected to show hydrogen whirls on the Mount Wilson plates.

Nevertheless, the writer feels that too much stress has been laid on the vortex structure around spot-groups, the general impression being that a sunspot vortex is one of the most spectacular features of the hydrogen chromosphere. This is occasionally true, but as a rule the structure is poorly defined and may be absent altogether. The misconception probably arises from the fact that the fine examples of hydrogen vortices are the ones most commonly reproduced and may thus seem typical except to those directly engaged in solar research.

Similarly, the vortices are referred to as "whirls," although no whirling motion has ever been actually observed in one. So far the sole motion detected is the rapid disappearance of dark hydrogen flocculi (prominences seen in projection against the disk) into the spot. The corresponding flow of matter outward has never been observed, with the exception of the Evershed effect, which refers to gases moving outward along the penumbra at the level of the reversing layer.

The foregoing discussion emphasizes the fact that the whole sunspot problem is still far from solution.

CARNEGIE INSTITUTION OF WASHINGTON
MOUNT WILSON OBSERVATORY
August 1940

[3] *Greenwich Photoheliographic Results.*

ON THE DETERMINATION OF MASS RATIOS OF SPECTROSCOPIC BINARIES*

O. C. WILSON

ABSTRACT

A method is described which permits the determination of the mass ratio and systemic velocity of a double-lined spectroscopic binary from much less observational material than that required for a complete orbit determination.

Knowledge of the relative masses of the components of spectroscopic binary stars necessarily depends entirely upon those systems in which both spectra are measurable. Moreover, it has thus far been limited to binaries in which the complete orbits of both components have been obtained. Since the determination of such orbits involves much work, it is not surprising that the existing data on mass ratios are not so extensive as might be desired. Furthermore, as more varied fields of astrophysical research are opened up, it appears very probable that less time will henceforth be spent on orbit computations than in the past. Accordingly, it seems appropriate to present here a method which permits the accurate determination of mass ratios from very much less observational material than is required for a complete orbit computation.

Consider a spectroscopic binary in which both spectra are visible. Let the measured radial velocities of the two components be u and v and the masses of the corresponding stars be m_u and m_v. Then, if γ is the radial velocity of the system, we have for the ratio of the masses, r, the rigorous relationship

$$r = \frac{m_u}{m_v} = \frac{v - \gamma}{\gamma - u} \tag{1}$$

or

$$v = \gamma(1 + r) - ru\,. \tag{2}$$

In principle, two spectrograms suffice to determine both r and γ. If the velocities from the two plates are u_1, v_1 and u_2, v_2, the results are

$$r = \frac{v_2 - v_1}{u_1 - u_2}$$

and

$$\gamma = \frac{u_1 v_2 - u_2 v_1}{(v_2 - v_1) - (u_2 - u_1)}\,.$$

In practice, the accuracy of measurement is seldom sufficient to permit satisfactory results from only two plates, and equation (2) must be solved for the best values of r and γ when the number of observations exceeds the number of unknowns.

Equation (2) may be solved most simply by graphical means, since it is linear in u and v. If the pairs of velocities u_n, v_n from the various spectrograms are plotted, they

* *Contributions from the Mount Wilson Observatory, Carnegie Institution of Washington*, No. 640.

will be found to define a straight line of negative slope in the u, v plane. The negative slope of the line is the mass ratio, since $dv/du = -r$ by equation (2). If u and v are chosen as abscissa and ordinate, respectively, and if the intercepts of the straight line are u_0 and v_0, it is readily seen that

$$r = \frac{v_0}{u_0} \qquad \text{and} \qquad \gamma = \frac{u_0 v_0}{u_0 + v_0} . \tag{3}$$

These equations are convenient to use when the line does not pass too close to the origin.

If it is felt that the graphical solution of equation (2) is not sufficiently accurate, the constants of the equation must be determined by the standard methods of least squares. Let

$$M_u = \frac{\Sigma u}{n} \qquad \text{and} \qquad M_v = \frac{\Sigma v}{n} ,$$

where n is the number of observations. Then application of the usual formulae leads to these results:

$$r = -\frac{\Sigma uv - nM_u M_v}{\Sigma u^2 - nM_u^2} \tag{4}$$

and

$$\gamma = \frac{M_v + rM_u}{1 + r} . \tag{5}$$

To obtain the probable errors, these quantities are inserted in equation (2), and the residuals s_n computed for each plate. Let

$$\epsilon_0 = 0.6745\sqrt{\frac{\Sigma s_n^2}{n - 2}} .$$

The weights of the parameters of equation (2) are

$$\left.\begin{aligned} p_r &= \Sigma u^2 - \frac{(\Sigma u)^2}{n} \\ \text{and} \qquad p_{\gamma(1+r)} &= n - \frac{(\Sigma u)^2}{\Sigma u^2} . \end{aligned}\right\} \tag{6}$$

It follows that the probable errors of r and γ are given by

$$\epsilon_r = \frac{\epsilon_0}{\sqrt{p_r}} \tag{7}$$

and

$$\epsilon_\gamma^2 = \frac{\epsilon_{\gamma(1+r)}^2 + \gamma^2 \epsilon_r^2}{(1 + r)^2} , \tag{8}$$

where

$$\epsilon_{\gamma(1+r)} = \frac{\epsilon_0}{\sqrt{p_{\gamma(1+r)}}} . \tag{9}$$

Usually, it is sufficiently accurate to write equation (8) as

$$\epsilon_\gamma = \frac{\epsilon_{\gamma(1+r)}}{1+r} . \tag{10}$$

The method outlined above has been tested on six double-lined binaries for which orbits have been computed. It was believed that, in general, six spectrograms should suffice to give satisfactory results. Therefore, the first six suitable spectrograms tabulated

TABLE 1

MASS RATIOS OF DOUBLE-LINED BINARIES

Star		Orbit	Ref.*	Graph	Least Squares
Boss 46.....	r	1.07	1	1.03	1.022±0.019
	γ	−29.3		−30.0	−29.00 ±1.52
HD 216014....	r	1.15	2	1.13	1.130±0.048
	γ	−24.8		−24.4	−25.69 ±3.68
RT Lac.....	r	1.87	3	1.68	1.709±0.020
	γ	−47.0		−47.0	−47.72 ±0.64
TV Cas.....	r	1.70	4	1.75	1.777±0.088
	γ	+ 0.5		+ 7.6	+ 7.53 ±1.99
Boss 35 Br....	r	1.04	5	1.07	1.073±0.054
	γ	+ 0.4		− 0.5	+ 0.23 ±2.11
Σ 227 A.....	r	1.00	6	1.00	0.974±0.043
	γ	−20.0		−20.0	−19.85 ±1.38

* 1. Pearce, *Pub. Dom. Ap. Obs.*, **3**, 275, 1926.
2. *Ibid.*, p. 171, 1925.
3. Joy, *Mt. W. Contr.*, No. 429; *Ap. J.*, **74**, 101, 1931.
4. Plaskett, *Pub. Dom. Ap. Obs.*, **2**, 141, 1922.
5. MacCormack, *Mt. W. Contr.*, No. 495; *Ap. J.*, **80**, 120, 1934.
6. Harper, *Pub. Dom. Ap. Obs.*, **2**, 129, 1921.

by the various orbit computers were used, except in one or two cases where a value was encountered which would not fit on the plot. Otherwise, no selection was exercised. After the values of r and γ were found graphically, least-squares solutions were made from the same data. The results are presented in Table 1.

The material in Table 1 exhibits two interesting features. In the first place, the generally excellent agreement between the results of the short method and those obtained from complete orbit determinations shows that entirely satisfactory mass ratios can be had from very limited observational data. Second, the graphical solutions are much more accurate than might have been anticipated. In only one star (RT Lac) do the differences between the graphical and the least-squares values exceed the probable errors of the latter, and then only very slightly. Thus, it appears that, unless the probable errors are desired, the simple graphical solution of equation (2) should suffice to give essentially all the accuracy obtainable from a few plates. Judgment must, of course, be exercised.

In cases where both components of a binary show numerous sharp lines, probably only three or four spectrograms would be required, but when only very few lines of poor quality are measurable the necessary number will naturally increase.

In the computation of spectroscopic orbits it is customary to include γ among the other parameters when corrections to the preliminary elements are being determined by least squares, and this procedure can hardly be avoided when only one spectrum is visible. When two spectra are measured, however, there appear to be very definite advantages in carrying out a least-squares solution for γ by means of equations (4) and (5) and eliminating it from further consideration at the very beginning. This solution can be made very rapidly and is inherently free of any of the errors due to uncertainties in the remaining elements. In addition, the value of r obtained in this way serves as a useful check on the mass ratio given by the final elements.

Last, it may be mentioned that if u and v are merely plotted against each other as the very first step in the computation of an orbit, any discordant or erroneous observations are immediately made apparent and can be corrected or eliminated before they are used in the numerical solutions. For example, this method is capable of distinguishing between true double-lined binaries and other objects which are not, even though two components have been measured in their spectra. A curious instance is afforded by the four Lick observations of 31 Camelopardalis.[1] When plotted, these measures define a straight line very well, but its slope is positive. This result is clearly impossible according to equation (2), and hence the second set of lines observed in this star cannot belong to the other member of the system.

It is a pleasure to acknowledge several helpful suggestions by Mr. G. Strömberg and by Mr. R. E. Wilson.

CARNEGIE INSTITUTION OF WASHINGTON
MOUNT WILSON OBSERVATORY
August 1940

[1] *Lick Obs. Pub.*, **14**, 80, 1928.

SYSTEMATIC AND ACCIDENTAL ERRORS IN THE SPECTROSCOPIC ABSOLUTE MAGNITUDES OF DWARF STARS OF TYPES F, LATE K, AND M*

GUSTAF STRÖMBERG

ABSTRACT

The systematic and the accidental errors in the spectroscopic absolute magnitude (M_s) for dwarf stars of spectral types F, K3–K9, and M have been determined by the method described in *Mt. W. Contr.* No. 628. The two regression lines have been determined by grouping the stars on the basis of M_s and $H = m + 5 \log \mu$, respectively, the mean value of M being derived from the trigonometric parallaxes. The two regression lines were then used as calibration lines for determining two new systems of spectroscopic absolute magnitudes. The first system, M'_s, based on the first regression lines, M on M_s, should be used when the stars are grouped on any basis directly connected with conditions in the stellar atmosphere that determine the spectral features which define M_s for a given spectral interval. The second system, M''_s, should be used when the stars are grouped on any basis directly correlated with the true absolute magnitude or with the energy generation in the interior of the star. The values of M_s, as published in *Mt. W. Contr.* No. 511, have the mean errors 0.60, 0.42, and 0.58, respectively, for the three spectral groups; of M_s, the mean errors are 0.27, 0.32, and 0.56; and of M''_s, 0.45, 0.39, and 0.62. The coefficient of correlation between M and M_s is approximately 0.85, 0.88, and 0.90 for the three spectral groups.

In *Mount Wilson Contribution* No. 628[1] the writer presented the results of a determination of the systematic and accidental errors in the spectroscopic absolute magnitudes of dwarf stars of spectral types G0–G7 and G8–K2 and gave formulae for deriving mean absolute magnitudes and for computing the dispersion in M from trigonometric parallaxes. This method has now been applied to dwarf stars of types F, K3–K9, and M. The trigonometric parallaxes used are those compiled by Schlesinger.[2] Three different systems of spectroscopic absolute magnitudes are used in these studies. The first is that given in *Mount Wilson Contribution* No. 511[3] and is denoted by M_s. The second is a corrected system in which the first regression line (M on M_s) is used as the calibration line and is denoted by M'_s. The third system is based on the second regression line (M_s on M) as a calibration line and is denoted by M''_s. The values of $\overline{M'_s}$ are derived by grouping the stars according to the size of M_s itself. The values of $\overline{M''_s}$ are in principle derived by grouping the stars according to the size of the true absolute magnitude (M); but since this in general cannot be done, the stars are grouped on a basis correlated to M, and the basis used in this as in the previous study is $H = m + 5 \log \mu$, which is a function of M and the linear tangential motion.

In the following discussion the dispersions in M, M_s, M'_s, and M''_s are denoted by q, q_s, q'_s, and q''_s, respectively. The mean errors of an individual determination of M in the three systems are designated by θ, θ', and θ''. The relations between the different dispersions and mean errors are given in *Mount Wilson Contribution* No. 628.[1]

In Table 1 are the results from a grouping according to H, which is a simple function of the reduced proper motion ($\mu\, 10^{0.2m}$) and is directly correlated to the true absolute magnitude M.

* *Contributions from the Mount Wilson Observatory, Carnegie Institution of Washington*, No. 641.

[1] *Ap. J.*, **92**, 156, 1940.

[2] *General Catalogue of Stellar Parallaxes*, 2d ed., 1935.

[3] *Ap. J.*, **81**, 187, 1935.

Table 2 shows the results from a grouping according to M_s itself. The data are shown in Figures 1, 2, and 3, in which the M_s and M are the abscissae and ordinates, and the

TABLE 1

GROUPING ACCORDING TO H

H	No.	$\overline{H}$	$\overline{M}$	Mean Error	q	$\overline{M}_s$	q_s	$\overline{M}-\overline{M}_s$	q/q_s
	Dwarfs Fo–F9								
−2.0	18	− 3.8	+ 0.85	±0.54	1.60	+2.41	0.70	−1.56	2.31
−1.9 to −0.6	19	− 1.0	2.19	.30	0.82	2.59	.58	−0.40	1.43
−0.5 to +0.5	23	+ 0.1	1.96	.37	1.34	2.71	.75	−0.75	1.78
+0.6 to +1.5	47	+ 1.1	2.73	.18	0.90	2.97	.60	−0.24	1.51
+1.6 to +1.9	34	+ 1.8	2.99	.16	0.38	3.26	.41	−0.27	0.93
+2.0 to +2.4	41	+ 2.2	3.24	.15	0.64	3.12	.45	+0.12	1.42
+2.5 to +2.8	46	+ 2.7	3.01	.16	0.76	3.37	.40	−0.36	1.92
+2.9 to +3.2	33	+ 3.0	3.37	.16	0.62	3.39	.38	−0.02	1.65
+3.3 to +3.7	38	+ 3.4	3.56	.16	0.70	3.56	.32	0.00	2.21
+3.8 to +4.2	35	+ 4.0	3.79	.17	0.69	3.73	.44	+0.06	1.55
+4.3 to +5.3	28	+ 4.8	3.83	.19	0.44	3.66	.30	+0.17	1.47
+5.4 to +9.7	32	+ 6.5	4.16	.28	1.16	3.69	0.33	+ 0.47	3.57
β Cass	1	+ 1.4	1.95	.07	.....	2.2	.....	− 0.2	.....
α Can Min	1	+ 1.0	2.8	.10	.....	3.1	.....	− 0.3	.....
η Cass	1	+ 4.1	+ 4.9	±0.10	.....	+ 4.8	.....	+ 0.1	.....
All	397	+ 2.4	+ 3.10	±0.06	1.09	+ 3.27	0.61	−0.17	1.80
	Dwarfs K3–K9								
+3.0 to +5.6	13	+ 4.7	+ 6.21	±0.25	0.64	+ 6.59	0.34	−0.38	1.93
5.7 to 6.2	13	6.0	6.19	.24	.72	6.46	.32	− .27	2.25
6.3 to 6.9	24	6.6	6.52	.12	.38	6.80	.38	− .28	1.00
7.0 to 7.4	23	7.2	6.61	.14	.49	6.85	.37	− .24	1.34
7.5 to 7.7	17	7.6	6.84	.20	.62	6.82	.30	+ .02	2.06
+7.8 to +9.2	20	8.4	6.96	.23	0.82	7.06	0.71	− .10	1.15
61′ Cygni	1	+ 9.2	+ 8.0	±0.10	.....	+ 7.7	.....	+0.3	.....
All	111	+ 6.8	+ 6.60	±0.08	0.68	+ 6.80	0.48	−0.20	1.42
	Dwarfs Mo–M9								
+ 6.0 to + 7.8	17	+ 7.1	+ 8.22	±0.20	0.75	+ 8.50	0.58	−0.28	1.29
7.9 to 8.7	18	8.4	8.35	.17	0.58	8.55	0.51	− .20	1.13
8.8 to 9.4	18	9.2	8.93	.19	0.65	8.75	0.56	+ .18	1.17
9.5 to 10.2	18	9.8	9.37	.34	1.26	9.38	0.79	− .01	1.60
10.3 to 11.4	14	10.6	10.10	.28	0.94	9.93	0.92	+ .17	1.03
+11.5 to +14.8	10	+12.5	+11.01	±0.53	1.43	+10.75	1.46	+0.26	0.99
All	95	+ 9.4	+ 9.17	±0.13	1.30	+ 9.17	1.08	0.00	1.20

means based on the grouping according to H and M_s are marked by dots and crosses. The first regression line (M on M_s) is marked by a dashed line and is determined by the crosses;

the second regression line (M_s on M) is marked as a continuous line and is determined by the dots. There is, of course, no a priori reason why the regression lines should be straight; this depends upon how accurately the preliminary calibration lines connecting line intensities with absolute magnitudes in the provisional system have been determined. The first regression line must lie below the second regression line in the region of

TABLE 2

GROUPING ACCORDING TO M_s

M_s	No.	$\overline{M}$	Mean Error	q	$\overline{M}_s$	$\overline{M}-\overline{M}_s$
	Dwarfs Fo–F9					
+1.3 to +2.5	39	+ 0.99	±0.32	1.36	+ 2.06	−1.07
2.6 to 3.0	76	2.42	.12	0.57	2.84	−0.42
3.1 to 3.3	87	3.17	.11	0.56	3.21	−0.04
3.4 to 3.6	90	3.46	.10	0.54	3.50	−0.04
3.7 to 4.0	84	3.92	.09	0.52	3.83	+0.09
+4.1 to +4.8	21	+ 4.39	±0.25	0.90	+ 4.22	+0.17
All	397	+ 3.10	±0.06	1.09	+ 3.28	−0.18
	Dwarfs K3–K9					
+5.9 to +6.4	29	+ 5.91	±0.14	0.49	+ 6.25	−0.34
6.5 to 6.7	27	6.40	.10	.34	6.59	.19
6.8 to 7.0	24	6.72	.13	.48	6.86	.14
7.1 to 7.3	13	7.16	.14	.37	7.22	.06
+7.4 to +7.9	19	+ 7.46	±0.14	0.38	+ 7.64	−0.18
All	112	+ 6.61	±0.08	0.68	+ 6.81	−0.20
	Dwarfs Mo–M9					
+ 7.5 to + 8.4	22	+ 7.97	±0.16	0.61	+ 8.11	−0.14
8.5 to 8.9	30	8.64	.10	0.48	8.68	− .04
9.0 to 9.9	22	9.30	.13	0.55	9.27	+ .03
+10.0 to +12.7	21	+11.02	±0.29	1.20	+10.85	+0.17
All	95	+ 9.16	±0.13	1.30	+ 9.16	0.00

large values of M, while for the smaller values of M the first regression line must lie above the second regression line. This fact helps to some extent to draw the two regression lines.

The mean error θ of an individual determination of M_s, as published in *Mount Wilson Contribution* No. 511, has been found to be 0.60, 0.42, and 0.58 for the F stars, late K, and M stars, respectively.

The two absolute-magnitude systems M_s' and M_s'' were determined from the first and second regression lines as calibration lines. Table 3 gives the values of M_s' and M_s'' for

different values of M_s. The values of M_s were then corrected to the system M_s'' by the data given in this table, and those of $\overline{M_s''}$ and q_s'' were determined. Table 4 shows those data from Table 1 which are changed in the new calibration.

The mean error θ' of an individual determination of M_s in the system M_s' is equal to 0.27, 0.32, and 0.56, respectively, for the three spectral groups. The corresponding values of θ'' for the system M_s'', which must always be larger than θ' for M_s', are 0.45, 0.39, and 0.62, respectively. The coefficients of correlation between M and M_s are, for the three spectral groups, approximately 0.85, 0.88, and 0.90.

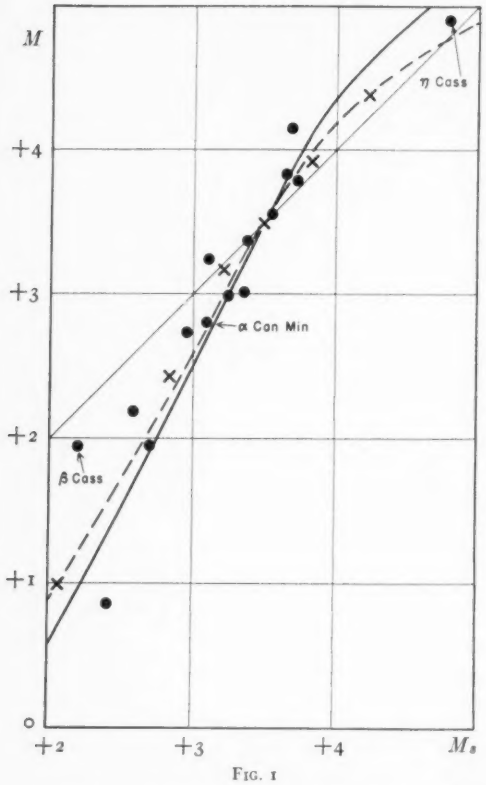

FIG. 1

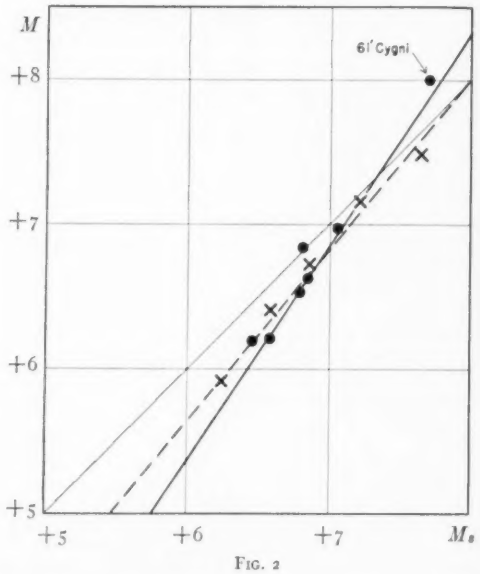

FIG. 2

FIG. 1.—Relation between spectroscopic absolute magnitudes M_s (abscissae) and true absolute magnitudes M (ordinates), derived from trigonometric parallaxes, for F0–F9 stars. Dots represent means of M and M_s when the stars are grouped according to $H = m + 5 + 5 \log \mu$; crosses, means for a grouping according to M_s. A few apparently bright stars are individually marked. The continuous curve is the second regression line and represents the dots. The dashed curve is the first regression line (M on M and represents the crosses. The straight line at 45° angle represents identity between M and M_s.

FIG. 2.—Diagram, similar to Fig. 1, for K3–K9 stars.

The question whether we should use the system M_s' and M_s'' as the most probable value of M depends upon several circumstances. When the stars are grouped on any basis *directly* correlated with M_s, that is, with the conditions in the reversing layer which are indicated by the intensity of the spectral lines used in determining the intrinsic brightness, we should use the system M_s'. When the stars are grouped on any basis directly correlated to the actual absolute magnitude M, that is, to any characteristic directly connected with the rate of energy generation in the interior of the stars, the system M_s''

TABLE 3

CONVERSION OF M_s INTO M' AND M''_s

Fo-F9			Ko-K9			Mo-M9		
M_s	M'_s	M''_s	M_s	M'_s	M''_s	M_s	M'_s	M''_s
+1.3	+0.2	−0.3	.....	.....	.....	.....	.....	.....
1.4	0.3	−0.2	.....	.....	.....	.....	.....	.....
1.5	0.4	−0.1	.....	.....	.....	7.5	7.3	6.2
1.6	0.5	0.0	.....	.....	.....	7.6	7.4	6.4
1.7	0.6	+0.1	.....	.....	.....	7.7	7.5	6.6
1.8	0.7	+0.3	.....	.....	.....	7.8	7.7	6.8
1.9	0.8	+0.4	5.9	5.5	5.2	7.9	7.8	7.0
2.0	0.9	+0.6	6.0	5.6	5.4	8.0	7.9	7.2
2.1	1.1	+0.7	6.1	5.8	5.5	8.1	8.0	7.4
2.2	1.2	+0.9	6.2	5.9	5.7	8.2	8.1	7.6
2.3	1.4	+1.1	6.3	6.0	5.8	8.3	8.2	7.8
2.4	1.5	+1.3	6.4	6.1	6.0	8.4	8.3	8.0
2.5	1.7	+1.5	6.5	6.3	6.1	8.5	8.4	8.3
2.6	1.9	+1.7	6.6	6.4	6.3	8.6	8.5	8.5
2.7	2.1	+1.9	6.7	6.5	6.4	8.7	8.6	8.6
2.8	2.2	+2.0	6.8	6.6	6.6	8.8	8.7	8.8
2.9	2.4	+2.2	6.9	6.7	6.7	8.9	8.8	8.9
3.0	2.6	+2.5	7.0	6.8	6.9	9.0	8.9	9.1
3.1	2.8	+2.7	7.1	6.9	7.0	9.1	9.1	9.2
3.2	3.0	+2.9	7.2	7.1	7.2	9.2	9.2	9.3
3.3	3.2	+3.1	7.3	7.2	7.3	9.3	9.3	9.4
3.4	3.4	+3.4	7.4	7.3	7.5	9.4	9.4	9.5
3.5	3.5	+3.6	7.5	7.4	7.6	9.5	9.5	9.6
3.6	3.7	+3.7	7.6	7.5	7.7	9.6	9.6	9.7
3.7	3.8	+3.9	7.7	7.6	7.9	9.7	9.7	9.8
3.8	3.9	+4.1	7.8	7.7	8.0	9.8	9.8	9.9
3.9	4.1	+4.2	7.9	7.9	8.2	9.9	9.9	10.1
4.0	4.2	+4.4	8.0	8.0	8.3	10.0	10.0	10.2
4.1	4.3	+4.5	.....	.....	.....	10.1	10.2	10.3
4.2	4.4	+4.6	.....	.....	.....	10.2	10.3	10.4
4.3	4.4	+4.7	.....	.....	.....	10.3	10.4	10.5
4.4	4.5	+4.8	.....	.....	.....	10.4	10.5	10.6
4.5	4.6	+4.9	.....	.....	.....	10.5	10.6	10.7
4.6	4.7	+5.0	.....	.....	.....	10.6	10.7	10.8
4.7	4.7	+5.0	.....	.....	.....	10.7	10.8	11.0
4.8	4.8	+5.1	.....	.....	.....	10.8	10.9	11.1
+4.9	+4.8	+5.1	.....	.....	.....	10.9	11.0	11.2
						11.0	11.1	11.3
						11.2	11.4	11.5
						11.4	11.6	11.8
						11.6	11.8	12.0
						11.8	12.0	12.2
						12.0	12.2	12.4
						12.2	12.4	12.7
						12.4	12.6	12.9
						12.6	12.8	13.1
						12.8	13.0	13.3

TABLE 4

GROUPING ACCORDING TO H: CORRECTED SYSTEM M_s''

H	No.	$\overline{M_s''}$	q_s''	$\overline{M}-\overline{M_s''}$	q/q_s''
	Dwarfs Fo–F9				
−2.0	18	1.42	1.22	−0.57	1.31
−1.9 to −0.6	19	1.70	1.13	+0.49	0.73
−0.5 to +0.5	23	1.93	1.10	+0.03	1.22
+0.6 to +1.5	47	2.45	1.12	+0.28	0.80
+1.6 to +1.9	34	3.01	0.83	−0.02	0.46
+2.0 to +2.4	41	2.74	0.98	+0.50	0.65
+2.5 to +2.8	46	3.21	0.79	−0.20	0.96
+2.9 to +3.2	33	3.29	0.75	+0.08	0.83
+3.3 to +3.7	38	3.59	0.58	−0.03	1.21
+3.8 to +4.2	35	3.83	0.69	−0.04	1.00
+4.3 to +5.3	28	3.79	0.54	+0.04	0.82
+5.4 to +9.7	32	3.84	0.60	+0.32	1.93
β Cass	1	0.9	.....	+1.0	.....
α Can Min	1	2.7	.....	+0.1	.....
η Cass	1	5.1	.....	−0.2	.....
All	397	3.01	1.11	+0.09	0.98
	Dwarfs Ko–K9				
+3.0 to +5.6	13	6.26	0.51	−0.05	1.27
5.7 to 6.2	13	6.06	0.49	+ .13	1.48
6.3 to 6.9	24	6.58	0.56	− .06	0.68
7.0 to 7.4	23	6.64	0.49	− .03	0.99
7.5 to 7.7	17	6.62	0.46	+ .22	1.36
+7.8 to +9.2	20	6.96	1.06	.00	0.77
61′ Cygni	1	7.9	.....	+0.1	.....
All	111	6.57	0.70	+0.03	0.97
	Dwarfs Mo–M9				
+ 6.0 to + 7.8	17	8.17	0.79	+0.05	0.95
7.9 to 8.7	18	8.24	0.85	+ .11	0.68
8.8 to 9.4	18	8.54	0.77	+ .39	0.85
9.5 to 10.2	18	9.43	1.01	− .06	1.25
10.3 to 11.4	14	10.08	1.08	+ .02	0.88
+11.5 to +14.8	10	11.01	1.63	0.00	0.88
All	95	9.07	1.38	+0.10	0.94

should be used. Most groupings, for instance, on the basis of m, H, period of light-variation, etc., are related to M rather than to the specific atmospheric conditions; hence, in general, M_s'' is the system of the greatest practical importance. For an *individual star*

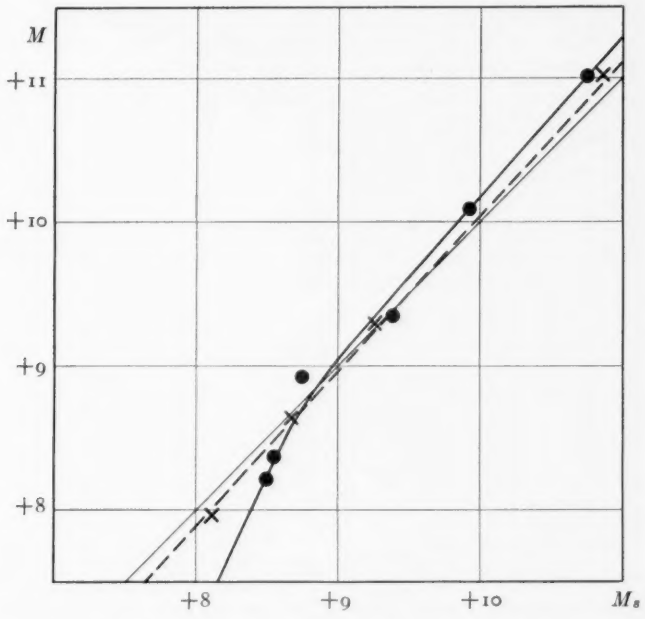

FIG. 3.—Diagram, similar to Fig. 1, for Mo–M9 stars

we do not usually know which system gives the best value of M. If nothing else than the intensity of the absolute-magnitude lines is known, M_s', which is based upon the regression of M on M_s, gives the best value we can assign to M.

CARNEGIE INSTITUTION OF WASHINGTON
MOUNT WILSON OBSERVATORY
August 1940

ULTRAVIOLET EMISSION LINES IN THE SPECTRA OF Me VARIABLES*

PAUL W. MERRILL

ABSTRACT

The lines studied are those between λ 4000 and λ 3700, observed near time of maximum light. Marked irregularities in the intensities of lines in the Balmer series are probably due to the abnormal weakness of certain members, notably $H\epsilon$, $H\kappa$, $H\mu$, and $H\xi$. On this assumption the general Balmer decrement does not differ greatly from that of the Be star BD+11°4673 or of the hydrogen spectrum observed in the laboratory. A few lines of *Si* I, *Fe* I, and *Mg* I were observed. $H\iota$ and $H\theta$ exhibit two components on a few plates. Most of the lines yield accordant radial velocities, but certain ones are subject to fairly large relative displacements.

Peculiarities in intensity, structure, and displacement tend to become less marked after maximum light. The absorption of overlying gases provides the best working explanation of the peculiarities.

Numerous emission lines of hydrogen were conspicuous on the early objective-prism spectrograms of Me variables taken at the Harvard Observatory, and their unusual relative intensities were at once evident. In describing her spectral classification Miss Antonia C. Maury wrote of Group XX (typical star *o* Ceti):

> The lines of hydrogen are bright. $H\gamma$, $H\delta$, $H\zeta$, $H\eta$, $H\theta$, $H\iota$, and frequently $H\kappa$, $H\lambda$, $H\mu$, and $H\nu$ are seen. The bright $H\beta$ may or may not be present; the line $H\epsilon$ is never seen bright, owing possibly to the superposed calcium band. The intensity is greatest in $H\delta$ and declines in either direction, except that $H\nu$ is next to $H\iota$ in brightness. The reversal of the hydrogen lines is complete; no accompanying dark lines are shown.[1]

Later investigations at several observatories have confirmed these results and have proved that the bright hydrogen lines in the spectra of typical long-period Me variables regularly exhibit certain striking deviations from the normal Balmer sequence of intensities steadily decreasing from $H\alpha$ to the head of the series in the ultraviolet. Bright lines due to iron, silicon, and other elements also have been recorded.

The present investigation deals with the bright lines in the ultraviolet portion of the spectrum observed near the time of maximum light. Most of the spectrograms have been obtained since September 1, 1938, with one-prism spectrographs attached to the 60-inch or the 100-inch reflector. Camera lenses of 18 inches focal length were employed, yielding a dispersion at $H\zeta$ of 24 A/mm. The combination of aluminum telescope mirrors and more transparent prisms (placed in the spectrographs on the date mentioned) affords an effective means of recording the bright lines in the near ultraviolet. The lines between $H\epsilon$ (λ 3970) and $H\iota$ (λ 3771) have been most extensively observed, but others down to $H\pi$ (λ 3692) appear on a few plates.

I am indebted to Mr. A. H. Joy for permission to include several spectrograms of χ Cygni taken by him in 1938.

INTENSITY

The estimated intensities of a number of the more important lines in the spectra of several variables will be found in Tables 1 and 2. For convenient comparison, intensity 10 is assigned to $H\zeta$ throughout Table 1 and to $H\iota$ throughout Table 2.

* *Contributions from the Mount Wilson Observatory, Carnegie Institution of Washington*, No. 642.

[1] *Harvard Ann.*, **28**, 45, 1897.

TABLE 1

INTENSITIES OF BRIGHT LINES, *Hε–Hκ*

DATE	MAG.	PHASE IN DAYS	INTENSITY							
			Hε	λ 3905	*Hζ*	λ 3852	*Hη*	*Hθ*	*Hι*	*Hκ*
			U Persei, 015254, M6e, 328 Days							
1939 Dec. 3...	8.0	+ 11	2	3	10	3	7	5	5	2
			R Aurigae, 050953, M7e, 462 Days							
1935 Sept. 19...	8.4	+ 31	<1	4	10	1	4	3	2	<1
			U Orionis, 054920a, M7e, 374 Days							
1939 Dec. 26...	6.5	− 6	<1	3	10	<2	5	4	5	<1
1940 Jan. 24...	6.8	+ 23	0.5	3	10	0.5	6	5	6	0.5
			R Leonis, 094211, M8e, 309 Days							
1921 Feb. 26...	6.9	+ 47	1	4	10	3	4	2	2	<1
Mar. 27...	7.7	76	2	6	10	6	2	<2	<2	<2
1928 Jan. 4...	7.0	62	1	4	10	3	2	<2	<2	<2
Feb. 11...	8.3	100	5	7	10	6	<5	<5	<5	<5
1938 Mar. 10...	8.0	42	1	3	10	4	5	3	2	<2
Apr. 17...	9.7	+ 80	5	10	10	15	5	<5	<5	<5
			T Ursae Majoris, 123160, M4e, 261 Days							
1940 Apr. 16...	7.8	− 9	<1	1	10	<1	4	2	2	<1
May 19...	8.1	+ 24	0.5	1	10	0.5	6	3	3	0.5
			U Virginis, 124606, M4e, 207 Days							
1939 June 8...	8.1	− 11	<1	1	10	<1	5	1	1	<1
			R Hydrae, 132422, M7e, 415 Days							
1926 June 20...	4.8	− 11	<1	3	10	<1	4	3	3	<1
1933 May 10...	3.9	+ 13	0.5	3	10	2	6	5	5	1
June 11...	5.4	+ 45	1	3	10	3	6	4	3	0.5
1939 Jan. 13...	6.7	+ 59	2	3	10	4	6	4	4	1
1940 Jan. 20...	5.9	+ 34	2	2	10	3	5	3	3	0.7

TABLE 1—*Continued*

Date	Mag.	Phase in Days	Intensity							
			$H\varepsilon$	λ 3905	$H\zeta$	λ 3852	$H\eta$	$H\theta$	$H\iota$	$H\kappa$
			R Canum Venaticorum, 134440, M6e, 331 Days							
1939 May 6...	8.0	− 21	<1	2	10	<1	5	3	3	<1
1940 Mar. 22...	8.1	− 24	<2	3	10	<2	5	3	3	<2
			U Ursae Minoris, 141567, M6e, 331 Days							
1940 May 21...	8.1	+ 1	<2	2	10	2	6	3	3	<2
			V Boötis, 142539, M6e, 259 Days							
1939 Apr. 16...	7.7	+ 18	3	2	10	2	6	3	2	0.8
			R Draconis, 163266, M5e, 246 Days							
1940 May 5...	7.4	− 6	<1	2	10	<1	6	3	3	1
May 30...	7.8	+ 19	1	2	10	1	6	4	4	2
			T Herculis, 180531, M3e, 165 Days							
1940 July 18...	8.9	+ 11	1	2	10	<1	6	3	3	0.7
			R Aquilae, 190108, M7e, 302 Days							
1939 May 6...	7.4	+ 36	1	3	10	3	7	4	4	1
			RT Cygni, 194048, M2e, 190 Days							
1940 May 18...	8.0	+ 2	4	0.5	10	0.4	6	5	4	2
			χ Cygni, 194632, Mpe, 413 Days							
1938 July 9...	5.3	+ 14	<1	3	10	3	6	5	5	1
Aug. 8...	6.4	+ 44	(1)	4	10	3	6	4	3	0.6
Sept. 6...	7.5	+ 73	1	5	10	5	6	4	4	1
Oct. 4...	9.0	+101	1	8	10	11	2	(0.5)	(0.5)	<0.5
Nov. 3...	10.5	+131	6	40	10	60	5	<5	<5	<5
1939 July 6...	7.6	− 47	<0.5	2	10	<0.5	1	2	2	<0.5
July 29...	6.3	− 24	<0.5	3	10	<0.5	4	5	5	0.5
Aug. 31...	5.5	+ 9	<0.5	4	10	0.6	6	5	6	0.6
Oct. 5...	7.2	+ 44	<0.5	4	10	3	6	5	6	1
Oct. 23...	8.3	+ 62	0.7	5	10	4	6	4	4	1

TABLE 1—*Continued*

Date	Mag.	Phase in Days	Intensity							
			$H\epsilon$	λ 3995	$H\zeta$	λ 3852	$H\eta$	$H\theta$	$H\iota$	$H\kappa$
			T Aquarii, 204405, M3e, 202 Days							
1940 July 18...	8.2	− 3	<1	1	10	<1	4	2	1	<1
			R Aquarii, 233815, M7e, 383 Days							
1939 Dec. 22...	6.5	− 4	<2	3	10	<2	4	3	3	<2
			R Cassiopeiae, 235350, M7e, 426 Days							
1939 June 8...	6.1	− 3	<1	2	10	<1	3	2	3	<1
July 6...	6.7	+ 25	<0.5	2	10	1	6	4	4	<0.5
July 29...	7.7	+ 48	1	3	10	2	6	4	4	(0.3)
Aug. 31...	8.4	+ 81	1	3	10	4	5	3	3	<1

TABLE 2

INTENSITIES OF BRIGHT LINES, $H\iota$–$H\pi$

Star	Date	Mag.	Phase in Days	Intensities							
				$H\iota$	$H\kappa$	$H\lambda$	$H\mu$	$H\nu$	$H\xi$	$H\sigma$	$H\pi$
U Per....	1939 Dec. 3	8.0	+11	10	3	4	1	2	1	1	<1
U Ori....	1939 Dec. 26	6.5	− 6	10	<1	1	<1	2	1	2	2
	1940 Jan. 24	6.8	+23	10	1	2	1	3	1	2	2
R Hya...	1933 May 10	3.9	+13	10	2	3	0.5	3	0.5	0.5	0.5
	1939 Jan. 13	6.7	+59	10	2	2	<1	2	<1	<1	<1
R Aql....	1939 May 6	7.4	+36	10	2	2	1	2	1	<1	1
RT Cyg....	1940 May 18	8.0	+ 2	10	5	7	2	2	(1)	(1)	<1
χ Cyg....	1938 July 9	5.3	+14	10	2	3	1	3	1	2	1
	1939 Aug. 31	5.5	+ 9	10	1	2	<1	2	1	1	<1
	Oct. 5	7.2	+44	10	2	2	<1	1	<1	<1	<1
	Oct. 23	8.3	+62	10	3	3	<1	1	<1	<1	<1
R Cas....	1939 July 17	7.2	+36	10	0.5	1	<0.5	2	<1	<1	<1

Typical intensities of the hydrogen lines near time of maximum light are listed in Table 3 and are plotted in Figure 1. The general Balmer decrement appears to be exhibited, at least to a first approximation, by $H\delta$, $H\zeta$, $H\iota$, $H\nu$, and $H\pi$. If this assumption is correct, the decrement is not greatly different from that of the Be star BD+11°4673 (see Pl. V) or of the hydrogen spectrum observed in the laboratory. This is an important fact to bear in mind in discussions of the physical origin of these lines in Me stars. The observed irregularity of the hydrogen series in the ultraviolet is probably due to the abnormally low intensities of certain members, notably $H\epsilon$, $H\kappa$, $H\mu$, and $H\xi$. The fact that the lines $H\theta$ and $H\iota$ are nearly equal in intensity makes the abrupt drop at $H\kappa$ very striking. A highly specialized and improbable mechanism would be required to produce these relative intensities in the actual emission of hydrogen atoms. Hence, as a working hypothesis the observed irregularities may be ascribed to the absorption of gases overlying (or possibly coincident with) the stratum of hydrogen emission.

TABLE 3

INTENSITIES OF BRIGHT HYDROGEN LINES

H	Me Variables		BD+11°4673
	Int.	Log.	Int.
δ	50	1.70	50
ϵ	1	0.00	40
ζ	25	1.40	(30)
η	15	1.18	20
θ	10	1.00	15
ι	10	1.00	11
κ	3	0.48	8
λ	3	0.48	6
μ	1	0.00	4
ν	3	0.48	3
ξ	1	0.00	3
o	2	0.30	2
π	2	0.30	2

It has long been believed that the low intensity of $H\epsilon$—which at maximum light is practically eliminated from the spectrum—is caused by absorption of the H line of calcium. C. D. Shane[2] suggested that $H\kappa$, $H\lambda$, and $H\mu$ are weakened by iron lines; $H\xi$, by a vanadium line. The suggestion concerning $H\xi$, ($H16$), seems to be confirmed by the recent measurements by W. S. Adams[3] with high dispersion.

The general pattern of deviation from a uniform Balmer decrement (see Table 3 and Fig. 1) is very persistent. The degree of deviation, however, varies considerably not only from star to star but in the same star at various times. The rather meager data indicate that the deviations are less marked in the earlier subdivisions of Me spectra (see Pl. V). In a given object the deviations probably become less during the post-maximum phase;[4] moreover, various cycles may not exhibit identical behavior.

Miss Maury's observation that in o Ceti, $H\nu$ is next to $H\iota$ in brightness applies to several of the more advanced variables, M6e–M8e, near the time of maximum light. It may not hold true for the post-maximum phase or for variables with less advanced spectra, e.g., RT Cygni, M2e (Pl. V). In general, $H\kappa$, $H\lambda$, and $H\nu$ have approximately equal intensities.

[2] *Lick Obs. Bull.*, **10**, 131, 1922.

[3] *Mt. W. Contr.*, No. 638; *Ap. J.*, **93**, 11, 1941.

[4] Cf. P. W. Merrill, *Spectra of Long-Period Variable Stars*, Pl. IV*c*, *d*. Chicago: University of Chicago Press, 1940.

PLATE V

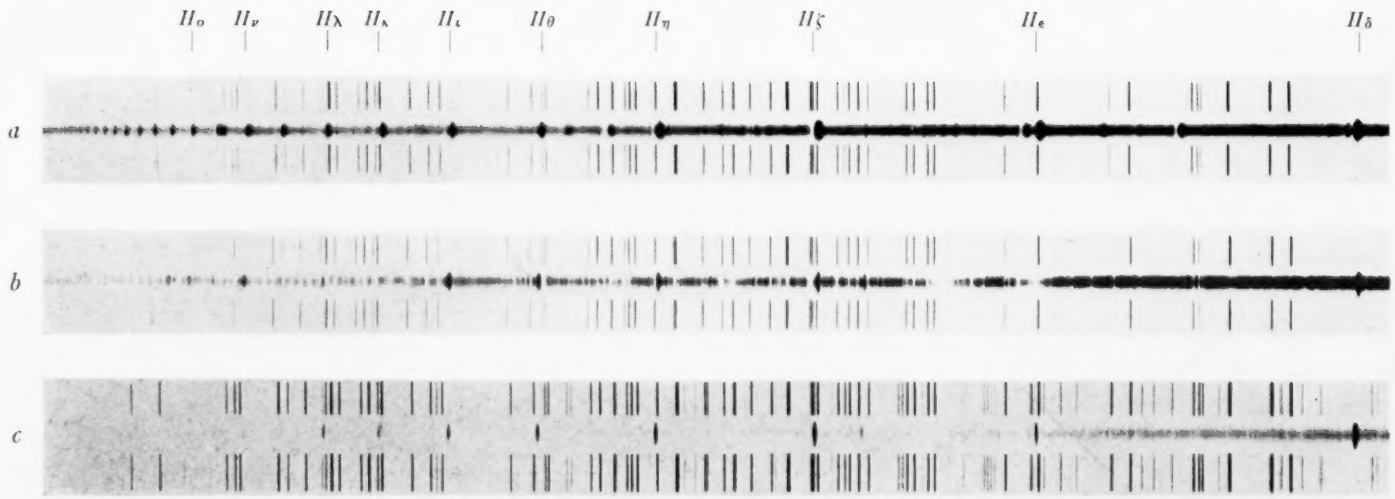

HYDROGEN EMISSION LINES IN THE ULTRAVIOLET

a) BD +11°4673, Bep, Dec. 3, 1939
b) U Orionis, M8e, Jan. 28, 1940
c) RT Cygni, M2e, May 19, 1940

Aside from the Balmer series, the two most prominent lines in the region studied are λ 3905 *Si* I and λ 3852, probably of *Fe* I. Both are stronger in the more advanced spectral types. The silicon line is seldom absent on well-exposed spectrograms regardless of phase. Its gain in relative intensity after maximum, shown in Table 1, probably arises largely from the fading of the hydrogen lines. The line λ 3852 appears about the time of maximum light and for two or three months steadily increases in intensity, its behavior thus resembling that of λ 4202.[5] The magnesium triplet λλ 3829, 3832, and 3838 frequently appears in low intensity a few weeks after maximum.

STRUCTURE

With low dispersion the bright lines in Me variables appear narrow and without structure. Spectrograms with high dispersion of *o* Ceti, chiefly by Campbell,[6] Joy,[7] and Adams,[3] have shown considerable structure in $H\gamma$, $H\delta$, and other lines.

With the intermediate dispersion employed in the present investigation, 24 A/mm at $H\zeta$, the bright lines frequently appear slightly wider than the iron lines of the compari-

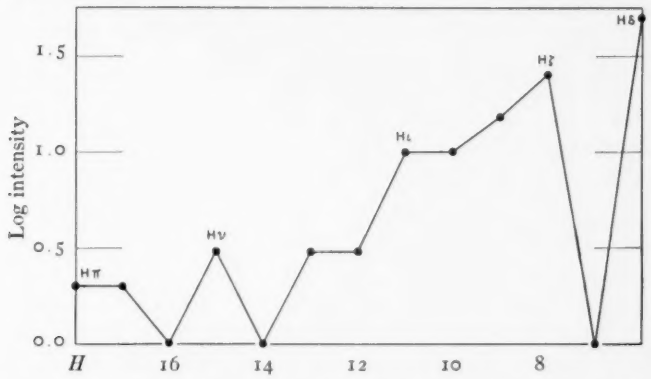

FIG. 1.—Typical intensities of bright hydrogen lines in the spectra of Me variables

son spectrum and in occasional instances are resolved into two close components. On my plates the images of the hydrogen lines $H\eta$, $H\theta$, and $H\iota$ are usually those best suited to the detection of structure. Measurements of $H\theta$ and $H\iota$ as double lines are collected in Table 4. The minimum within $H\theta$ may correspond to a blend of the lines λ 3797.72 *Cr* and λ 3797.52 *Fe*, measured by Adams with high dispersion.[3] The minimum of $H\iota$ is unidentified. The line $H\eta$ has never appeared clearly double. The post-maximum line λ 3852 and the *Mg* triplet λλ 3829, 3832, and 3838 are narrow, sharply defined lines. The silicon line λ 3905 may be somewhat narrower than the hydrogen lines.

The peculiarities of structure, as well as those of total intensity, may become less marked during the post-maximum phase.

Since the minima within the various bright lines are brought out clearly only with high dispersion, it is evident that most of the absorption lines to which they presumably correspond are relatively weak and may therefore be difficult to identify.

DISPLACEMENT

Previous data on the displacements of the ultraviolet emission lines are meager. Measurements at Ann Arbor[8] and at Mount Wilson[9] showed that $H\zeta$ frequently has an

[5] *Mt. W. Contr.*, No. 399; *Ap. J.*, **71**, 285, 1930.

[6] *Ap. J.*, **9**, 31, 1899. [7] *Mt. W. Contr.*, No. 311; *Ap. J.*, **63**, 281, 1926.

[8] Merrill, *Pub. Astr. Obs. U. Michigan*, **2**, 45, 1916.

[9] Merrill, *Mt. W. Contr.*, No. 264; *Ap. J.*, **58**, 215, 1923.

appreciable positive displacement with respect to other bright lines. C. D. Shane's investigation[2] at Lick Observatory yielded fairly small displacements for about a dozen bright lines in the ultraviolet. Near the time of maximum light, however, $H\kappa$ was displaced an angstrom toward longer wave lengths, whereas two months later it was approximately in its normal position.

The lines in Me spectra hitherto most frequently used for determinations of radial velocity are $H\beta$, $H\gamma$, $H\delta$, λ 4571.11 *Mg* I, λ 4308.91 *Fe* I, and λ 4202.03 *Fe* II. These lines have been found to give displacements which agree well—probably within errors of measurement. According to the present investigation, ultraviolet bright lines that regularly

TABLE 4

DATA CONCERNING DOUBLE LINES

Star	Date	Phase in Days	$H\iota$ λ 3770.63		$H\theta$ λ 3797.90	
			Separation	λ of Min.*	Separation	λ of Min.*
U Ori	1939 Dec. 28	− 4	0.54 A	3770.43	0.50 A	3797.64
	1940 Jan. 20	+19	.55	3770.46	.....	.....
	Jan. 28	+27	.54	3770.49	.....	.....
R CVn	1939 May 7	−20	(.56)	(3770.54)	.....	.....
	1940 Mar. 27	−19	(.67)	(3770.52)	.....	.....
χ Cyg	1939 July 6	−47	.54	3770.55	.....	.....
	July 29	−24	.58	3770.49	.....	.....
	Aug. 31	+ 9	(.56)	(3770.57)	(.48)	(3797.68)
R Cas	1939 June 8	− 3	.49	3770.45	(0.38)	(3797.70)
	July 6	+25	(0.41)	(3770.43)	.....	.....

* Corrected for the mean displacement of numerous absorption lines.

yield displacements closely agreeing with those of the above-mentioned lines of longer wave length are

$H\epsilon$, $H\eta$, ($H\iota$)	
Si I	3905.51
Fe I?	3852.58
Mg I	3838.30, 3832.31, 3829.37

$H\iota$ has a small preponderance of positive residuals.

Lines often yielding fairly large positive residuals (say more than 0.1 A) are $H\zeta$, $H\kappa$, ($H\mu$), while those often yielding negative residuals are $H\theta$, $H\lambda$, ($H\xi$). The positive residual of $H\zeta$ may be due to the weakening (real or photographic) of the edge of shorter wave length by the absorption line λ 3888.52 *Fe* I, measured by Adams with high dispersion.[3]

The meager data suggest that large residuals tend to disappear after maximum and that especially narrow lines usually yield small residuals.

The best working hypothesis of the origin of the peculiarities in intensity, structure, and displacement of the bright lines in Me variables is that of selective absorption by overlying gases. The effects of absorption apparently decrease after maximum light.

CARNEGIE INSTITUTION OF WASHINGTON
MOUNT WILSON OBSERVATORY
September 1940

THE CONTINUOUS SPECTRUM OF STELLAR ATMOSPHERES CONSISTING ONLY OF ATOMS AND NEGATIVE IONS OF HYDROGEN

RUPERT WILDT

ABSTRACT

Theoretical color temperatures have been derived for stellar atmospheres consisting only of H and H^- in ionization equilibrium, over the range of effective temperatures $5040/T_e = 0.5$–1.2 and for different electron pressures. Choosing the electron pressure so as to reproduce the value of the Balmer discontinuity observed by Barbier and Chalonge, the color temperatures of the spectral types Ao–Fo determined by the same authors can be tolerably well represented by the H–H^- mixture. For the later spectral types the theoretical color temperatures fall considerably below the corresponding effective temperatures, while the observed color temperatures are distinctly higher than the effective ones. It does not seem possible to remove this discrepancy by adding the conventional metallic absorption to that of H and H^-.

It is generally realized now that the continuous radiation of the stars cannot even approximately be represented by a single Planck function over the entire range of wave lengths accessible to astronomical observations. Consequently, the assignment of color temperatures to the energy-curves of stellar spectra is merely an abbreviated description of the results of the spectrophotometric measurements. The rea interest lies in deducing the observed energy-curves from purely physical data, i.e., from the theoretical absorption coefficients, as functions of the frequencies and the temperature, of a stellar atmosphere of suitable composition. Aside from the lack of sufficiently reliable data on the composition of stellar atmospheres, this task meets with several difficulties. Above all, the theoretically computed color temperatures depend in an extremely sensitive manner on the frequency distribution of the assumed absorption coefficients. Moreover, the variation of $k_\nu/\bar{k}$ (the ratio of the monochromatic absorption coefficient to the Rosseland mean) with the optical depth in the stellar atmosphere, if properly taken account of, involves an almost prohibitive amount of numerical work. Hence, most investigators had to resign themselves to introducing a value of $k_\nu/\bar{k}$ constant throughout the atmosphere, as a first approximation. Then there remains one outstanding uncertainty, namely, the lack of a trustworthy theory of the absorption produced by metallic atoms. In particular, the theory of metallic absorption utilized by Unsöld and Pannekoek implies for the alkali metals values of the absorption coefficients that are more than ten times too large as compared with those measured in the laboratory. This fact and the recent discovery that the negative ions of hydrogen make an important contribution to the opacity of stellar atmospheres have induced the writer to investigate the theoretical color temperatures of atmospheres consisting solely of atoms and negative ions of hydrogen, completely disregarding the quantitatively most uncertain metallic absorption. The results are not satisfactory, but it does not seem possible to improve on them by superimposing the conventional metallic absorption on that of H and H^-.

Table 1 contains the theoretical color temperatures (expressed in the form of the parameter $\theta_c = 5040/T_c$), which were computed with the help of Burkhardt's[1] table. For each value of the electron pressure (P_e) and of the effective temperature ($\theta_e = 5040/T_e$) there are listed four numbers. The quantity D denotes the Balmer discontinuity ($D = \Delta \log_{10} I$), following the notation adopted by Barbier and Chalonge. The quantities A, B, and C are the values of θ_c referring to the frequency ranges 1.40–1.80, 2.20–2.60, 2.74 (Balmer limit)–3.00, respectively (the unit of $1/\lambda$ is 10^4 cm^{-1}). At the bottom of Table 1 there are given the limiting values of A, B, and C that are reached

[1] *Zs. f. Ap.* **13**, 56, 1936.

at electron pressures greater than a certain critical one (P_e^*), i.e., when the absorption by hydrogen atoms becomes negligible beside that of the negative ions. These limiting values, which are constant in each column of θ_e, account for the empty places in the lower right half of the table, while the empty places in the upper left half result from the fact that Burkhardt's table extends only to the value 2.0 of the argument k/k_ν (:: marks results derived by slight extrapolation of Burkhardt's table).

TABLE 1

THEORETICAL COLOR TEMPERATURES OF H–H^- ATMOSPHERES

$5040/T_e =$ A, B, C

$10^4/\lambda = 1.40$–1.80, 2.20–2.60, 2.74–3.00 cm^{-1}

$D = \Delta \log_{10} I$ at the Balmer limit

P_e (DYNES/CM^2)		$5040/T_e$							
		0.5	0.6	0.7	0.8	0.9	1.0	1.1	1.2
10	A				0.87	1.11			
	B				0.80	0.97			
	C				0.75	0.89			
	D				*0.41*	*0.04*			
10^2	A		0.37::	0.66	0.95	1.11			
	B		0.30::	0.64	0.85	0.98			
	C		0.60	0.66	0.77	0.89			
	D			*0.39*	*0.06*	*0.004*			
10^3	A	0.30::	0.47	0.81	0.96				
	B	0.25::	0.49	0.73	0.86				
	C	0.50::	0.58	0.65	0.80				
	D	*0.50::*	*0.42*	*0.09*	*0.006*				
10^4	A		0.66	0.83					
	B		0.60	0.73					
	C		0.53	0.68					
	D		*0.12*	*0.01*					
Limit	A	0.62	0.72	0.85	0.96	1.11	1.20	1.24	1.46
	B	0.53	0.64	0.74	0.87	0.98	1.15	1.20	1.39
	C	0.50	0.59	0.69	0.80	0.89	0.96		
P_e^*		10^6	10^5	10^4	10^3	10^2	1		

It has already been emphasized by Unsöld that at the highest temperatures (spectral types earlier than A0) at which the H^- absorption is negligible for normal stars, the color temperatures of pure hydrogen atmospheres do not tally with the observations and, moreover, do not even vary monotonically with the effective temperature. This means that for the early spectral types the metallic absorption cannot be disregarded. Figure 1 displays a comparison of Unsöld's[2] color temperatures (based on an abundance ratio $H:M = 13.7:1$) with those of Table 1 for the stars later than A5, all data referring to an electron pressure of 100 dynes per square centimeter. Although the ranges of wave lengths to which the color temperatures A and B of Table 1 apply do not coincide exactly with those assumed by Unsöld for the visual and photographic region, this circumstance

[2] *Physik der Sternatmosphären*, Table 35 and Fig. 54, Berlin: Julius Springer, 1938.

does not vitiate the comparison. While the curves of Figure 1 do run rather closely parallel over the entire range of effective temperatures, there is an important difference between the two curves pertaining to Unsöld's and the writer's data, respectively. Unsöld's color temperatures for the photographic region are systematically lower than that for the visual region, but the writer's color temperatures behave in just the opposite way. Unsöld's data are in qualitative agreement with the spectrophotometric observations of Jensen[3] and of Kienle and his collaborators,[4] who found that the difference of the spectrophotometric gradients ($\varphi_{\text{blue}} - \varphi_{\text{red}}$) increases steadily upon progressing to later spectral types or, in other words, that the color temperatures of the photographic region are systematically lower than that of the visual region. The failure of the H–H^- mixture to reproduce this most conspicuous feature of the observations can clearly be traced to the absorption-curve of the H^- ions,[5] which has a flat maximum near λ 4000 and drops rapidly throughout the visual region toward the infrared. A look at the limiting color temperatures of pure H^- atmospheres (bottom of Table 1) will confirm this statement. According to Massey and Bates, a high degree of confidence must be placed in the theoretical absorption-curve of the H^- ions (the small corrections for the free-free transitions do not alter its shape to any remarkable extent). The superposition of the conventional metallic absorption on that of H^- would not serve to remove the discrepancy under discussion. On the contrary, since for the later spectral types the metallic absorption-curve rises steeply toward the violet, its superposition could not reverse the gradient of the H^- curve, which has the very same sign. It rather looks as if there had to be introduced a hitherto unknown mechanism producing an absorption coefficient strongly decreasing from the near infrared toward the violet. This is also indicated by the empirical absorption-curve of the solar atmosphere derived from the monochromatic limb darkening, which cannot be represented by the combination of metallic and H^- absorption.[6]

Barbier and Chalonge[7] have recently homogenized and summarized the results of their spectrophotometric work in the ordinary photographic region and in the ultraviolet beyond the Balmer limit, including the determination of the Balmer discontinuity. Their color temperatures, T_1 (λλ 4600–3700) and T_2 (λλ 3700–3150), have been entered in Figure 2, together with the color temperatures B and C of Table 1 (both for P_e = 100 and 1000 dynes per square centimeter), which refer approximately to the same spectral ranges. Figure 2 also contains a new determination by Arnulf, Barbier, and Chalonge[8] of the color temperature of the sun. Over the entire range of λλ 4500–3300 the intensity-curve of the integrated solar radiation can be represented by a single color temperature (6200° K). This remarkable result was achieved by using spectrograms of high dispersion and carefully avoiding all regions affected by line absorption. The color temperatures of the various spectral classes were plotted at the abscissae corresponding to Kuiper's[9] scale of effective stellar temperatures. Concerning the reality of the crossing of the curves pertaining to T_1 and T_2 at about $\theta_e = 0.7$, the French authors maintain some reservations, on account of the insufficient dispersion of the stellar spectra and the crowding of absorption lines in the F stars. For the earlier spectral types, however, there are obvious physical reasons why T_1 should be larger than T_2. The most important phenomenon discernible in Figure 2 (note the straight line of 45° slope) is that all observed color temperatures T_1 and T_2 are higher than the effective tempera-

[3] *A.N.*, **248**, 217, 1933.

[4] *Zs. f. Ap.*, **16**, 201, 1938.

[5] H. S. W. Massey and D. R. Bates, *Ap. J.*, **91**, 202, 1940.

[6] R. Wildt, *Ap. J.*, **90**, 611, 1939.

[7] *C.R.*, **210**, 99, 1940.

[8] *C.R.*, **210**, 325, 1940.

[9] *Ap. J.*, **88**, 429, 1938.

tures of the respective spectral types. In view of the small dispersion of the stellar spectra, which tends to depress the apparent continuous background toward the shorter wave lengths by blending of the absorption lines in the later spectral types, this phenomenon must be regarded as firmly established. The theoretical color temperatures B and C are definitely lower than the corresponding effective ones, for the later spectral types, but the curves B and C show qualitatively the same crossing over each other as the observational curves T_1 and T_2. In judging the discrepancies between theory and observation it cannot be assumed that the effective electron pressure is constant along the spectral sequence, but this uncertainty may be overcome by recourse to the value D of the Balmer discontinuity, as given in Table 1. The observed values of D^7 are

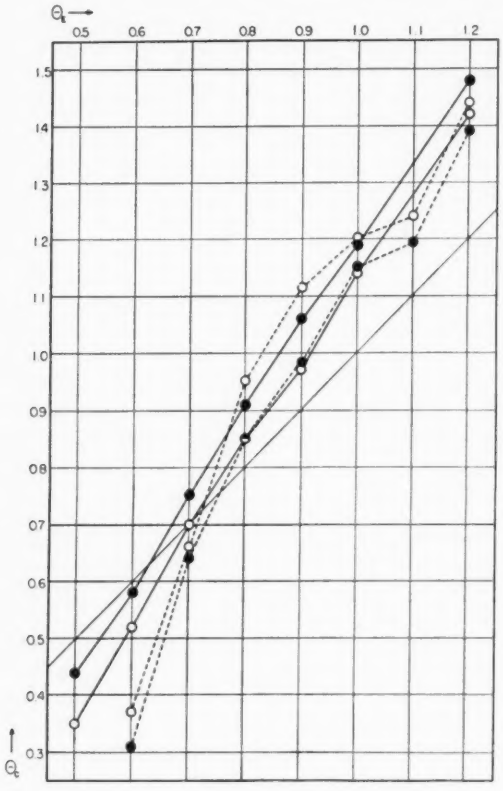

FIG. 1.—*Heavy lines:* Unsöld ($H : M = 13.7 : 1$); *broken lines:* Wildt ($H + H^-$); *empty circles:* visual range; *filled circles:* ordinary photographic range.

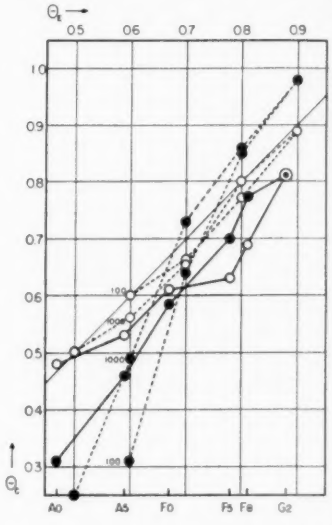

FIG. 2.—*Heavy lines:* observations by Barbier and Chalonge; *broken lines:* theoretical values ($H + H^-$); *empty circles:* ultraviolet beyond the Balmer limit; *filled circles:* ordinary photographic range; ⊙: sun.

$$A0: 0.47,\ A5: 0.39,\ F0: 0.28,\ dF5: 0.17,\ dF8: 0.11\ .$$

With due regard, finally, to the intrinsic uncertainties of the observed scales of the effective and the color temperatures, it may be concluded that the representation of the observational data by the theoretical values of Table 1 is rather satisfactory if an electron pressure of about 10^3 dynes per square centimeter is assigned to the A0 and A5 stars, and a somewhat smaller one, closer to 10^2 dynes per square centimeter, to the F0 stars. For the later F dwarfs and the sun the observed values of D imply still smaller electron pressures, which in turn yield color temperatures far lower than the effective

ones. The electron pressures found for the stars between Ao and Fo are not unreasonable, nor are the smaller ones of the later F dwarfs and of the sun. The serious deficiency of the H–H^- mixture is that it makes the color temperatures of stars later than F_5 considerably too low. Yet the same fault is to be found with Unsöld's color temperatures (Fig. 1) and to an even greater extent with those of Pannekoek.[10] As these two authors differ widely in their assumptions as to the relative abundance of hydrogen to metals, and as, further, their results show the same deficiency as the H–H^- mixture, it does not seem likely that the combination of the metallic absorption with that of H^- would be of any avail. In order to test this surmise, the color temperatures of the sun were computed from the absorption coefficients given in Tables 2 and 3 of the preceding paper,[6] which are Pannekoek's absorption coefficients corrected for the presence of H^- ions. It may suffice to state briefly that again the color temperatures turned out to be considerably lower than the effective solar temperature.

The problem of deriving theoretical color temperatures, then, has to be left in a quite unsatisfactory state. It must be kept in mind that all the color temperatures discussed have been derived on the basis of a theory neglecting the variability of $k_\nu/\bar{k}$ with the optical depth, but this can hardly account for the systematic discrepancies pointed out. The writer is inclined to believe that the solution is to be sought in some additional mechanism of absorption, which may have been overlooked thus far. If such should be found, it might render adequate account, together with the H^- absorption, of the color temperatures of the later spectral types. The combination of metallic and H^- absorption has definitely failed to reproduce the observationally well-founded, high-color temperature of the sun. In conclusion a word may be said concerning the "blanketing effect," which has been disregarded in Burkhardt's treatment of the radiative equilibrium. The density of distribution of the absorption lines throughout the solar spectrum increases greatly from the infrared toward the ultraviolet, and consequently the contribution of the line absorption to the opacity of the solar atmosphere shows the same trend. But a trend of the very opposite sign would be required in order to reduce the discrepancy between the theoretical and the observed color temperature of the sun, because the H^- absorption is too weak in the red anyhow. By way of generalization it may be surmised therefore that the neglect of the blanketing effect cannot be held responsible for the systematic discrepancies between the theoretical and the observed color temperatures of all the later spectral types.

PRINCETON UNIVERSITY OBSERVATORY
June 1940

[10] *Ap. J.*, **84**, 486, 1936.

RT AURIGAE

ARTHUR L. BENNETT

ABSTRACT

RT Aurigae was observed during the two seasons 1938–1940 with the infrared photometer on the Loomis Telescope at an effective wave length near λ 8000. The range of variation is 0^m521, and minimum occurs 0^p255 (0^d95) before maximum.

RT Aurigae (BS 2332) is the second typical Cepheid observed at the request of Dr. Martin Schwarzschild.[1] The star was selected as a suitable example of shorter period.

The phases were computed with Kukarkin's elements[2]

$$\text{Max} = \text{JD } 2420957.478 + 3.728261E\,.$$

Heliocentric Greenwich astronomical time is used.

Two comparison stars were chosen which, in the mean, approximate both the color and the magnitude of the variable. Although they were both south following, the difference in air-mass between the mean position and that of the variable exceeded 0.10 for only nine observations. The data for the three stars are given in the accompanying table. If the infrared magnitude of *a* is taken the same as the visual magnitude, the data in column "m_r" are obtained.

Star	BS	α (1900)	δ (1900)	m_v	Spectrum		m_r
					Harvard	Wilson	
v	2332	6^h22^m1	+30°6	5.0–5.9	.....	F1–G0	4.33–4.85
a	2398	6 28.9	+28.1	5.05	A0	.....	5.05
b	2480	6 38.4	+29.1	5.54	K0	K3	3.85

Extinction corrections were applied for the difference in air-mass between the mean of the comparison stars and the variable. The coefficients were determined for estimated transparencies as follows: T10 and T9, 0.125; T8, 0.145; T7, 0.196; T6, 0.220.

The individual observations are in Table 1. A set consists of eight readings on the variable and four on each of the comparison stars. The values of the difference between the magnitude of the variable and the mean magnitude of the comparison stars, reduced to the zenith, are in the column "Δm_1."

The light-curve was plotted, and a smooth free-hand curve was drawn through the observations. The residuals from this curve were used to derive the weights as follows: T10 and T9, 1.0; T8, 0.8; T7, 0.5. There was no close correlation of the size of the average residual with the hour angle. The weight is taken as unity for hour angles less than 4^h30^m (air-mass, 1.80) and 0.5 for greater hour angles.

During the first season, 1938–1939, no observations were obtained near maximum. The residuals of the second season's observations which fell on the part of the light-curve well established in the first season were obtained. A systematic difference was apparent which was in some measure dependent upon the phase. The difference is definitely not

[1] See "S Sagittae," *Ap. J.*, **90**, 289, 1939.

[2] *Veränderliche Sterne*, **4**, 385, 1935.

TABLE 1

OBSERVATIONS OF RT AURIGAE

JD Hel. G.A.T.	Phase	Δm_1	p	T	JD Hel. G.A.T.	Phase	Δm_1	p	T
9166.838	0.927	+0.029	1.0	9	9217.795	0.595	+0.339	1.0	9
.857	.932	+ .006	1.0	.....	.810	.599	+ .344	0.8	8
.875	.937	− .010	1.0	.....	.823	.603	+ .353	0.8	.....
9167.869	.204	+ .057	1.0	9	.872	.616	+ .348	0.8	.....
.882	.207	+ .056	1.0	.....	.887	.620	+ .355	0.8	.....
.895	.211	+ .062	1.0	.....	9218.733	.847	+ .308	1.0	10
9173.782	.790	+ .383	0.8	8	.746	.850	+ .296	1.0	.....
.802	.795	+ .386	0.8	.....	.843	.876	+ .215	1.0	9
.887	.818	+ .352	0.8	.....	9223.763	.196	+ .042	0.8	8
.902	.822	+ .358	0.8	.....	.778	.200	+ .049	0.8	.....
9174.869	.081	− .048	0.8	8	9224.640	.431	+ .253	0.8	8
9176.793	.598	+ .330	0.8	8	.790	.471	+ .267	0.8	.....
.809	.602	+ .340	0.8	.....	.807	.476	+ .271	0.8	.....
.857	.615	+ .346	0.8	.....	.879	.495	+ .286	0.8	.....
.873	.619	+ .351	0.8	.....	.894	.499	+ .290	0.8	.....
9179.821	.410	+ .223	1.0	9	.906	.502	+ .297	0.8	.....
.833	.413	+ .233	1.0	.....	9228.634	.502	+ .297	1.0	10
.890	.428	+ .245	1.0	.....	.647	.506	+ .299	1.0	.....
.905	.432	+ .238	1.0	.....	.693	.518	+ .297	1.0	.....
9182.793	.207	+ .055	0.8	8	9230.639	.040	− .091	1.0	9
.811	.212	+ .067	0.8	.....	.653	.044	− .085	1.0	.....
.861	.225	+ .076	0.8	.....	.669	.048	− .083	1.0	.....
.875	.229	+ .083	0.8	.....	.688	.053	− .086	1.0	.....
9190.764	.345	+ .161	0.5	7	.748	.069	− .057	1.0	.....
.780	.349	+ .173	0.5	.....	.766	.074	− .057	1.0	.....
9197.837	.242	+ .102	0.8	8	.781	.078	− .046	1.0	.....
.851	.246	+ .081	0.8	.....	.828	.091	− .047	1.0	.....
.864	.249	+ .091	0.8	.....	.843	.095	− .035	1.0	.....
9203.791	.839	+ .321	0.8	8	.859	.099	− .030	1.0	.....
.803	.842	+ .314	0.8	.....	.873	.103	− .029	1.0	.....
.855	.856	+ .267	0.8	.....	9231.699	.325	+ .166	0.8	8
.871	.860	+ .273	0.8	.....	.713	.328	+ .158	0.8	.....
9204.766	.100	− .040	0.8	8	9235.574	.364	+ .205	0.5	10
.781	.105	− .029	0.8	.....	.588	.368	+ .194	0.5	.....
.793	.108	− .028	0.8	.....	.600	.371	+ .191	1.0	.....
.807	.111	− .028	0.8	.....	.651	.385	+ .204	1.0	.....
.839	.120	− .018	0.8	.....	.682	.393	+ .218	1.0	.....
.875	.130	− .009	0.8	.....	.743	.409	+ .229	1.0	.....
.888	.133	− .011	0.8	.....	9240.652	.726	+ .400	0.5	7
.902	.137	+ .002	0.8	.....	.686	.735	+ .398	0.5	.....
.914	.140	− .001	0.8	.....	9246.764	.365	+ .196	0.8	8
9212.646	.214	+ .065	0.5	9	.900	.402	+ .226	0.8	.....
.681	.223	+ .076	1.0	.....	9247.751	.630	+ .357	1.0	9
.788	.252	+ .087	1.0	.....	.766	.634	+ .371	1.0	9
.802	.256	+ .098	1.0	.....	.782	.638	+ .368	1.0	.....
.826	.262	+ .110	1.0	.....	.820	.649	+ .368	1.0	.....
.865	.273	+ .113	1.0	.....	.865	.661	+ .373	1.0	.....
.878	.276	+ .116	1.0	.....	.905	.671	+ .376	1.0	.....
.897	.281	+ .133	1.0	.....	.920	.675	+ .369	1.0	.....
.910	.285	+ .128	1.0	.....	.934	.679	+ .383	0.5	.....
.922	.288	+ .134	1.0	.....	9248.557	.846	+ .315	1.0	9
9213.811	.527	+ .286	0.5	7	.573	.850	+ .294	1.0	.....
.830	.532	+ .304	0.5	.....	.611	.861	+ .261	1.0	.....
9216.784	.324	+ .156	1.0	9	.626	.865	+ .260	1.0	.....
.801	.329	+ .166	1.0	.....	.655	.872	+ .234	1.0	.....
.857	.344	+ .175	1.0	.....	.667	.876	+ .222	1.0	.....
9217.629	.551	+ .324	0.5	9	.724	.891	+ .160	1.0	.....
.643	.554	+ .324	0.5	.....	.737	.894	+ .148	1.0	.....
.688	0.566	+0.320	1.0	.....	.773	0.904	+0.111	1.0	.....

TABLE 1—*Continued*

JD Hel. G.A.T.	Phase	Δm_1	p	T
9248.787	0.908	+0.092	1.0	9
.821	.917	+ .052	1.0	.....
.832	.920	+ .045	1.0	.....
.873	.931	+ .010	1.0	.....
.887	.935	− .027	0.8	.....
9255.541	.719	+ .409	0.8	8
.553	.723	+ .402	0.8	.....
.601	.736	+ .395	0.8	.....
.637	.745	+ .397	0.8	.....
9258.573	.533	+ .310	0.8	8
.587	.536	+ .314	0.8	.....
.720	.572	+ .337	0.8	.....
9260.721	.109	− .020	0.8	8
9270.527	.739	+ .408	0.5	7
.544	.744	+ .410	0.5	.....
.564	.749	+ .396	0.5	.....
.581	.753	+ .399	0.5	.....
.615	.763	+ .408	0.5	.....
.629	.766	+ .388	0.5	.....
.643	.770	+ .406	0.5	.....
.657	.774	+ .395	0.5	.....
9279.630	.181	+ .052	1.0	9
.645	.185	+ .040	1.0	.....
.659	.188	+ .053	1.0	.....
.680	.194	+ .046	1.0	.....
.693	.198	+ .051	1.0	.....
.717	.204	+ .062	1.0	.....
.773	.219	+ .083	1.0	.....
.783	.222	+ .074	1.0	.....
9287.508	.294	+ .136	1.0	9
.523	.298	+ .129	1.0	.....
.575	.312	+ .143	1.0	.....
9289.621	.860	+ .270	0.5	7
.640	.866	+ .262	0.5	.....
.704	.883	+ .185	0.5	.....
.717	.886	+ .193	0.5	7
.759	.897	+ .138	0.8	8
.814	.912	+ .072	0.8	.....
9299.521	.516	+ .298	1.0	9
.537	.520	+ .303	1.0	.....
.584	.533	+ .307	1.0	.....
.597	.536	+ .313	1.0	.....
.637	.547	+ .324	1.0	.....
.652	.551	+ .326	1.0	.....
.700	.564	+ .329	1.0	.....
.769	.582	+ .332	1.0	.....
.782	.586	+ .351	1.0	.....
9306.612	.418	+ .231	0.8	8
.668	.433	+ .245	0.8	.....
.695	.440	+ .251	0.8	.....
.768	.460	+ .270	0.8	.....
.794	.467	+ .269	0.4	.....
.825	.475	+ .259	0.4	.....
9311.574	.749	+ .406	1.0	9
.632	.764	+ .396	1.0	.....
.730	.791	+ .386	1.0	.....
.766	.800	+ .387	0.5	.....
.794	.808	+ .367	0.5	.....
9317.584	0.361	+0.192	1.0	9
9317.646	0.377	+0.204	1.0	9
.787	.415	+ .244	0.5	.....
9318.577	.627	+ .354	0.5	7
.591	.631	+ .359	0.5	.....
9325.518	.489	+ .288	1.0	9
.583	.506	+ .293	0.8	8
.608	.513	+ .306	0.8	.....
.644	.523	+ .304	0.8	8
9330.550	.838	+ .323	0.8	8
.610	.855	+ .287	0.8	.....
.655	.867	+ .253	0.8	.....
.733	.888	+ .167	0.5	9
.765	.896	+ .134	0.5	.....
9336.537	.444	+ .258	1.0	9
.553	.449	+ .262	1.0	.....
9337.529	.710	+ .405	0.8	8
.544	.714	+ .401	0.8	.....
.588	.726	+ .401	0.8	.....
.605	.731	+ .406	0.8	.....
.632	.738	+ .402	0.6	.....
.654	.744	+ .400	0.8	.....
9345.586	.871	+ .232	0.8	8
.599	.875	+ .222	0.8	.....
.622	.892	+ .174	0.4	.....
.689	.899	+ .138	0.4	.....
9363.602	.704	+ .389	0.8	8
.619	.708	+ .401	0.4	.....
9517.860	.079	− .045	0.6	9
.873	.083	− .041	0.6	.....
9524.804	.942	− .048	0.5	8
.823	.947	− .065	0.5	.....
.837	.950	− .082	0.5	.....
.852	.954	− .096	0.5	.....
9551.768	.174	+ .031	0.5	8
.782	.178	+ .036	0.5	.....
.807	.184	+ .033	0.5	.....
.820	.188	+ .040	0.5	.....
.833	.191	+ .035	0.5	.....
9553.833	.728	+ .397	0.3	7
.848	.732	+ .397	0.3	.....
.886	.742	+ .406	0.3	.....
.901	.746	+ .398	0.3	.....
9554.797	.986	− .115	0.6	9
.810	.990	− .125	0.6	.....
.822	.993	− .121	0.6	.....
.858	.003	− .114	0.6	.....
.872	.006	− .119	0.6	.....
.883	.009	− .113	0.6	.....
.896	.012	− .115	0.6	.....
.908	.016	− .104	0.6	.....
9594.797	.715	+ .395	0.6	9
9595.691	.955	− .085	0.5	8
.703	.958	− .099	0.5	.....
.716	.962	− .100	0.5	.....
.732	.966	− .107	0.5	.....
.744	.969	− .091	0.5	.....
9596.774	.245	+ .094	0.5	8
.787	.249	+ .085	0.5	.....
9606.834	0.944	−0.066	0.6	9

TABLE 1—*Continued*

JD Hel. G.A.T.	Phase	Δm_1	p	T	JD Hel. G.A.T.	Phase	Δm_1	p	T
9606.849	0.948	−0.075	0.6	9	9658.625	0.835	+0.341	0.3	7
9620.934	.726	+ .394	0.2	8	.640	.839	+ .298	0.3	.....
9624.824	.769	+ .397	0.6	9	9660.671	.384	+ .209	0.6	9
.838	.773	+ .391	0.6	.....	9671.652	.329	+ .159	0.5	8
9625.780	.026	− .103	0.6	9	.669	.334	+ .180	0.5	.....
.860	.047	− .091	0.6	.....	.683	.338	+ .169	0.5	.....
.872	.050	− .081	0.6	.....	.754	.357	+ .178	0.5	.....
.886	.054	− .071	0.6	.....	9676.512	.633	+ .378	0.6	9
.899	.057	− .083	0.3	.....	.525	.636	+ .365	0.6	.....
9631.772	.633	+ .348	0.3	7	.586	.653	+ .364	0.6	.....
.785	.636	+ .366	0.3	.....	.598	.656	+ .370	0.6	.....
9635.607	.661	+ .377	0.5	8	.645	.669	+ .373	0.6	.....
.620	.665	+ .379	0.5	.....	.657	.672	+ .386	0.6	.....
.634	.669	+ .377	0.5	.....	9681.539	.981	− .113	0.6	9
.647	.672	+ .392	0.5	.....	.553	.985	− .117	0.6	.....
.683	.682	+ .382	0.5	.....	.567	.989	− .122	0.6	.....
.697	.685	+ .393	0.5	.....	.580	.992	− .120	0.6	.....
.710	.689	+ .384	0.5	8	.629	.005	− .117	0.6	.....
.727	.694	+ .400	0.5	.....	.641	.009	− .112	0.6	.....
.761	.703	+ .394	0.5	.....	.653	.012	− .115	0.6	.....
.774	.706	+ .391	0.5	.....	.665	.015	− .107	0.6	.....
.787	.710	+ .398	0.5	.....	.721	.030	− .112	0.5	8
9638.645	.476	+ .285	0.5	8	.734	.034	− .102	0.5	.....
.659	.480	+ .279	0.5	.....	9682.531	.247	+ .099	0.2	6
.781	.513	+ .301	0.5	.....	.579	.260	+ .119	0.2	.....
.795	.516	+ .307	0.5	.....	.591	.263	+ .106	0.2	.....
9645.755	.383	+ .216	0.5	8	.630	.274	+ .117	0.2	.....
.775	.389	+ .205	0.5	.....	.642	.277	+ .114	0.2	.....
.789	.392	+ .229	0.5	.....	.655	.281	+ .136	0.2	.....
9657.625	.567	+ .324	0.6	9	9686.555	.327	+ .152	0.5	8
.644	.572	+ .339	0.6	.....	.568	.330	+ .163	0.5	.....
.659	.576	+ .350	0.6	.....	.639	.349	+ .182	0.5	.....
.706	0.589	+0.341	0.5	8	.651	0.352	+0.177	0.5	.....

TABLE 2

NORMALS

$\bar{P}$	$\overline{\Delta m_1}$	p	$\bar{P}$	$\overline{\Delta m_1}$	p	$\bar{P}$	$\overline{\Delta m_1}$	p
0.008	−0.115	4.2	0.354	+0.182	4.0	0.696	+0.391	4.2
.028	− .102	3.8	.374	+ .200	4.4	.715	+ .402	4.3
.048	− .085	4.2	.396	+ .218	4.8	.729	+ .401	4.2
.070	− .057	4.5	.416	+ .234	4.3	.742	+ .401	4.6
.092	− .040	5.2	.436	+ .249	4.4	.757	+ .400	4.0
.107	− .027	4.2	.465	+ .267	4.2	.780	+ .392	4.0
.132	− .007	4.0	.492	+ .289	4.6	.816	+ .359	4.5
.182	+ .040	4.0	.509	+ .299	4.9	.844	+ .313	3.9
.194	+ .047	4.3	.522	+ .300	4.3	.854	+ .285	4.4
.205	+ .056	4.6	.538	+ .314	4.6	.865	+ .255	4.6
.216	+ .071	4.3	.560	+ .325	4.6	.875	+ .216	4.8
.231	+ .085	3.9	.580	+ .341	4.5	.894	+ .151	4.6
.250	+ .090	4.3	.599	+ .341	4.2	.910	+ .082	3.8
.270	+ .114	4.0	.621	+ .352	4.7	.928	+ .022	4.0
.289	+ .132	5.0	.635	+ .367	4.3	.941	− .043	4.0
.322	+ .155	4.1	.657	+ .371	4.2	.962	− .097	4.1
0.334	+0.169	4.0	0.672	+0.378	4.7	0.989	−0.120	3.6

due to a change in phase but might be caused by a change in color response dependent upon the change from a silver to an aluminum coating on the mirror of the telescope. This is not shown in the measured difference of magnitude between the comparison stars, however. A correction of $-0^m.005$ has, therefore, been applied to all values of Δm_1 for JD 9517 and all succeeding observations. The residuals of the second season's observations showed a larger scatter. All observations have, accordingly, received a weight 0.6 of those of the first season. The probable error of an observation of unit weight, derived from the average residual, is $0^m.003$.

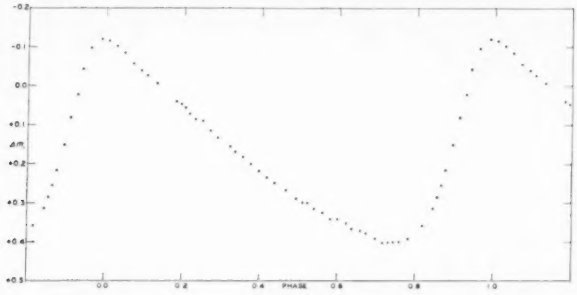

FIG. 1.—RT Aurigae. Infrared photoelectric normals

The observations were arranged according to phase and were combined into normals, in Table 2, of average weight 4.3. These normals are plotted in Figure 1.

The light-curve is remarkably smooth. Occasional large residuals affect the normals, but it is improbable that the minor fluctuations are real. The maximum occurs at phase 0.990, minimum at 0.735; $M - m = 0.255$ ($0^d.95$). The range is $0^m.521$, as compared with $0^m.87$ visual and $1^m.18$ photographic.[3]

YALE UNIVERSITY OBSERVATORY
July 1940

[3] Kukarkin, *op. cit.*, p. 387.

AN INTERPRETATION OF STELLAR MOTIONS IN TERMS OF A NONSTEADY-STATE MODEL FOR THE GALAXY

JOHN TITUS

ABSTRACT

In the theory of stellar systems in nonsteady states a deviation of the vertex of star streaming from the galactic center is predicted for a model consisting of a central mass and a flattened homogeneous spheroid. In this paper a comparison of this model with our galactic system is made. The constants required to give the motions at points within the galaxy are determined from the five observed quantities in the neighborhood of the sun, namely, the deviation of the vertex, the ratio of the axes of the velocity ellipse, the longitude of the node of the double harmonic wave in the radial velocities, the K-term proportional to the distance, and Oort's constant A. From these the motion of the local centroid at the sun is computed and compared with the observed value. The curves for radial velocity to be expected on this model are also illustrated.

I

A model which was first introduced by Oort and which has since been used extensively in dynamical investigations idealizes the distribution of stars in the galaxy as consisting of a central mass and a uniform spheroidal distribution of matter. The force function for such a model is given by

$$K(\bar{\omega}) = \frac{\partial V}{\partial \bar{\omega}} = C\bar{\omega} + \frac{D}{\bar{\omega}^2}, \tag{1}$$

where C and D are related to the mass of the homogeneous spheroid and the central condensation, respectively. Now a potential function of the form (1) plays a critical role in Chandrasekhar's theory of stellar systems in nonsteady states. According to this theory, when

$$\frac{\partial V}{\partial \bar{\omega}} = -\frac{\ddot{\phi}}{\phi}\bar{\omega} + \frac{q}{\phi}\frac{1}{\bar{\omega}^2}, \tag{2}$$

where ϕ is an arbitrary function of the time and q an arbitrary constant, the appropriate solutions for the coefficients of the velocity ellipse indicate a deviation of the vertex. It will be recalled in this connection that a similar deviation of the vertex is predicted also in the steady-state theory. But in this case the force function must have one of the two forms

$$K(\bar{\omega}) = C\bar{\omega} \tag{3}$$

or

$$K(\bar{\omega}) = \frac{D}{\bar{\omega}^2}. \tag{4}$$

Since these two forms are much too special, it is generally agreed that the phenomenon of the deviation of the vertex cannot find an explanation within the framework of the steady-state theory. However, since in the nonsteady-state theory the deviation of the vertex is predicted for a form of the potential function which seems useful from other considerations, it is of interest to compare the detailed consequences of the case of equation (2) with observed data. This is the object of the present paper.

II

For a distribution function assumed to be of the form

$$\Psi \equiv \Psi[a(\Pi - \Pi_0)^2 + 2h(\Pi - \Pi_0)(\Theta - \Theta_0) + b(\Theta - \Theta_0)^2 + \sigma] , \tag{5}$$

the solutions for the various quantities appropriate for the case (2) are given by[1]

$$a = \phi^2 , \tag{6}$$

$$b' = \frac{b}{a} = 1 + \frac{b_{20}}{a}\tilde{\omega}^2 - \frac{2a\phi\tilde{\omega}}{a}\sin(\theta - \theta_0) , \tag{7}$$

$$h' = \frac{h}{a} = \frac{a\phi\tilde{\omega}}{a}\cos(\theta - \theta_0) . \tag{8}$$

Furthermore, the motions of the local centroid are given according to

$$\Delta_1 = a\Pi_0 + h\Theta_0 = a\tilde{\omega}\psi , \tag{9}$$

$$\Delta_2 = h\Pi_0 + b\Theta_0 = h\tilde{\omega}\psi + ap\tilde{\omega} , \tag{10}$$

where

$$\psi = \frac{\dot{\phi}}{\phi} .$$

It should be noted that in equation (10) we have used ap in place of "p" in Chandrasekhar's equation (1054).

Solving equations (9) and (10) for Π_0 and Θ_0, we find

$$\Pi_0 = \tilde{\omega}\psi - \frac{h'p\tilde{\omega}}{b' - h'^2} , \tag{11}$$

$$\Theta_0 = \frac{p\tilde{\omega}}{b' - h'^2} . \tag{12}$$

In the foregoing equations, ϕ and hence ψ are functions of time only, while b_{20}, a, ap, and θ_0 are constants of integration. It is seen that the solution involves the five quantities $a\phi/a$, ψ, b_{20}/a, p, and θ_0. These are to be determined in terms of quantities which may be found from observation.

Now, the equation for the velocity ellipse, referred to axes along the radial II, and the transverse Θ, directions is

$$a(\Pi - \Pi_0)^2 + 2h(\Pi - \Pi_0)(\Theta - \Theta_0) + b(\Theta - \Theta_0)^2 = Q , \tag{13}$$

[1] S. Chandrasekhar, "The Dynamics of Stellar Systems," *Ap. J.* **92**, 474, 1940 (see Eqs.[1050]–[1054]).

where Q is a constant. Let the ratio of the minor to the major axis be denoted by κ, and let the major axis of the ellipse (13) be inclined at an angle ϵ to the radial direction. By definition this is the deviation of the vertex. It is clear that we should be able to express b' and h' in terms of κ and ϵ and elementary geometrical considerations show that

$$b' = \frac{\kappa^2 \sin^2 \epsilon + \cos^2 \epsilon}{\sin^2 \epsilon + \kappa^2 \cos^2 \epsilon}, \tag{14}$$

$$h' = -\frac{(1 - \kappa^2) \sin \epsilon \cos \epsilon}{\sin^2 \epsilon + \kappa^2 \cos^2 \epsilon}. \tag{15}$$

Thus a knowledge of κ and ϵ will furnish b'_s and h'_s, the values of b' and h' at the sun.

Turning next to the differential motions, it is well known that, if Π_0 and Θ_0 are arbitrary continuous functions of position in the neighborhood of the sun, the observed radial velocity-curve for objects at a distance r from the sun will reduce to a double harmonic wave as r approaches zero. Thus to the first order in r the radial velocity V due to the differential motions is given by

$$V = r[A \sin 2(l - l_0) + C \cos 2(l - l_0) + K], \tag{16}$$

where A, C, and K are given by the following differential expressions,

$$A = \frac{1}{2}\left\{\frac{1}{\bar{\omega}}\frac{\partial \Pi_0}{\partial \theta} - \frac{\Theta_0}{\bar{\omega}} + \frac{\partial \Theta_0}{\partial \bar{\omega}}\right\}_s, \tag{17}$$

$$C = \frac{1}{2}\left\{\frac{\partial \Pi_0}{\partial \bar{\omega}} - \frac{\Pi_0}{\bar{\omega}} - \frac{1}{\bar{\omega}}\frac{\partial \Theta_0}{\partial \theta}\right\}_s, \tag{18}$$

$$K = \frac{1}{2}\left\{\frac{\partial \Pi_0}{\partial \bar{\omega}} + \frac{\Pi_0}{\bar{\omega}} + \frac{1}{\bar{\omega}}\frac{\partial \Theta_0}{\partial \theta}\right\}_s, \tag{19}$$

the subscript s denoting that the respective quantities are to be evaluated at the sun.[2]

If C is different from zero, the node of the double wave is displaced from the origin. Since it is known that this point agrees quite well with the longitude of the galactic center as determined, for example, from the distribution of the globular clusters, we shall assume that

$$C = 0. \tag{20}$$

From equations (18) and (19) we get[3]

$$\frac{\partial \Pi_0}{\partial \bar{\omega}} = K, \tag{21}$$

$$\frac{\Pi_0}{\bar{\omega}} + \frac{1}{\bar{\omega}}\frac{\partial \Theta_0}{\partial \theta} = K. \tag{22}$$

[2] Cf., e.g., Smart, *Stellar Dynamics*, pp. 417–18, Cambridge, England, 1938.

[3] Cf. Pilowski, *A.N.*, **257**, 225, 1935; Smart, *op. cit.*, p. 413.

Using the expressions for Π_0 and Θ_0 given by equations (11) and (12) and carrying out the necessary differentiations, we find that equations (21) and (22) reduce to

$$K = \psi - \frac{2h'_s p\left[1 - \frac{a\phi\bar{\omega}_s}{a}\sin(\theta_s - \theta_0)\right]}{(b'_s - h'^2_s)^2}, \tag{23}$$

and

$$K = \psi - \frac{h'_s p}{b'_s - h'^2_s} + \frac{2h'_s p\left[1 - \frac{a\phi\bar{\omega}_s}{a}\sin(\theta_s - \theta_0)\right]}{(b'_s - h'^2_s)^2}. \tag{24}$$

From these we find that

$$\tfrac{1}{4}(b'_s - h'^2_s) = 1 - h'_s \tan(\theta_s - \theta_0), \tag{25}$$

and

$$\psi = K + \tfrac{1}{2}\frac{h'_s p}{b'_s - h'^2_s}. \tag{26}$$

Again, evaluating A according to equation (17), we find, after some reductions and the use of equation (25),

$$p = -\frac{8A(b'_s - h'^2_s)}{2 + b'_s + h'^2_s}. \tag{27}$$

Finally, the computation of b_{20}/a and $a\phi/a$ in terms of known quantities is simple, and we find

$$\frac{a\phi}{a} = \frac{h'_s}{\bar{\omega}_s \cos(\theta_s - \theta_0)} \tag{28}$$

and

$$\frac{b_{20}}{a} = \frac{1}{\bar{\omega}_s^2}\left[b'_s - 1 + 2\frac{a\phi\bar{\omega}_s}{a}\sin(\theta_s - \theta_0)\right]. \tag{29}$$

III

We now have the following data of observation:

1. The deviation of the vertex
2. The ratio of the axes of the velocity ellipse
3. $C = 0$
4. The value of Oort's constant A (this is assumed to be 18 km/sec/kp)
5. The value of K, the term in the radial velocities which is proportional to the distance (according to Trumpler,[4] this is equal to -4.3 km/sec/kp)

[4] *Ap. J.*, **91**, 195, 1940.

It is now seen that these five data provide just the required number of equations to determine the various quantities occurring in the expressions for Π_0 and Θ_0.

The method of evaluating the various constants proceeds as follows. For given values of κ and ϵ, b_s' and h_s' can be calculated from equations (14) and (15), and $\theta_s - \theta_0$ from equation (25). Next, for an assumed value of A, p can be found from equation (27), and ψ from equation (26). It is to be noted that ψ is the sum of K and a term in p, b_s', and

TABLE 1

DEPENDENCE OF THE CONSTANTS ON ϵ AND κ

ϵ	+10°	+10°	+10°	+10°	+10°	+15°	+15°	+15°	+15°	+15°
κ	0.4	0.5	0.6	0.7	0.8	0.4	0.5	0.6	0.7	0.8
b_s'	+5.260	+3.585	+2.586	+1.948	+1.520	+4.363	+3.164	+2.376	+1.842	+1.470
h_s'	−0.775	−0.470	−0.288	−0.173	−0.095	−0.971	−0.625	−0.397	−0.243	−0.136
$\theta_s - \theta_0$	+ 12°0′	− 18°40′	− 52°20′	− 71°30′	− 81°20′	− 8°30′	− 26°10′	− 48°20′	− 66°20′	− 78°0′
p(km/sec/kp)	− 85.3	− 83.3	− 77.2	− 69.5	− 61.6	− 67.3	− 71.8	− 70.4	− 65.9	− 59.9
ψ(km/sec/kp)	+ 2.8	+ 1.5	+ 0.2	− 1.2	− 2.4	+ 5.2	+ 3.8	+ 2.0	+ 0.2	− 1.5
$(\Theta_0)_s$(km/sec)	− 146	− 198	− 247	− 290	− 326	− 157	− 207	− 254	− 296	− 330
$(\Pi_0)_s$(km/sec)	− 91	− 81	− 70	− 60	− 50	− 110	− 99	− 85	− 70	− 57

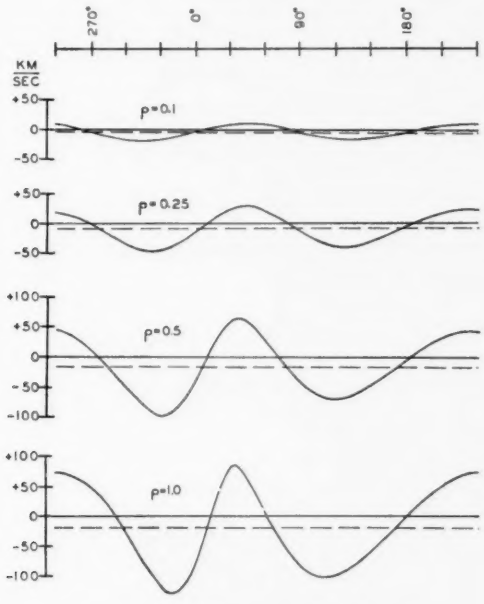

FIG. 1.—The curves for radial velocity

h_s', so that a change in K will produce an identical change in ψ. Finally, $a\phi/a$ and b_{20}/a can be calculated, since all the quantities entering into the expressions are now known. Table 1 shows the dependence of the constants upon the value of κ and ϵ. The various lines give these quantities for $\epsilon = 10°$ and $15°$, and $\kappa = 0.4, 0.5, 0.6, 0.7$, and 0.8; $A = 18$ km/sec/kp, and $\bar{\omega}_s = 8$ kp.

Since the theory predicts the motions of the local centroids at all points in the system, we may compute the curves for radial velocity to be expected on this model. This is done by subtracting the projection of the motion of the sun upon the line of sight from the corresponding projection of the motion at the given point. It is convenient to introduce

galactic co-ordinates, the longitude l and the distance $\rho = r/\bar{\omega}_s$. For the case $\kappa = 0.6$ and $\epsilon = 15°$, the expressions for b' and h' are

$$b' = 2.376 + 2.265\rho^2 - \rho\{3.641 \cos (l - l_0) + 0.794 \sin (l - l_0)\}, \quad (30)$$

$$h' = -0.397 + \rho\{0.397 \cos (l - l_0) + 0.445 \sin (l - l_0)\}. \quad (31)$$

The radial velocity is given by

$$V = p\bar{\omega}_s \left[\frac{h' \{\cos (l - l_0) - \rho\} - \sin (l - l_0)}{b' - h'^2} - \frac{h'_s \cos (l - l_0) - \sin (l - l_0)}{b'_s - h'^2_s} \right] + \rho\bar{\omega}_s\psi . \quad (32)$$

The curves of Figure 1 have been computed for $\rho = 0.1, 0.25, 0.5$, and 1.0. The dotted line represents the position of the zero point when the K-term has been eliminated, as would be done in practice.

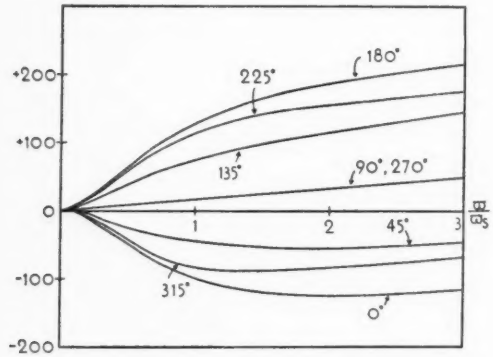

FIG. 2.—The radial motion in km/sec in various directions from the center.

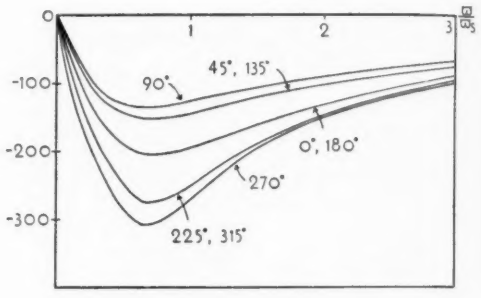

FIG. 3.—The transverse motion in km/sec

Figures 2 and 3 show the values of Π_0 and Θ_0 as functions of distance from the center of the system (in terms of galactic units) in various directions outward from the center. The figures attached to the curves show the values of $\theta - \theta_0$. Finally, Figure 4 shows the values of the deviation of the vertex to be expected. The abscissa gives $\theta - \theta_0$, and the curves are for

$$\frac{\bar{\omega}}{\bar{\omega}_s} = 1 \quad \text{and} \quad \frac{\bar{\omega}}{\bar{\omega}_s} = 2 .$$

IV

The purpose of this investigation has been to interpret the state of stellar motions in terms of a nonsteady-state model for the galaxy. The results are not to be regarded as more than tentative for several reasons. First, the numerical quantities used are very inaccurately known. For example, it is generally agreed that there is a positive deviation of the vertex, but whether it amounts to 10° or 15° is not known with certainty. Again, it may be that the constants, as calculated from the stars near the sun, are not applicable to other sets of objects—such as clusters or planetary nebulae—or even to stars at other points in the galaxy. In other words, we may have the superposition of different systems, each with its own set of constants. However, it is possible that the essential features may remain unchanged.

The values $\kappa = 0.6$, $\epsilon = +15°$, and $A = 18$ km/sec/kp seem at present to be the most probable. For these, Θ_0 for the sun is -254 km/sec, in quite good agreement with the observed value, derived from radial velocities of globular clusters.[5] The value of Π_0 equal to -85 km/sec is not verified by the clusters, but there is certain other information tending to indicate a negative radial motion. It is hard to see how the contraction associated with the negative K-term which is frequently found can be reconciled with a positive radial velocity. Berman[6] finds an increase in the longitude of the galactic center with increasing distance. For $\rho = 0.1$, $l_0 = 325°$, while for $\rho = 0.5$, $l_0 = 330°$, and for $\rho = 1.0$, $l_0 = 333°$. This effect can be explained most easily (as the curves of Fig. 1 show) by a negative value of Π_0. Thus, for example, for stars at the center (if such were observable) for which $\rho = 1$, $l = l_0$, the motions would be zero, and the only contribution to the radial

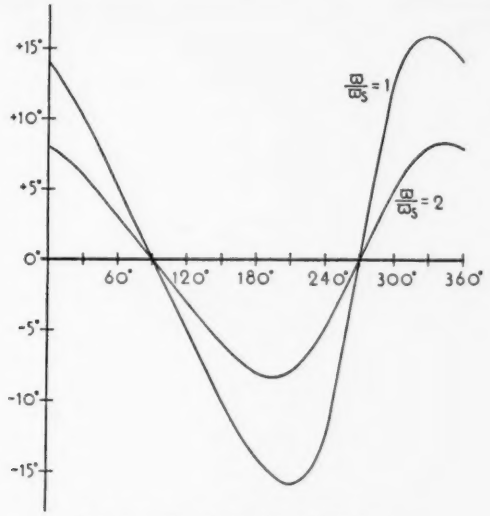

FIG. 4.—The deviation of the vertex

velocity would be the inward solar motion, so that a negative velocity would be found, and as the curve is inclined at that point it must of necessity cross the axis at a longitude greater than l_0. It is to be noticed that this effect exists even when the K-term has been removed.

A quantity of considerable interest is $\dot{\phi}/\phi$. According to equation (2), this measures the fractional decrease of the central mass with time. At the same time, it is also a measure of the fractional increase of the mean residual speed with time. Since it is now believed that the age of the galaxy is of the order of 10^9 years, it appears that we can expect

$$\psi \simeq 10^{-9} = 1 \text{ km/sec/kp} .$$

An examination of Table 1 shows that for $\kappa = 0.6$ and $\epsilon = 10°$ or $15°$ the theory predicts a ψ of this order of magnitude. Further, on this interpretation, a negative K-term appears essential, for otherwise we would have larger values for ψ than would appear reasonable.

It is a pleasure to thank Dr. Chandrasekhar for his help and encouragement in this investigation.

YERKES OBSERVATORY
June 5, 1940

[5] Smart, *op. cit.*, p. 368.

[6] *Lick Obs. Bull.*, **18**, 66, 1937.

INTERSTELLAR ABSORPTION NEAR THE NORTH POLE OF ROTATION

PHILIP C. KEENAN AND HORACE W. BABCOCK

ABSTRACT

Revised spectral classes for B8–A5 stars north of +80° declination confirm essentially the variation of interstellar absorption with distance found by Stebbins, Huffer, and Whitford for these stars. The total visual absorption, which is inappreciable for distances less than 200 parsecs, increases to 0.3 mag. at 400 parsecs.

The zero point of the scale of normal colors of the stars—the relation between spectral type and intrinsic color—is closely bound up with the amount of reddening due to interstellar absorption in the neighborhood of the north pole. The normal spectrum-color relation must be established by means of bright stars with galactic latitudes so high that it can safely be assumed that they are unreddened; but, since the scales of visual and photographic color indices were set up for the stars of the North Polar Sequence, it is important to determine the amount of reddening at the pole as a function of apparent magnitude. It is only when this has been done that the North Polar Sequence and the stars in the surrounding polar cap can be used also as color standards from which the reddening in other parts of the sky can be accurately determined.

Until recently it appeared that the bright stars around the pole were considerably reddened, with a color excess of the order of +0.10 mag. on the International Scale.[1] However, the photoelectric colors measured by Stebbins, Huffer, and Whitford[2] for the brighter A0 stars around the pole indicated that the reddening becomes appreciable only at about the seventh visual magnitude. In the meantime, an investigation of spectral types in the North Polar Sequence[3] showed that these stars had previously been classified from one to two spectral subdivisions too early, compared with the bright standards in the HD system. Since a shift of one subdivision at A0 corresponds to a change in color index of several hundredths of a magnitude, this result suggested that systematic differences in the spectral types were responsible for at least part of the color excesses which had been ascribed to these stars.

In view of this possibility, it was evidently important to reclassify on spectrograms of uniform quality the stars measured by Stebbins, Huffer, and Whitford. For this purpose Professor Stebbins made available a list of the 80 stars with HD types between B8 and A0 lying north of +80° and of the 49 B8–A5 stars in high galactic latitude and with m_v brighter than 7.0 which had served as unreddened standards for his intrinsic color-curve. The photoelectric colors of the high-latitude stars and the polar stars brighter than 8.0 were measured at Madison. The fainter stars were taken at Mount Wilson, both series being referred to the same polar standards.

The spectrographic observations were carried out with the Bruce spectrograph on the 40-inch refractor. All spectrograms were taken with the 6-inch camera (scale: 120 A/mm at $H\gamma$). In order to keep the density and width of spectrum uniform it was necessary to expose as long as 90 minutes for the faintest stars on the program, but for all except a few of the stars at least two good spectrograms each were obtained.

[1] *Trans. I.A.U.*, Report of Committee on Stellar Photometry, VI, 215, 1938.

[2] *Ap. J.*, **90**, 209, 1939; see esp. Fig. 6.

[3] Keenan, *Ap. J.*, **91**, 113, 1940.

Classification on the system of the bright stars of the *Henry Draper Catalogue* was carried out by direct comparison with similar spectrograms[4] of the following standard stars:

β Tau	B8s	μ Ori	A3s
α Lyr	A0s	β Leo	A3n
α Cor Bor	A0n	β Tri	A5s
o Peg	A0s	ι Urs Maj	A5n
π Dra	A2s	ρ Gem	F0s
α Pis Aus	A3	ϵ Cep	F0n

With spectrograms of this dispersion it is possible to refine the classification over the original HD system. For that reason the types in the list above, due for the most part to

TABLE 1

UNREDDENED STARS FOR NORMAL COLOR-CURVE

HD	HR	R.A. 1900	Decl. 1900	m_v	Spectrum		C_1	E'_1	Remarks
					HD	Yerkes			
66824	3167	8^h00^m	+43°33′	6.24	A0	B8.5	$-0^m.06$	$+0^m.03$	
76644	3569	8 52	48 26	3.12	A5	A5n	+ .06	+ .02	ι Urs Maj
77327	3594	8 57	47 33	4.3, 4.5	A0	A0n	− .06	− .01	χ Urs Maj
79158	3652	9 07	43 38	5.30	B8	B8	− .14	− .03	
79763	3676	9 11	47 14	5.70	A0	A0s	− .02	+ .03	
83869	3854	9 36	48 53	6.34	A0	A0n	− .07	− .02	
89021	4033	10 11	43 25	3.52	A2	A2s	− .04	− .03	λ Urs Maj
90470	4096	10 22	42 07	5.80	A2	A5	+ .04	.00	
91312	4132	10 27	40 56	4.84	A5	A9	+ .08	.00	
94334	4248	10 48	43 43	4.84	A0	B9.5	− .07	− .01	ω Urs Maj
103483	4560	11 50	47 02	6.46	A0	A2n	.00	+ .01	
109980	4811	12 34	41 25	6.29	A3	A7n	+ .06	.00	
115271	5004	13 11	41 23	5.68	A5	F4	+ .08	.....	
116303	5045	13 18	44 26	6.41	A3	A7	+ .10	+ .04	
118232	5112	13 30	49 32	4.63	A3	A4	+ .02	+ .01	
120047	5179	13 42	41 35	5.69	A3	A5n	+ .02	− .02	
125162	5351	14 13	46 33	4.26	A0	B9.5n	− .02	+ .04	λ Boo
129002	5468	14 35	44 50	5.39	A0	A0	− .06	− .01	
133029*	5597	14 57	47 40	6.16	A0p	B9sp	− .10	− .02	Si+strong
133962	5627	15 02	48 32	5.59	A0	A0s	− .07	− .02	
138213	5752	15 26	47 33	5.96	A0	A3	+ .01	.00	Metals strong
142926	5938	15 52	42 51	5.61	B8	B8.5	− .11	− .02	
144206	5982	16 00	46 19	4.64	B9	B8s	− .11	.00	υ Her
145389	6023	16 06	45 12	4.26	B9p	B9s	− .09	− .01	φ Her
149303	6162	16 29	45 49	5.55	A0	A4n	+ .03	.00	
149631	6168	16 31	42 39	4.25	A0	B9.5n	− .05	+ .01	σ Her
152107*	6254	16 46	46 10	4.86	A2p	B9.5p	+ .02	+ .08	52 Her, Sr+ strong
60178–9	2890–1	7 28	32 06	1.99, 2.85	A0	A0s	− .04	+ .01	α Gem
79248	3657	9 08	21 42	6.09	A0	A2:	− .02	− .01	
79469	3665	9 09	2 44	3.84	A0	B9n	− .08	.00	θ Hyd
80024	3686	9 12	35 47	5.76	A5	A5n	+ .05	+ .01	
81937	3757	9 24	63 30	3.75	F0	F0	+ .14	+ .04	23 Urs Maj
82621	3799	9 28	52 30	4.65	A0	A2n	− .01	.00	26 Urs Maj
87696	3974	10 02	35 44	4.47	A5	A7	+ .04	− .02	21 Leo Min
92769	4189	10 38	26 51	5.55	A2	A5n	+ .05	+ .01	
95382	4294	10 56	6 38	5.08	A5	A7n	+ .06	.00	
136849	5718	15 18	33 17	5.36	B9	B8	−0.12	−0.01	

* The two stars marked with asterisks have peculiar spectra and were not included in the derivation of the normal color-curve.

[4] We are indebted to Dr. Morgan and Dr. Titus for the use of spectrograms of several of these stars.

TABLE 2

STARS NORTH OF +80 DECLINATION

HD	R.A. 1900	Decl. 1900	m_v	Spectrum		C_1	E'_1	Distance (Parsecs)	Remarks
				HD	Yerkes				
56.....	0^h00^m	+80°31′	9.0	Ao	A2−	+0.04	+0.05	400	
2534.....	0 24	+80 49	8.10	Ao	A2	.00	+ .01	280	
7505.....	1 10	+80 22	6.73	Ao	Ao+n	− .07	− .03	170	
7939.....	1 14	+84 13	9.2	Ao	B9.5s	.00	+ .06	500	
9653.....	1 30	+80 55	7.10	Ao	B8	− .08	+ .03	280	
10648.....	1 39	+80 23	7.23	Ao	B9.5n	− .07	− .01	200	
12467.....	1 57	+80 49	5.99	Ao	A2	+ .01	+ .02	110	
13714.....	2 09	+80 16	7.47	Ao	Ao	− .06	− .01	230	
13828.....	2 10	+83 13	8.1	Ao	A3n	+ .04	+ .03	280	
14500.....	2 15	+80 10	8.25	Ao	A2n	+ .02	+ .03	340	
15374.....	2 23	+85 22	7.8	Ao	Ao+	− .02	+ .02	250	m_v From Mt. Wilson
17243.....	2 41	+85 28	8.7	Ao	A1s	− .03	.00	350	
22677.....	3 34	+83 14	7.52	B9	B8.5n	− .08	+ .01	300	
24716.....	3 51	+80 42	7.8	Ao	A1	+ .01	+ .04	240	
26012.....	4 02	+81 43	7.33	Ao	A1n	− .03	.00	200	
26209.....	4 04	+81 23	7.50	Ao	A2s	+ .04	+ .05	210	
30881.....	4 46	+86 10	7.96	B9	B9	− .04	+ .04	300	
30932.....	4 47	+80 38	9.0	Ao	B9.5s	− .05	+ .01	450	
33972.....	5 09	+81 16	9.2	Ao	A5	+ .09	+ .05	330	
34109.....	5 10	+85 35	6.55	Ao	Aon	− .07	− .02	120	
40158.....	5 52	+80 02	9.02	Ao	B9.5n	− .03	+ .03	450	
55075.....	7 06	+81 26	6.20	B9	B9	− .07	+ .01	140	
56049.....	7 10	+86 33	8.7	Ao	Ao	− .03	+ .02	360	
60062.....	7 28	+81 55	7.60	B9	B8n	− .06	+ .05	340	
63834.....	7 46	+84 41	7.38	Ao	A1	− .04	− .01	200	
65299.....	7 53	+84 21	6.39	Ao	A2s	− .04	− .03	130	
66368.....	7 58	+88 56	7.01	Ao	A3	+ .04	+ .03	170	NPS 6
67934.....	8 05	+82 44	6.17	Ao	B9.5n	− .04	+ .02	145	
72520.....	8 28	+82 36	6.69	Ao	B9s	− .12	− .04	200	
74776.....	8 41	+80 24	7.47	Ao	B9.5	− .07	+ .01	240	
82371.....	9 26	+82 49	7.49	Ao	A3	− .04	− .05	210	
87787.....	10 02	+85 56	9.2	Ao	A1s	+ .01	+ .04	430	Metallic lines slightly strong
92192.....	10 34	+80 57	6.70	Ao	A1	− .04	− .01	170	
99150.....	11 20	+81 06	9.4	Ao	A2n:	+ .03	+ .04	440	
99945.....	11 25	+81 41	6.13	Ao	A3sp	+ .11	+ .10	.....	Sr+ strong
108149.....	12 20	+85 52	8.9	Ao	A1s	+ .04	+ .07	380	
111112.....	12 42	+81 10	6.26	Ao	A5	+ .04	. 00	110	
118478.....	13 32	+82 30	9.1	B8	B5:	− .21	.....	.....	Interstellar K?
121952.....	13 54	+87 48	8.92	Ao	A7	+ .07	+ .01	270	
126047.....	14 18	+87 52	8.78	B9	B9	.00	+ .08	460	
132610.....	14 55	+81 09	7.20	Ao	A1n	− .03	.00	210	
139305.....	15 32	+80 06	8.40	Ao	B9	− .05	+ .03	380	
144800.....	16 03	+81 07	8.35	Ao	A2	.00	+ .01	280	
149444.....	16 30	+80 57	8.8	Ao	A2	+ .02	+ .03	350	
150265.....	16 35	+86 26	8.8	Ao	A2	+ .06	+ .07	350	W Urs Min
156401.....	17 12	+84 54	7.73	Ao	A4	+ .06	+ .03	200	Metallic lines slightly strong
159386.....	17 29	+82 49	8.1	Ao	Aon	+ .07	+ .12	280	
166205.....	18 04	+86 37	4.44	Ao	A2	− .04	− .03	54	NPS 1, δ Urs Min
166926.....	18 08	+87 00	5.86	A3	A3p	+ .07	+ .06	.....	NPS 4 Metallic lines strong
166818.....	18 08	+84 40	8.2	Ao	A1s	− .03	.00	280	

TABLE 2—*Continued*

HD	R.A. 1900	Decl. 1900	m_v	Spectrum		C_1	E'_1	Distance (Parsecs)	Remarks
				HD	Yerkes				
169470	18^h20^m	+82°22′	9.0	A0	A5n:	+ .09	+ .05	330	
170151	18 23	+82 54	7.29	B9	B8n	− .10	+ .01	290	
178738	19 05	+82 14	6.83	A0	A1n	− .05	− .02	170	
180499	19 12	+82 31	7.99	B9	B8	− .03	+ .08	380	
183381	19 24	+81 45	8.03	B9	A2	− .01	.00	250	
189205	19 54	+84 31	8.0	A0	A1n	+ .03	+ .06	260	
191562	20 06	+84 26	8.9	A0	A2	+ .07	+ .08	360	
194375	20 20	+80 13	6.79	A0	B8	− .09	+ .02	240	
195212	20 25	+82 44	8.9	A0	A0	− .05	.00	400	
199095	20 50	+82 10	5.69	A0	A0	− .04	+ .01	100	
203398	21 17	+80 23	7.20	A0	A1	− .02	+ .01	190	
205937	21 34	+81 45	9.0	A0	A1s	+ .02	+ .03	400	
210979	22 09	+82 10	7.68	A0	A2	+ .03	+ .04	220	
212664	22 21	+84 00	7.49	A0	A1	− .04	− .01	220	
212710	22 21	+85 36	5.38	A0	B9	− .08	.00	110	NPS 2
213809	22 29	+81 39	8.6	A0	A0:	+ .04	+ .09	350	
215743	22 42	+86 46	8.07	A0	A1n	− .03	.00	280	
215971	22 44	+82 45	7.46	B8	B9.5n	− .07	− .01	230	
218737	23 05	+80 06	7.71	B9	B9	− .06	+ .02	280	
219168	23 09	+80 28	8.7	A0	A2s	+ .03	+ .04	330	
219748	23 13	+83 42	7.76	B9	B9:	− .07	+ .01	300	
221468	23 27	+80 27	8.3	A0	A0s	+ .03	+ .08	300	
222821	23 39	+80 45	7.87	A0	A0	− .02	+ .03	260	
223257	23 43	+87 47	8.9	A0	A3:	+ .03	+ .01	350	
224309	23 52	+82 38	6.42	A0	A1	0.00	+0.03	140	V Cephei

Morgan, differ somewhat from the entries in the *Henry Draper Catalogue*. The subtypes actually used for the program stars were B8, B8.5, B9, B9.5, A0, A1, A2, A3, A4, A5, A7, A9, F0, F2, and F4.

Of the stars in high galactic latitudes, most of those with m_v fainter than 6.4 were eliminated in order to avoid any danger of appreciable reddening. The remaining 37 stars are listed in Table 1, which, in addition to the HD identification, gives in the second column the number of each star in the *Harvard Revised Photometry*.

In order to obtain the intrinsic photoelectric color-curve the colors of the standard stars in Table 1 were plotted against the revised spectral types (Fig. 1). Between types B9 and F4 the straight line in the diagram fits the points well and was used in forming Table 3.

By comparison with these normal colors, the color excesses of the individual stars were found and are given in the column headed E'_1 in Tables 1 and 2. The ninth column of Table 2 contains the distances of the polar stars, corrected for absorption from a preliminary plot of color excess against apparent magnitude. The distances were computed by assigning visual absolute magnitudes as follows:

Spectral Type	M_v	Spectral Type	M_v
B8	−0.3	A3	+1.0
B9	+ .2	A4	+1.2
A0	+ .6	A5	+1.4
A1	+ .7	A7	+1.6
A2	+0.8		

It did not appear feasible to estimate differences of luminosity within a given type, but it should be noted that none of the spectra showed supergiant characteristics. The intrinsic dispersion in the luminosities necessarily gives rise to considerable uncertainty in the derived distances.

The relation of color excess to distance for all the stars in the polar cap excepting the peculiar ones HD 99945 and 118478, and North Polar Sequence 4 is shown in Figure 2.

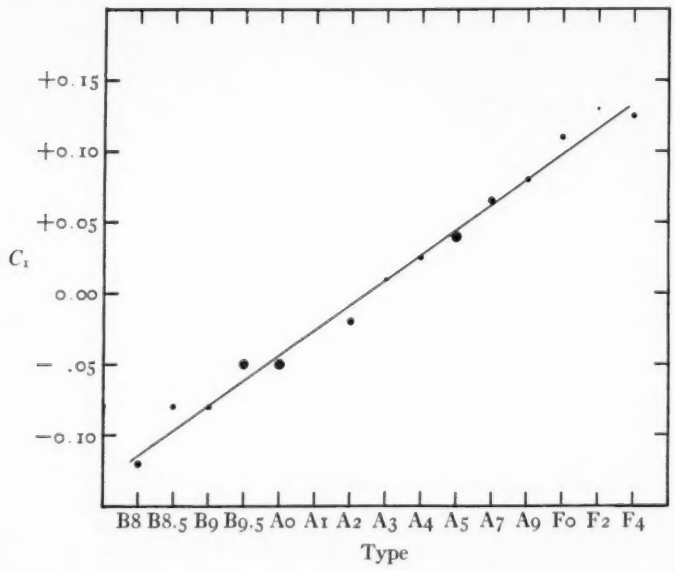

FIG. 1.—Intrinsic color-curve from 34 standard stars. Mean points are plotted for each type, with size of dot indicating weight.

TABLE 3

INTRINSIC COLORS FOR SPECTRAL CLASSES B8 TO F0

Type	C_1	Type	C_1	Type	C_1
B8	−0.11	A1	−0.03	A5	+0.04
B8.5	− .09	A2	− .01	A7	+ .06
B9	− .08	A3	+ .01	A9	+ .08
B9.5	− .06	A4	+0.03	F0	+0.10
A0	−0.05				

The normal points on the diagram define a curve which agrees closely with that given by Stebbins, Huffer, and Whitford[2] on the basis of the original HD types. The observations can be best represented by assuming absorption to set in at about 200 parsecs distance ($m_v = 7$), the reddening increasing to 0.04 mag. at 400 parsecs, but the data do not preclude the possibility of an absorption coefficient increasing linearly with distance throughout the whole observed range of apparent magnitude. If the total visual absorption is taken as $A_v = 7E_1'$, the value of A_v at 400 parsecs is 0.30 mag., as compared to about 0.4 mag. indicated by Stebbins' diagram. The decrease is due to slight systematic differences

in $\Delta Sp = (Sp)_{Yerkes} - (Sp)_{HD}$. The differences are brought out by grouping the data as follows:

Polar stars with m_v brighter than 7.5: $\Delta Sp = +0.7$ subdivisions
Polar stars with m_v fainter than 7.5: $\Delta Sp = +1.1$ subdivisions
Unreddened comparison stars A3 or earlier: $\Delta Sp = +0.5$ subdivisions

The standard stars with HD types A5 and later give $\Delta Sp = +2.5$, but, since no types later than A3 are included among the polar stars, these should be left out of the comparison. Since the revised types for the two regions are homogeneous, it is evident that the

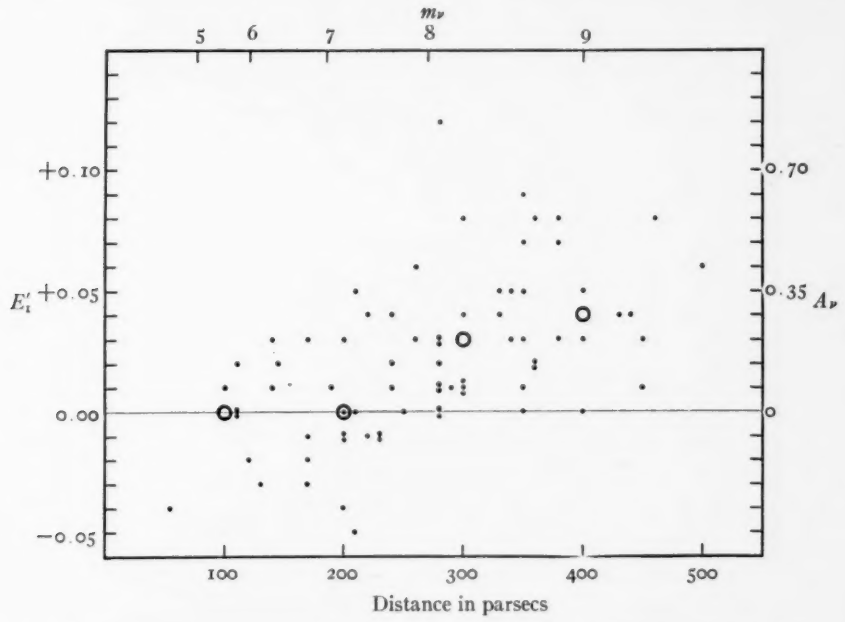

FIG. 2.—Absorption as a function of distance at the pole of rotation. Normal points are shown as large circles. On the left the ordinates give color excess; on the right, total visual absorption. The scale of visual magnitudes on the top holds for Ao stars.

HD types for faint polar stars are systematically slightly earlier than for the brighter stars, which are in turn a little earlier in this part of the sky than in the regions containing the comparison stars. Both differences act in the same direction in making the color excesses of the fainter stars at the pole appear too large when the HD types are used.

We are grateful to Professor Stebbins and his staff for permission to include their unpublished photoelectric colors in the tables.

YERKES OBSERVATORY
June 1940

DIFFUSE RADIATION IN THE GALAXY

L. G. HENYEY AND J. L. GREENSTEIN[1]

ABSTRACT

Observations have been obtained to verify the existence of diffuse interstellar radiation. A Fabry photometer, attached to the 40-inch refractor at the Yerkes Observatory, was used to measure the brightness of regions over a wide range of galactic latitude. The intensities in the photographic region of the spectrum were calibrated by means of the Polar Sequence stars. The mean of four such runs across the Milky Way, on circles of nearly constant longitude, $l = 40°$, shows a maximum of brightness of 80 stars of the tenth magnitude per square degree for the diffuse extra-terrestrial radiation. The mean of three runs near $l = 140°$ shows a maximum of 35 in the same units.

It is shown that the observed intensity of diffuse light may be explained as scattered stellar radiation if the phase function governing the scattering of starlight by the interstellar matter is strongly forward-throwing. The concentration of the diffuse light toward the galactic circle is also in agreement with this property of the phase function. The observations also indicate that the scattering efficiency, or albedo, of the particles is greater than 0.3.

INTRODUCTION

The light of the night sky has been partly resolved into its various components by van Rhijn,[2] Dufay,[3] Wang Shih-Ky,[4] and others. After subtracting the contributions to the total radiation which arise from the permanent aurora, the zodiacal light, and starlight, a residual illumination was found which was ascribed to stellar radiation diffused by interstellar material. In view of the great optical thickness of a dark nebula, the scattering power of such an object should be high; and a dark nebula, illuminated by stars, should be brighter than the surrounding regions of the Milky Way if they are relatively transparent. Observations by Struve and Elvey[5] revealed only small contrast between the dark nebulae and normal regions of the Milky Way. From this observation they concluded that either the scattering efficiency (albedo) of the particles was very low or there existed considerable diffuse radiation in the Milky Way. The latter hypothesis was shown to be correct by Elvey and Roach,[6] who measured photoelectrically the surface brightness of the night sky and determined the variation of the intensity of light of galactic origin with galactic latitude and longitude. After subtracting the component arising from starlight, a considerable residual intensity was found, the mean value of which was 57 stars of the tenth magnitude per square degree in the galactic plane.

The measures by Elvey and Roach are subject to some uncertainty because of the large area of the sky included in each measurement. The measured intensity must be corrected for the light of all stars within a field of 9 square degrees. The Fabry photometer, constructed by Struve and Elvey[5] for the 40-inch refractor at the Yerkes Observatory, can be used for a more detailed study. The photometer records the surface brightness of the sky, or of a star, in an image 0.5 mm in diameter, with five minutes' exposure on Eastman 40 plates. A complete set of observations covering 60° across the Milky Way, and including exposures on standard stars, requires four hours for completion. Observations can be made only on perfect photometric nights free from any trace of

[1] National Research Fellow, at the time of the beginning of this investigation.

[2] *Pub. Astr. Lab. Groningen*, **31**, 1921.

[3] *Etude de la lumière du fond du ciel nocturne*, Paris, 1934.

[4] *Pub. Obs. Lyon*, **1**, No. 19, 1936.

[5] *Ap. J.*, **83**, 162, 1936.

[6] *Ap. J.*, **85**, 213, 1937.

polar aurora. We present here the results of the detailed investigation of two regions in the Milky Way—one in Cygnus near $l = 40°$, the other in the region of the dark nebulae in Taurus and Auriga, near $l = 140°$.

OBSERVATIONAL TECHNIQUE

The field of the sky included in each exposure is defined by a circular diaphragm in the focal plane of the 40-inch, with a diameter of 126″. The observer chooses a field, near a predetermined galactic latitude and longitude, such that all stars brighter than the limit of visibility with the 40-inch refractor are excluded from the field of the diaphragm. This limit is fainter than visual magnitude 15, and it is probable that all stars are excluded brighter than photographic magnitude 16. For this reason the correction for unresolved starlight is less serious than it was in the observations of Elvey and Roach and is probably free from large systematic errors depending on galactic latitude. The observing program for each night was so designed that points at a nearly constant galactic longitude, with galactic latitudes ranging from $+30°$ to $-30°$, could be observed with a minimum change in zenith distance. The observations were taken near the height of the pole. For purposes of calibration, exposures were made on stars of the North Polar Sequence, usually on numbers 14, 15, 16, and 17, with the same exposure time but with a diaphragm 18″ in diameter. The images produced by the stars are of the same quality and size as those of the sky; the smaller diaphragm serves merely to reduce the effect of the sky background on the stellar images. Exposures with the larger diaphragm were made on the sky at the North Pole, to serve as a check on the constancy of the polar aurora and on the transparency. The surface brightness of the night sky in the Milky Way is only 0.3–0.4 mag. brighter than near the galactic pole. The North Polar Sequence stars are too widely separated in magnitude to define the characteristic curve of the plate adequately, and a tube photometer was used to supply the plate calibration. The zero point of the photometer curve was set by the densities of the stellar images. The densities were measured on a Ross photometer. It was found that the total mean error of a determination of surface brightness was of the order of ± 0.03 mag. The image density of the sky exposures was close to that at the center of the straight-line portion of the characteristic curve. No systematic deviation of the North Polar Sequence stars from the characteristic curve could be detected.

The measured surface brightnesses include direct and scattered auroral light, zodiacal light, and the light of faint stars. The auroral and zodiacal light both vary from night to night, and their absolute amounts are not accurately known. The procedure of reduction comprises two steps. The intensity of the zodiacal light at the ecliptic latitude and longitude may be derived, approximately, from the isophotes published by Elvey and Roach.[6] The variation of the auroral light with zenith distance can be theoretically predicted if the absolute intensity is known at any one point. Unfortunately, it was found that the auroral light usually varies with azimuth at Yerkes, being stronger at the North Pole than at equal altitude in other azimuths. A variation of the permanent auroral emission with the geomagnetic latitude may be present. It seems best to assume that the diffuse galactic radiation is small, or zero, at points 30° distant from the galactic circle. We use the observed values of the residual surface brightness at these points, after subtracting the zodiacal light and starlight, to fix the absolute amount of the auroral light for the mean azimuth of the observations. This method of reduction also corrects for any errors in the adopted values of the zodiacal light, as well as for the extra-terrestrial radiation scattered in the earth's atmosphere. The theoretical variation of auroral light with zenith distance permits us to subtract out the auroral light at each point, and we finally obtain the residual galactic light. We depend, essentially, on the rather sudden increase in the galactic light near the Milky Way plane.

The observations must also be corrected for the light of the stars fainter than the

sixteenth magnitude. Since the star counts are not available for the actual fields observed, the corrections were based on the star counts of Seares and Joyner[7] and of van Rhijn,[8] interpolated for the galactic latitude and longitude of the observations. The extrapolation of the tables for fainter stars introduces, in general, only small uncertainty into the correction for the unresolved stars. To determine more precisely the total starlight, the mean star counts were corrected by using the detailed counts to the eighteenth magnitude by Miller[9] in Cygnus and to the fifteenth magnitude by McCuskey[10] in Tau-Aur. The star correction is uncertain near the galactic plane in Cygnus, where the actual illumination contributed by stars of each successively fainter magnitude group is only slowly decreasing at the limit of the available star counts.

TABLE 1

MEAN INTENSITY OF STARLIGHT IN TENTH-MAGNITUDE STARS PER SQUARE DEGREE

b	Seares and Joyner	Van Rhijn	b	Seares and Joyner	Van Rhijn
0°	121	201	40°	34	33
5	109	139	50	28	28
10	88	93	70	22	22
20	57	61	90	20	20
30	42	44			

While investigating the problem of the correction of the observed light for the contribution of the faint stars, a serious difficulty was encountered which does not seem to have been noticed previously. Since our knowledge of the frequency of faint stars is based on the Mount Wilson counts in the Selected Areas, we may expect the distribution tables of Seares and Joyner and of van Rhijn to yield accordant results. The methods used in these two investigations in extrapolating the counts to the galactic circle and in reducing the data for the southern Milky Way seem, however, to have been quite different. The nature of this discrepancy may be seen from an examination of Table 1, which gives the integrated starlight, I_0, from 1 square degree, as derived from the distribution tables of Seares and Joyner[7] (Table XIV) and van Rhijn[8] (Table 6). If the counted number of stars between apparent magnitude $m + \frac{1}{2}$ and $m - \frac{1}{2}$, at galactic latitude b, is $A_{m,b}$, then

$$I_0(b) = \int_{-\infty}^{\infty} A_{m,b}\, 10^{-0.4(m-10)}\, dm\,.$$

Counts in the catalogues of the bright stars were made for stars brighter than magnitude 5, and an extrapolation was made for the fainter stars which contribute only a small fraction of the light.

It is necessary to distinguish between these two results, and it was found that the counts of Miller and of McCuskey agreed more closely with the distribution tables of van Rhijn (Table 10) than with those of Seares and Joyner. The final adopted values of the starlight, based on van Rhijn's tables, are displayed in Figure 1. Little uncertainty

[7] *Ap. J.*, **67**, 24, 1928.

[8] *Pub. Astr. Lab. Groningen*, **43**, 1929.

[9] *Harvard Ann.*, **105**, No. 15, 1937; *Contr. Perkins Obs.*, No. 13, 1939.

[10] *Ap. J.*, **88**, 209, 1938.

PLATE VI

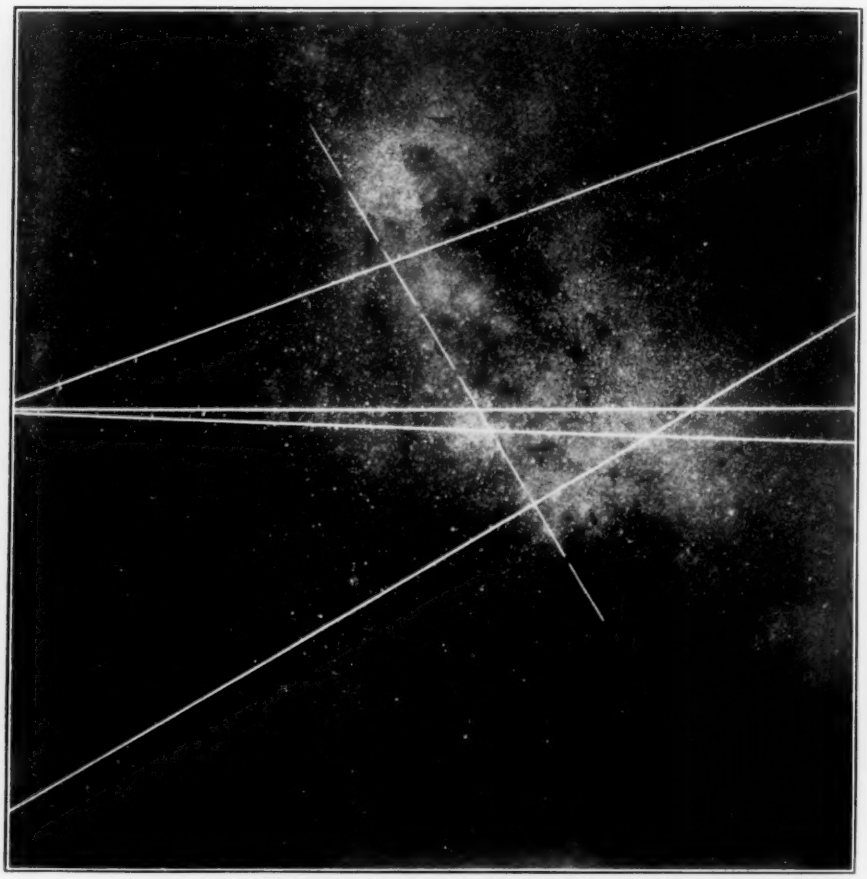

PHOTOGRAPH FROM THE ROSS AND CALVERT *Atlas of the Milky Way* OF THE REGION IN CYGNUS IN WHICH THE DIFFUSE RADIATION WAS MEASURED

The solid lines indicate the tracks along which observations were made. The broken line indicates the galactic equator.

exists in the correction for unresolved stars in the field of the photometer; in any case, we have used the larger values.

The surface brightness of the Cygnus region, one of the brightest found by Elvey and Roach, has been investigated in four complete runs across the Milky Way, from $b = -30°$ to $b = +20°$. The regions covered by the observations are shown in Plate VI. The individual observations are shown in Figure 2, *b*, where we have plotted the corrected intensities of the diffuse light against galactic latitude. Some uncertainty exists in the northern half of the Milky Way because of the large correction for starlight. The radiation in the southern half is determined more exactly because of the small star correction required in the regions of great obscuration by the dark nebulae of the rift. The diffuse light is roughly the same in the rift and in the star clouds, in agreement with the measures of Struve and Elvey.[5]

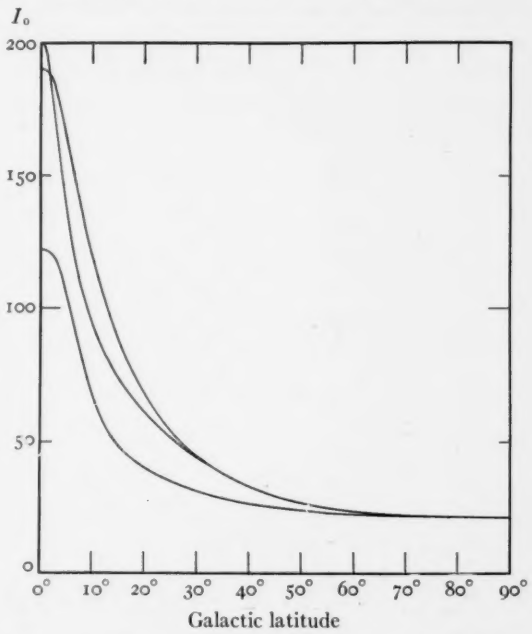

FIG. 1.—The adopted values of I_0, the surface brightness of the starlight, are given. The curve reaching the highest value is based on the mean star counts over all longitudes. The next curve is for the Cygnus region, $l = 40°$; the bottom curve is for the Tau-Aur region, $l = 140°$. The intensities per square degree are expressed in terms of the photographic brightness of one tenth-magnitude star.

In spite of the lack of knowledge of the diffuse intensity at high galactic latitudes it is probable that the galactic light is more sharply concentrated to the Milky Way plane than is the mean starlight. From the mean star counts around the sky the increase of starlight in the range $b = 15°$ to $b = 0°$ is found to be 60 per cent of its value at $b = 0°$. For the diffuse light our method of reduction makes this increase 100 per cent. To reduce it to the same ratio of increase as the starlight, however, we would have to assume that the diffuse light is 90 (in units of tenth-magnitude stars per square degree) at $b = 15°$. So high a value seems improbable on the basis of the photoelectric observations.

We must also consider the possible effects of the extended regions with bright emission-line spectra, discovered by Struve and Elvey.[11] The photographic emulsion we have used has low sensitivity at $H\beta$, and the absorption of the optical system excludes the lines $H\zeta$ and λ 3727. The line emissions at $H\beta$, $H\gamma$, $H\delta$, and $H\epsilon$ may affect our measured surface brightnesses. If we use the Balmer decrement obtained in our study of diffuse nebulae,[12] we can compute a maximum total brightness of the pertinent lines, in terms of $H\alpha$. Struve and Elvey have estimated the order of magnitude of the emission in $H\alpha$, and after some correction we obtain the photographic surface brightness of the extended nebulae as about 3 tenth-magnitude stars per square degree. The uncertainty of the surface brightness of $H\alpha$ is considerable, but it is safe to assume that the intensity is less than 15 and that only a small fraction of the diffuse radiation in the Milky Way is in the form of line emission. This is reasonable on the basis of the theory of nebular

[11] *Ap. J.*, **88**, 364, 1938.

[12] Greenstein and Henyey, *Ap. J.*, **89**, 653, 1939.

excitation, since the mean temperature of the stimulating radiation in the Milky Way is low, compared to that in normal diffuse emission nebulae. We may expect the spectrum of the nebula associated with the Galaxy as a whole to be dominantly of the reflection type.

The results of three sets of observations of the Milky Way near $l = 140°$ are shown in Figure 2, *a*. As a result of preliminary trials it was found necessary to begin far south of the Milky Way, near $b = -40°$, to obtain measures free from diffuse radiation. The very extended dark nebulosities in Tau-Aur stretch far south, and Hubble[13] has found regions of deficiency in the counted number of extragalactic nebulae at $-40°$ in this longitude. The effect of these absorbing regions is visible in the asymmetry of the intensity of the diffuse light. At northern galactic latitudes it falls sharply to the adjusted

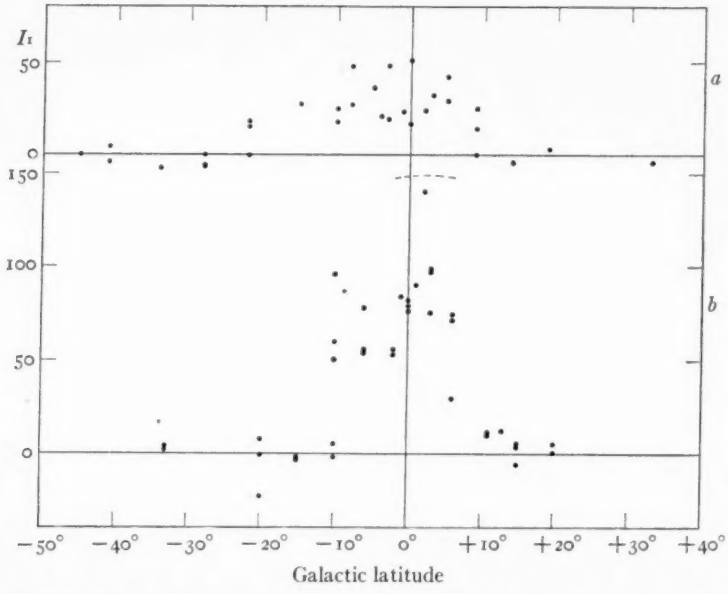

FIG. 2.—The individual measured values of I_1, the surface brightness of the diffuse radiation, are plotted as a function of galactic latitude. Fig. 2, *a*, at top, refers to the region in Tau-Aur near $l = 140°$; Fig. 2, *b*, refers to the region in Cygnus, near $l = 40°$.

zero near $b = +15°$. The intensity is high as far south as $-20°$, however. The maximum light in the Milky Way is less than in Cygnus and reaches a value of less than 50. The concentration of the diffuse light would be no greater than that of starlight if the intensity of the diffuse light were 20 at $b = 20°$; this possibility cannot be excluded by our data.

In the course of the surveys exposures were obtained at various points of special interest. The dark nebula near *o* Persei (*Barnard Atlas of Selected Regions of the Milky Way*, Chart 3, *B4*) has an intensity of about 15 brighter than the normal fields around it. The faintly luminous nebulosity preceding *o* Persei is brighter than its surroundings, by 55. The Pleiades are very bright, and we have observed a surface brightness of 2.5 mag. per square degree in the nebula near Merope. NGC 1977, which has a faint emission spectrum as well as a reflection spectrum, reaches 1.8 mag. per square degree. The center of NGC 1976 is too bright for accurate measurement with our present technique and is probably brighter than 0 mag. per square degree.

[13] *Ap. J.*, **79**, 8, 1934.

The results of our detailed investigations may be compared with those of Elvey and Roach. For the Cygnus dark region they obtain 110; for the bright region, 78. Both these figures are based on zero intensity at 40°. Since we have set our zero of intensity at $b = 15°$ in Cygnus, we should transform their values to 96 and 58, respectively, on our scale. Our observed values are 80 and 100; the difference may depend on the actual regions observed and on the star corrections they have used. In the Tau-Aur region they find the maximum diffuse radiation in the galactic plane to be 50, compared to our value of 35. Their observations do not reveal the considerable intensity at southern galactic latitudes, because of the overcorrection for starlight involved in the use of the mean star counts in the star-poor regions of the dark nebulae. Nevertheless, the order of magnitude of the diffuse light found by two completely independent methods is essentially the same, and the presence of diffuse radiation throughout most of the Milky Way may be considered established. The mean value of the galactic light in the Milky Way plane is given by Elvey and Roach as 57. This is almost identical with the mean intensity, over all galactic latitudes and longitudes, of starlight as derived from the star counts, i.e., 61 from the van Rhijn tables.

THEORETICAL DISCUSSION

In comparing the observational results with theoretical predictions, it is convenient to divide the problem into two parts. We consider first the intensity of diffuse light along the galactic circle and then the concentration toward the galactic circle.

The diffuse light has its origin at each point along the line of sight in the scattering of starlight and diffuse light. The contribution of an element of optical thickness, $d\tau$, is

$$d\tau \int I \Phi d\omega ,$$

where the integral[14] represents the amount of radiation scattered into the line of sight. The total intensity of starlight and diffuse light is I, and the scattering is governed by the phase function, Φ. The intensity of light reaching us is reduced by the factor $e^{-\tau}$, where τ is the optical thickness between the point at which the scattering takes place and the observer. The observed intensity of diffuse light, I_1, is the integral of the contributions up to some limiting optical thickness, τ_0, or

$$I_1 = \int_0^{\tau_0} e^{-\tau} d\tau \int I \Phi d\omega = \overline{\int I \Phi d\omega}(1 - e^{-\tau_0}) \qquad (1)$$

if we take the appropriate mean value of the term $\int I \Phi d\omega$ along the line of sight. In computing I_1, we restrict our attention, for the time being, to its value along the galactic circle.

Our region of the Galaxy may be regarded, to a first approximation, as a slab of emitting and scattering matter, stratified along parallel planes. The observed diffuse light originates within comparatively short distances, of the order of 1500 parsecs, from the sun. Within such distances we have no reason to expect violent fluctuations of the term $\int I \Phi d\omega$. This integral depends on the incident intensity, which is a function of the density of absorbing and emitting matter averaged over large regions of space. Its value varies more slowly than does the star density. We shall compute the value of the observable intensity by using the value of $\int I \Phi d\omega$ near the sun.

Little information concerning the nature of the phase function for interstellar scatter-

[14] Henyey, *Ap. J.*, **85**, 107, 1937.

ing is now available. We have carried out our computations, using a phase function of the form

$$\Phi(a) = \frac{\gamma(1 - g^2)}{4\pi} \frac{1}{(1 + g^2 - 2g \cos a)^{3/2}} . \tag{2}$$

The phase angle is a, defined as the deviation of the ray from the forward direction; γ is the spherical albedo; the parameter g measures the asymmetry of the phase function, according to the expression

$$\gamma g = \int \Phi(a) \cos a \, d\omega . \tag{3}$$

For $g = 0$ we have an isotropic distribution of the scattered radiation; for $g = +1$ all the radiation is thrown forward. A representation of the cases $g = +\frac{1}{3}$ and $g = +\frac{2}{3}$, with $\gamma = 1$, is given in Figure 3. Such forward-throwing functions resemble those com-

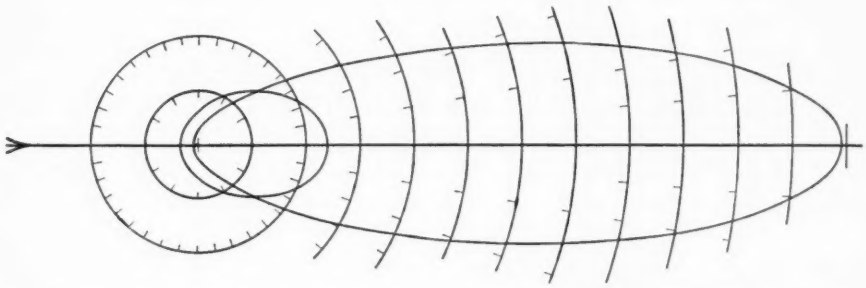

FIG. 3.—Polar diagram of the phase function of equation (2), for $\gamma = 1$. The more elongated curve is for $g = +\frac{2}{3}$; the other, for $g = +\frac{1}{3}$. The radiation is incident on the particle from the left, as shown by the arrow.

puted on the basis of the Mie theory for particles whose radius is near a wave length. If the sign of g is negative, we have backward-throwing phase functions of the same form as those in Figure 3. Suitable combinations of forward and backward phase functions of the form of (2) can also be used.

In order to compute the quantity $\int I \Phi d\omega$, we must know I as a function of position over the sky. The principal variation of I is in galactic latitude, with a smaller variation in longitude. Let us carry out the computation of $\int I \Phi d\omega$ as though the longitude variation is zero and the variation with latitude is (*a*) the mean over the sky and (*b*) the actual variation at the particular longitude which we are considering. The true value is evidently intermediate between these two. For this purpose we have used the mean star counts of van Rhijn[8] and have computed the light of the stars, $I_0(b)$. The results have been given in Figure 1 for the mean over all longitudes and for $l = 40°$ and $l = 140°$. We have already discussed the difficulty arising from the discrepancy between the distribution tables of Seares and Joyner[7] and of van Rhijn.[8] To $I_0(b)$ must be added $I_1(b)$, the diffuse light, which can be obtained from our Figure 2, *a* and *b*, for Cygnus and Tau-Aur. For the average over all longitudes the values observed by Elvey and Roach[6] were used. As may be seen from the curves in Figure 1, the values of $I_0(b)$ for Cygnus are close to those for the average over all longitudes; in view of the uncertainty of the diffuse light arising from the absence of data for the southern hemisphere the mean light was taken equal to that in Cygnus.

The results of the integration, which was carried out numerically, are shown in Figure 4. In the figure we have plotted the ratio, Γ, of the observed maximum intensity of diffuse light to the value predicted for $\gamma = 1$, $\tau_0 = \infty$, and various values of g. The ratio, Γ, measures the effectiveness of the interstellar matter in scattering light; according to equation (1), it is

$$\Gamma = \gamma(1 - e^{-\tau_0}) = \frac{\text{Observed light}}{\text{Predicted light}} . \tag{4}$$

The results for Cygnus are given by the top curve, where case (*a*) and (*b*) coincide. The two other full-line curves were obtained for Tau-Aur; the upper of these curves is for

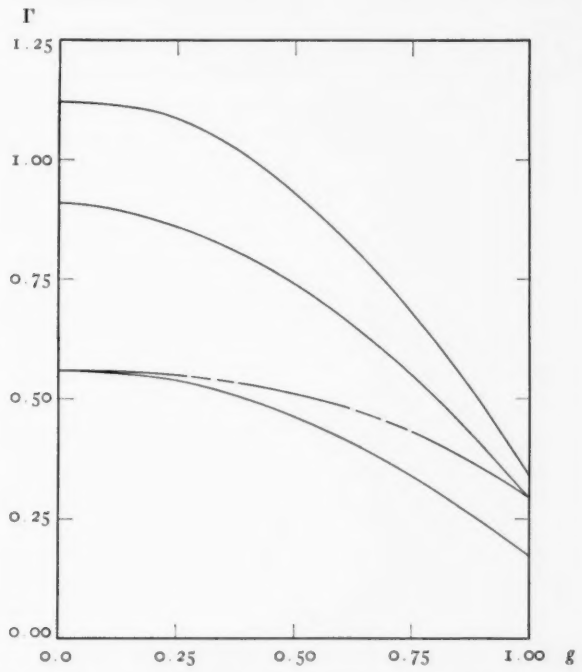

FIG. 4.—The ratio, Γ, of the observed diffuse intensity to the predicted value for albedo unity is plotted as a function of g. The uppermost curve refers to the results for Cygnus; the three lower curves, to the results for Tau-Aur.

case (*b*), the bottom curve for case (*a*). The broken-line curve indicates the probable trend of the actual value of Γ for Tau-Aur.

The first point of interest is the systematic difference between Cygnus and Tau-Aur. The ratio of the value of Γ for Tau-Aur to that for Cygnus lies between 0.50 and 0.85. This difference may arise either from a real variation of the optical properties of the interstellar matter from point to point in the Galaxy or from a much smaller total optical thickness, τ_0, in Tau-Aur. That there is a real difference in the total amount of material seems quite reasonable. Let us accept this possibility and assume that the optical thickness in the direction of Cygnus is effectively infinite. For Tau-Aur

$$1 - e^{-\tau_0} = \frac{\Gamma_{\text{Tau-Aur}}}{\Gamma_{\text{Cygnus}}} ,$$

and we have the condition $0.50 < 1 - e^{-\tau_0} < 0.85$. Then,

$$0.7 < \tau_0 < 1.9 .$$

The upper limit corresponds to $g = +1$. We require, therefore, considering the uncertainty of the observations, that τ_0 be less than 2.5.

Since counts of extragalactic nebulae have originally indicated large absorption in the Milky Way, the low total absorption required in Tau-Aur must be examined. An absorption of 2.7 mag. ($\tau_0 = 2.5$) corresponds to a decrease in the counted number of nebulae, to a given limiting magnitude, to one-thirtieth the number at the galactic pole. On the plates used by Hubble this would leave about 3 nebulae per plate. Such a number could possibly escape detection. A lower absorption, say $\tau_0 = 1.5$ mag., corresponds to 12 nebulae per plate—probably sufficient to be mentioned, in spite of the high star density in the Milky Way. These values of τ_0 may gain some support from the colors of distant B stars in this region of the Milky Way. Stebbins, Huffer, and Whitford[15] find no color excesses as large as 0.25 mag. between $l = 120°$ and $l = 210°$, up to distances of 1500 parsecs. We may summarize by the statement that the observed weakness of the diffuse light in Taurus can be explained by the condition

$$1.5 < \tau_0 < 2.5$$

and an extremely forward-throwing phase function. The value of g required, $> +0.9$, cannot be taken as a definite lower limit, because of observational uncertainties. The observations indicate that there is about an even chance that $g > 0.9$; it is almost certain that $g > 0.65$.

Examining the curve in Figure 4 for the Cygnus region, we find that for $g < 0.4$ the possible values of Γ exceed unity. By the nature of Γ this is impossible. We thus have another strong indication that the phase function is moderately or strongly forward-throwing. Since the total absorption, τ_0, in Cygnus is effectively infinite, the quantity Γ equals the spherical albedo, γ. Then, since $g > 0.65$, it follows that

$$0.3 < \gamma < 0.8 ,$$

with some preference for the lower limit. These limits depend on the observations and on our assumptions concerning $\int I \Phi d\omega$; they are somewhat uncertain. In any case, there exists a strong indication that γ is not very small. It should be remembered that, if the interstellar material consisted of small metallic particles, γ would be much smaller,[16] because of the consumptive absorption within the particles.

We have considered the intensity of light on the galactic circle. Our observations can be used to define another observational quantity, the concentration of the diffuse light toward the galactic plane. To discuss this problem we must introduce some model for the Galaxy of stars and interstellar matter. We will regard the Galaxy as a slab of emitting and scattering material stratified along parallel planes and extending to infinity in all directions along the galactic circle. The most serious deviations from such a model in the actual Galaxy arise from the existence of local clouds of absorbing material, or dark nebulae. Provided they are concentrated toward the galactic plane, they have little effect on the intensity of the diffuse light. For example, the galactic light in Cygnus (Fig. 2, *b*) hardly varies, from the brilliant star cloud to the dark nebulae in the rift.

[15] *Ap. J.*, **90**, 209, 1939.

[16] Henyey and Greenstein, *Ap. J.*, **88**, 601, Table 2, 1938.

The illumination of a slab such as we are considering is governed by the following equation of transfer:

$$\cos\theta \frac{dI}{d\tau} = I - \int I\Phi d\omega - a . \tag{5}$$

The meaning of some of the symbols is given by Figure 5. The differential equation refers to the intensity, I, traveling in the direction of a ray defined by θ at point τ. The optical thickness is τ measured from the central plane; and τ_1 is the half-thickness of the slab. To make the problem specific, we have assumed that the sun is actually in the central plane, at the point $\odot$, in Figure 5. The scattering term is $\int I\Phi d\omega$.[14] The quantity a is the ratio of the stellar emission per unit volume into unit solid angle to the absorption coefficient per unit distance. The intensity I is the total intensity, in-

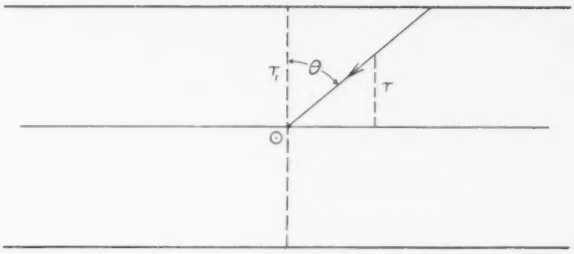

FIG. 5.—Sketch illustrating the meaning of the symbols used in the discussion of the plane-parallel model.

cluding both starlight and diffuse light. The intensity of the starlight, I_0, is the solution of the equation

$$\cos\theta \frac{dI_0}{d\tau} = I_0 - a . \tag{6}$$

The diffuse intensity, I_1, is

$$I_1 = I - I_0 . \tag{7}$$

The solution of equation (5) for I is, for $0 < \theta < \pi/2$,

$$I = \sec\theta\, e^{\tau \sec\theta} \int_{\tau}^{\tau_1} e^{-\tau' \sec\theta} \left(\int I\Phi d\omega + a \right) d\tau' .$$

Likewise, for I_0,

$$I_0 = \sec\theta\, e^{\tau \sec\theta} \int_{\tau}^{\tau_1} e^{-\tau' \sec\theta}\, a\, d\tau' . \tag{8}$$

Hence, the diffuse light I_1 is

$$I_1 = \sec\theta\, e^{\tau \sec\theta} \int_{\tau}^{\tau_1} e^{-\tau' \sec\theta} \left(\int I\Phi d\omega \right) d\tau' . \tag{9}$$

It may be seen from this discussion that the illumination depends on the values of a at various points in the slab. Bottlinger[17] considered the problem of the representation of the observed intensity of starlight in terms of a model for the Galaxy. He found that the light, averaged over all longitudes, could be represented by a plane-parallel model with, in our terminology, a constant value of a. In case a is constant we have from equation (8), for $\tau = 0$,

$$I_0 = a(1 - e^{-\tau_1 \sec \theta}) . \tag{10}$$

We have examined the representation by equation (10) of the star counts by van Rhijn, averaged over all longitudes and over the northern and southern hemispheres. We find that a good fit is given by taking $a = 195$ and $\tau_1 = 0.12$. Table 2 gives a comparison of the observed and the predicted starlight. It may be seen that the observations are represented within an error of 10 per cent. We choose, therefore, to carry through our analysis regarding a as constant.

TABLE 2

OBSERVED AND PREDICTED STARLIGHT

b	Van Rhijn Observed	I_0 Predicted	b	Van Rhijn Observed	I_0 Predicted
90°	20	22	20°	61	58
70	22	23	10	93	96
50	28	28	5	139	146
40	33	33	0	201	195
30	44	41			

To compute I_1, we must have information concerning $\int I\Phi d\omega$ at all points along the ray. A solution of a restricted case of the present problem of the diffusion of radiation in the Galaxy has been made by Wang Shih-Ky,[4] who considered the problem of a uniform phase function and unit albedo. A more general solution may be obtained by considering the well-known symbols, J, F, and K.[18] Then we have

$$\left.\begin{aligned} \tfrac{1}{4}\frac{dF}{d\tau} &= (1 - \gamma)J - a , \\ \frac{dK}{d\tau} &= \tfrac{1}{4}(1 - \gamma g)F , \end{aligned}\right\} \tag{11}$$

where γ is the spherical albedo and g the asymmetry of the phase function, given by equation (3). Using the approximation $K = \frac{1}{3}J$ and assuming that γ and g are constants, we find that equations (11) lead to the equation

$$\frac{d^2J}{d\tau^2} = p^2J - 3a(1 - \gamma g) , \tag{12}$$

where

$$p^2 = 3(1 - \gamma)(1 - \gamma g) .$$

[17] *Zs. f. Ap.*, **4**, 370, 1932.

[18] Cf. Milne, *Handb. d. Ap.*, **3**, 121.

The solution of (12) for constant a is

$$J = \frac{a}{1-\gamma} - A \cosh p\tau ,$$

where A is a constant of integration. (No term in sinh $p\tau$ appears, because the model is symmetrical about the central plane, $\tau = 0$.) To evaluate the constant of integration, we use the usual boundary condition, $|F| = 2J$, at the surface $\tau = \tau_1$. The application of this condition leads to

$$J = \frac{a}{1-\gamma}\left[1 - \frac{\cosh p\tau}{\cosh p\tau_1 + \frac{2}{3}\frac{p}{1-\gamma g}\sinh p\tau_1}\right]. \tag{13}$$

We must here introduce some form of the phase function to evaluate the scattering term, $\int I\Phi d\omega$. The optical properties of our model for the Galaxy should depend primarily upon those properties of the phase function which we specify by γ and g. We have seen that in the differential equations (11) and (12), at least as far as J and F are concerned, this is certainly true, within the range of validity of the approximation, $K = \frac{1}{3}J$. There is, consequently, little loss of generality in supposing that the phase function is of the form

$$\Phi = \frac{\gamma(1-g)}{4\pi} + \gamma g\Psi , \tag{14}$$

where Ψ is a perfectly forward-throwing phase function of unit albedo. It can be verified that γ and g in this relationship conform to their former definitions. It follows that

$$\int I\Phi d\omega = \gamma(1-g)J + \gamma g I .$$

Introducing this expression into equation (5), we have

$$\cos\theta \frac{dI}{d\tau} = (1-\gamma g)I - \gamma(1-g)J - a .$$

The value of I at $\tau = 0$ may be computed as before:

$$I = \sec\theta \int_0^{\tau_1} e^{\tau'(1-\gamma g)\sec\theta}(\gamma(1-g)J + a)d\tau' .$$

Substituting for J from (13) and carrying out the integration, we find for I:

$$I = \frac{a}{1-\gamma}\left[1 - e^{-\tau_1(1-\gamma g)\sec\theta} - \frac{\gamma(1-g)}{(1-\gamma g)} \times \frac{1 - e^{-\tau_1(1-\gamma g)\sec\theta}\left(\cosh p\tau_1 + \frac{p}{1-\gamma g}\cos\theta\sinh p\tau_1\right)}{\left(1 - \frac{3(1-\gamma)}{1-\gamma g}\cos^2\theta\right)\left(\cosh p\tau_1 + \frac{2p}{3(1-\gamma g)}\sinh p\tau_1\right)}\right].$$

Subtracting the intensity of starlight as given by equation (10), we have, finally, the diffuse light, I_1, as

$$I_1 = \frac{a}{1-\gamma}\left[\gamma + (1-\gamma)e^{-\tau_1 \sec\theta} - e^{-\tau_1(1-\gamma g)\sec\theta} - \frac{\gamma(1-g)}{(1-\gamma g)} \times \frac{1 - e^{-\tau_1(1-\gamma g)\sec\theta}\left(\cosh p\tau_1 + \frac{p}{1-\gamma g}\cos\theta \sinh p\tau_1\right)}{\left(1 - \frac{3(1-\gamma)}{1-\gamma g}\cos^2\theta\right)\left(\cosh p\tau_1 + \frac{2p}{3(1-\gamma g)}\sinh p\tau_1\right)}\right]. \quad (15)$$

When $\gamma = 1$, the right-hand side in equation (15) becomes indeterminate, but the correct form may be obtained by passing to the limit.

TABLE 3

RELATIVE CONCENTRATION, σ, DIFFUSE LIGHT *minus* STARLIGHT

g	γ			
	0	1/3	2/3	1
	$\tau_1 = 0.1$			
0	0.00	0.00	0.00	0.00
1/2	.18	.19	.21	.22
1	0.22	0.23	0.24	0.25
	$\tau_1 = 0.2$			
0	0.00	0.00	0.01	0.01
1/2	.24	.27	.30	.33
1	0.33	0.37	0.40	0.44

In view of the uncertainties inherent in the observational problem, it seems undesirable to make a detailed comparison between the observational and the theoretical results. We can, however, make a comparison between the observed and the predicted concentration of light toward the galactic circle. For this purpose we introduce a parameter, μ, to measure the concentration.

$$\mu = \frac{I(b = 0^\circ) - I(b = 20^\circ)}{I(b = 0^\circ)}. \quad (16)$$

The relative concentration, diffuse light *minus* starlight, is

$$\sigma = \mu_1 - \mu_0 .$$

In the Cygnus region the observed value of μ_0 is 0.64 ± 0.07. This probable error has been estimated by allowing for the errors of sampling and for the errors due to the faint stars. According to equation (10), this corresponds to $\tau_1 = 0.15 \pm 0.04$. The value of μ_1 as derived in the Cygnus region becomes exactly unity. The concentration can never exceed unity, and the error must be all one-sided. The situation can be represented by saying that $\mu_1 = 0.95 \pm 0.06$. From this set of values we find the relative concentration, σ, to be $\sigma = 0.31 \pm 0.09$.

Equations (10) and (15) have been used to compute σ for a number of values of γ, g, and τ_1. Table 3 contains the results of these computations. It may be seen that for $g = 0$ there is very little relative concentration.

TABLE 4

RELATION BETWEEN γ AND g FOR THE OBSERVED CONCENTRATION

γ	0	1/3	2/3	1
g	>1	1.0	0.9	0.8

Let us adopt a value of $\tau_1 = 0.15$; then we find in Table 4 for each value of γ the value of g which is required to yield the observed relative concentration in Cygnus. Here, again, we have a positive indication of the strongly forward-throwing character of the phase function. The observational errors again limit our conclusions, but we may state that the observed concentration supports our former statement that g is very probably greater than 0.65. Table 4 also confirms our conclusion that γ is very probably greater than 0.3.

It is a pleasure to acknowledge our indebtedness to Dr. C. T. Elvey for his discussion of the possibility of investigating the diffuse galactic light by means of the Fabry photometer.

YERKES OBSERVATORY
March 1940

THE SPECTROSCOPIC BINARY 29 CANIS MAJORIS*

OTTO STRUVE AND FRANCES SHERMAN

ABSTRACT

A new orbit has been derived from spectrograms taken at the McDonald Observatory. A large difference in the velocity of the center of mass, as compared with previous observations, may be caused by a third body. The emission lines show a large red shift which is tentatively attributed to self-absorption in an expanding and rotating shell. The structure and intensity of the emission lines undergo large periodic changes. P Cygni type absorption lines are observed on the violet borders of the emission lines between secondary minimum of light and primary minimum.

1. In 1935 Luyten and Ebbighausen[1] determined the orbit of this binary from a series of spectrograms secured at the Yerkes Observatory between 1931 and 1935. This investigation confirmed the earlier orbital elements derived by Harper[2] at Ottawa in 1917, with the exception of the eccentricity, which, according to Harper, was 0.156, while Luyten and Ebbighausen found 0.077. From a short series of spectrograms taken at Victoria in 1927 and 1928 Pearce[3] derived small corrections to Harper's elements γ and K_1, assuming his results for T, ω, and e. Pearce also measured a very faint secondary spectrum, from which he found $m_2/m_1 = 0.75$.

Shortly after the publication of the orbit by Luyten and Ebbighausen, S. Gaposchkin[4] announced the variability of this star in light and derived the elements from his light-curve. A photoelectric light-curve was determined by Elvey and Rudnick at the McDonald Observatory,[5] and their results were announced by Kuiper.[6] A photographic light-curve by Seyfert,[7] obtained in 1939–1940, is now under discussion.

The spectrum of 29 Canis Majoris shows fairly strong emission lines of *He* II 4686, *N* III 4634, and *N* III 4640. These lines frequently occur in emission in O-type stars, and in some normal stars they occasionally have a P Cygni character.[8] Struve, Elvey, and Morgan announced[9] in 1935 that these emission lines are variable in 29 Canis Majoris. Soon afterward, Luyten and Ebbighausen[10] found that the velocity-curve determined from the emission lines gave a value of γ which was 109 km/sec larger than that deduced from the absorption lines. Struve[11] called attention to the fact that the same systematic difference was already present in Harper's observations, although it was concealed through the use of an adjusted wave length for the *He* II line. Struve also pointed out that "measures of the *He* II 4686 line, when it occurs in emission in O-type stars, nearly always indicate a red displacement of one or two angstrom units." This statement was based upon measurements by J. S. Plaskett[12] and by C. S. Beals.[13]

This remarkable phenomenon in many respects resembles the systematic displacement recently found by O. C. Wilson[14] for the two components of the spectroscopic binary HD 193576. One component is a normal B star, and its value of γ is -34 km/sec. The other component is a Wolf-Rayet star, and its value of γ is $+56$ km/sec. In an

* *Contributions from the McDonald Observatory, University of Texas*, No. 27.

[1] *Ap. J.*, **82**, 246, 1935.

[2] *Pub. Dom. Obs., Ottawa*, **4**, 115, 1917.

[3] *Pub. Dom. Ap. Obs., Victoria*, **6**, 50, 1932.

[4] *Harvard Bull.*, No. 902, p. 17, 1936.

[5] Unpublished.

[6] *Ap. J.*, **88**, 503, 1938.

[7] Unpublished.

[8] Swings and Struve, *Ap. J.*, **91**, 546, 1940.

[9] *Ap. J.*, **82**, 95, 1935.

[10] *Ap. J.*, **82**, 248, 1935.

[11] *Ap. J.*, **82**, 249, 1935.

[12] *Pub. Dom. Ap. Obs., Victoria*, **2**, 16, 1930.

[13] *Pub. Dom. Ap. Obs., Victoria*, **4**, 271, 1930.

[14] *Ap. J.*, **91**, 379, 1940.

attempt to explain this result, Wilson[15] has also made use of the measurements by Beals[13] in Wolf-Rayet stars.

Luyten[16] has already stressed the importance of 29 Canis Majoris for studies of apsidal motion.[17] Chandrasekhar has pointed out its importance for studies of the internal constitution of stars.[18] Accordingly, the star was placed upon the observing program of the quartz Cassegrain spectrograph of the McDonald Observatory, and 34 spectrograms were obtained between January 29 and February 14, 1940.

2. The results of the measurements are given in Table 1. The measurements of the absorption lines were combined in 14 normal places, as shown in Table 2. The preliminary elements obtained from a graphical solution and the final elements resulting from a least-squares solution, following Schlesinger's method,[19] are given in Table 3. The probable error of one normal point of unit weight is ± 5.1 km/sec, and that of a single spectrogram of average quality is ± 9.6 km/sec. Nine spectrograms (Nos. CQ 295, 296, 297, 302, 308, 311, 320, 323, and 325) were obtained with the dispersion of 40 A/mm at λ 3933 on Eastman Process emulsion. The probable error of one such plate is $\pm$ 7.8 km/sec. Seventeen spectrograms (Nos. CQ 300, 303, 309, 310, 312, 313, 314, 319, 321, 322, 324, 326, 329, 330, 333, 335, and 336) were taken on Agfa Super Pan Press film with the same dispersion. The probable error is ± 9.2 km/sec. Eight spectrograms (Nos. G $f/2$ 763, 764, 770, 771, 778, 779, 787, and 788) were taken on Process film, with a dispersion of 50 A/mm. The probable error is ± 12.0 km/sec. The marked superiority of the Process plates is apparent, and the use of film for radial velocity work of high precision is obviously not to be recommended. The weighted sum of the squares of the residuals was $\Sigma pv^2 = 1192.0$ for the preliminary elements and $\Sigma pv^2 = 510.4$ for the final elements.

The mean velocity from the interstellar calcium line K is $V_{Ca} = +32.9 \pm 1.1$. Former determinations[20] gave +29 km/sec. The difference is not much larger than can be explained by the internal scatter.

Our value of γ is +9.3 km/sec. Luyten and Ebbighausen find −9.0; Harper gives −12.1; and Pearce gives −10.6. The difference between our new value and the old determinations is in the same sense as that found for interstellar calcium but is much larger and is hardly compatible with the probable errors.

Table 4 shows the wave lengths used for the absorption lines as well as for the emission lines. The curvature correction was computed from Ditscheiner's formula and was later tested on spectrograms. In order to test the instrumental errors Dr. D. Popper measured a number of spectrograms of stars and of the sky. The corrections to the McDonald velocities are small and are, on the average, in the opposite direction from that required to bring our measures of 29 Canis Majoris in harmony with the older measures (Table 5). The tests show conclusively that the spectrograph performs admirably and that the systematic difference in γ must have some other explanation.

Perhaps we should consider an explanation in terms of a guiding error produced by atmospheric dispersion. At the Yerkes Observatory, and we believe also at Ottawa and at Victoria, the slit of the spectrograph is normally placed in the parallel. At the McDonald Observatory, for all far southern stars, the slit is kept north and south. Since the declination of 29 Canis Majoris is $-24°$ the atmospheric dispersion must be very serious

[15] *Ap. J.*, **91**, 394, 1940.

[16] *Pub. Yerkes Obs.*, **7**, 297, 1939; *Ap. J.*, **82**, 250, 1935.

[17] Professor H. N. Russell has also, in a private discussion, suggested that we reobserve 29 Canis Majoris, both spectroscopically and photometrically.

[18] *Stellar Structure*, p. 319, Chicago: University of Chicago Press, 1939.

[19] *Pub. Allegheny Obs.*, **1**, 33, 1908.

[20] Luyten and Ebbighausen find +29 km/sec, and Pearce finds +29.5 km/sec.

at all northern observatories. The violet image will be markedly displaced from the center of the slit, and accurate guiding is difficult—even when the violet fringe of the image is clearly visible. At the Yerkes Observatory this is rarely the case, and the tendency must be to keep the violet image too close to the lower slit jaw. Since the prism is mounted with its edge down when the telescope, west of the pier, is pointed south, the effect of atmospheric dispersion will be to produce a line which has a spurious dis-

TABLE 1

RADIAL VELOCITIES OF 29 CANIS MAJORIS

No.	Date	U.T.	JD	Phase	V_{abs}	V_{em}	$V_{Ca\,II}$	O−C V_{abs}	O−C V_{em}
CQ 295	1940 Jan. 29	5:00	2429657.70	1.40	−193	−196	+32.1	+ 5	−49
296	30	4:10	658.67	2.37	− 44	− 87	+38.7	+19	−75
297		5:30	658.73	2.43	− 38	− 84	+31.0	+10	−89
300	31	6:19	659.76	3.46	+214	+239	+39.9	+ 4	−16
302	Feb. 1	5:00	660.71	0.01	+133	+268	+35.8	0	+ 4
303		5:43	660.74	0.04	+102	+290	+19.0	−22	+46
308	2	4:48	661.70	1.00	−154	− 89	+36.8	+ 7	+ 8
309		5:33	661.73	1.03	−167	−129	+39.1	− 1	−25
310	3	6:00	662.75	2.05	−139	−118	+28.1	− 4	−37
311		6:43	662.78	2.08	−131	− 50	+30.4	− 2	+25
312		7:27	662.81	2.11	−118	.....	+13.6	+ 5	.....
313		7:40	662.82	2.12	−130	.....	+31.2	− 9	.....
314		7:58	662.83	2.13	−125	.....	+37.2	− 7	.....
319	4	3:40	663.65	2.95	+ 97	+201	+33.0	+ 1	+65
320		4:13	663.68	2.98	+121	+197	+30.0	+16	+54
321		4:46	663.70	3.00	+103	+151	+51.3	− 7	+ 3
322	5	4:07	664.67	3.97	+233	+311	+50.4	− 1	− 4
323		4:44	664.70	4.00	+225	+286	+31.2	+ 4	−29
324		5:24	664.72	4.02	+220	+319	+33.5	+ 2	+ 4
325		6:02	664.75	4.05	+229	+283	+40.4	+15	−31
326		6:41	664.78	4.08	+202	.....	+21.3	− 8	.....
G *f*/2 763	7	5:38	666.73	1.64	−219	− 86	+47.3	−28	+53
764		5:53	666.74	1.65	−216	−116	+32.0	−26	+22
770	8	5:13	667.72	2.63	+ 3	.....	+26.4	− 4	.....
771		5:22	667.72	2.63	+ 18	+ 73	+32.5	+11	+19
778	10	5:19	669.72	0.23	+ 72	+192	+31.8	+11	− 1
779		5:27	669.73	0.24	+ 53	+210	+34.8	− 6	+11
787	11	6:18	670.76	1.27	−179	−169	+23.1	+14	−29
788		6:29	670.77	1.28	−180	−106	+39.9	+14	+35
CQ 329	12	6:54	671.79	2.30	− 80	− 48	+12.1	+ 1	−20
330		7:06	671.80	2.31	− 82	−104	+36.5	− 4	−78
333	13	7:09	672.80	3.31	+149	+243	.....	−35	+20
335	14	4:31	673.69	4.20	+212	.....	.....	+25	.....
336		5:18	673.72	4.23	+174	.....	.....	− 6	.....

placement toward the violet. With a slit width of 0.05 mm and a scale of about 1500 km/mm, a systematic error of several kilometers is to be expected. In this connection it will be recalled that a similar large error was suspected by ten Bruggencate[21] in the radial velocities of Y Sagittarii.

It is difficult, without extensive tests of the Yerkes spectrograph, to determine the effect of atmospheric dispersion for stars near the horizon. For stars at higher altitudes this error is negligible. It is probably safe to attribute to this cause the small difference

[21] *Harvard Circ.*, No. 351, 1930.

in the calcium velocities, but the large difference in γ remains unexplained unless it is caused by a third body. In view of the large systematic difference in γ it is reassuring

TABLE 2

NORMAL PLACES

Phase	Numbers of Plates Included	Weight	Velocity	O−C
0.02.....	CQ 302, 303	0.4	+118	−12
0.24.....	G *f*/2 778, 779	0.4	+ 62	+ 3
1.02.....	CQ 308, 309	0.4	−160	+ 3
1.28.....	G *f*/2 787, 788	0.4	−180	+14
1.56.....	CQ 295, G *f*/2 763, 764	0.6	−209	−13
2.10.....	CQ 310, 311, 312, 313, 314	1.0	−129	− 3
2.30.....	CQ 329, 330	0.4	− 81	− 1
2.40.....	CQ 296, 297	0.4	− 41	+14
2.63.....	G *f*/2 770, 771	0.4	+ 10	+ 2
2.98.....	CQ 319, 320, 321	0.6	+107	+ 2
3.38.....	CQ 300, 333	0.4	+182	−15
4.01.....	CQ 322, 323, 324, 325	0.8	+227	+ 8
4.14.....	CQ 326, 335	0.4	+207	+ 8
4.23.....	CQ 336	0.2	+174	− 6

TABLE 3

ORBITAL ELEMENTS FROM ABSORPTION LINES

Preliminary Elements	Corrected Elements ± p.e.
K = 221 km/sec	K = 216.4 ± 3.1 km/sec
$\omega = 55^\circ$	$\omega = 51^\circ.5 \pm 10^\circ$
e = 0.08	e = 0.062 ± 0.015
T = 4.33 days	T = 4.338 ± 0.122 days
γ = +7.5 km/sec	γ = +9.3 ± 4.7 km/sec
P = 4.39351 days (assumed)	P = 4.39351 days
$a \sin i$ = 13,309,000 km	$a \sin i$ = 13,046,000 km

TABLE 4

WAVE LENGTHS OF LINES

ABSORPTION LINES

N IV	3478.69	*Si* IV	4088.86
N IV	3482.98	*N* III	4097.31
He I	3634.27	*He* II / *N* III	4199.95
H_{10}	3797.90	$H\gamma$	4340.48
He I	3819.62	*He* I	4387.59
H_9	3835.39	*He* I	4471.49
He II	3923.51	*He* II	4541.61
Ca II	3933.68		
He I	4026.20		

EMISSION LINES

N III	4634.14	*He* II	4685.74
N III	4640.63	$H\beta$	4861.33

to find that the other elements are in excellent agreement with the determination by Luyten and Ebbighausen.

Nine of our spectrograms, well distributed in phase, were obtained on the high-contrast Eastman Process emulsion. We have carefully searched these plates for the lines of the fainter component but have not been able to find any trace of them. The new spectrograms are very much better than the older Yerkes plates, and a re-examination of the latter suggests that the fainter component could not be seen on them.[22] The relative displacement of the lines of the two components and the reasonably good sharpness of the absorption lines are such that the components would be completely separated on our plates. This negative result is unfortunate, as it throws some doubt upon the mass ratio and other conclusions dependent upon it.

TABLE 5

RADIAL VELOCITIES OBTAINED WITH 500-MM CAMERA

Plate	Star	Type	Measured Velocity in Km/Sec	Velocity from Moore's Catalogue	Correction
CQ 185	ν Cep	cA2	-23.4 ± 2.1	-21.5 ± 1.1	$+1.9$
186	10 Lac	O9s	-10.5 ± 2.0	-9.5 ± 0.4	$+1.0$
187	61 Cyg A	K5	-62.3 ± 1.9	-65.1 ± 0.2	-2.8
203	α Cas*	K1	-0.7 ± 1.0	-3.8 ± 0.1	-3.1
205	2H Cam	cB6	-1.4 ± 1.3	-7.2 ± 0.3	-5.8
206	α Per*	cF5	-7.0 ± 2.1	-2.4 ± 0.1	$+4.6$
212	α Per*	cF5	-4.9 ± 1.5	-2.4 ± 0.1	$+2.5$
229	α Cas*	K1	-8.1 ± 0.9	-3.8 ± 0.1	$+4.3$
232	α Cet*	Mo	-29.4 ± 1.4	-25.7 ± 0.1	$+3.7$
237	β Peg	Mo	$+8.3\pm1.1$	$+8.8\pm0.2$	$+0.5$
Sky 1			-5.7 ± 1.1		$+6.2$
2			-6.5 ± 1.0		$+7.0$
3			-1.6 ± 1.0		$+2.1$
4			-2.3 ± 1.3		$+2.8$
5			-1.7 ± 1.2		$+2.2$
6			-2.6 ± 1.7		$+3.1$
7			$+0.5\pm1.4$		0.0
Mean correction					$+1.78\pm0.54$

* IAU velocity standard.

The velocity-curve derived from the absorption lines is shown in Figure 1. Phase zero corresponds to JD 2424981.613, as was adopted by Pearce.

3. The emission lines give a velocity-curve which is shown in Figure 2. As Luyten and Ebbighausen[1] have pointed out, the principal difference from the velocity-curve of Figure 1 is a shift in γ. But the shape of the curve is also appreciably different. The most conspicuous features are the greater width of the minimum of the emission-line curve and the relatively small difference between the two curves at phases between 2.0 and 2.5 days. This is a very remarkable phenomenon, and it has been verified by differential measurements in a spectrocomparator.

The elements derived from the emission lines are given in Table 6. Because of the uncertainty in the measures—the emission lines are faint at certain phases and often diffuse—the agreement with the elements deduced by Luyten and Ebbighausen is satisfactory. The relatively smaller value of γ, which we have found, is caused largely by the small value of the shift near phase $2^d.0$.

[22] Kuiper states (*Ap. J.*, **88**, 503, 1938) that Morgan had confirmed the presence of an extremely faint companion. The possibility of a real change in the relative intensities of the two components is not altogether excluded.

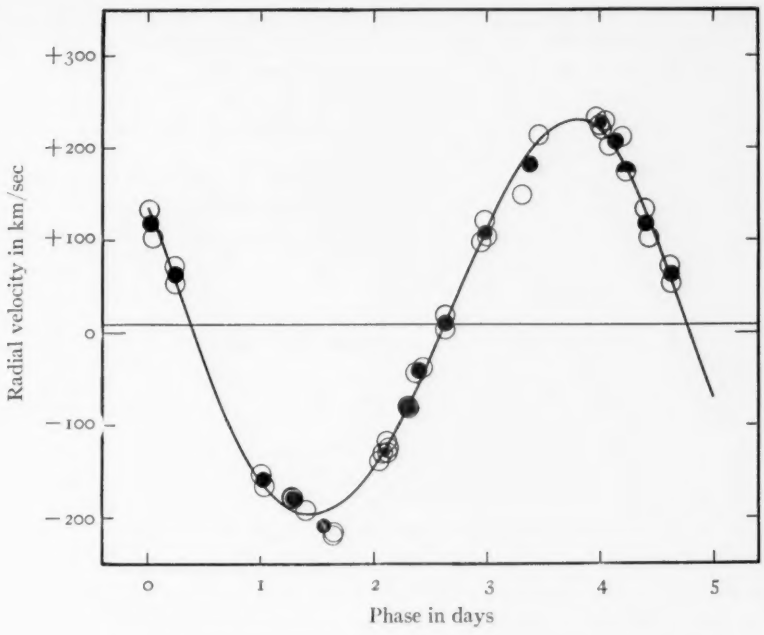

FIG. 1.—Velocity-curve of 29 Canis Majoris from absorption lines

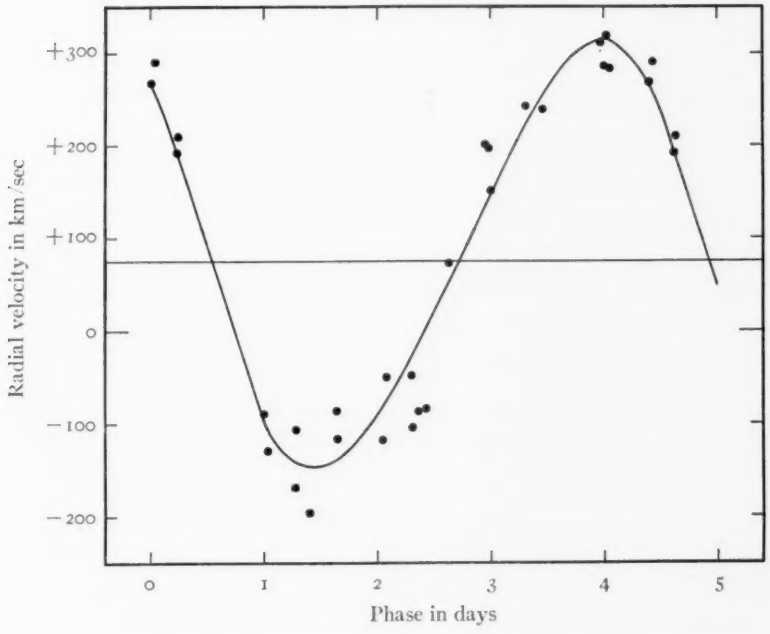

FIG. 2.—Velocity-curve of 29 Canis Majoris from emission lines

The emission lines vary in intensity and in structure. The new Process plates are so much superior to the old series of spectrograms that we have given in Table 7 a description of the lines. The large change in the intensity of the emission lines is in good accord with the preliminary account from the Yerkes plates.[9] But the most important result is unquestionably the discovery that between phases $2^d.43$ and $4^d.05$ the emission line is flanked by a P Cygni type of absorption line whose violet displacement corresponds to a velocity of expansion of about 350 km/sec. This value applies to the center of the rather broad P Cygni absorption line at *He* II 4686 for phase $4^d.00$. The existence of expansion in several normal Oe stars has been recently demonstrated by Swings and Struve,[23] and the phenomenon in 29 Canis Majoris is of a similar nature. However,

TABLE 6

ORBITAL ELEMENTS FROM EMISSION LINES

$K = 231$ km/sec	$T = 0^d.40$
$e = 0.13$	$\gamma = +75$ km/sec
$\omega = 80°$	$a \sin i = 14{,}000{,}000$ km

TABLE 7

EMISSION LINES IN 29 CANIS MAJORIS

Phase in Days	Intensity of *He* II 4686	Width of *He* II 4686	Description of *He* II 4686	Quality
0.01	10	4.6 A	Narrow, no structure	Good
1.00	12	3.5	Narrow, no structure	Good
1.40	8	5.0	Narrow, no structure	Poor
2.08	2	8.0	Very diffuse	Good
2.37	4	6.9	Very narrow central absorption	Good
2.43	7	6.8	Fairly strong narrow absorption and conspicuous P Cygni type of absorption line on violet border of emission	Good
2.98	10	4.8	Central absorption has disappeared. Broad and diffuse P Cygni absorption on violet border of emission	Good
4.00	10	6.8	No central absorption. P Cygni absorption very conspicuous, also in the two *N* III lines	Good
4.05	10	5.5	No central absorption. A very weak P Cygni absorption is still present	Good

in this spectroscopic binary it is complicated by the variation in the width and intensity of the emission lines and by the occurrence of a central absorption at phases $2^d.37$ and $2^d.43$.

One of the most remarkable results is the fact that the variations shown by the emission lines are unsymmetrical with respect to primary minimum of the light-curve. The latter occurs at phase $0^d.4$—where the lines are near maximum strength. But minimum line strength takes place at phase $2^d.08$ and definitely precedes secondary eclipse. The narrow central absorption line appears only near secondary minimum, but the P Cygni type of absorption line is present from a phase prior to secondary minimum to a phase prior to primary minimum.

It is clear that the emission lines are produced in an expanding nebulous shell. The fact that the star 29 Canis Majoris has an appreciable axial rotation[24] suggests that

[23] *Ap. J.*, **91**, 546, 1940.

[24] *Pub. Yerkes Obs.*, **7**, 293, 1939.

the expanding envelope must revolve around the more massive component in a complicated orbit. Disregarding, for the moment, self-absorption within the shell, we can take the total observed emission of the line to represent a quantity which is proportional to the total number of emitting atoms which are not obscured by the components of the binary and are not projected upon their apparent discs. The minimum intensity is not accompanied by strong absorption of the P Cygni type. Hence, it would be reasonable to conclude that at phase $2^d.0$ the obscuration by one of the two components is greatest. In that case we should expect strong absorption at the opposite point of the orbit, at phase $4^d.2$. The observations are not sufficiently numerous, but we do observe some P Cygni type absorption at phase $4^d.05$.

The nature of the red shift of the emission lines is obscure. There can be little doubt that the phenomenon is, indeed, similar to that shown by HD 193576. O. C. Wilson[25] has discussed various explanations applicable to this star. The gravitational explanation, which he favors, does not account for the observations of 29 Canis Majoris. We can also discard, with Wilson, explanations in terms of (1) motion of the star and envelope as a whole; (2) geometrical effect, such as occultation or unsymmetrical ejection; and (3) Stark effect. But Wilson's fourth suggestion, namely, that the effect is caused by absorption within the shell, is more promising. The fact that broad P Cygni absorptions are observed in 29 Canis Majoris shows that a distortion of the violet edge of the emission lines must be present. We are reminded, in this connection, of the fact that in Be stars with double emission lines the violet component is often weaker than the red component. McLaughlin's[26] qualitative interpretation of this effect involves self-absorption in a shell which expands and rotates. It should be profitable to derive the theoretical contours of the emission lines produced by such a shell. But the fundamental question—whether sufficient self-absorption can be produced within the shell—is answered by our recognition of P Cygni type of absorption lines.

YERKES OBSERVATORY
May 31, 1940

[25] *Ap. J.*, **91**, 398, 1940. [26] *Proc. Nat. Acad. Sci.*, **19**, 44, 1933.

ON THE NATURE OF THE SYSTEM OF β LYRAE

ZDENĚK KOPAL

ABSTRACT

An analysis of the photometric and spectroscopic evidence available on β Lyrae leads to the following conclusions:

1. The cB9 component is the larger, the more massive, and the more luminous of the two.

2. The mass ratio derived from the ellipticity constant is $m_2/m_1 = 0.82$ for a centrally condensed model, and $m_2/m_1 = 0.74$ for a polytrope with index $n = 1.5$. Irrespective of structure, the masses of the two components do not seem to differ greatly.

3. An approximate interpretation of the rotational effect leads to results that are consistent with the dynamical mass ratio.

4. Two sets of absolute dimensions, corresponding to two models of different density condensation, were derived. Except for the masses, there is but little difference between the two sets. The minimum combined mass of the system results in the value 95 $\odot$, making β Lyrae the most massive eclipsing system known.

5. There is no indication whatever of any motion of the apsidal line in the β Lyrae system. As a high degree of density condensation is at variance with considerations of the hydrogen content of the primary component, the orbital eccentricity of 0.0137 ± 0.0018 (p.e.) found by Rossiter appears questionable.

1. *Introduction.*—The system of β Lyrae has often been denoted as the most puzzling binary in the sky. Its variability was discovered by Goodricke in 1784, and its character as a spectroscopic binary was first recognized by Pickering in 1891. An enormous amount of photometric and spectroscopic material on this system now exists;[1] but, in spite of much laborious investigation, the many attempts to obtain a definite picture of the system have resulted in widely differing models, each of which succeeded only partly in interpreting the available evidence. The present paper originated in the writer's desire to discuss the main observational features *de novo*, in order to clarify, if possible, the nature of the ambiguities. It led to the rather unexpected conclusion that there is no necessity for any ambiguity at all and that the existing photometric and spectroscopic material can be harmonized into a model fitting all the observed features. In the following five sections the individual steps leading to this conclusion will be discussed, and the final results presented in § 7; the concluding section will contain some remarks of a more general character.

2. *Photometric evidence.*—The main photometric features of β Lyrae are well known. The light-curve displays two broad and unequally deep minima with continuous light-changes between, undoubtedly caused by the elliptical form of two components of unequal surface brightnesses revolving in a very close orbit. An orbital solution by Russell's method was first carried out by Shapley[2] on the basis of Stratonov's visual light-curve. Shapley found the solution to be largely indeterminate, which he attributed to the inaccuracy of the underlying light-curve. His opinion, however, that "from the standpoint of photometric study there is no opportunity of further advance until a good light curve is produced"[3] has not been confirmed by later investigations. Three photoelectric light-curves of β Lyrae have been produced in the past twenty-five years (Guthnick and Prager,[4] Stebbins and Huffer,[5] Smart and Green);[6] these curves have proved the reality of the irregular fluctuations of brightness, changing from one cycle to another, so that the de-

[1] Cf. *Geschichte und Literatur der veränderlichen Sterne*, **2**, 156, 1920, and Appen., **2**, 244, 1936.

[2] *Princeton Contr.*, No. 3, 1915.

[3] *Ibid.*, p. 72.

[4] *Sitzungsber. d. Preuss. Akad. d. Wiss.*, p. 222, 1917.

[5] *Washburn Obs. Pub.*, **15**, 209, 1931.

[6] *M.N.*, **95**, 644, 1935.

viations of individual observations from a mean light-curve are likely to exceed widely their accidental errors.

Another and equally serious source of difficulty is inherent in the method employed in computing the orbit. First, the interval between minima being comparatively short, it is difficult to determine the values of the ellipticity and reflection constants with the desired accuracy; and any error of the rectification constants will naturally jeopardize the true form of the light-curve within minima, which serves for the derivation of the geometrical elements. In addition, both components are not likely to be of the same geometrical form, and in such cases the rectification does not render the light-curve strictly similar to one produced by two spherical components. Finally, the Russell-Shapley method as developed thus far fails to take account of the proper distribution of brightness over the eclipsed disk. Both components of the β Lyrae system appear to be strongly distorted. In such cases, in addition to normal limb darkening, the surface brightness varies proportionally to the local gravity, and the system of isophotes will then depend on the phase as well as on the inclination of the axis of rotation to the line of sight; in particular, it will generally be unsymmetrical with respect to the geometrical center of the disk. As long as methods for computing orbital elements from light-curves are not sufficiently refined to meet these requirements, any results obtained for close pairs, such as β Lyrae, can be regarded merely as a first approximation—no matter how accurate the underlying light-curve may be.

The light-curve which will be adopted in § 4 for the purposes of the present investigation is that by Danjon.[7] It is based on 211 observations, 1923–1926, with a Pickering photometer and a Wratten No. 21 filter which specifies the effective wave length to about λ 5780.

3. *Spectroscopic evidence.*—The complexity of the spectroscopic evidence has largely contributed toward making the system of β Lyrae so puzzling. Its spectrum is composite: on a perfectly normal spectrum, now classified as cB9, is superposed a most remarkable spectrum resembling class B5 but exhibiting a number of peculiar characteristics.[8] The B9 lines display a variable radial velocity and lend themselves to the derivation of the spectroscopic orbit. The B5 lines, however, show practically no periodic variation and give average velocities some 50 km/sec more negative than the velocity of the center of mass of the system determined from the B9 lines. This, coupled with the generally abnormal appearance of the B5 spectrum, recently led Struve to advance the idea that the B5 spectrum originates not in the reversing layer of any star but in an expanding shell of gas in which the whole system is imbedded.[9] His hypothesis is doubtless correct. It enabled him to explain a series of anomalous features of the B5 spectrum, the details of which—however interesting—are of but secondary importance for the dynamics of the system, which is the primary objective of this study. From the dynamical point of view β Lyrae is a typical single-spectrum binary whose spectroscopic elements, unlike the photometric ones, are very accurately established, notably by the work of Rossiter.[10]

Spectroscopic observations have brought out two features of fundamental importance. First, as has been pointed out by Stratton, the B9 lines are visible in nearly unchanged intensity throughout the whole cycle. This was doubted by Struve, but it appears to be established in a recent study by Baker,[11] who found the B9 spectrum clearly visible and without any conspicuous fall in intensity on a spectrogram taken little more than one hour (phase angle 1°.4) before primary minimum. Second, Rossiter found that the B9 lines exhibit a rotational effect at the time of primary minimum. These two indications, coupled with the photometric evidence that both components are probably very unequal

[7] *Strasbourg Ann.*, **2**, Part 1, 1928.

[8] Cf., e.g., Struve, *Observatory*, **57**, 265, 1934.

[9] *Ibid.*

[10] *Michigan Pub.*, **5**, No. 6, 1933.

[11] *Harvard Ann.*, **105**, 107, 1937.

in size and that the eclipses must be almost grazing, lead unmistakably to the following conclusions: (*a*) The B9 component is the larger one and is eclipsed at primary minimum.[12] (*b*) The invisible companion must be smaller in size and of a lower effective temperature. The second point is a logical consequence of the fact that in the primary minimum the component with higher surface brightness (and therefore higher temperature) must be eclipsed. Colorimetric measurements by several investigators (Schwarzschild, Danjon, Schneller) have confirmed the increase of the color index during the primary minimum in accordance with expectations.

The scheme presented by the two foregoing points is contrary to almost all the models devised thus far on the basis of the light-curves alone; but in § 2 we have listed the reasons why, under present conditions, any photometric solution must be highly ambiguous. We proceed now to examine whether the above picture, suggested so strongly by the spectroscopic evidence, is really at variance with the photometric results or whether the two pieces of evidence can be harmonized.

4. *A model of the system.*—According to Danjon, the fractional rectified intensity of the system at the time of secondary minimum is 0.88. The secondary eclipse being total or nearly total, this must be equal to the luminosity of the primary. Thus,

$$\frac{L_2}{L_1} = 0.136 \; ; \tag{1}$$

and, owing to the ratio of surface brightnesses,

$$\frac{J_1}{J_2} = 3.0 \, , \tag{2}$$

obtained from the rectified depths of both minima (anticipating the degree of darkening of the primary to be about 0.5), we have

$$k^2 = \left(\frac{r_2}{r_1}\right)^2 = \frac{J_1}{J_2} \cdot \frac{L_2}{L_1} \, .$$

Hence,[13]

$$k = 0.62 \, . \tag{3}$$

With the aid of the above ratio of surface brightnesses, the temperature of the secondary component can be estimated. If we adopt $T_1 = 11{,}300°$ and $\lambda_{\text{eff}} = 5780$, Planck's formula yields $T_2 = 7700°$.

[12] Struve attempted (*op. cit.*) to consider a second B9 component as the eclipsing star at primary minimum. However, even if its ellipsoidal form and all the possible implications arising therefrom are taken into account, one cannot see what could evoke the observed rotational effect in this case.

[13] Danjon (*op. cit.*, p. 138) suggested an interesting way of inferring the ratio of the radii from changes of the color index in both minima and obtained a somewhat lower value of k than ours. However, it must be pointed out that the underlying color indices are still highly uncertain. More recently, a series of photoelectric color indices of β Lyrae has been published by Schneller (*Berlin-Babelsberg Kl. Ver.*, No. 17, 1936). While showing a marked color-index variation at the time of primary minimum, the series failed to establish any evidence of variation at secondary minimum and so failed to provide us with a basis for a colorimetric determination of k.

The radii and inclination are then obtained under the assumption of grazing eclipses from

$$\left.\begin{aligned} a_1^2(1 - z_g \cos^2 \psi')(1 + k)^2 &= \cos^2 i \cdot \cos^2 \psi' + \sin^2 \psi \,, \\ a_1^2(1 - z_g)(1 - k)^2 &= \cos^2 i \,, \end{aligned}\right\} \tag{4}$$

and

$$a_2 = k \cdot a_1 \,,$$

where $a_{1,2}$ are the semimajor axes of the two components (expressed in terms of the orbital radius as unity), i is the angle of inclination, ψ' the phase angle at the first contact, and z_g $(= \epsilon^2 \sin^2 i)$ the geometrical ellipticity of the primary.

The determination of the first contact is somewhat difficult, as the continuous light-changes do not make it evident where the eclipse sets in. In such cases determination of ψ' may largely depend upon the adopted rectification constants. However, in the case of β Lyrae the beginning of the eclipse is independently indicated by the appearance of the rotational effect. Rossiter estimated its semiduration at $1^d.6$, which agrees very closely with Danjon's value of $1^d.75$ ($\psi' = 49°$). At the beginning of the eclipse the rotational effect is necessarily small and is more likely to escape attention; the photometric value is probably more correct and therefore will be adopted. The close agreement between the two reflects favorably on the correctness of Danjon's rectification constants.

The last factor deserving our attention is z_g. Let us suppose, for a moment, that the geometrical form of both components is the same. Observations supply us with the value of the *optical* ellipticity of the system which is twice the coefficient of $\cos^2 \psi$. For β Lyrae, according to Danjon,

$$z_o = 0.415 \,. \tag{5}$$

The theory shows[14] that the ratio of optical to geometrical ellipticities is

$$\frac{z_o}{z_g} = \frac{15 + u}{5(3 - u)} \left\{ 1 + \frac{\tau}{4} \left(\frac{5}{\Delta_2} - 1 \right) \right\} , \tag{6}$$

where u is the coefficient of limb darkening,

$$\tau = \frac{1}{4} \frac{c_2}{\lambda T (1 - e^{-c_2/\lambda T})} \,,$$

and Δ_2 is a constant depending on the internal structure.[15] The term outside of the braces in (6) represents the effect of limb darkening, while the second term in brackets takes account of the gravity effect.

The system of β Lyrae does not lend itself to an empirical determination of the limb darkening. However, the hypothesis of a constant, continuous absorption coefficient (closely compatible with reality as far as the present observational evidence goes) leads

[14] See the writer's forthcoming paper in *Ann. New York Acad. Sci.*, **40**, 1940 (Harv. Reprints, No. 211).

[15] For its definition, cf., e.g., Chandrasekhar, *M.N.*, **93**, 453, 1933.

to $u = 0.5$, which can be safely adopted. Furthermore, if we insert $\Delta_2 = 1$ (pronounced central condensation) and the appropriate temperature and wave length, we find that

$$\frac{z_0}{z_g} = 2.0\,, \tag{6.1}$$

that is, that the limb darkening and gravity effect combined just double the geometrical ellipticity of the components. Therefore,

$$z_g = 0.21\,; \tag{5.1}$$

if we insert this value in equation (4) and solve the equations, we obtain

$$\left.\begin{aligned} a_1 &= 0.50\,, \\ a_2 &= 0.31\,, \\ i &= 80^\circ.4\,. \end{aligned}\right\} \tag{7}$$

Thus, a model in which the primary (B9) component is the larger one is found to be perfectly consistent with photometric evidence. The alternative model (B9 being the smaller) can satisfy the observed light-changes nearly equally well but is definitely at variance with the spectroscopic evidence. Apart from the latter, there are also some purely photometric indications favoring the model proposed above. One such consideration concerns the reflection effect. Were the secondary component the larger one (as in Danjon's model), the theoretical reflection constant at λ 5780 should be $s = 0.06$, while, according to Danjon, it amounts to only about $s = 0.01 \pm 0.01$. The theoretical value corresponding to our model, $s = 0.02$, is not inconsistent with the observations. Furthermore, if analogy can be any guide, in all eclipsing systems similar in some respects to β Lyrae (V Puppis, VV Orionis, SZ Camelopardalis, etc.), the primary component is the larger one.

The final and most important consideration is the visibility of the secondary's spectrum. According to all models in which the low-temperature component exceeds its companion in size, the total luminosity of both components should be nearly the same, or the secondary should be even more luminous than the B9 component (Danjon). But this would leave us with the puzzling question why the lines of the secondary's spectrum (displaying velocity changes synchronous with the orbit) are invisible. The model proposed in the present paper removes this difficulty altogether. With the ratio of the radii and with the temperatures derived above, both components should differ in their total brightness by 2.7 mag. during full light, and the difference should decrease only to 2.2 mag. at mid-eclipse during primary minimum. Yet, it is well known that a difference of only 1 mag. is sufficient to extinguish all traces of the lines of the fainter star in the combined spectrum. Thus, the absence of the secondary's spectrum in β Lyrae is in agreement with the proposed general properties of the system and could have been expected.

5. *Mass ratio.*—The invisibility of the secondary's lines prohibits determination of the mass ratio of the two components from the semiamplitudes of their radial velocities. However, in the case of β Lyrae, as well as in many other single-spectrum eclipsing binaries that are not too widely separated, the mass ratio can be otherwise obtained. If the secondary's luminosity is smaller than, say, four-tenths of the primary's (which corresponds to the difference of 1 mag.), its mass can, nevertheless, be sufficient to distort the primary tidally and in this way to generate an observable phase effect, a measure of which is the well-known ellipticity constant.

The theoretical value of the proper ellipticity effect, varying as $\cos^2\psi$, is [16]

$$\left.\begin{aligned} z = {}& \tfrac{3}{5}\sin^2 i \sum_{i=1}^{2} \frac{15+u_i}{3-u_i}\left[\Delta_2 + \frac{\tau_i}{4}(5-\Delta_2)\right] L_i \frac{m_j}{m_i} r_i^3 \\ & + \tfrac{1}{4}\tfrac{5}{2}\sin^2 i \sum_{i=1}^{2} \frac{1-u_i}{3-u_i}\left[\Delta_4 + \frac{\tau_i}{4}(9-3\Delta_4)\right] L_i \frac{m_j}{m_i} r_i^5 + \dots . \end{aligned}\right\} \quad (8)$$

while the reflection effect generates also a term varying as $\cos^2\psi$, which, approximately (for $i = 90°$), takes the form[16]

$$z_r = \sum_{i=1}^{2} L_i r_j^2 \left(\frac{T_j}{T_i}\right)^4 \{0.185 + 0.75 r_i + 0.94 r_i^2 + \dots .\} , \quad (9)$$

where m_j/m_i denotes the mass ratio and r_i is the radius of a sphere having the same volume as the distorted ellipsoid. In our case we can put, with sufficient accuracy,

$$r_i^3 = a_i^3 (1 - z_0) . \quad (10)$$

Equations (8) and (9) are correct as far as terms of the order of r^5 and r^4, respectively, are concerned.

The theoretical ellipticity and reflection coefficients of $\cos^2\psi$ differ in sign; therefore, if z_0 is the observed (optical) ellipticity constant, z_r is to be *added*, in order to obtain the proper ellipticity effect, z, as defined by equation (8).

For β Lyrae we have $z_0 = 0.415$ (Danjon), and we find $z_r = 0.043$. Therefore, $z = 0.458$. The only unknown quantities in (8) are the mass ratio and Δ_2, Δ_4, etc. These constants, specifying the internal structure, converge rapidly to unity with increasing density condensation, so that, if the latter is not smaller than that of a polytrope—say, $n = 2.5$—we may put $\Delta_2 = \Delta_4 = 1$. If so, equation (8) can be used for evaluating the mass ratio necessary to produce the observed tidal effect. Explicitly it takes the form

$$0.530 \frac{m_2}{m_1} + 0.019 \frac{m_1}{m_2} = 0.458 . \quad (8.1)$$

This is a quadratic equation the roots of which are

$$\frac{m_2}{m_1} = 0.82 ; \qquad \frac{m_2}{m_1} = 0.04 .$$

The physical significance of the two roots is simple. If the first root is the true one, both components are moderately distorted and the primary is responsible for the main part of the observed ellipticity. The second root would imply that most of the observed ellipticity is due to the secondary; but in this case the distortion of the latter would have to be enormous—probably beyond the limit of its stability. In addition, a mass ratio of $m_2/m_1 = 0.04$, combined with the spectroscopic mass function of $8.32\ \odot$ (Rossiter), would lead to illusory masses for the individual components. There is, therefore, no room

[16] For its derivation see the writer's forthcoming paper in *Ann. New York Acad. Sci.*

for doubt that the former root is the true one—provided only that the adopted model holds good.

Recent investigations on the ellipticities and apsidal motions of some representative eclipsing systems have shown that stellar density condensations are generally high. Exception has been noted only in the behavior of some very massive systems (e.g., V Puppis), the central condensations of which are probably lower than those of genuine main-sequence stars. As β Lyrae is probably a very massive system, it seems desirable to evaluate its mass ratio for still another model—one of lower density condensation, in order to see the extent of the uncertainty arising from our ignorance of the true model. Let us take, say, the polytrope $n = 1.5$, for which $\Delta_2 = 1.2892$, $\Delta_4 = 1.0562$. Equation (8) then takes the form

$$0.585 \frac{m_2}{m_1} + 0.021 \frac{m_1}{m_2} = 0.458 , \tag{8.2}$$

and its roots are

$$\frac{m_2}{m_1} = 0.74 ; \qquad \frac{m_2}{m_1} = 0.05 .$$

As we should expect, the first root is, in this case, farther from, and the second nearer to, unity than for the former model, for it is well known that ellipticity increases with diminishing density condensation, and a less massive secondary is then able to produce the same effect. But we see that the uncertainty arising from our ignorance of the true model is not large; a transition from an infinite density condensation to that of the polytrope $n = 1.5$ ($\rho_c/\bar{\rho} = 5.9907$) changes the mass ratio from 0.82 to 0.74. *Thus, despite an apparent inequality in brightness, the masses of the components of β Lyrae cannot be very different.*

Elements of the single-spectrum orbit of the B9 component have been very accurately derived by Rossiter.[17] Those which interest us most are

$$a_1 \sin i = 32.6 \cdot 10^6 \text{ km} ,$$

and

$$\frac{m_2^3 \sin^3 i}{(m_1 + m_2)^2} = 8.32 \odot .$$

Inserting the inclination $i = 80°.4$ and the foregoing mass ratios, we find

I. $5 > n > 3$:	II. $n = 1.5$:
$m_1 = 52.2 \odot$	$m_1 = 64.7 \odot$
$m_2 = 42.8 \odot$	$m_2 = 47.9 \odot$
$(a_1 + a_2) = 73.4 \cdot 10^6$ km	$(a_1 + a_2) = 77.7 \cdot 10^6$ km

where a_1 and a_2 denote the semimajor axes of the orbits of the two components. We note that, given the ellipticity constant and the mass function, the lower the density condensation, the larger and more massive is the system. Under these conditions the centrally condensed model yields the minimum possible masses and dimensions.

[17] *Op. cit.*

6. *Rotational effect.*—The interpretation of the rotational effect appears to be another way of determining the absolute dimensions and hence the mass ratios in single-spectrum eclipsing systems. This method is less general than that based on the ellipticities, for it involves the assumption that an eclipsed star rotates in the same period as the system revolves, whereas the method based on the ellipticities is free from this assumption, under certain conditions at least.[18] In the system of β Lyrae, however, the powerful tidal interaction between the two components makes synchronism between rotation and revolution very probable, and we may thus expect that both methods will lead to concordant results.

The system of β Lyrae was the first system in which the rotational effect was discovered.[19] Rossiter found that it reaches its maximum of 13 km/sec at phase $\pm 1^d0$ ($\psi = \pm 27°.8$). The relation between the observed rotational effect, V_r, and the equatorial velocity, V_{eq}, is

$$V_r = V_{eq} \cdot F \cdot \sin i ,$$

where F, the rotation factor, is the mean value of the rotational component in the line of sight, averaged over the portion of the eclipsed star visible at the corresponding phase. The value of F obviously depends on the distribution of brightness over the surface of the eclipsed star, and its exact calculation would no doubt be very difficult. In order to get merely an idea whether the observed rotational effect is compatible with the mass ratio derived in the preceding paragraph, we introduce the following simplifications: (*a*) the eclipsed star shall be spherical (with a radius equal to the geometrical mean of the three actual semiaxes); (*b*) its disk shall be uniformly bright. For this case, analytical formulae were recently set up by Petrie,[20] giving F as a function of the geometrical elements. Using them, we find $F = 0.14$, which yields $V_{eq} = 94$ km/sec. If the primary rotates with Kepler angular velocity, then $r_1 = 1.7 \times 10^7$ km. But in § 5 (eq. 10) we found that $r_1 = 0.46$ of the orbital radius. Hence, the latter would be equal to $3.8 \cdot 10^7$ km, which is of the expected order of magnitude but is less than we found in § 5, by a factor of about 2. However, it must be remembered that F, calculated under the assumption of uniform disks, is the maximum possible value, leading consequently to minimum dimensions. Also, the area eclipsed at $\psi = 27°.8$ is comparatively small, and consequently a small error in the adopted geometrical elements can largely affect the computed equatorial velocity. Whether these circumstances can explain the whole discrepancy is difficult to assert, but the possibility is by no means excluded. An approximate graphical solution, carried out by Danjon for his model, indicates that the limb darkening itself can account for a factor of about 1.6. A detailed analysis, taking account of the actual distribution of brightness over the visible portion of the eclipsed primary, seems too laborious to be expedient. However, the above result shows at least that the observed rotational effect is approximately of the expected magnitude.

7. *Absolute dimensions.*—Had the rotational effect fixed the absolute scale of the system, the ellipticity constant could have been used for the determination of the internal

[18] That is, provided that the period of free oscillation of either component is shorter than that of a forced oscillation (equal to the orbital period). The free period of a gaseous sphere is (cf., e.g., Emden, *Gaskugeln*, p. 451, 1907), approximately

$$P_{free} = 11{,}897 \sqrt{\frac{1}{m \cdot \bar{\rho}}} \text{ seconds} ,$$

where $\bar{\rho}$ is the mean density and m the mode of oscillation. For the first-order tidal deformation, $m = 2$. In the system of β Lyrae the primary component is the one of lower density; inserting $\bar{\rho}_1 = 0.0008$ gm/cm^3 (cf. § 7), we find $P_{free} = 3^d4$, while $P_{forced} = 12^d9$. Therefore, the inequality $P_{free} \ll P_{forced}$ is amply fulfilled for the B9 component and all the more so for the secondary.

[19] Rossiter, *Ap. J.*, **60**, 15, 1924.

[20] *Pub. Dom. Ap. Obs., Victoria*, **7**, No. 6, 1938.

structure, and the system could thus have been completely specified without knowledge of the secondary's spectrum. However, this was not the case, and the density condensation of β Lyrae remains unknown. In the following listings, two sets of absolute dimensions of the system are given, one derived under the assumption of a centrally condensed model (polytropic index $5 > n > 3$), the other for a polytrope of $n = 1.5$.

I:

$m_1 = 52.2 \odot$ $\quad m_2 = 42.8 \odot$

$a_1 = 53 \odot$ $\quad a_2 = 33 \odot$

$b_1 = 46 \odot$ $\quad b_2 = 31 \odot$

$c_1 = 41 \odot$ $\quad c_2 = 30 \odot$

$\bar{\rho}_1 = 0.00052 \odot$ $\quad \bar{\rho}_2 = 0.00139 \odot$

Orbital radius $= 73.4 \times 10^6$ km

II:

$m_1 = 64.7 \odot$ $\quad m_2 = 47.9 \odot$

$a_1 = 56 \odot$ $\quad a_2 = 35 \odot$

$b_1 = 48 \odot$ $\quad b_2 = 32 \odot$

$c_1 = 41 \odot$ $\quad c_2 = 31 \odot$

$\rho_1 = 0.00059 \odot$ $\quad \bar{\rho}_2 = 0.00138 \odot$

Orbital radius $= 77.7 \times 10^6$ km

The relative dimensions and the form of the components of β Lyrae and their orbit, as seen from the earth, are graphically exhibited in Figure 1. The diagonal cross ($\times$) in-

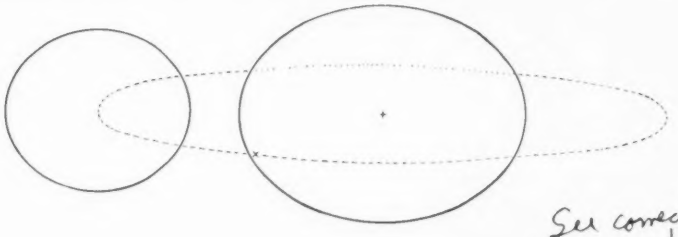

FIG. 1.—The system of β Lyrae

See correction, p. 368 this volume

dicates the position of the secondary's center at the moment of maximum rotational effect. The open circle in the lower right-hand corner represents the proportional size of the sun.

The absolute bolometric magnitudes of the components are practically the same in both cases: $M_1 = -6^m.6$, $M_2 = -4^m.0$. The primary component (B9 supergiant) is found to conform to the empirical mass-luminosity law as closely as could be expected; but the luminosity of the secondary seems to be too low for its mass. It is possible to make both components fit the mass-luminosity law by a further decrease in their density

condensations; but in so doing, we may depart too much from the absolute dimensions set by the rotational effect. It is also questionable whether the effort to bring both components into agreement with the mass-luminosity law has much meaning. In particular, it is uncertain whether the effective temperature of 7700°, derived from the surface brightness in the vicinity of λ 5780, is a correct measure of the total energy output of the secondary component. Its radiation, on the other hand, seems to be intense enough to excite the lines of a B5 spectrum in the envelope—a fact plainly at variance with a low effective temperature.[21] It is probable, as was suggested by Struve, that while the primary component of β Lyrae is a perfectly normal star, the secondary is an abnormal "yellow" B star, the total radiation of which is not completely specified by its surface brightness at a single particular wave length.

8. *Concluding remarks.*—At the conclusion of the present survey of the β Lyrae system two considerations of a dynamical nature may be mentioned. The presence of stationary lines in its composite spectrum points to the existence of a gaseous envelope in which the components revolve. Such a resisting medium must produce perturbations of all the orbital elements except the node and the inclination; but only the perturbations of the orbital period have any chance of being detected. The theory of orbits shows that the resisting medium causes a secular acceleration of the orbital period (in addition to periodic terms), at a rate depending on the resistance. Actually, the period of β Lyrae has been lengthening all the time, by about 9.38 seconds a year. The nature of a perturbing function which can give rise to the observed increase is still quite obscure;[22] but it seems certain that the effect of the resisting medium must be smaller than that—a circumstance which may lead to an estimate of the limiting density of the envelope.

[21] The question whether it is the secondary component which is responsible for the excitation of the lines of the envelope admits of a simple and crucial test. In the preceding paragraphs we have seen that the secondary is undoubtedly much smaller than its more luminous companion and that its eclipse is total or nearly total. Therefore, during the time of the secondary minimum a large section of the envelope between the giant primary and us should be in the shadow of the primary star and hence cut off from the source of excitation. The envelope lines should consequently display marked decrease in intensity during the secondary minimum, while remaining nearly unchanged throughout the rest of the cycle. So far, the only study of the variations of the line intensities of the envelope appears to be that by Baker (*op. cit.*). He has, indeed, established some evidence that certain stationary lines, presumably originating in the envelope (such as *He* I 3888 or 4471), show the expected decrease in intensity, while others (such as *He* I 3613 or 4387) seem to disappear altogether during secondary minimum. However, considerably more material will be required to give a definite picture of the actual, rather complicated, state of affairs.

Note added in proof.—The writer is indebted to Professor Struve for calling his attention to the fact that the decrease in intensity of the emission envelope lines at the time of secondary minimum has already been established by Miss Maury (*Harvard Ann.*, **84**, 207, 1933). So our suggestion that the secondary component is responsible for the excitation of envelope lines appears substantiated.

[22] A secular increase in the orbital period might tentatively be explained by a secular decrease of mass. Owing to the well-known integral $P \cdot m^2 = \text{const}$ (where m is the combined mass of the system; cf. Jeans, *Astronomy and Cosmogony*, p. 293, 1928), we would put $dP/P = -2\,dm/m$ and calculate from the observed value of dP/P the secular loss of mass. In the case of β Lyrae this suggestion seems strengthened by the fact that spectroscopic observations show that the envelope matter exhibiting B5 lines is constantly streaming outward, with a velocity of some 50 km/sec relative to the center of mass of the system. Nevertheless, this explanation seems to fail at the very outset.

The parabolic velocity of escape is generally given by $V_e^2 = 2G \cdot m/R$, where G is the gravitational constant. Now we have seen that, approximately, $m = 100\odot$, while R, the distance of streaming matter from the center of mass of the system, will certainly not be larger than, say, the radius of the orbit. Inserting these values in the above formula, we find $V_e = 600$ km/sec, which is more than ten times as large as the observed velocity of the expanding shell. Therefore, no matter moving with velocities actually observed can be lost, and after some time the excited atoms emitting B5 lines must inevitably fall back. The fact that these atoms radiate only during levitation strongly suggests radiation pressure.

The system does, of course, lose matter by radiation. The total energy output of β Lyrae is, according to our picture, about 33,000 times larger than that of our sun, i.e., about 1.25×10^{38} erg/sec, or, converted into matter, 1.39×10^{17} gm/sec. Thus, $dm/m = -7.76 \times 10^{-13}$ per cycle, which would correspond to a period increase $dP/P = 1.55 \times 10^{-12}$. In reality, however, $dP/P = 2.97 \times 10^{-7}$; i.e., the period of β Lyrae actually increases about 100,000 times more rapidly than loss of matter by radiation alone would permit.

Another consideration of some interest is the apsidal motion in the β Lyrae system. Rossiter, analyzing his extensive spectroscopic material, found the small but significant orbital eccentricity $e = 0.0137 \pm 0.0018$ (p. e.) and longitude of periastron $\omega = 325°$. The latter seems to have been constant within the interval 1907–1921 (Rossiter) and probably even from 1892 (Tichov,[23] Belopolsky,[24] Stein[25]). Moreover, Baker's velocity-curve,[26] derived from Tremblot's spectrograms taken in 1934, agrees so closely with that by Rossiter that there is certainly no indication of any change in ω up to 1934. But, unless the internal density condensation of both components is infinite, a stationary apsidal line is a dynamical impossibility. An application of Sterne's formula to the model developed in the preceding paragraphs leads to the following theoretically expected rate of apsidal motion:

n	P/U	$\Delta\omega$ per Cycle	U
1.5	0.0784	+28°.2	165 days
3	.00850	3.06	4.17 years
4	0.00073	+ 0.26	48.5 years

where U denotes the period of revolution of the apsidal line.

In addition, apsidal revolution should invoke an apparent inequality of the orbital period of the form

$$a \cdot \sin (b \cdot E + c) ,$$

where E is the epoch, c the longitude of periastron at $E = 0$, and

$$a = \frac{e}{\pi} \cdot P = 0.056 \pm 0.007 \text{ (p.e.)}$$

$$b = 360 \cdot \frac{P}{U} .$$

Spectroscopic observations cover an interval of more than forty years, while photometric observations extend over about one and one-half centuries. Neither method, however, has established the slightest evidence of any of the observable consequences of apsidal motion.

An indirect indication of stellar density condensations may be obtained from the study of the hydrogen content of the stars. Chandrasekhar[27] has recently generalized the procedure of calculating the hydrogen content for any degree of central condensation, and his method can be applied to the present case. The procedure need not be repeated here;[28] since it also involves a knowledge of the luminosity, it can thus far be safely applied only to the primary (B9) component of β Lyrae. The guillotine factor (related to the photoelectric absorption) is sensibly equal to 1; electron scattering decreases its "effective" value to slightly below unity. If X_0 denotes the percentage of hydrogen content (by

[23] *Mem. Soc. spett. ital.*, **26**, 107, 1897.

[24] *Ap. J.*, **6**, 328, 1897.

[25] *Proc. Acad. Amsterdam*, **10**, 459, 1908.

[26] *Loc. cit.*

[27] *M.N.*, **96**, 647, 1936.

[28] Cf. Chandrasekhar, *Introduction to the Study of Stellar Structure*, pp. 292–320, Chicago, 1939.

weight), and ξ^* is the radius of a volume containing 90 per cent of the total mass and is expressed in terms of the stellar radius as unity, we obtain the following results:

X_0	ξ^*	X_0	ξ^*
0.10	0.81	0.60	0.68
.20	.78	.70	.67
.30	.75	.80	.67
.40	.72	0.90	0.68
0.50	0.70		

It has already been noted by Chandrasekhar[29] that for massive B stars the hydrogen content depends largely on ξ^*. In the present case the range of possible values of ξ^* shows that, no matter what is the true hydrogen content of β Lyrae A, its density condensation must be weak if the "astronomical" and "physical" opacities are to be reconciled at all.

The range $0.81 > \xi^* > 0.67$ corresponds, very approximately, to variation of the polytropic index n within the limits $1 < n < 2$. But we have already seen that for $n = 1.5$ (which can be considered as the mean) the revolution of the apsidal line would be completed in about thirteen cycles ($U = 165$ days).[30] Consequently, any determination of the longitude of periastron from observations distributed over an interval long compared with U would be meaningless, and the ω's derived from such a series of observations should be distributed at random. Rossiter's results, however, do not indicate this. He divided his whole series into seven intervals of approximately two years each, and the individual ω's for each interval came out remarkably concordant. This agreement as it stands would seem to disprove the possibility of rapid apsidal progression. Thus, we find ourselves faced with two alternatives. Either the density condensations of the components of β Lyrae are indeed extremely high ($n \gg 4.5$) and the period of apsidal revolution is of the order of several hundred years at least, as Rossiter's measurements seem to indicate (but in this case no possible hydrogen admixture can bring the "astronomical" and "physical" opacities into agreement); or, alternatively, the density condensation of β Lyrae A at least is low, as the theory of hydrogen content indicates (but in this case the orbital eccentricity and the longitudes of periastron as derived by Rossiter could not be real). It is possible—and, in fact, quite likely—that in such close systems as β Lyrae the velocity-curve will suffer deformations arising from the non-uniform distribution of brightness over the distorted surfaces of the two components, and such deformations might be interpreted formally as spurious eccentricity. Whether or not the eccentricity found by Rossiter for β Lyrae can be quantitatively accounted for in this way cannot be decided at the moment; but, as long as there is no more convincing evidence to the contrary, the orbital eccentricity of β Lyrae should be considered as questionable.

In conclusion, the writer takes pleasure in expressing his indebtedness to Mr. James G. Baker for stimulating discussions on some aspects of the problems connected with the system of β Lyrae.

HARVARD COLLEGE OBSERVATORY
June 1940[31]

[29] *Op. cit.*

[30] It is interesting to note in this connection that, according to Danjon (*op. cit.*, pp. 122–127), both maxima are not constantly of the same brightness, but the greatest height of one maximum changes periodically and inversely with respect to that of the other maximum. Danjon finds that the amplitude of these fluctuations is $0^m.1$ and their period 157 days, which is remarkably close to the period of apsidal revolution when n is in the vicinity of 1.5.

[31] The manuscript was received by the editors on August 5, 1940.

THE SPECTRUM OF β LYRAE

OTTO STRUVE

ABSTRACT

The system of β Lyrae consists of a normal B9 giant of lower luminosity than β Orionis. Those of its absorption lines which are not associated with emission lines from a nebula change little in intensity outside of eclipse. But those absorption lines which are associated with emission are weak and variable in intensity.

The B5 absorption lines come from a nebula which has a condensation 29° after principal minimum. Dilution effects place the average distance of the nebula at about twice the radius of the B9 star from the latter's surface. The constancy of the normal B9 lines implies that the continuous absorption of the nebula has little effect upon the formation of these lines, and this is interpreted to mean that the nebula is a ring in the equatorial plane of the B9 star, not a complete shell.

During principal eclipse the B9 star is eclipsed by a smaller star, so that the lines of the B9 star remain visible. Satellites appear on the red side before central eclipse and on the violet side after central eclipse. These satellites show less dilution than does the B5 spectrum of the ring, and the outflowing stream corresponds to a hotter temperature than the inflowing stream. The violet satellites are interpreted as a stream flowing from the B9 star, along that side of the invisible second component which becomes uncovered after minimum light. A part of the stream forms an expanding ring, while another part flows around the invisible component and returns to the B9 star, giving rise to the red satellites.

The emission lines show a rotational velocity of more than 300 km/sec, and their changes in structure and intensity agree with the proposed picture of β Lyrae.

THE PROBLEM

Although β Lyrae has been known as a variable star since 1784 and although its spectrum has been investigated more minutely than that of any other star, the physical nature of this remarkable and unique object has not yet been fully explained. The spectrum consists, essentially, of three distinct sources: (1) a normal giant-type absorption spectrum of class B9, which shows a regular variation in velocity with a range of 367 km/sec and which is identified with that component of the binary system which is obscured at primary eclipse; (2) an abnormal absorption spectrum resembling spectral class B2 or B5, varying in intensity but showing little or no variation in velocity during the 12.9-day cycle of the binary; and (3) an emission spectrum of variable intensity, corresponding to the B5 absorption lines and consisting of very broad emission bands which have been suspected by some, but not by all, observers to vary in a peculiar manner in wave length or in radial velocity.

Several years ago I suggested[1] that, contrary to the then commonly held opinion, the B5 absorption lines do not represent the spectrum of that component of the binary which is in front at primary minimum but are produced in an expanding nebulous mass of gas between the B9 component and the observer. This conclusion has since been confirmed by J. G. Baker,[2] whose measurements of the radial velocities of the strong ultraviolet *He* I lines leave no doubt that the phenomenon of the B5 spectrum is essentially similar to that of P Cygni–type absorption.

This advance in the interpretation of β Lyrae promised within a short time to dispose of the many mysterious changes and peculiarities in the spectrum which had been described by previous investigators.[3] However, in spite of several attempts, no important advance has been announced in recent years, and the variation of the B5 lines in in-

[1] *Observatory*, **57**, 265, 1934. [2] *Harvard Ann.*, **105**, 107, 1937.

[3] R. H. Curtiss, *Pub. Allegheny Obs.*, **2**, 73, 1911; F. E. Baxandall and F. J. M. Stratton, *Ann. Sol. Phys. Obs.* (Cambridge), **7**, Part I, 1930; A. C. Maury, *Harvard Ann.*, **84**, 207, 1933; R. A. Rossiter, *Pub. Obs. U. of Michigan*, **5**, No. 6, 1933.

PLATE VII

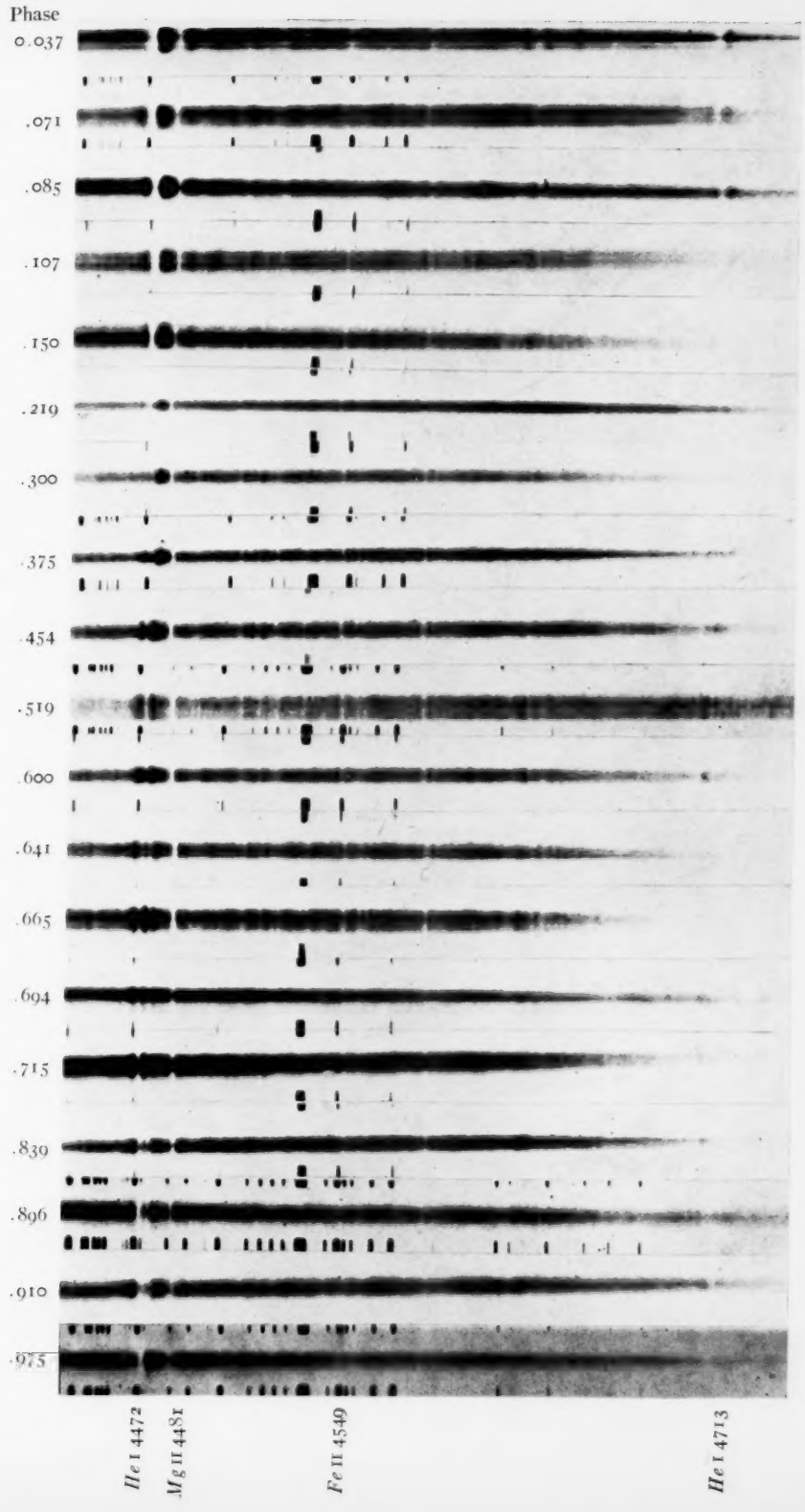

UNIV. OF MICH.

PLATE VIII

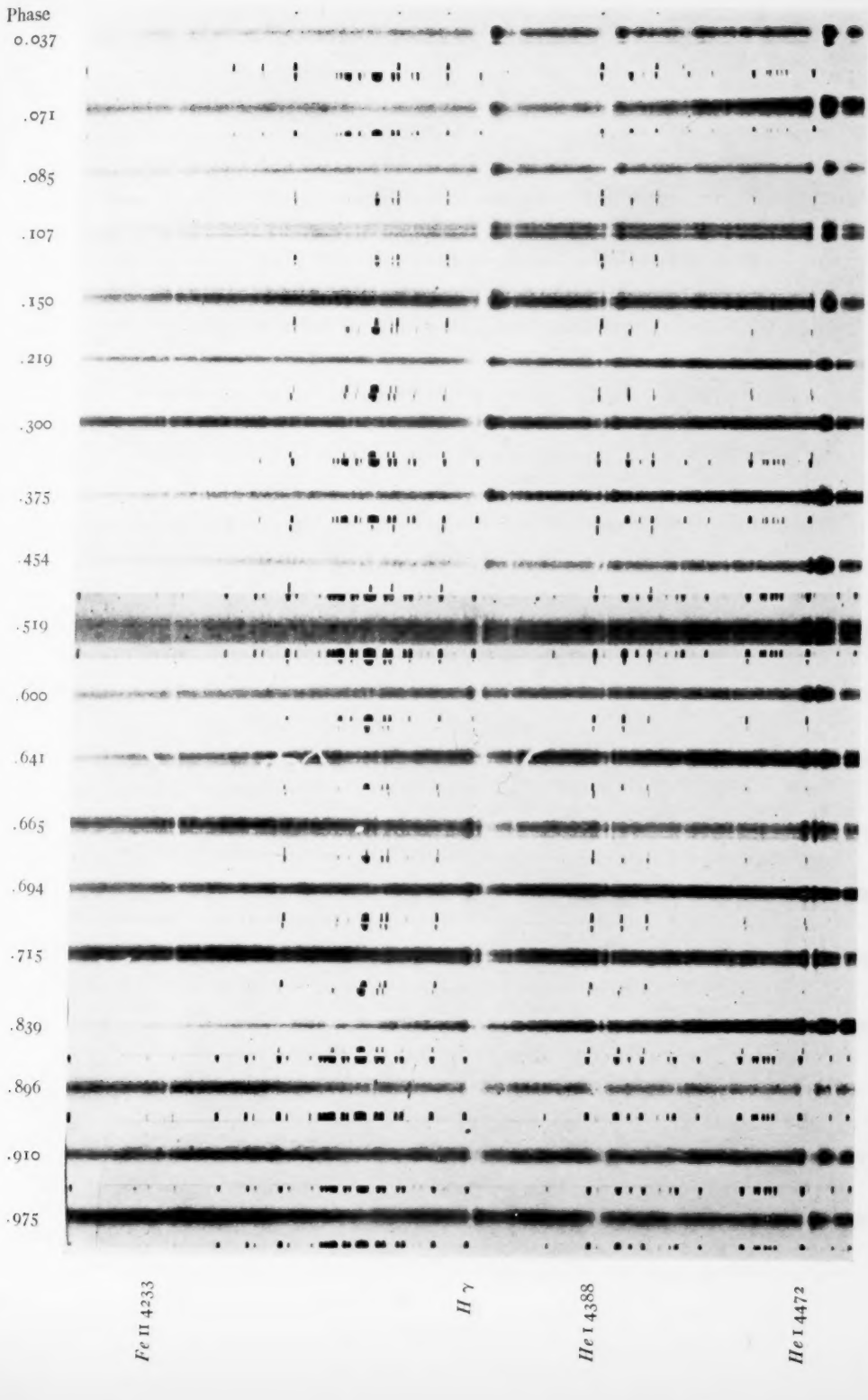

UNIV. OF MICH.

PLATE IX

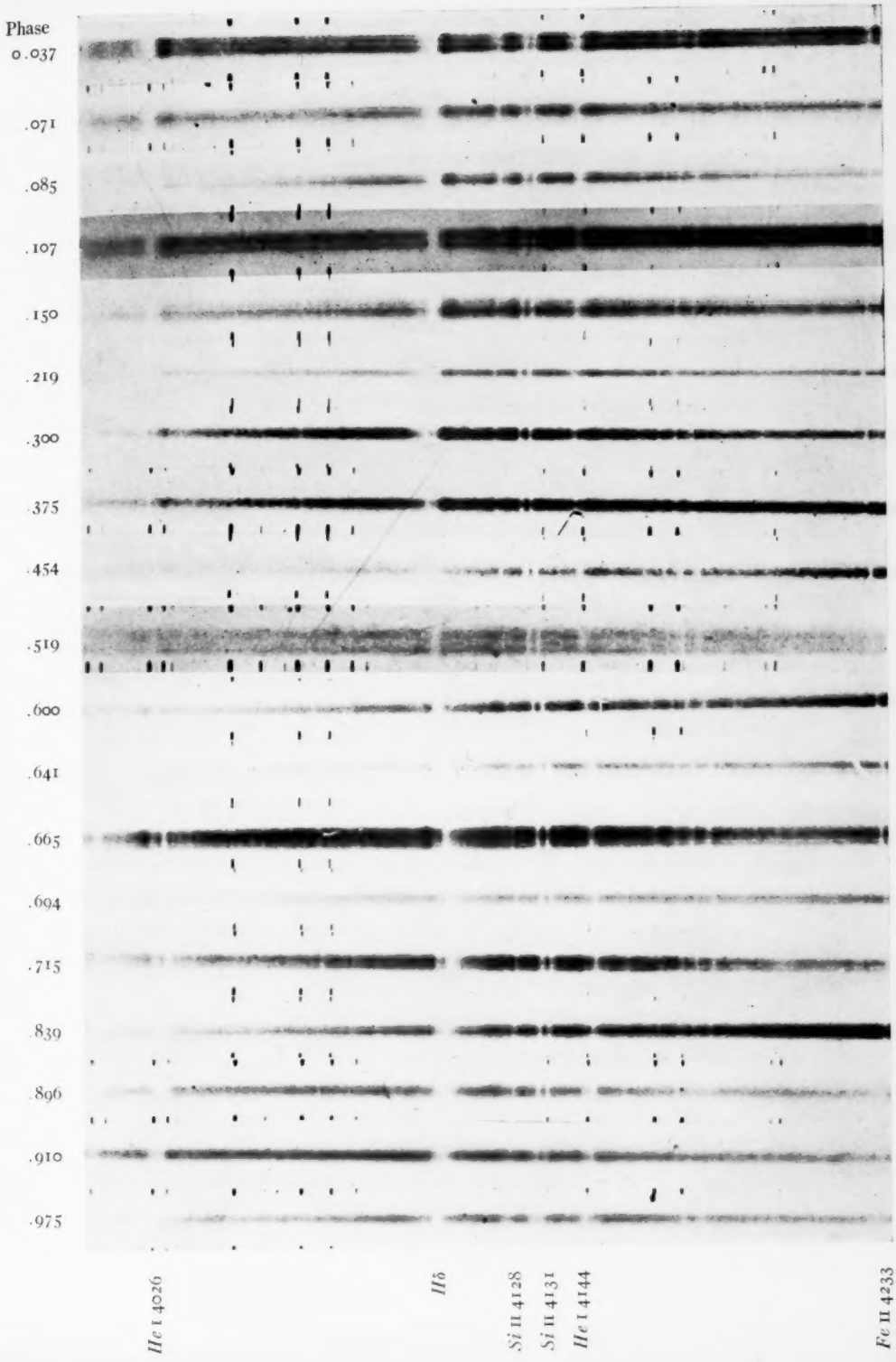

UNIV. OF MICH.

PLATE X

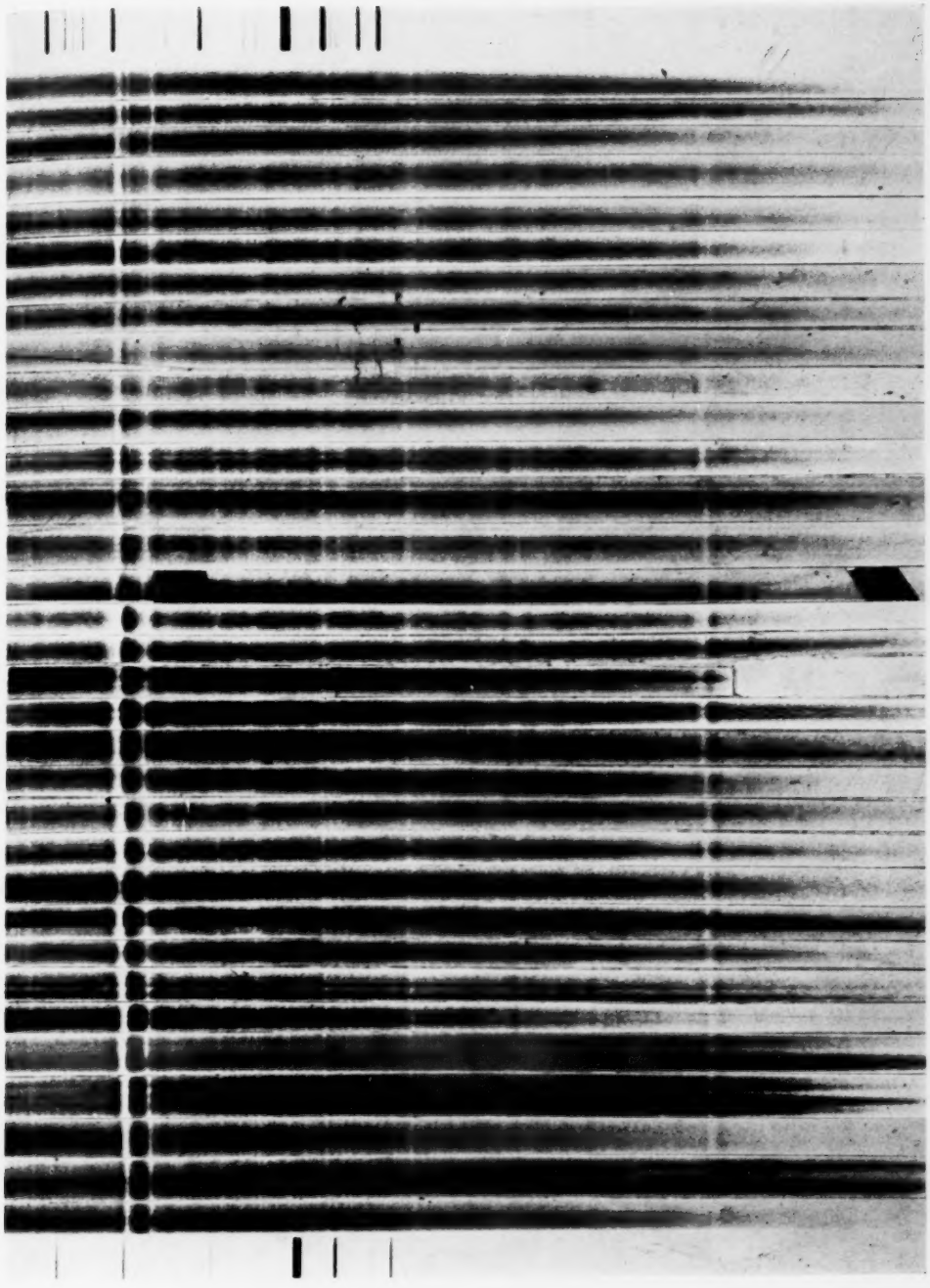

UNIV. OF MICH.

PLATE XI

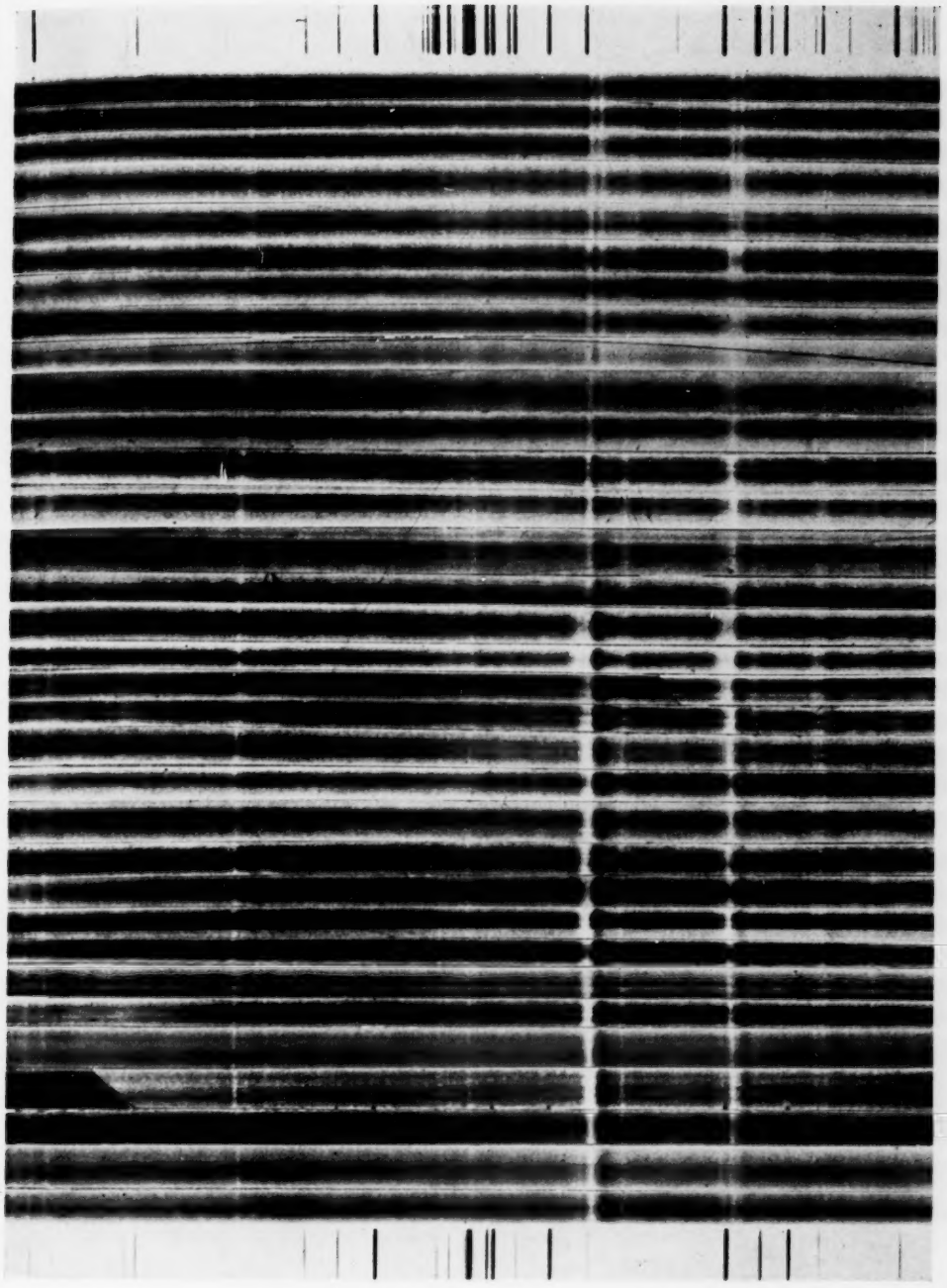

UNIV. OF MICH.

PLATE XII

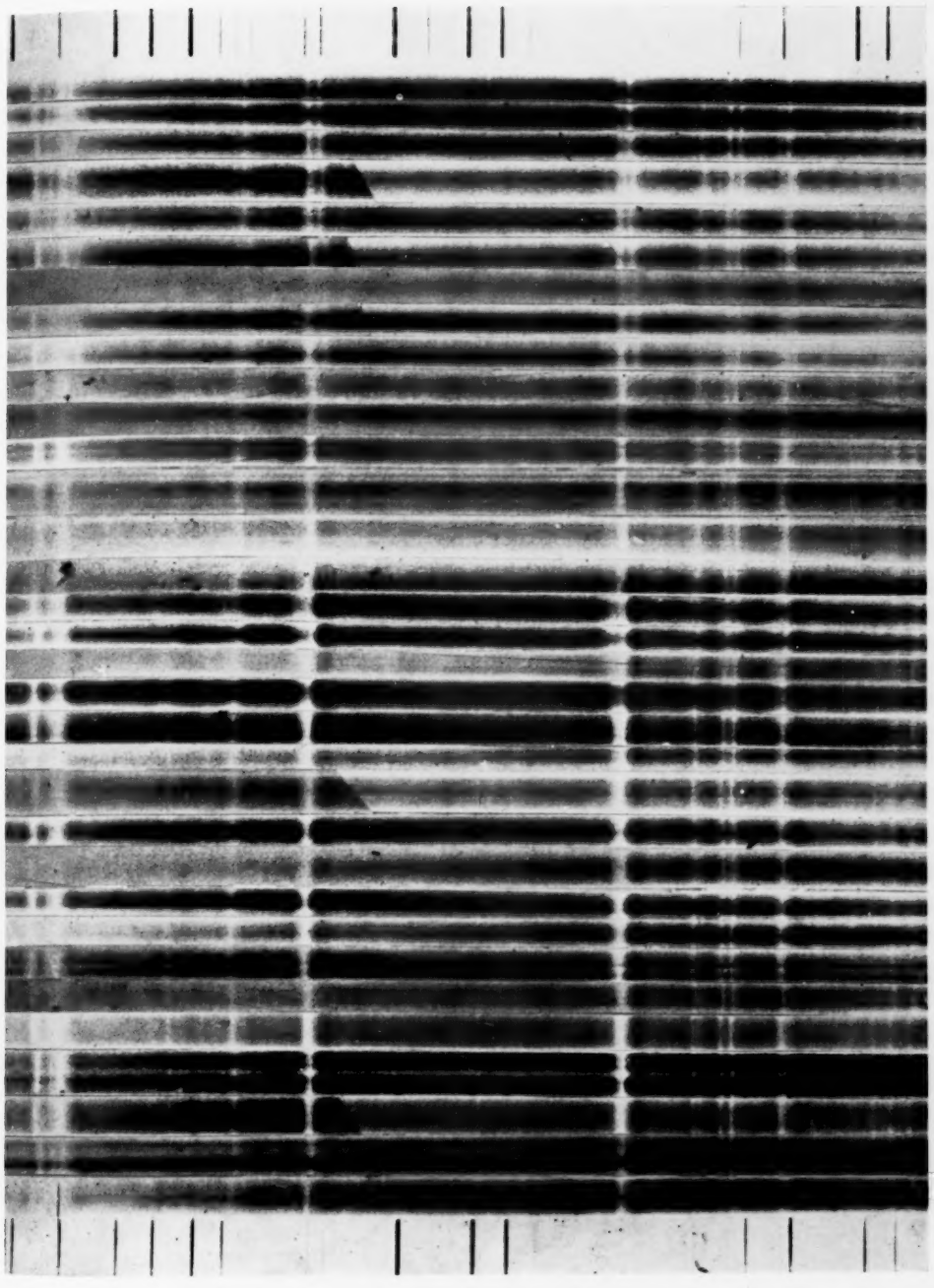

UNIV. OF MICH.

tensity and perhaps in velocity, the absence of the spectrum of the eclipsing star at primary minimum, the origin of red and violet satellite lines just preceding and following central eclipse, the peculiar variations in intensity of some B9 lines of *He* I and their abnormal weakness, and the variations in intensity and, probably, in velocity of the emission lines are some of the outstanding puzzles of β Lyrae.

It does not seem reasonable that with the progress in recent years in the interpretation of the formation of stellar and nebular absorption and emission lines we should continue to countenance such spectroscopic mysteries. Hence, a new attempt at a solution of the β Lyrae problem is justified at this time. We are now able to take advantage of two new methods: A study of the dilution effects[4] in the various sources should yield information concerning the relative distances between the absorbing gases and the exciting photosphere of the B9 star; and a search for obscuration effects produced by the continuous opacity[5] of the gases responsible for the B5 absorption lines should clarify our picture of the nebulous structure around β Lyrae.

Conventional methods of measuring the radial velocities of the centers of the lines and of tabulating the equivalent widths of lines, which are sometimes unsymmetrical and often are complicated by emission, give little promise at this stage. It is not now necessary or desirable to duplicate the excellent radial-velocity work of Rossiter or to give a new description of the spectrum in general. As a matter of fact, the work of Curtiss, of Baxandall and Stratton, and of Miss Maury is so complete, in the photographic region of the spectrum, that conventional methods would yield little more information than is contained in their publications. Baker has analyzed the ultraviolet region, but the visual region has not yet been sufficiently investigated.

In order to make progress, I have presented in Plates VII–XII a part of the material secured at the Yerkes Observatory between February 26, 1932, and December 15, 1938. All spectrograms are on Eastman Process emulsion, and special care was taken in the photographic procedure to secure the highest possible contrast. Plates VII, VIII, and IX represent a selection of spectrograms covering all phases, starting at primary minimum. Plates X, XI, and XII show a larger number of spectrograms taken near primary minimum. All phases are counted from primary minimum in fractions of the period, 12.922 days, and are computed by means of Rossiter's[6] formula. This formula fairly satisfactorily represents the Yerkes observations, as may be seen from Figure 1, and the correction to the period is very small.

THE B9 STAR

From a study of the Yerkes plates Miss Pillans[7] concluded that the B9 star is a normal supergiant of spectral class intermediate between β Orionis and σ Cygni. This result is essentially confirmed by an inspection of the spectrograms in Plates VII, VIII, and IX. A closer study shows that the *H* lines of the B9 component have fairly pronounced wings of the type produced by Stark effect. Near phase 0.75, when the velocity is near maximum, the entire red wing is uncovered, and there can be no doubt that it is stronger than the corresponding wing in β Orionis. At phase 0.25, when the velocity is near minimum, the violet wing is uncovered, but it is appreciably weaker than the red wing is at phase 0.75. The difference in the appearance of the two wings is of considerable interest. As far as I know, these wings have not previously been associated with the Stark effect but have been considered as separate, multiple components of the *H* lines. But their appearance strongly suggests the exponential decrease of absorption found empirically

[4] Struve and Wurm, *Ap. J.*, **88**, 84, 1938; Struve, *Proc. Amer. Phil. Soc.*, **81**, 211, 1939.

[5] Struve, *Proc. Nat. Acad.*, **26**, 117, 1940. In this paper on page 119, line 15 from the top, read "and at λ 4000 is" instead of "and at λ 5000 is." On the same page, line 17 from the top read "depth produced by $10^{2\tau}$" instead of "depth produced by 10^{τ}."

[6] *Pub. Obs. U. of Michigan*, **5**, 69, 1933.

[7] *Ap. J.*, **80**, 51, 1934.

by Elvey for lines broadened by Stark effect. It is almost certain, therefore, that the new interpretation is correct. This implies a luminosity somewhat lower than that of β Orionis but higher than that of a main-sequence B star.

For our purpose the most significant result of an inspection of the spectra is the fact—long known, but perhaps not sufficiently appreciated—that those lines of the B9 component which are not appreciably complicated by emission or by the B5-type absorption remain almost constant in intensity, except during primary eclipse, when they are strengthened and rotationally broadened. Miss Maury has indicated small variations in the intensities of these lines, with a shallow maximum at secondary eclipse. These variations are seen to be, from our spectrograms, of minor importance; and, since they can be easily explained,[8] we shall not consider them here. The important thing is that outside of primary eclipse the B9 lines vary so little. This behavior is important in connection with the continuous absorption of the B5 gases, which we shall discuss in the following section. *Mg* II 4481 and *Si* II 4128 and 4132 show this constant intensity very clearly, but essentially the same behavior is presented by all lines of *Fe* II and by the ($2^1P - n^1D$) lines of *He* I.

In view of this constancy of all B9 lines not complicated by emission or B5-type absorption, it is strange to find that the ($2^3P - n^3D$) lines of *He* I show large changes in intensity. These changes have, doubtless, been seen by all previous observers, but they have not received the attention they deserve. Near minimum velocity, at phases around 0.25, these lines are extraordinarily weak. Near maximum velocity, at phases around 0.75, they are fairly strong. I suppose it has been thought that overlapping emission or blending with the B5 absorption is the cause of this phenomenal variation. But, if we compare the B9 line λ 4472 at phases 0.63–0.83 with the same line at phases 0.21–0.36, we conclude that (*a*) there is no blending in either group with the B5 line; (*b*) the emission may complicate the first group of lines, having positive velocities, but does not seriously overlap the second group, having negative velocities; and (*c*) the lines of the second group are not only weak but are also narrow. Hence, we are not simply dealing with a phenomenon of superposition of light over the normal contour of a strong B9 absorption line; the contour itself is altered in a manner which must represent intrinsic variation, not merely an effect of photographic blending.

The recognition of this, as yet unexplained effect, is significant for two reasons: (*a*) it is almost certainly related to the difference in the appearance of the Stark-effect wings of *H*, described previously; and (*b*) it is probably connected with the conclusion by J. G. Baker[9] with regard to the B9 spectrum: "The strongest helium lines are weak and the lines of medium intensity are strong." It is significant that within the region covered by the Yerkes plates it is precisely the ($2^3P - n^3D$) lines of *He* I which are strong.

If it is admitted that the general weakness of the ($2^3P - n^3D$) lines of *He* I and their variations in intensity are intrinsic, we are faced with a remarkable case of departures from thermodynamic equilibrium. The ($2^1P - n^1D$) lines of *He* I are normal; yet the excitation potential of their lower state differs by only a fraction of a volt from that of state 2^3P. Probably the key to the solution of this problem lies in the fact that strong emission lines accompany all those lines of *He* I and of *H* which show the anomaly. As seen from the earth, the Doppler shift causes a relative displacement of the B9 absorption lines against the emission lines. But from the surface of the B9 star the shift will be small. We shall see later that the widening of the emission lines is caused largely by rotation. Hence, apart from a relatively small Doppler shift caused by the expansion of the nebula, the reversing layer of the B9 star will be subjected to the intense and concentrated[10] radiation of *He* I from the nebula in almost exactly those frequencies in which the *He* atoms of the reversing layer are prepared to absorb. This effect is comparable to

[8] *Observatory*, **57**, 272, 1934. [9] *Harvard Ann.*, **105**, 134, 1937.

[10] The emission line as seen by an observer in the B9 star will be fairly narrow.

a local radiation several times greater than that which comes from the photosphere of the B9 star, and it may depopulate the particular *He* I levels to such an extent that only a weak line remains in the outgoing flux of radiation.

The variation in the intensities of these lines is probably due to the fact that the approaching hemisphere of the B9 star is subjected to a much stronger nebular radiation than the receding hemisphere. This will become clearer after we have discussed the variations of the B5 lines.

It would be premature to attempt a numerical computation of the depopulation of the 2^3P level. The observations indicate a factor ranging between about 0.1 at phase 0.25 and perhaps 0.8 at phase 0.75.

Apart from this peculiar depopulation of the 2^3P level, the B9 spectrum presents no conspicuous departures from equilibrium conditions. The great strength of *Mg* II 4481 and of *Si* II 4128 and 4131 shows conclusively that there is no appreciable dilution of radiation due to great distance from the photosphere. This is also brought out by the normal intensities of the ($2^1P - n^1D$) lines of *He* I and by the lack of abnormal strengthening[11] of the line λ 3965 ($2^1S - 4^1P$).

THE B5 ABSORPTION SPECTRUM

The B5 spectrum undergoes large variations in intensity. When it is strong, it shows a weak line of *Mg* II 4481[12] and probably very weak lines of *Si* II 4128 and 4131. This shows that the dilution of radiation in the B5 gas is appreciable, though not excessive. Without a curve of growth, which cannot now be obtained for the B5 spectrum, we can make only an estimate of the factor by which the equivalent widths of these lines are reduced, as compared with stars having similar *He* I lines. The result is between 10^{-1} and 10^{-2}. Since the B5 lines show large turbulence broadening, we assume that the curve of growth is linear. In this case the dilution factor[13]

$$0.01 < W < 0.1 ,$$

and since, approximately,

$$W = \frac{R^2}{4r^2} ,$$

we find:

$$\text{For} \quad W = 10^{-1} , \qquad r = 1.5R ,$$

$$\text{For} \quad W = 10^{-2} , \qquad r = 5.0R ,$$

where r is the effective distance of the B5 gas from the center of the B9 star and R is the radius of the B9 star.

A similar estimate is obtained from the *He* I lines. The singlet lines ($2^1P - n^1D$) are abnormally faint, but they are not completely extinguished, as they are in the shells of ζ Tauri and φ Persei.[14] Relative to the triplet lines ($2^3P - n^3D$), they are perhaps weakened by a factor of 10. Table 4 of the paper by Struve and Wurm[4] shows that this would correspond to

$$W = 10^{-2} .$$

[11] This line, arising from a metastable level, remains strong when other lines arising from normal excited levels are weakened by dilution (see *Ap. J.*, **88**, 84, 1938).

[12] Pillans, *op. cit.*, p. 57.

[13] *Proc. Amer. Phil. Soc.*, **81**, 213, 1939.

[14] *Ap. J.*, **88**, 89, 1938.

At the same time, λ 3965 ($2^1S - 4^1P$) is very strong. I estimate that the populations of the two states are

$$\left(\frac{2^1S}{2^3P}\right)_{\beta\ \mathrm{Lyrae}} = 10\left(\frac{2^1S}{2^3P}\right)_{\mathrm{Boltzmann}}$$

Referring again to Table 4 of Struve and Wurm, we find, for $T = 25{,}000°$,

$$\left(\frac{2^1S}{2^3P}\right)_{\mathrm{Boltzmann}} = 0.14 .$$

For three different dilution factors we have

$$W = 0.10 \qquad 2^1S/2^3P = 0.31 ,$$

$$W = 0.02 \qquad 2^1S/2^3P = 1.42 ,$$

$$W = 0.01 \qquad 2^1S/2^3P = 2.50 .$$

The estimated intensity of λ 3965 thus leads to

$$W = 0.02 .$$

We shall adopt $r = 3R$. This value is little more than an estimate, but it does give us a rough idea of the structure of the nebulous mass. We have no way to determine the thickness of the layer. But from the absence of any conspicuous effects of stratification, of the type observed in P Cygni,[15] we may conclude that this thickness is not very great. At least that part of the layer which contributes appreciably to the absorption and emission lines shows only a small range in the ionization potentials represented (*He* II is absent in emission, while *He* I is strong) and must, therefore, be fairly thin and of fairly uniform density. Perhaps we may assume a thickness of about $2R$, centered at a distance of $3R$ from the center of the B9 star.

It is significant that the dimensions of the nebula are comparable to the dimensions of the orbit of the binary system and that the secondary (invisible) component is enveloped by the B5 gases. This conclusion would not have been possible without a study of the dilution effects. An important conclusion is that obscuration of the B5 gases by the components of the binary should not be altogether negligible.

The B5 lines vary in intensity, reaching a maximum at about phase 0.08. This very pronounced asymmetry with respect to primary minimum has been previously known.[16] Its significance becomes apparent when we recall that the equivalent widths of the B5 lines measure the numbers of atoms per square centimeter in the nebulous layer. Actual measurements are presented in the following paper by Miss Gill. The lines are very broad, and all but the strongest must lie on the straight-line portion of the curve of growth, where $A \propto N$. Miss Gill has listed the equivalent widths of some B5 lines. They all vary in the same manner and clearly represent varying amounts of nebular material projected upon the disk of the B9 star. Whether we are dealing with changes in extent of the layer or with changes in density, or with both, cannot be decided. There are no large changes in the ionization of the B5 layer as we pass through the 12.9-day cycle. Following the maximum at phase 0.08, the lines rapidly decline in strength. They are very weak at phase 0.25, although their intensities are not the same in different cycles. Near phases 0.4 and 0.5 they are blended with the B9 lines, but be-

[15] *Ap. J.*, **81**, 66, 1935.

[16] See, e.g., Miss Maury's Fig. 3, *Harvard Ann.*, **84**, 221, 1933.

ginning with phase 0.6 the B5 lines again rapidly increase in strength. At phase 0.65 they are much stronger than at phase 0.35. Similarly, at phase 0.75 they are stronger than at phase 0.25. But because of the unsymmetrical location of maximum intensity they are weaker at phases 0.85, 0.90, and 0.95 than at phases 0.15, 0.10, and 0.05.

Since the presence of emission makes it difficult to measure the B5 lines without ambiguity—should they be referred to the continuous spectrum of the B9 star, to the intensity of the broad emission line, or to the sum of the two sources?—we must again rely upon estimates. The ratio N max/N min of the numbers of atoms per square centimeter is of the order of 10^2 or 10^3.

The spectrographic observations as such give no explanation of the asymmetry of maximum intensity. This has been provided by Kuiper's dynamical theory, which is presented elsewhere in this issue. We accept it as an observational fact that the nebula contains vastly more atoms per square centimeter at phase 0,08, corresponding to an angle of 29° after primary minimum, than at any other phase.

Our observations have not yet shown whether the nebulous layer is a spherical shell or a ring in the equatorial plane of the B9 star. To distinguish between the two alternatives, we shall consider the continuous absorption and emission of the nebula.

The significant observational data are: (1) Those absorption lines of the B9 component which are not complicated by emission phenomena or by the B5 absorption lines show no appreciable change in intensity except for those variations which are directly related to primary eclipse. (2) The B9 lines are always strong and suggest little or no effect of continuous absorption and emission in the B5 layer. (3) Those B9 lines which are blended with emission components (*He* I 4472, *H*, etc.) are variable in intensity.

We can discuss these observational results in the following way: Consider phase $1^d0 = 0^p08$. The B5 lines are then at maximum and resemble those of a strong-lined B supergiant. The composition of the B5 gases and their ionization must also be similar to those of a B5 supergiant reversing layer. This is uncertain by a considerable factor because we have no accurate curves of growth. But since turbulence is so large that approximately $A \propto N$, we find for the numbers of atoms producing these lines values which are comparable to those for the same lines in ordinary supergiants. Hence, it is obvious that the general opacity of the B5 gases at phase 0.08 cannot be very small. Since the theory of the continuous absorption coefficient of a highly ionized stellar atmosphere is not sufficiently well known, we shall rely upon former computations[5] and shall conclude that, since the lines are identical in strength with those of a normal reversing layer, where τ goes to infinity, the optical thickness of the B5 gases must be at least that found by Milne and others for the depth of the fictitious photosphere. It is probably safe to say that $0.1 < \tau_1 < 0.5$, and a value of $\tau_1 = 0.3$ should be close to the truth. Any uncertainty in τ_1 will affect the following discussion.

In this case we can apply the formula[17]

$$I(0, \theta) = \int_0^{\tau_1} J(x) e^{-x \sec \theta} \sec \theta \, dx$$

or

$$I(0, \theta) = \tfrac{1}{2} F \int_0^{\tau_1} (1 + \tfrac{3}{2}\tau) e^{-\tau \sec \theta} \sec \theta \, d\tau \, .$$

Unsöld[18] has plotted the integrand as a function of τ for different values of θ. If we use an average θ—for example, $\sec \theta = 1.5$—so that $I(0, \theta) = F$, we find by graphical integration that the average surface brightness of the continuous spectrum of the B5 gas is approximately one-quarter of that of a normal star.

[17] Unsöld, *Physik der Sternatmosphären*, p. 94, 1938.

[18] *Ibid.*, p. 95.

The B5 line (*He* I 4472) cuts deep into the B9 star's continuous spectrum long before the B9 line is blended with the B5 line (e.g., at phase $0^{p}71 = 9^{d}165$). This shows that the projected area of the B5 gases cannot be much smaller than the B9 disk.

On the other hand, the continuous spectrum would tend to fill in the B9 lines if the B5 area were very much larger than the B9 disk. As a matter of fact, if the area of the B5 gases were four times larger than the B9 disk, the lines of the latter would be reduced in intensity to one-half their normal strength. A comparison of the B9 spectrum with β Orionis and σ Cygni by Miss Pillans shows that the B9 lines are not noticeably weakened, as compared with normal lines of a B9 supergiant. Hence, the projected area of the B5 gases must be approximately equal to the area of the B9 component.

If this is the case, the filling-in by overlapping of the continuous spectrum of the B5 gases with the lines of the B9 component would be

$$\frac{1}{1 + \frac{I_2}{I_1}} = \frac{1}{1 + 0.25} = 0.80 .$$

A point on the contour which normally has an intensity of 0.60 (absorption of 0.40) would now have an intensity of 0.68 (absorption of 0.32). This difference, which would be constant throughout the 12.9-day cycle, would probably not be noticeable.

We have tacitly assumed that star and nebula do not affect one another; in other words, that the light of the B9 star is not weakened by absorption in the nebula. This will be approximately true at phases 0.3–0.5, where the B5 lines are weak but where the total emission of the nebula must be normal (except for obscuration by the B9 star). At phases near 0.08 we must allow for the fact that the B9 star shines through a mass of gas of optical thickness $\tau_1 = 0.3$. Hence, we apply the formula

$$I(0, \theta) = I_0 e^{-\tau_1 \sec\theta} + \tfrac{1}{2}F \int_0^{\tau_1} (1 + \tfrac{3}{2}\tau) e^{-\tau \sec\theta} \sec\theta \, d\tau .$$

For a point on the contour which normally has an intensity of 0.60, we now find 0.70. The entire range in intensity with phase is between 0.68 and 0.70, which cannot be detected observationally. This treatment presupposes that the B5 gases have no effect upon the formation of the line of the B9 star. If the B5 shell were complete and everywhere similar to that which gives rise to the strong absorption at phase $1^{d}0 = 0^{p}08$, we must solve the equations of transfer of radiation, giving[19]

$$\frac{H^1}{H} = 1 - \frac{\sqrt{3}\,\eta}{2\left\{\left[1 + \eta + \frac{\sqrt{3(1+\eta)}}{2}\right] \sin h\sqrt{3}\,\tau_1 + \left[\sqrt{1+\eta} + \frac{\sqrt{3}(1+\eta)}{2}\right] \cos h\sqrt{3}\,\tau_1\right\}} .$$

For comparison we select again a point on the contour, where $\eta = 2$ and where normally $(\tau_1 = 0) H^1/H = 0.60$. Then

$$\frac{H^1}{H} = 1 - \frac{\sqrt{3}}{(3 + \frac{3}{2}) \sin h\sqrt{3}\,\tau_1 + \left(\sqrt{3} + \frac{3\sqrt{3}}{2}\right) \cos h\sqrt{3}\,\tau_1} .$$

[19] *Proc. Nat. Acad.*, **26**, 118, 1940.

For $\tau_1 = 0.3$ we compute $H^1/H = 0.72$, instead of 0.60. The filling-in of the lines would be somewhat greater in this case of a shell than in the case of a detached mass of B5 gas. But we could not, in practice, distinguish between the two results were it not for the fact that the second method would give no appreciable τ_1 at phases near $0^p.5$ and would thus require a variation of the B9 lines such that the point for which $\eta = 2$ would oscillate between $I = 0.60$ at phase $0^p.5$ and $I = 0.72$ at phase $0^p.08$. It is certain that no such variation exists. Hence the B5 gases not only do not envelop the star with uniform thickness—this we already know from the changes of the B5 intensities—but do not even envelop one hemisphere. We conclude that the B5 gases form a ring around the B9 star with a small but compact condensation in the direction of phase 0.08.

The question arises whether the continuous spectrum of those portions of the nebulous ring which are not projected upon the disk of the B9 star and which contribute to the emission lines is strong enough to fill in appreciably the B5 absorption lines. Miss Gill's measures show that even at maximum the residual central intensities of the B5 lines are appreciable. For example, *He* I 4472 has a central intensity $I_0 = 53$ per cent at phase 0.017. Such large central intensities are not normal for lines broadened by turbulence. For example, in 17 Leporis, F. E. Roach finds on a spectrogram taken January 1, 1940:

Line	Central Intensity
H_ϵ + *Ca* II H	1 per cent
Ca II K	5
$H\zeta$	10
H (2–9)	13
H (2–10)	12

The high residual intensity of the B5 lines in β Lyrae may well be produced by continuous emission in the nebula. However, both components of the binary may also contribute to the residual intensities of the B5 lines of *He* I. The spectral type of the secondary is later than B8.[20] Hence, it cannot possess strong lines of *He* I, and its continuous spectrum will be superposed over the *He* I line of the B5 spectrum.

PHENOMENA DURING PRIMARY ECLIPSE

Until very recently it was generally believed that the principal eclipse of β Lyrae is either total or almost total and that the B9 star is much smaller than the other, invisible, component. For example, Danjon in 1928 found $a_1/a_2 = 0.42$, while Guthnick and Prager in 1919 found $a_1/a_2 = 0.53$. Here a_1 designates the semimajor axis of the B9 star, and a_2 refers to the invisible component. Spectroscopically this result presents certain difficulties. The B9 lines remain visible throughout the primary eclipse, and their rotational broadening is not compatible with the idea that only a narrow polar cap of the B9 star remains visible. In 1934 I attempted[1] to remove the difficulty by assuming that the spectral type of the second component is not later than A0 and that the broadened lines at principal eclipse are due to it and not to the B9 star. This interpretation was somewhat strained because color observations by Danjon and by Elvey suggested a type at least as late as A0 and probably later. Yet, there is reason to believe that the *He* I lines ($2^1P - n^1D$) at principal eclipse belong, in a large part, to the same source that produces *Mg* II 4481, *Fe* II, etc. Even more precarious was my interpretation of the satellite lines. These lines appear shortly before central eclipse on the red sides of the B9 lines and definitely show *He* I. They disappear at central eclipse and reappear a few hours later on the violet sides of the B9 lines, again with strong *He* I. I suggested that these lines originate in an extended atmosphere surrounding the A0 component when this atmosphere is projected upon the B9 disk. The displacement of ± 200 km/sec would then be due to the rotation of the A0 star. There are two things wrong with this inter-

[20] *Observatory*, **57**, 268, 1924.

pretation: the strength of the *He* I lines is not compatible with spectral type A0, and the rotation of 200 km/sec is considerably larger than can reasonably be expected for the A0 star. Wares found a rotational velocity of 40 km/sec at the equator of the B9 star. The older photometric solutions make the A0 star two or three times larger than the B9 star, so that its equatorial rotation may be as large as 120 km/sec. But we observe a large part of the rim of the A0 star when it is projected over the B9 disk, and it is difficult to see how the observed displacement could be more than ±100 km/sec. All observers agree that the satellites are displaced nearly twice this amount.

The solution of this fundamental difficulty is due independently to Kuiper and to S. Gaposchkin. The former informed me two years ago[21] that the photometric observations are well represented if the eclipsing star at primary eclipse is made considerably smaller than the B9 star, so that this eclipse is annular. The spectral type of the secondary thus becomes about A5. Unpublished computations by Wesselink[21] support this conclusion. Independently, S. Gaposchkin[22] derived a set of elements for β Lyrae, in which

$a_1 = 0.480$ (B9 star) $\quad L_2 = 0.04$
$a_2 = .245$ (invisible star) $\quad Sp_1 =$ B9 (observed)
$L_1 = 0.96$ $\quad Sp_2 =$ F5 (computed)

The agreement between these independent discussions leaves no doubt that the eclipse is annular, that the lines of the B9 star are visible throughout eclipse, and that even at central eclipse the light of the secondary is but a small fraction of the total light, so that its spectrum should not be visible. One discrepancy has thus been removed. There remains the difficulty of the satellites, which now cannot even remotely be due to the axial rotation of the small, invisible, component.

Since in most previous investigations the phenomena during eclipse have been treated rather briefly, I have measured all Yerkes spectrograms between phases 0.839 and 0.157. The velocities in Table 1 have been corrected to the sun. The numbers of whole cycles elapsed since Rossiter's epoch are given in front of the decimal point, under "Phase." The observations are plotted in Figure 1, where the continuous line represents Rossiter's velocity-curve of the B9 component. There is a small systematic difference between my measurements and Rossiter's curve. Lowering the latter by about 5 km/sec would improve the agreement and would bring out more clearly the rotational displacements of the lines first discovered by Rossiter. We notice that between phases 0.980 and 0.020, where Rossiter's curve should pass through the computed velocity-curve, the observations give systematically negative residuals. Even if the velocity-curve is lowered 5 km/sec, my observations cross the curve at phase 0.960 instead of at phase 0.000. This discrepancy cannot be completely removed by a correction in the period, which, at most, may explain the systematic difference of 5 km/sec. Rossiter excluded from consideration all spectrograms taken between phases $12^d4 = 0^p96$ and $0^d4 = 0^p03$.

It should be noted that the limiting phases of the rotational effect, as given by Rossiter, are $1^d6 = 0^p125 = 45°$ and $11^d3 = 0^p876 = -45°$. These values agree well with the beginning and the end of the eclipse as computed from the photometric elements by Gaposchkin.

We see in Figure 1 that the B5 line *He* I 4472 shows a small change in velocity, which is probably not caused by blending with the relatively very weak line of the B9 star (designated as B8 in Fig. 1). This variation is of opposite sense to that required if the B5 line belonged to the second binary component. The velocity of the B5 line *Mg* II 4481, which is always weak and somewhat complicated by the red emission wing of *He* I 4472, gives a systematically smaller radial velocity. Of particular interest are the satellites of

[21] *Annual Report of the Yerkes Obs. for 1938–1939; Pub. A.A.S.*, **9**, 304, 1939.

[22] *Pub. A.A.S.*, **9**, 152, 1939; *Proc. Amer. Phil. Soc.*, **82**, 305, 1940. I am indebted to Dr. Gaposchkin for the use of his unpublished data concerning the photometric solution of β Lyrae.

TABLE 1

RADIAL VELOCITIES OF β LYRAE IN KM/SEC

Plate	Phase	B9 (4481, 4128, 4131)	B5 (4472)	B5 (4481)	B9 (4472)	Satellites (4481, 4128, 4131)
10164	2189.839	+137.0	− 67.4	.....	+144.5	.....
11052	240.846	+132.8	− 93.9	−115.1	+167.0	.....
11105	243.848	+131.0	− 87.1	−124.4	+151.6	.....
11139	245.852	+126.6	− 55.0	−155.9	+158.3	.....
11106	243.855	+129.1	− 85.2	−120.5	+157.6	.....
11140	245.857	+120.0	− 69.2	−106.5	+152.2	.....
11141	245.861	+120.5	− 59.2	.....	+152.1	.....
11142	245.863	+121.4	− 59.2	− 98.5	+146.0	.....
11143	245.870	+125.4	− 59.3	− 86.6	+154.0	.....
10052	181.896	+ 99.1	− 84.3	−104.2	+146.4	.....
11127	244.925	+ 79.1	− 85.6	−120.9	+183.3	+171.6
11087	242.929	+ 78.1	− 92.3	−130.8	+177.4	+183.3
11128	244.935	+ 65.7	− 92.0	−119.8	+179.0	+187.3
11149	246.938	+ 52.0	− 74.7	−110.0	+216.4	+184.9
10636	217.940	+ 54.2	− 70.3	−109.6	+208.8	+223.0
11150	246.947	+ 44.2	− 71.6	−137.7	+229.5	+199.3
11151	246.954	+ 27.7	− 81.2	−156.0	+209.9	+173.5
12290	361.973	− 5.9	− 50.5	.....	+250.7	+183.9
10076	182.975	− 10.6	− 84.6	.....	+223.9	+161.2
11324	254.981	− 7.3	− 70.5	.....	.....	+126.9
10577	210.982	− 8.0	− 81.0	.....	.....	.....
12291	361.984	− 14.5	− 66.1	.....	.....	.....
12292	362.985	− 19.1	− 73.5	.....	.....	.....
10139	187.988	− 5.2	− 59.2	.....	.....	.....
10116	185.988	− 25.1	− 65.4	.....	.....	.....
12293	362.994	− 30.3	− 62.3	.....	.....	.....
10175	191.003	− 33.5	− 96.2	.....	.....	.....
11130	245.003	− 30.4	− 94.0	.....	−275.7	−214.8
11145	246.015	− 48.0	− 93.1	.....	−305.7	−249.5
11131	245.017	− 54.8	−104.3	.....	−285.4	−226.5
10352	197.037	− 64.2	− 82.8	.....	−238.4	−205.8
11332	255.057	− 96.2	−112.1	.....	−206.6	−184.8
11055	241.069	−116.6	−119.3	.....	.....	.....
10151	189.071	−119.3	−101.8	.....	.....	.....
12294	363.072	−123.3	−113.6	.....	.....	.....
11056	241.077	−118.2	−121.5	.....	.....	.....
10625	217.077	−113.0	−101.0	.....	.....	.....
11113	244.081	−121.4	−121.7	.....	.....	.....
10192	192.085	−119.3	−100.0	.....	.....	.....
11114	244.089	−122.6	−111.2	.....	.....	.....
10284	195.107	−144.7	−107.0	.....	.....	.....
12285	361.120	−163.0	− 95.5	.....	.....	.....
12286	361.126	−161.9	−102.4	.....	.....	.....
10550	209.129	−150.0	−110.2	.....	.....	.....
10102	185.139	−154.4	−105.7	.....	.....	.....
12310	366.145	−163.5	− 93.9	.....	.....	.....
10168	190.150	−166.4	−112.7	.....	.....	.....
11067	242.157	−172.2	−110.0	.....	.....	.....

Mg II 4481, of *Si* II 4128 and 4131, and of what was at first interpreted as a B9 line of *He* I 4472. At phases 0.84–0.87 the B9 component of *He* I 4472 is fairly strong and easily measurable. The velocities derived from this line are systematically larger, by about 25 km/sec, than those of *Mg* II 4481 and of *Si* II 4128 and 4131. It is possible that the true B9 line, which is definitely present long before, is already slightly blended with a satellite line at phase 0.845. With increasing phases the satellite line becomes stronger and clearly dominates between phases 0.92 and 0.97. The satellite lines of *Mg* II 4481 and of *Si* II 4128 and 4131 appear at phase 0.925, rapidly gain in intensity, and then equally rapidly become too weak to be seen at phase 0.980. The radial velocities of the latter remain roughly constant at +180 km/sec, while those of *He* I 4472, after blending with the true B9 line has ceased, are of the order of +225 km/sec.

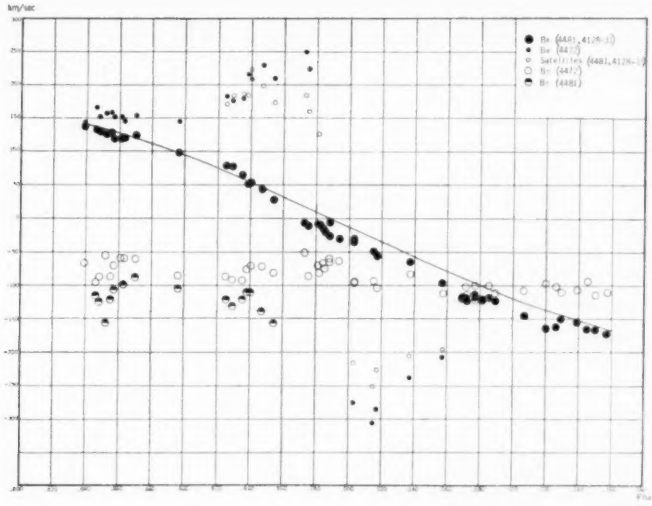

FIG. 1.—Radial velocities measured in the spectrum of β Lyrae near primary eclipse

A remarkable result is the complete absence of the true B9 line around phase 0.95, when it should be about halfway between the strong B5 line and the fainter satellite. It would, however, in this phase be covered by a strong emission line. If any further proof were required, this observation would suffice to show that the B9 absorption takes place below the *He* I emission.

The violet satellites start immediately after phase 0.000, when they flash out with great intensity. The velocities increase with phase from −300 km/sec to −200 km/sec for *He* I 4472 and from −225 km/sec to −200 km/sec for *Mg* II 4481. Their intensities rapidly diminish, and they disappear at phase 0.06.

In interpreting these phenomena the disappearance of the red satellites $0^{p}02$ before central eclipse and the appearance of the violet satellites suddenly at $0^{p}003$ are significant. The star is at minimum light soon after the disappearance of the red satellites, and only obscuration by the invisible component can be responsible. On the other hand, the times of appearance of the red satellites and disappearance of the violet satellites is affected by the rapid change in the brightness of the uneclipsed portion of the B9 star.

An inspection of Plates X, XI, and XII shows that the spectra of the red and the violet satellites are different. The former are narrow and show little turbulence; the latter are broad, shading off toward the violet, and indicate large turbulent velocities. The red satellites are very strong in *Fe* II, the satellites being as strong as the normal B9 lines. The violet satellites show no *Fe* II. Both sets of satellites show *H* and *He* I, the violet

ones being especially conspicuous—perhaps as a result of their larger turbulent widths. *Mg* II 4481 is present in both sets: it is rather weak in the red satellites and very diffuse and weak in the violet satellites. The same probably holds also for *Si* II 4128 and 4131. Of special interest is *He* I 3965 because it permits us to estimate the dilution of radiation in the satellites. The red satellite shows this line clearly, but it is much weaker than the corresponding B5 line. The violet satellite shows only a very weak λ 3965.

From the relatively greater intensities of *Mg* II and *Si* II in the red satellites than in the B5 spectrum, and from the moderate intensity of *He* I 3965 we conclude that there is

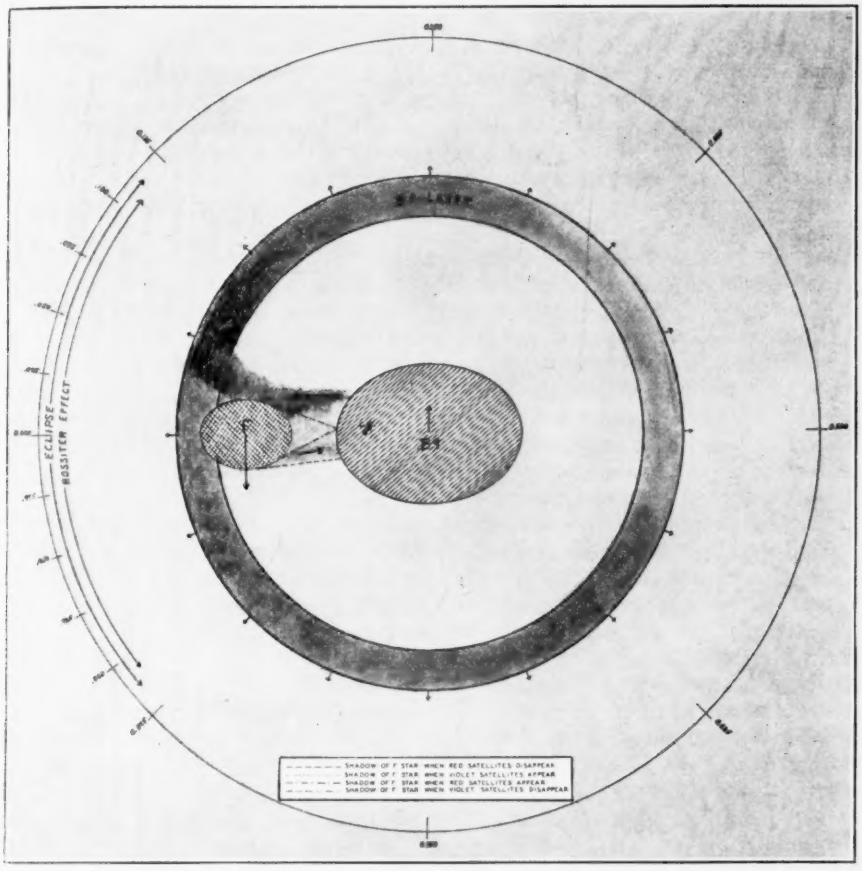

FIG. 2.—A schematic representation of the spectrographic observations of β Lyrae

some effect of dilution but that it is smaller than for the B5 spectrum. The gas giving rise to the satellites lies between the B9 star and the nebulous ring.

The weakness of *He* I 3965 in the violet satellites proves that they, too, originate between the B9 star and the B5 ring. Moreover, the spectral type of the red satellites corresponds to a lower temperature than that of the violet satellites.

SUMMARY

We are now prepared to form a physical picture of β Lyrae (see Fig 2). There are two stars, one of which is of type B9 and contributes 96 per cent of the light of the system.

This star is a giant, but its luminosity is lower than that of β Orionis. The other star is too faint to impress its light upon the spectrum, but its temperature must correspond to that of a star of class late A or early F. The semimajor axis of the B9 star is about twice that of the F star, and the separation between their centers is about twice the semimajor axis of the B9 star.

A stream of gas passes from the B9 star in the direction of the F star, along that side of the latter which becomes exposed to sight after central eclipse. These gases stream out with a velocity of about 300 km/sec, but the dispersion is large and, hence, the violet satellites are broad. The gas is hot, coming from the surface of the B9 star, and the spectrum shows some evidence of dilution. The F component hides this stream from our view until phase 0.003, when quite suddenly it becomes visible in absorption. As the stream passes along the surface of the F star, a part becomes deflected, essentially through conservation of angular momentum, in a manner discussed by Kuiper, and forms a condensation at phase 0.08 which has an average distance of about twice the radius from the surface of the B9 star. The condensation continually receives matter from the outgoing stream of gas and dissipates it in the form of an expanding ring, whose size increases while its density decreases as we pass from phase 0.08 to phase 0.25 and beyond.

However, a part of the stream which gives rise to the violet satellites—perhaps that which consists of the slower atoms—flows around the F star and, after having been cooled along the surface of the latter, while the exciting radiation of the B9 star is hidden by the mass of the F5 component, returns to the B9 star as a stream having a velocity of about 200 km/sec. This stream gives rise to the red satellites. It becomes hidden from view $0^{p}02$ before central eclipse.

That side of the B9 star which is subjected from above to the intense nebular radiation of *H* and *He* I from the outgoing stream and from the condensation at phase 0.08 shows marked departures in the populations of those levels from which strong B9 absorption lines should normally originate.

The emission lines come from the nebula, and much of their strengthening at primary and secondary eclipses is, as Mrs. McLaughlin[23] has suggested, due to the longer exposures required when the star is faint. But there are some definite changes in the intensities and structure of the emission lines which cannot be attributed to variation in light. In a general way, these changes can be accounted for by obscuration effects, but as yet no detailed investigation has been made. The fact that most of the nebular material is concentrated near phase 0.08 suggests that Belopolsky's[24] early orbit for the emission lines may, after all, be physically significant. Curtiss[25] has formally verified Belopolsky's elements for $H\beta$ but has expressed doubt as to the physical significance of the results, for reasons which are perhaps not completely binding. Baxandall,[3] after carefully reviewing the arguments of Curtiss, concludes:

> . . . . With all these uncertainties in the measurements there is an unexpected agreement in the results obtained for separate bands—and these results do not point to an orbital shift of the band so much as to the suppression of half the band at a time. During the first half of the cycle the bright bands lie wholly to the red of the undisplaced lines, during the second half of the cycle they lie to the violet with occasional extensions to the red side.

The value of K derived for $H\beta$ by Curtiss is 75 km/sec. This is much smaller than Rossiter's K for the B9 star, 184 km/sec, and is in good agreement with the fact that, by averaging the measures of the edges of the bright bands, we determine the velocity of the center of gravity of the entire nebulous ring, not only of the condensation at phase 0.08.

[23] *Pub. A.A.S.*, **6**, 272, 1931.

[24] *Mem. d. Soc. spett. ital.*, **22**, 101, 1893; **26**, 135, 1897.

[25] *Pub. Allegheny Obs.*, **2**, 113, 1911.

The total widths of the emission lines are of the order of 10 A, corresponding to about 685 km/sec. This is much wider than can be accounted for by expansion alone, and we conclude that the nebulous ring has a velocity of rotation of more than 300 km/sec. This is compatible with the dimensions of the ring and with the orbital velocity of 184 km/sec of the B9 component.

The picture of β Lyrae presented by its spectroscopic characteristics removes most of the difficulties encountered by previous workers. It is rendered intelligible by Kuiper's dynamical theory,[26] and I wish here to record my indebtedness to Dr. Kuiper for many stimulating discussions of this problem. Two aspects of the problem deserve further study: the remarkable departures from equilibrium conditions in certain *He* I lines of the B9 star and the variations in the structure and intensity of the emission lines.

YERKES OBSERVATORY
August 8, 1940

[26] *Ap. J.*, **93**, 133, 1941.

SOME LINE INTENSITIES IN β LYRAE

JOCELYN R. GILL

ABSTRACT

Microphotometer tracings have been made from sixteen Yerkes spectrograms covering the light-cycle of β Lyrae at various phases. Profiles of the lines *Si* II 4128–4130, *Mg* II 4481, $H\gamma$, $H\delta$, and *He* I 4472 are reproduced, and a table of equivalent widths of certain of the B9 (stellar) and B5 (nebular) components is given. It is found that the lines *Si* II 4128–4130 and *Mg* II 4481 of the B9 spectrum are not constant throughout the light-cycle but are strongest near primary minimum. These line intensities of *Si* II and *Mg* II must be further qualified, however, since the measured equivalent widths of these lines include the satellites and might, therefore, be found constant throughout the light-cycle if the satellites were subtracted.

The B5 components of $H\gamma$, $H\delta$, and *He* I 4472 are found to be strongest near primary minimum.

The B9 component of λ 4472 is variable and notably *weaker* in the first half of the cycle than in the second half.

I

In order to make progress in the solution of the general problem of β Lyrae a photometric study of the line intensities is required. The spectrum of β Lyrae is composed of a normal star spectrum of class B8 or B9 and a set of hydrogen and helium lines of class B5 which are not those of a normal star.[1] The B5 lines are, in fact, thought to originate in a nebula surrounding in some manner the two components of the β Lyrae system. For this reason we are interested in the behavior of the B9 stellar lines and in that of the B5 nebular absorption lines.

The first problem considered was whether the B9 lines—that is, the lines due to the normal star spectrum—were constant in equivalent width throughout the cycle of light-variation. In order to test whether the B9 lines were affected by the nebulous material surrounding the system, the lines $\lambda\lambda$ 4128–4130 of *Si* II and λ 4481 of *Mg* II were measured.

The second problem concerned the B5 lines. For the purpose of ascertaining the behavior of the B5 component throughout the light-cycle the lines $H\gamma$, $H\delta$, and λ 4472 of *He* I were chosen and equivalent widths obtained. These data determine the optical thickness of the B5 material in the several position angles given by the phases of light-variation. The measurement of the B5 components in $H\gamma$, $H\delta$, and λ 4472 should, further, permit us to test whether the nebula is thick enough to weaken the ordinary absorption lines produced in the reversing layers of the B9 star.[2]

The third problem involved the measure of the B9 component of λ 4472 of *He* I. Whereas the lines $\lambda\lambda$ 4128–4130 of *Si* II and λ 4481 of *Mg* II belong entirely to the normal B9 star spectrum, the line λ 4472 occurs in both the B9 and the B5 spectra and presents a case combining the effects of the B9 star and of the nebula. It should be interesting to determine whether the behavior of the B9 component of λ 4472 parallels that of the B9 components of $\lambda\lambda$ 4128–4130 and λ 4481 or whether it is different.

II

Sixteen spectrograms were used in this discussion, covering the cycle of light-variation in β Lyrae and selected from a large collection of plates taken with the Bruce spectro-

[1] Helen M. Pillans, *Ap. J.*, **80**, 51, 1934.

[2] O. Struve, *Proc. Nat. Acad.*, **26**, 118, 1940.

TABLE 1*

LIST OF PLATES USED IN MAKING THE MICROPHOTOMETER TRACINGS

Plate No.	Computed Cycles+Phase	Date Taken	Universal Time	Exposure Time (in Minutes)	Quality of Plate
1R 11130	2245.003	1934, May 31	3^h55^m	253	E†
1R 11131	2245.017	1934, May 31	7 56	221	G
1RM 12294	2363.072	1938, Aug. 4	8 26	170	G
1R 10550	2209.129	1933, Feb. 21	11 02	125	E
1R 11092	2243.235	1934, May 8	7 21	92	G
1R 10131	2187.300	1932, May 15	7 29	134	E
1RM 12298	2363.363	1938, Aug. 8	2 46	125	G
1R 10148	2188.454	1932, May 30	5 21	213	G
1RM 12314	2367.614	1938, Oct. 2	1 30	141	G
1R 10547	2208.665	1933, Feb. 15	11 07	150	E
1R 10567	2209.746	1933, Mar. 1	10 25	160	E
1R 11121	2244.769	1934, May 28	3 12	139	G
1R 10052	2181.896	1932, Mar. 6	11 16	75	G
1R 11127	2244.925	1934, May 30	3 24	156	G
1R 11128	2244.935	1934, May 30	6 37	224	VG
1RM 12291	2361.984	1938, July 21	6 47	252	G

*The plates were taken by O. Struve, W. W. Morgan, F. R. Sullivan, L. G. Henyey, G. Wares, Miss Helen Pillans, and C. C. C. Crump.

† E = excellent; G = good; VG = very good.

TABLE 2

EQUIVALENT WIDTHS OF THE LINES IN β LYRAE

Phase	B5 $H\gamma$	B5 $H\delta$	B5 *He* I 4472	B8 *He* I 4472	B8 *Si* II λλ 4128–4130	B8 *Mg* II λ 4481†
.003	1.82 A	1.83 A	2.07 A	0 A	0.86 A	0.91 A
.017	1.64	1.87	2.14	0	0.66	0.70
.072	1.20	1.69	1.07	0	0.72	0.57
.129	1.77	1.85	0.96	0	0.53	0.32
.235	0.57	0.52	0.18	0.12	0.40	0.24
.300	0.38	0.37	0	0.01	0.42	0.24
.363	0.36	0.29	0	0	0.34	0.22
.454	0.56	0.75	0	0	0.58	0.37
.614	0.18	0.29	0.01	0	0.67	0.29
.665	0.03	0.17	0	0	0.53	0.41
.746	0.20	0.32	0.19	0.05	0.45	0.42
.769	0.18	0.36	0.22	0.09	0.47	0.37
.896	0.52	0.92	0.91	0.36	0.79	0.36
.925	0.48	0.87	0.81	0.10	0.70–0.81*	0.55
.935	0.36	0.90	0.86	0.07	0.94–1.08*	0.78
.984	0.82	2.32	0.98	0	1.02	0.81

*The smaller value does not include the violet wing, whereas the larger value includes the entire area shown in the reproduced profile of the line.

† The equivalent widths of *Mg* II 4481 include satellites whenever they are present in the profile.

graph of the Yerkes Observatory over a period of several years (1932–1938). These plates are single-prism spectrograms having a dispersion of 30 A/mm at λ 4500 and were taken on Eastman Process emulsion. The plates were sensitized with a tube sensitometer which has been accurately calibrated by several observers and is in regular use at the Yerkes Observatory.

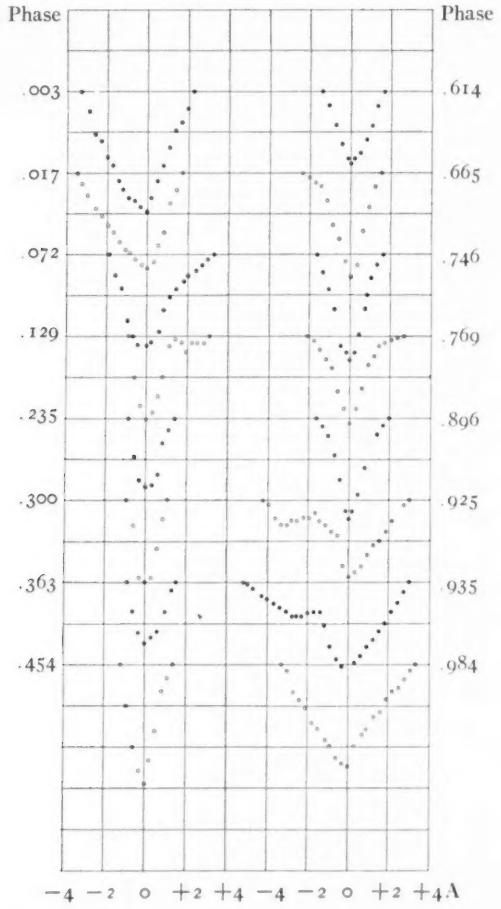

FIG. 1.—Profiles of *Mg* II 4481

Microphotometer tracings were made from the sixteen spectrograms by Miss Frances Sherman and the writer, using the Yerkes microphotometer designed by Dr. C. S. Beals of the Dominion Astrophysical Observatory. The magnification used on the tracings was one hundred times the linear dispersion of the plates.

Table 1 is arranged according to successive phases of the light-cycle and gives, first, the series plate number; second, the computed number of cycles and the decimal fraction of the period, i.e., the phase;[3] third, the date on which the plate was obtained;

[3] The phases were computed by Miss Sherman using Rossiter's formula (cf. R. A. Rossiter, *Pub. U. of Michigan Obs.*, **5**, No. 6, 69, 1933).

fourth, the Universal Time at which the plate was taken; fifth, the exposure time; and sixth, the quality of the plate.

The profiles were reduced in terms of percentages of the continuous spectrum, following the usual method for the reduction of tracings. Measurements were made every millimeter for λλ 4128–4130 and λ 4481, every two millimeters for *Hγ*, Hδ, and *He* I

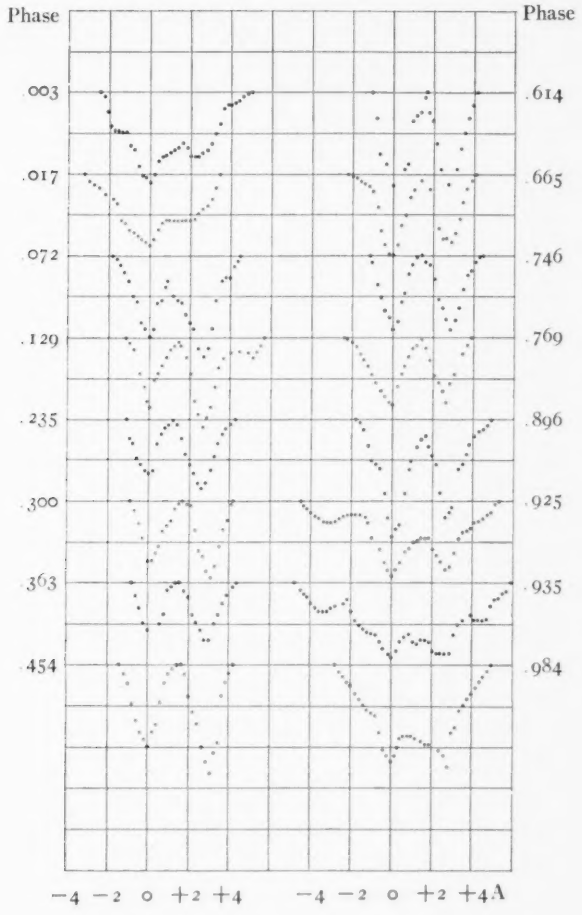

FIG. 2.—Profiles of *Si* II 4128–4131

4472, except for the wings, where measures were occasionally separated by intervals of three or four millimeters. The equivalent widths were obtained from the profiles by measuring the area under the curve with a planimeter. The unit of equivalent width is one angstrom of the continuous background, and this unit was separately determined on each sheet of cross-section paper on which the profiles were plotted.

Table 2 summarizes the equivalent widths determined from the plotted profiles. The B5 components were measured in Hγ, Hδ, and λ 4472 of *He* I; the B9 components were measured in λλ 4128–4130 of *Si* II and λ 4481 of *Mg* II and also in λ 4472. The zero values shown at certain phases for either the B5 or the B9 component of *He* I 4472 indi-

cate either that the absorption is entirely covered by emission or that the absorption does not cut below the continuous spectrum, as an inspection of the figures will show.

The complete profiles, including both emission and absorption components of λλ 4128–4130, λ 4481, *Hγ*, *Hδ*, and *He* I 4472 are reproduced in Figures 1–5. The central intensities of the B5 components of *Hγ*, *Hδ*, and *He* I 4472 are placed on the zero

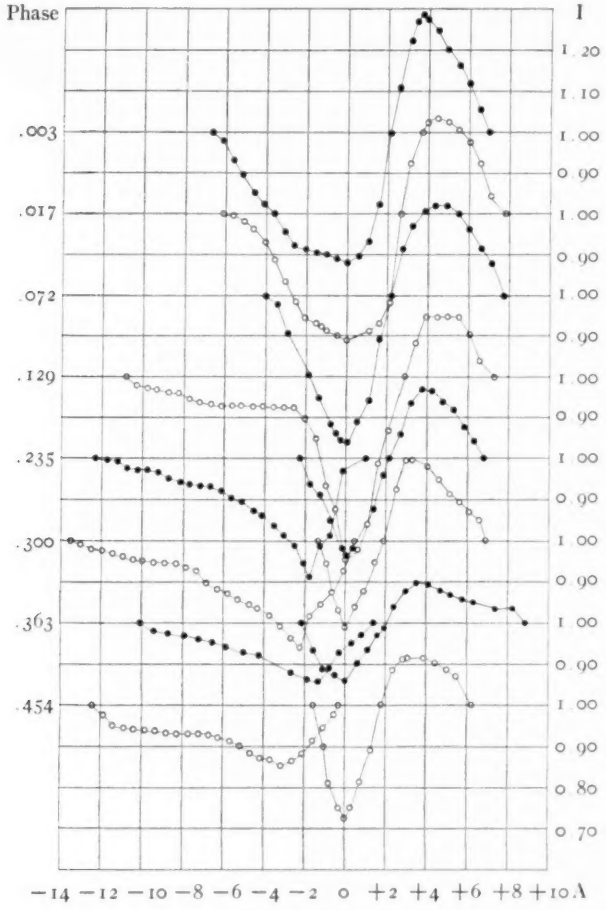

FIG. 3*a*.—Profiles of *Hγ*

point of the abscissa scale. For *Mg* II 4481 the central intensities are plotted on the zero point of the abscissa scale; for *Si* II 4128–4130 the deepest point of λ 4128 is plotted on the zero point. Each step of the ordinate scale represents 10 per cent absorption of the continuous background. In *He* I 4472 this B5 line disappears in absorption at phases .300, .363, and .454, and consequently it was necessary to estimate its position from the behavior of *Hγ* and *Hδ* at those phases. The separation into two components of *Hδ* and *Hγ* at phase .363 and of *Hδ* at phase .454 is problematical; the original tracing shows only a single line with a pronounced violet wing and does not indicate a definite

separation of the B5 and the B9 components. The characteristic curve used in calibrating the intensities for $H\delta$ at phase .017 had to be extrapolated to get the highest points of the emission portion of the profile.

III

The profiles of *Mg* II 4481 of the B9 star show at times rather unsymmetrical lines. With the small dispersion used, this assymmetry, observed between phases .925 and

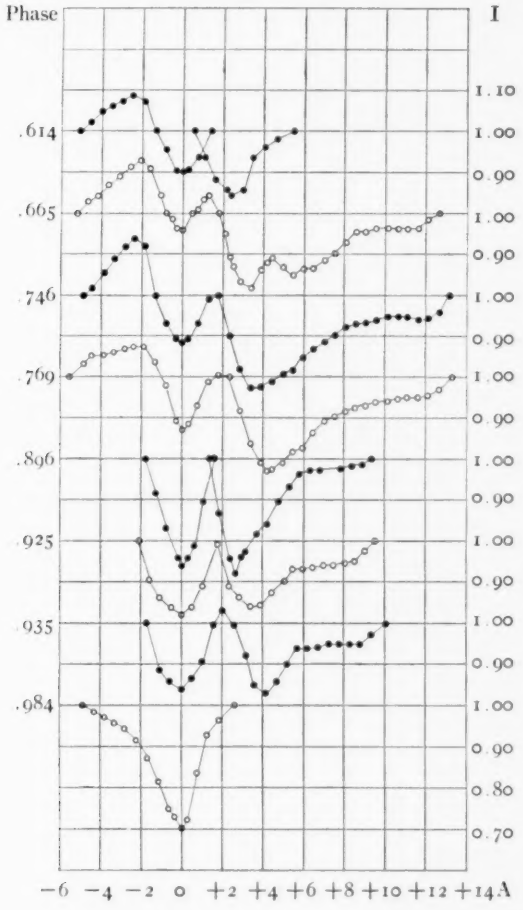

FIG. 3*b*.—Profiles of $H\gamma$

.072, is probably caused by the satellite lines rather than by Rossiter's rotation effect. There is a suggestion of a red satellite at phase .129, although its existence is by no means definite. The violet satellites, which are very pronounced at phases .925 and .935 are, however, not the satellites observed by Struve and others for *Mg* II 4481. The red satellite of *Mg* II 4481 is included in the red wings of the profiles at phases .925, .935, and .984. The values of the equivalent widths show that λ 4481 is strongest near primary minimum—that is, at phases .925, .935, .984, .003, .017, and .072—whereas

it is fairly constant throughout the rest of the cycle. It is weakest between phases .235 and .363.

In plotting the profiles of λλ 4128–4130, well-known doublet of *Si* II, no attempt has been made to separate the two lines because they are blended near primary minimum. The equivalent widths for *Si* II are, therefore, those of the entire doublet. Like *Mg* II 4481 the lines of *Si* II 4128–4130 have a suggestion of satellites between phases .925

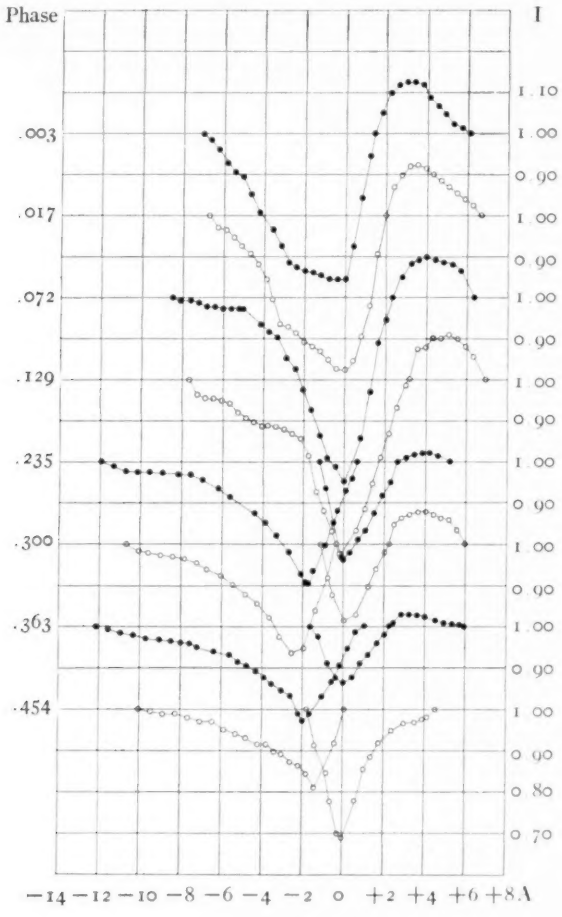

FIG. 4*a*.—Profiles of *Hδ*

and .129. The measured line intensities of *Si* II show a behavior similar to that of *Mg* II and have their greatest strength near primary minimum at phases .896, .925, .935, .984, .003, .017, and .072. *Si* II 4128–4130 are weakest between phases .235 and .454.

The behavior of *Hγ* and *Hδ* is sufficiently parallel to be considered simultaneously. The B5 components, arising in the nebulous material surrounding the β Lyrae system, are strongest near primary minimum at phases .984, .003, .017, .072, and .129, as both the profiles and the equivalent widths indicate. The lines *Hγ* and *Hδ* are weakest somewhere between phases .614 and .746.

Although the relative behavior of $H\gamma$ and $H\delta$ is apparently parallel, the absolute behavior of the two lines is not. Inspection of the table of equivalent widths shows that $H\delta$ is often of the order of twice the strength of $H\gamma$ and about three times its strength just preceding primary minimum (phase .984). The discrepancies between the intensities of $H\gamma$ and $H\delta$ are partly explained by the Stark wings which are known to be stronger in $H\delta$ than in $H\gamma$.[4]

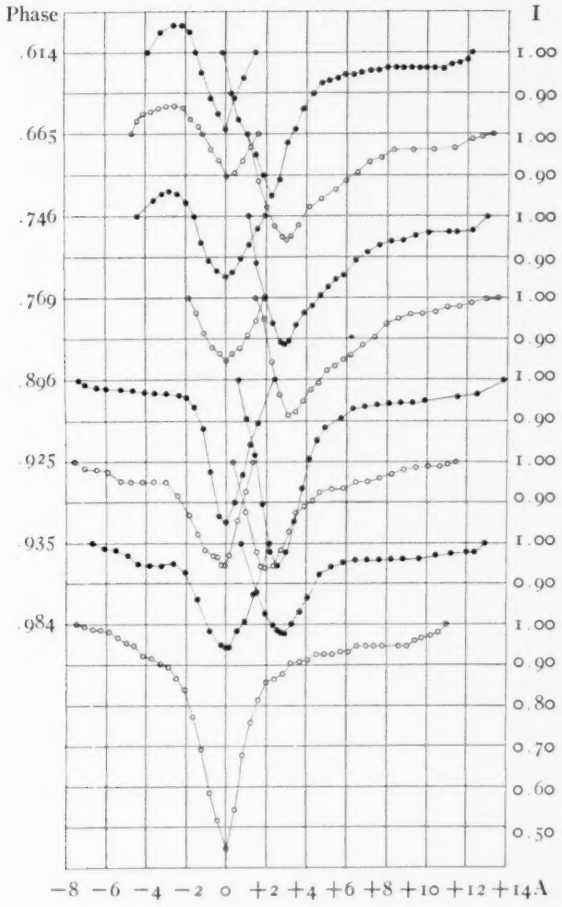

FIG. 4*b*.—Profiles of $H\delta$

Another interesting fact about the hydrogen lines is the characteristic behavior of their wings. For $H\delta$ the phases from .235 through .454 show an increasingly wide violet wing of the B9 component with the red wing covered by emission. Beginning with phase .614 there is an indication of a red wing almost until primary minimum. $H\gamma$ shows a behavior very similar to that of $H\delta$, having a violet wing throughout phases .235–.454 with the red wing covered by emission. By phase .614 the uncovered wing is on the red side, and this situation continues until phase .925.

[4] Elvey and Struve, *Ap. J.*, **72**, 300, 1930.

The line of *He* I 4472 is very complicated, having several emission and absorption components throughout most of the light-cycle. The profiles at phases .003 and .017 resemble those of *Hδ* and *Hγ*; but those at phases .072 and .129 are quite different, having emission components both on the violet and on the red sides. From phases .003 to .235 the main absorption is due to the B5 component, but by phase .300 the B5 component is covered by emission, with the B9 component in evidence. From phases .614

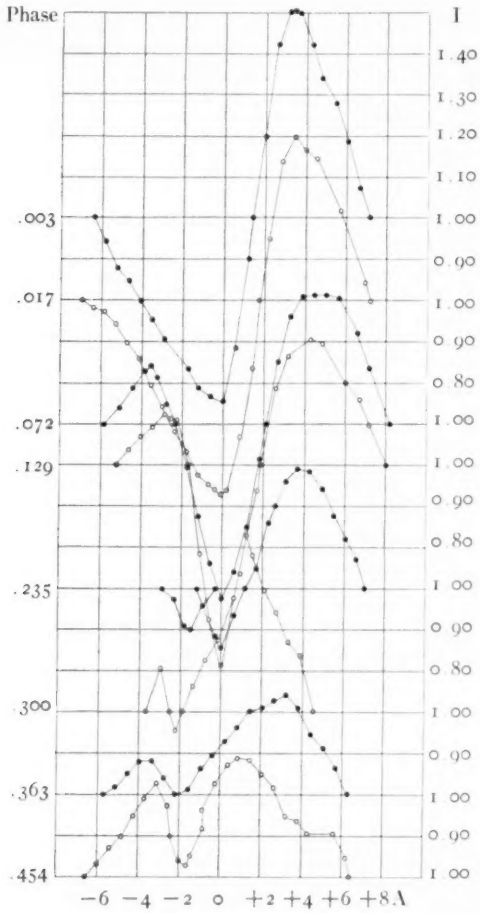

FIG. 5*a*.—Profiles of *He* I 4472

to .984 both the B9 and the B5 absorption components show, being at certain phases more or less covered by emission. The table of equivalent widths shows the B5 absorption in λ 4472 to be strongest at phases .003 and .017. At these two positions λ 4472 is stronger than *Hδ* or *Hγ*, although just preceding primary minimum (phase .984) *Hδ* is the strongest line measured, being more than twice as strong as *He* I 4472 and nearly three times as strong as *Hγ*.

The measures of the intensities of the B9 lines of *Si* II 4128–4130 and *Mg* II 4481 show not only that the B9 lines are not constant in equivalent width throughout the light-cycle but also that the B9 lines are themselves strongest near primary minimum—a

remarkable fact since the B5 lines, originating in the nebulous envelope, are also strongest near primary minimum and do not weaken the B9 lines as expected.[5] This is at least in part caused by the satellites. It is possible that the B9 lines would remain constant in equivalent width if the intensities of the satellites were subtracted.

The B9 component of λ 4472 is variable and notably weaker in the first half of the cycle than in the second half.

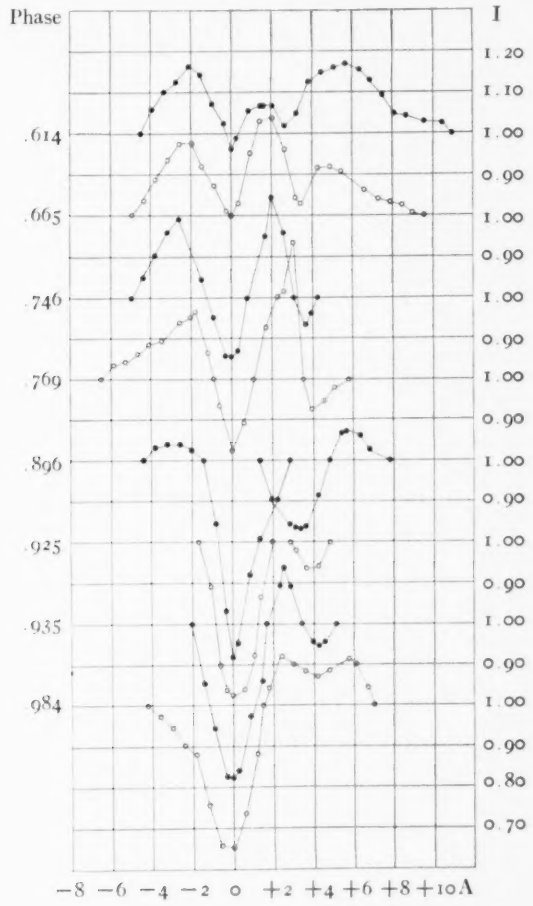

FIG. 5*b*.—Profiles of *He* I 4472

I am grateful to Dr. Struve for the suggestion of this problem and also for his constant encouragement and assistance while the work was being done. I also wish to express my appreciation to Dr. Page and Dr. Keenan for the assistance they gave me while I was working at the University. Thanks are due Miss Sherman for her share in making the microphotometer tracings.

YERKES OBSERVATORY
September 1940

[5] Struve, *loc. cit.*

THE SPECTRUM OF β LYRAE IN THE VISUAL REGION

J. L. GREENSTEIN AND T. L. PAGE

ABSTRACT

Nine grating spectrograms of the visual region of β Lyrae have been discussed. Table 1 contains a list of wave lengths and identifications in the spectrum of the primary star, of type cB9. Lines of *Fe* II, *Si* II, *S* II, and *Ne* I are present. The usually strong hydrogen and helium lines are not clearly seen; presumably, they are weakened by the presence of strong emission lines in the "stationary" spectrum. The stationary or B5 spectrum consists of strong emission lines of *H* and *He* I with strong superposed absorption lines. *Na* I is present as an absorption line with two components; one component at -5 km/sec may possibly be interstellar, the other at about -125 km/sec must originate in the nebulous shell. Table 2 contains the measured displacements of the B5 absorption lines; they seem to be independent of the orbital motion of the cB9 star. The measured intensities of the emission components and of the absorption lines are given in Table 3. The absorption is greatest near the phase of primary minimum; the material is too small to reveal the asymmetry discussed by Struve. The absorption line *He* I 5016, originating from a metastable level, is stronger relative to its emission line than are the B5 absorption lines from normal levels, such as λ 5876.

A preliminary investigation of the visual spectrum of β Lyrae has been carried out with the Yerkes autocollimating grating spectrograph. Nine exposures at various phases of different cycles were obtained between July and September, 1940. The description of the spectrum may, therefore, be affected by possible changes between cycles. The spectrograph has a mean dispersion of 27.1 A/mm and covers the region from $H\beta$ to $H\alpha$. Agfa Super Pan Press films were used. The films are good in the interval from λ 5100 to λ 6500 but are usually underexposed at $H\beta$ and at λ 6678.

THE CB9 SPECTRUM

The spectrum of β Lyr has been divided into two components—one arising in expanding shell, the B5 spectrum,[1,2] the other in a supergiant B9 star. The lines of the B5 spectrum show nearly constant velocity of approach. The lines of the B9 spectrum show large orbital velocities. They are broad and rather shallow in the visual region. This shallowness, together with the possible variability of the lines with phase, results in some doubt concerning the reality of some of the fainter lines. Wave lengths of all lines were measured on six plates, while the B5 lines were also measured on three additional plates. In Table 1 we give a list of those lines of the B9 spectrum which were measured on three or more plates. The probable error of a final wave length is ± 0.11 A. Thirty-three other lines measured on two plates have been satisfactorily identified with laboratory sources and are undoubtedly real. While not included in Table 1, they have been used to aid in identifications.

The spectroscopic orbit derived by Rossiter[3] was used to obtain preliminary radial velocities for the first identifications of the lines. The final velocities derived from the six plates differ only negligibly from the predicted orbital velocities, except for rotation effect. The systematic residual velocity is $+1$ km/sec referred to the predicted orbital velocities and $+2$ km/sec referred to the atmospheric lines. The observed wave lengths were corrected for the orbital velocity of the B9 component and were combined to form the list given in Table 1. Intensity estimates and identifications are included. Under λ_1 and I_1 are the laboratory wave lengths and intensities.

The identifications are based mainly on Miss Moore's *A Multiplet Table of Astro-*

[1] Struve, *Observatory*, **57**, 265, 1934.

[2] Struve, *Ap. J.*, this issue.

[3] *Pub. Obs. U. of Michigan*, **5**, No. 6, 1933.

physical Interest and on Dobbie's[4] list of *Fe* II lines. *Fe* II, *Si* II, and *S* II dominate the spectrum, and *Ne* I is definitely present. The strength of *S* II is remarkable; the lines, however, have been classified and are all extremely strong in the spark spectrum of sulphur. Certain of the unidentified lines are found in other stellar spectra, i.e., α Cyg[5] and υ Sgr[6]; they are so indicated in Table 1. The lack of identifications for some lines is not surprising in view of the incompleteness of the laboratory investigations of the visual region of the spectra of ionized metals. The major peculiarity of this B9 spectrum is the absence of the usual strong hydrogen and helium lines seen in spectra

TABLE 1

THE B9 SPECTRUM

λ	I	Element	λ_1	I_1	λ	I	Element	λ_1	I_1
5041.25	2	*Si* II	1.13	8	92.73	1	(*Fe* II	3.87	1)
48.01	2	*He* I	7.74	2			υ Sgr	2.60	3
56.05	3	*Si* II	6.17	10	5565.04	1	*S* II	4.94	4
5127.48	1	(*Fe* II	7.87	1)	89.85	1n	?	.....	.....
		υ Sgr	7.09	3	5600.35:	0–1	?	.....	.....
56.67	2	(*S* II	7.04	4)	12.17	0–1	?	.....	.....
		υ Sgr	6.26	3			*S* II	9.96	8
69.55	5	*Fe* II	9.03	12	40.01	3	*S* II	0.32	5
5227.89	2	(*Ti* II	6.55	5)			*Si* II	9.49	2
		υ Sgr	7.30	5n	47.43	0–1	*S* II	6.98	6
34.78	1	*Fe* II	4.62	7	5957.96:	2	*Si* II	7.61	5
60.26	1–0	*Fe* II	0.33	5	79.15	3	*Si* II	8.97	7
64.92	1	*Fe* II	4.80	2	6029.38	2	(*Ne* I	0.00	10)
		Mg II	4.14	5	67.52:	1–0	?	.....	.....
5316.51	3	*Fe* II	6.61	8	75.02:	0–1	?	.....	.....
44.52:	1	?	.....	.....	79.89	1	?	.....	.....
63.05	2	*Fe* II	2.86	5	6108.84	1	?	.....	.....
70.06	0	α Cyg	9.68	2	43.28	1–0	*Ne* I	3.06	12
87.19	2	*Fe* II	7.14	2	48.01	1–0	*Fe* II	7.74	2
96.18	0	*Fe* II	5.86	1			*Fe* II	9.24	2
5401.61	2	*Fe* II	2.11	2	75.31	0–1	*Fe* II	5.14	1
		Mg II	1.05	5	6202.58:	0–1	?	.....	.....
09.28	1	*Fe* II	8.84	1	66.43	2	*Ne* I	6.54	15
28.88	1	*Fe* II	7.82	3	6347.24	6	*Si* II	7.10	10
		S II	8.64	5	61.93	1	?	.....	.....
32.63	3	*S* II	2.77	9	71.46	5	*Si* II	1.36	8
44.25	0	?	.....	.....	6402.43	3n	*Ne* I	2.25	20
54.13	2	*S* II	3.81	10	6506.45:	2	*Ne* I	6.53	15
73.46	0	*S* II	3.59	5	12.28	2	α Cyg	2.19	2
88.43	1–0	*S* II	8.28	3					

in the range B8 to A2. The great strength of the emission lines of hydrogen and helium in the shell weaken the B9 absorption lines in two ways. The strong superposed emission wings cover the B9 lines except near the phase of maximum positive velocity. Further, as suggested by Struve,[2] the strong emission lines may de-excite atoms in the B9 atmosphere. The weaker helium lines are actually present in the B9 spectrum. The line λ 4922 ($2^1P^o - 4^1D$) has only weak emission in the B5 spectrum; the observed complex line, which includes a *Fe* II line, λ 4924, shows definite displacements correlated with the orbital velocity of the B9 star. The very weak line *He* I 5048 ($2^1P^o - 4^1S$) has no detectable emission; its displacements follow the B9 star's orbital motion, and the line should be ascribed to the star.

[4] *Ann. Solar Phys. Obs., Cambridge*, **5**, Part 1, 1938.

[5] Marshall, *Ap. J.*, **82**, 97, 1935.

[6] J. L. Greenstein, unpublished.

The spectrum of the B9 star has been compared with that of β Ori, cB8, and of σ Cyg, cA0, on plates taken with the grating spectrograph. The lines of *Fe* II are roughly equal in β Ori and β Lyr, while *S* II is stronger in β Lyr. The *C* II lines at λ 6578 and λ 6583 are definitely much stronger in β Ori. In σ Cyg, *Fe* II is stronger, *S* II weaker, than in β Lyr. The level of ionization and excitation in β Lyr is intermediate between that in the two other stars, and we might classify β Lyr as cB9 in agreement with previous investigators.[7,8] The possible existence of the important satellites to the B9 lines and the phenomena at primary minima remain to be studied on more complete series of plates. On one plate taken 0^d7 before the primary minimum the lines are very broad or even double. The *Si* II lines at λ 6347 and λ 6371 seem to be considerably weaker than normal.

THE STATIONARY OR B5 SPECTRUM

Struve[1,2] has suggested that the emission and absorption lines of hydrogen and helium originate in a nebulous mass at considerable distance from the B9 star. He has extensively discussed the spectroscopic features of this appendage and has shown that it possesses variable density, with a maximum soon after primary minimum. A dynamical model for this asymmetrical mass of material has been suggested by Kuiper.[9] Besides the hydrogen lines the visual region contains four helium lines originating at the normal levels, 2^1P^o and 2^3P^o, and one line, λ 5016, from the metastable level, 2^1S. These lines are of variable intensity and consist of a broad emission line on which is superposed a broad absorption line, displaced to the violet. An additional feature is a very complex structure of variable intensity between wave lengths λ 5888 and λ 5896, the resonance lines of neutral sodium. There is no obvious emission at the D1 and D2 lines. The B5 lines all show considerable Doppler broadening arising from the velocity dispersion or from turbulent motions within the nebulous material.

The probable error of the measured position of a line on one plate corresponds to perhaps ± 8 km/sec. All the measured displacements have been interpreted as velocity shifts, and Table 2 gives the measured velocities for each plate. The first column contains the phase, the second the predicted orbital velocity of the B9 star, and the following columns the velocities in km/sec.

The general features of the observed displacements resemble those of the displacements in the photographic[2] and ultraviolet[10] regions of the spectrum. The hydrogen lines show displacements averaging -100 km/sec at phases 1^d, 2^d, and 12^d and -85 km/sec at 3^d, 4^d, and 10^d. The displacements are greater for the metastable line λ 5016 than for the other lines. Little influence of the orbital motion of the B9 star is detectable in any of these lines. The sodium lines are more difficult to interpret. Each sodium line is usually double, and at some phases other components are suspected. One of the sodium lines is nearly stationary near zero displacement. The mean displacement of these red components of D1 and D2, r, is -5 km/sec; either the lines may be interstellar in origin, or they may arise in a nebulous envelope with a small velocity of expansion. The equivalent width of D2 is about 0.65 A; since the star is at a distance of 500 parsecs, this strength is greater than average but perhaps not excessively so. When the displaced component of D1 and D2 is weak and at large negative displacements, the red component seems sharp and may well be interstellar. The velocities of the displaced component, v, of the sodium lines are somewhat anomalous. They are the largest observed in the visual region—about -125 km/sec; the largest displacements occur at phases 3^d and 4^d, when the B9 star has large negative velocity. It is probable that the sodium lines in the envelope are slightly affected by blends with the B9 star.

The existence of neutral sodium in any appreciable quantity in a nebulous mass

[7] Maury, *Harvard Ann.*, **84**, 207, 1933.

[8] Pillans, *Ap. J.*, **80**, 51, 1934.

[9] *Ap. J.*, this issue.

[10] J. G. Baker, *Harvard Ann.*, **105**, 107, 1937.

which has strong hydrogen and helium lines is interesting. Let us assume that the ionization and excitation can be described by a temperature $T = 15{,}000°$, an electron pressure which need not be known directly, and a dilution W. Struve[2] has shown that $W \approx 0.02$. Hydrogen, helium, and sodium are all dominantly ionized, but we need not consider the second ionization of sodium unless the electron pressure is exceedingly low. The ratio of the number of atoms of sodium (ground state) to hydrogen (second states) is given by

$$\log_{10} \frac{N(Na\ 1)}{N(H)_2} = \log_{10} \frac{\zeta(Na)}{\zeta(H)} + 1.74 \left(\frac{5040°}{T}\right) - \log_{10} W - 0.60\,, \qquad (1)$$

where the total abundance by number of atoms is ζ. If we deal with weak lines, for

TABLE 2

VELOCITY DISPLACEMENTS OF THE STATIONARY LINES (B5 SPECTRUM)

Phase	B9 Velocity	*Hβ*	*Hα*	*He* λ 4922	*He* λ 5016	*He* λ 5876	*He* λ 6678	*Na* λ 5890	*Na* λ 5896
0^{d}95*	− 92	−98	−110	−115	−118	−110	−61	−101*d* −07*d*	−39*dd*
2.04	−166	.....	− 92	.....	.....	− 94	.....	−143: −28	−118: +05
2.07	−167	−77	− 81	− 93	−106	− 99	−79	−100 −06	−115 −13
3.26	−200	−71	− 73	−115	−110	− 96	−43	−160 −06	−188 +01
4.29	−188	.....	− 35:	+ 15*d*:†	− 92	− 61	−06:	−160 +04	−142 +06
10.14	+163	−77	− 74	− 73*d*:	− 89	− 77	−51	−136 −03	−107 +04
11.15	+125	−77	− 87	− 78	−110	− 90	−74	−111 −03	−108 −10
11.93*	+ 70	−60:	−120	+ 29*d*:	−108	−100	−91:	−151*d*: −40*d*:	−113: −21
12.23	+ 48	−37:	−104	− 41	−120	−104	−71	−128 −01	−109 −10

* At phases 0^{d}95 and 11^{d}93 the sodium lines were badly blended and could not be accurately measured.

† Lines marked *d* are clearly double or are blended and are therefore probably affected by lines of the B9 star or by other components.

which we can assume that the equivalent width, $A \propto Nhf$, or with lines originating in a highly turbulent atmosphere, we obtain

$$\log_{10} \frac{\zeta(Na)}{\zeta(H)} = \log_{10} \frac{A(Na)}{A(H\alpha)} - 1.74 \left(\frac{5040°}{T}\right) + \log_{10} W + 0.60 - \log_{10} \frac{f(Na)}{f(H\alpha)}\,. \qquad (2)$$

The *f*-values in the last term are known, and the equivalent widths are given in Table 3. Since the hydrogen lines are strong in the visual region, we are underestimating the number of hydrogen atoms and are, therefore, overestimating the abundance of sodium.

From our measures of plates near primary minimum, the equivalent width of the absorption component of *Hα* is about 9 A and of the displaced components of D1+D2 about 1.5 A. The abundance of sodium is then less than one four-hundredth of that of hydrogen—an upper limit which seems reasonable. While neutral sodium is unusual in normal B5 spectra, dilution of the radiation favors its appearance, as can be seen in equation (1).

LINE INTENSITIES IN THE B5 SPECTRUM

The nature of the variation of the emission and absorption-line intensities with phase has been studied on the available plates. The results are subject to possible variations from cycle to cycle. Four lines were studied in the visual region—*He* I 5016 ($2^1S - 3^1P^o$), *He* I 5876 ($2^3P^o - 3^3D$), *Hα*, and the *Na* I lines. Microphotometer tracings were made with a dispersion of 0.27 A/mm. Photometric standardization on seven plates was

afforded by a tube sensitometer of rather uncertain effective wave length. For two plates a step-slit spectrosensitometer was used. The profiles of the complex emission and absorption lines were then obtained on an intensity scale.

We have measured, in general, four quantities for each line. For most lines the central absorption cuts below the neighboring continuous spectrum and leaves two distinct emission lines, V and R, which are easily measured. The intensity is given in units of 1 A of the neighboring stellar continuous spectrum; during eclipse, of course, this unit will vary. The strong, nearly central, absorption line obviously has blotted out what should have been the strong central part of the emission line. An attempt has been made to reconstruct this total emission line by reflecting the relatively undisturbed red emission wing about the undisplaced position of the line. This total emission is denoted by E in Table 3. The total absorption of the absorption line has been obtained with respect to the hypothetical background of the reconstructed emission line and is affected by the uncertainties of drawing that line. All equivalent widths were measured with

TABLE 3

EQUIVALENT WIDTHS IN THE B_5 SPECTRUM

Phase	*He* I 5016				*He* I 5876				*Hα*				*D*2*	*D*1*
	Abs.	*V*	*R*	*E*	Abs.	*V*	*R*	*E*	Abs.	*V*	*R*	*E*	*v r*	*v r*
0^d.95	2.1	0.13	0.32	1.4	8.3	1.8	6.3	15	7.1	3.8	12	23	1.7*d*	1.2*d*
2.04	2.9	.....	.46	2.3	4.7	1.2	3.5	8.7	6.8	3.0	8.4	17	0.58 0.71	.....
2.07	2.4	.19	.77	2.4	4.6	1.3	3.4	8.3	8.8	3.3	9.6	21	1.3*d*	0.33 0.47
3.26	1.5:	.36:	.51:	2.0:	4.4	1.8	5.1	11	6.5	5.9	13	26	0.64 0.68	0.68*d*
4.29	1.5	.11	.60	1.7	3.8	1.8	4.6	9.9	7.4	6.6	12	25	0.34 0.70	0.68*d*
10.14	1.7	.28	.71	1.9	4.8	1.7	3.4	9.2	6.4	4.2	8.4	19	0.28 0.43	.....
11.15	2.2	.24	.22	1.4	4.4	1.3	2.6	7.4	6.8	4.4	9.8	20	.....	.....
11.93	1.6	.47	.....	1.2	3.9	1.0	4.1	8.9	8.7	5.6	14	29	.....	.....
12.23	2.5	0.13	0.21	1.4	6.4	1.7	5.7	13	11	5.1	15	31	1.9*d*	1.4*d*:

* The fixed component of D1 and D2 is r, the displaced and variable component is v. Where these lines could not be separated, the total blended equivalent width was measured. This is indicated in Table 3 by the symbol *d*.

a planimeter; the accidental error is of the order of 5 per cent; the photometric errors and the uncertainty of the drawing of the original emission line are much more serious and may attain 20 per cent. It was not always possible on the tracings to separate the components of the D lines, and they have not always been measured. The tracings give the impression that the entire region of the D lines is depressed below the neighboring continuum. Table 3 contains the results of these measurements.

Some general conclusions as to the behavior of the emission lines may be drawn from the data of Table 3. The red emission component is always much stronger than the violet, with an average ratio $V/R = 0.3$. The total emission E fluctuates rather irregularly during the cycle, with some tendency for higher values in the first half of the cycle. The absorption lines are strongest just before and just after primary minimum, but there is no material for the study of the asymmetrical increase soon after primary minimum, which was discussed by Struve.[2] The displaced sodium lines are weak at phases 4^d and 10^d. While *Hα* and λ 5876 behave similarly as far as variation with phase is concerned, they show a different ratio of absorption to emission intensities. The ratio E/Abs. for *Hα* is 3.0, for λ 5876 it is 2.0, and for the metastable line λ 5016 the ratio falls to 0.9. The latter phenomenon is connected with the relative overpopulation of the metastable level in an extended atmosphere.

YERKES OBSERVATORY
October 1940

ON THE INTERPRETATION OF β LYRAE AND OTHER CLOSE BINARIES*

GERARD P. KUIPER

ABSTRACT

In this paper a model for β Lyrae is developed which attempts to account for the complex photometric and spectroscopic phenomena and which is consistent with dynamics.

In the introduction the dimensions of the system are discussed, and the conclusion is reached that the components have a common envelope (they form a "contact binary"). In section 2 it is shown that contact binaries with unequal components are unstable. It is shown that matter streams from A to B as long as the masses are unequal; that Δm and Δ(Spectral type) are abnormally large for the mass ratio; and that a system of currents will be set up (Fig. 4, *b*). These currents account for the satellite components of spectral lines observed near the primary minimum of β Lyrae.

If the common envelope attains great height and/or if the currents attain large velocities, ejection of matter from the outer point of B will take place. This ejection is considered to supply the source of the mysterious B_5 spectrum and to cause the asymmetry and irregularity of the photometric minimum. Ejection of another type (type A), arising in a separated binary composed of one giant and one dwarf star, is also considered, and its application to peculiar emission stars with composite spectra is stressed. The theory of both types of ejection based on Jacobi's integral is given in section 4. The orbits of ejected particles are determined in sections 5–7. Section 5 contains the first-order theory for the vicinity of the point of ejection; Figures 6 and 7 illustrate the results. Numerical integrations are used in sections 6 and 7 with Figures 8–12 showing the orbits obtained. Section 8 gives applications to β Lyrae and other stars. A schematic picture of the gaseous tail in which β Lyrae winds itself is given in Figure 13. The effect is that of a giant pinwheel with one streamer. The shadow cast by B on the streamer appears to play an important role in the spectral features, as it appears to de-ionize the gas. The change of period in β Lyrae is also considered. It appears that both the process of mass transfer from A to B and the ejection from B would tend to shorten the period. The effect on the period of the pressure at the interface of the components is examined in the addendum.

1. INTRODUCTION

It is a well-known fact that β Lyrae shows peculiar asymmetries which have not yet found an adequate explanation. These asymmetries appear in the light-curve as well as in the spectral features. We mention below the chief data and the interpretation they have thus far received.[1]

a) *The light-curve.*—Stebbins,[2] using a rubidium cell, found "a marked asymmetry of the light curve at primary minimum, the decrease of light being more rapid than the increase. This difference extends as far as the maxima on each side of the minimum, the phases of the maxima being -2.95 days and $+3.45$ days respectively." The depths of the minima were found to be 0.98 and 0.47 mag., respectively, and the maximum following the primary minimum was found to be 0.02 mag. lower than the other maximum. Such an inequality had already been suspected by K. Schwarzschild.[3]

Huffer,[4] using a potassium cell, confirmed the asymmetry of the primary minimum but found the maxima nearly equal in brightness. He obtained somewhat smaller values for the amplitudes, 0.88 and 0.40 mag. However, Smart,[5] also using a potassium cell, found amplitudes in good accord with those of Stebbins (0.97 and 0.44 mag.), so that intrinsic variations, rather than differences in the color sensitivity of the cells, may be re-

* *Contributions from the McDonald Observatory, University of Texas*, No. 28.

[1] A complete bibliography is given in the *Geschichte und Literatur des Lichtwechsels*, **2**, 156, 1920, and *Zweite Ausgabe*, **2**, 244, 1936.

[2] *Lick Obs. Bull.*, **8**, 186, 1916.

[3] *Pub. d. Kuffnerschen Sternwarte*, **5**, C 127, 1899.

[4] *Pub. Washburn Obs.*, **15**, 209, 1931.

[5] *M.N.*, **95**, 647, 1935.

sponsible for these differences in amplitude. Smart agreed with Stebbins in finding the maximum after the primary minimum about 0.02 mag. fainter than the other maximum.

A good visual light-curve has been published by Danjon,[6] who found marked changes in the light-curve during three successive observing seasons; but in all three seasons the primary minimum was strikingly asymmetrical, as is shown in Figure 1, which is reproduced from Danjon's paper. The amplitudes were 0.81 and 0.43 mag.; these values, in connection with the values found photoelectrically, suggest, as Danjon points out,[7] that the star eclipsed at primary minimum is the bluer of the two, consistent with the ratio of the surface brightnesses found from the minima.

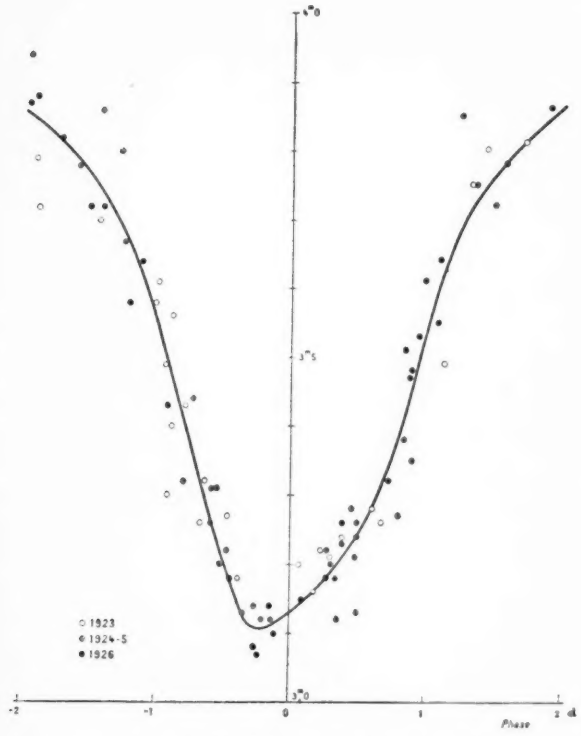

FIG. 1.—Primary minimum of β Lyrae (Danjon)

b) *The color.*—Stebbins and Huffer[8] found the color index to be $-0^{m}13$ in their system, corresponding to a normal B8 star. Hall's infrared index[9] corresponds to about A0.

Of particular interest are the color measures related to phase. The visual determinations by L. Terkan[10] were not confirmed by the more reliable photoelectric measures by Elvey[11] and by Schneller.[12] Both these observers found the binary to be reddest at primary minimum and bluest at secondary minimum. The range was found to be 0.03 mag. by Elvey (base line, 4750–4250A) and about 0.06 mag. by Schneller. These results are consistent with those by Danjon and with the ratio of the surface brightnesses.

c) *The spectroscopic observations.*—These are very numerous and need not be mentioned here in view of Dr. Struve's article in this issue.[13]

d) *The interpretation.*—Much progress in astronomy has been the direct result of attempts to interpret the observations of β Lyrae. Plassmann seems to have been the first[14] to emphasize that the double-star hypothesis, previously used to explain light-curves of the Algol type, would also be applicable to β Lyrae if tidally elongated components were assumed. That this hypothesis was correct, rather than E. C. Pickering's earlier suggestion of a single, rotating ellipsoid covered with spots,[15] was already indi-

[6] *Ann. Obs. Strasbourg*, **2**, 114, 1933.

[7] *Ibid.*, p. 130.

[8] *Pub. Washburn Obs.*, **15**, 233, 1931.

[9] *Ap. J.*, **79**, 169, 1934.

[10] *A.N.*, **226**, 345, 1926.

[11] *Ap. J.*, **81**, 173, 1935.

[12] *Kl. Veröff. Berlin-Babelsberg*, No. 17, 1936.

[13] P. 104.

[14] Cf. J. Stein, *Die veränderlichen Sterne*, **2**, 307, 1924.

[15] *Proc. Amer. Acad. Arts and Sci.*, **16**, 270, 1881.

cated by Pickering's observations of the spectrum[16] and was conclusively shown by G. W. Myers[17] with the aid of Belopolsky's radial velocities of 1892.

The first determination of the photometric elements was made by Myers,[17] who developed the necessary formulae for ellipsoidal bodies; a summary of this work was presented at the dedication of the Yerkes Observatory.[18] J. Stein found[19] that some of Myers' formulae needed correction, and he derived a new set of elements. By that time the photometric theory was practically complete.

Several photometric solutions have been published; those prior to 1924 are listed by Stein.[14] With the exception of some of von Hepperger's solutions the darker star (in front at primary minimum) was found to be the larger. This is also true of Danjon's solution[6] and of several solutions made by Sandig.[20]

TABLE 1

COMPUTED ABSOLUTE MAGNITUDES FOR β LYRAE

M_A/M_B	M_A	M_B	$M_{bol}(A)$	$M_{bol}(B)$	ΔM_{bol}	$M_{vis}(A)$
1.0	33	33	− 6.6:	− 6.6:	0.0:	− 5.6:
1.5	78	52	8.6::	7.7:	0.9:	7.6::
2.0	150	75	10:	8.6::	1.4::	9:
2.5	255	102	11:	9:	2:	10:
3.0	399	133	−11::	−10:	1–2::	−10::

The fact that the same light-curve can be explained by such widely different ratios of the radii as assumed by von Hepperger (5 and 0.6) shows that other considerations should be used as well as the conventional ones. Struve has shown[21] that the B5 spectrum is not due to a star and that only one component of the binary is visible. This means that $L_B \ll L_A$. Hence the round maxima of the light-curve are due chiefly to the elongation of A, since B is too faint. Since the composition of B and A are presumably similar, the mass-luminosity relation may be used to derive the result $M_B \ll M_A$. The considerable elongation of A then shows that the center of B must be close to A, at the most about one radius of A from A's surface. This shows that B cannot be larger than A.

A lower limit to the mass ratio and the relative size of B can be set in the following manner. From measures of the B8 component Rossiter[22] found the mass function to be $8.32\odot$. In Table 1 we give the resulting masses of the two components for different mass ratios ($B \leqslant A$), adopting $i = 90°$ in each case. (The masses so obtained will be minimum masses.) With the aid of an empirical mean mass-luminosity relation[23] bolometric magnitudes may now be derived; but, owing to the great scatter in the upper part of the mass-luminosity diagram, the star may easily differ by 1 or 2 mag. from these computed values.

We have the following information as to the true absolute magnitude of β Lyrae. Spectroscopically Struve[24] found the luminosity of the B8 component high, but less than that of Rigel, which by its double companion of type B5 may be estimated to be about −8 visually. But β Lyrae has also a visual companion. On the basis of the measures in Aitken's *Catalogue of Double Stars* (after correction for precession in angle amounting to

[16] *A.N.*, **128**, 42, 1891. Cf. also *Harvard Obs. Circ.*, No. 7, 1896; *Ap. J.*, **4**, 142, 1896.

[17] *Untersuchungen über den Lichtwechsel des Sternes β Lyrae*, Munich, 1896.

[18] *Ap. J.*, **7**, 1, 1898.

[19] *Proc. Acad. Amsterdam*, **10**, 459, 1907.

[20] *Zs. f. Ap.*, **8**, 29, 1934.

[21] *Observatory*, **57**, 265, 1934.

[22] *Pub. Michigan Obs.*, **5**, 86, 1934.

[23] *Ap. J.*, **88**, 489, 1938; 29 Canis Majoris was omitted.

[24] *Ap. J.*, **93**, 105, 1941.

$-0^{m}65$ per century), the proper motions in Boss's *General Catalogue*, and the radial velocities (-19.0 km/sec for β_1 and -13 ± 5 for β_2), it is probable that the stars form a physical system. The magnitude of β_1 at maximum is 0.17 mag. fainter than the A0 star γ Lyrae according to Smart,[5] and 0.15 mag. according to Stebbins.[2] For γ Lyrae we find 3.37 IPv; hence, β(max.) = 3.53 IPv. Adopting in the bright binary $\Delta m = 3$, for reasons given later, we find for the apparent magnitude of A, 3.6.

The magnitude of the companion, β_2, is given as 7.78 in the *Henry Draper Catalogue*, as 7.40 by Danjon on the basis of measures on 17 nights,[25] and as 7.73 IPv by Mrs. Gaposchkin.[26] Danjon finds $\beta_2 - \beta_1$ (max.) = 3.95 mag.; this leads to $\beta_2 = 3.53 + 3.95 = 7.48$. We adopt 7.5. The spectral type was found to be B3 $\pm$ in the *Henry Draper Catalogue*, B8n at Victoria, and B8 by the writer. The companion is probably itself a spectroscopic binary; assuming $\Delta m = 1.0$ we find then 7.9, B8 for its brighter component. If the star is an ordinary main-sequence star, the distance modulus of β Lyrae comes out to be about 8.1; and the absolute magnitude of the B8 component of β_1, -4.5. The uncertainty of the distance modulus is probably about 1 mag. We see that this result is consistent with Struve's spectroscopic determination. A third argument leads to the same value as an upper limit; the galactic longitude being 30°, the star would be expected to show the effects of galactic rotation if the distance were as large as 1000 parsecs; actually it shows only the reflex of the solar motion, so that the distance is probably not over 400 parsecs. We have, accordingly, $M(A) = -4.5 \pm 1$.

This value, in connection with Table 1, shows that almost certainly $M_A/M_B < 2$. However, on account of the faintness of B, this ratio should well exceed unity. It seems difficult to obtain a more precise determination, and the compromise ratio, 1.5, will be adopted in the following pages. The results obtained are, with some numerical modifications, also valid for other mass ratios.

As a test of these considerations Dr. Wesselink made in 1938 a solution based upon all the major photometric series, assuming the size of B to be about two-thirds that of A. He found that a good representation could be made.[27] Later S. Gaposchkin published[28] another solution, also assuming $R_B < R_A$. But he has not used the spectroscopic observations of this star; his mass ratio $A/B = 3.8$ would lead, in connection with Rossiter's mass function, to masses thirty-seven and forty-seven times larger than those given in Gaposchkin's two solutions.

Wesselink's solution has not yet been published.[27] It is clear that the values are approximate in view of the large indeterminacy of the solution and because of the roughness of the assumption that the stars are ellipsoids with uniform disks.

On the basis of Wesselink's or Gaposchkin's solutions it follows that the components of β Lyrae are very close. The writer has pointed out[29] that for equal components built on the Roche model actual contact exists whenever $a_1/a > 0.43$ and $b_1/a > 0.38$. Here a_1 and b_1 are the true dimensions of the "ellipsoids," not necessarily those derived from the light-curve. More extensive data, also for different mass ratios, are given in Table 3. The relation between the empirical values of a_1 and b_1 and the true values cannot be found without extensive computations. It will be necessary to assume the bolometric intensity distribution over the surface to be given by the theorem $H \propto g$, although this cannot be (strictly) valid if the components are unequal; this is shown in section 2. The distribution of gravity may be obtained from Figure 3 and Tables 4*b* and 4*c*, gravity being proportional to the reciprocal of the distance between consecutive equipotential surfaces. It appears that maximum brightness will be found in a belt at right angles to the line joining the centers. The effect will be an increase of the maxima of the light-curve and con-

[25] *Op. cit.*, p. 121.

[26] *Harvard Obs. Mimeogr.*, **3**, No. 2, 1938.

[27] *Pub. A.A.S.*, **9**, 304, 1939.

[28] *Proc. Amer. Phil. Soc.*, **82**, 305, 1940; Struve, *Ap. J.*, **93**, 112, 1941.

[29] *Ap. J.*, **88**, 497 and 501, 1938.

sequently an exaggerated empirically determined ellipticity of the components. Near the minima a brightening toward the limb will be present, which, in view of the experience that darkened solutions often give larger radii than uniform solutions, may be expected to result in an underestimation of the radii. This enhances the probability that the components of β Lyrae are in contact.[30]

During the primary minimum the companion is much darker than at other phases, partly because of the low gravity at the outer point of B and partly because of obscuration to be discussed later. Hence, an exaggerated value of Δm is found from the photometric solution, and too late a spectral type is computed from the surface brightness or color.

Although we have now obtained the approximate dimensions of the system, we have, as yet, no clue to the cause of the asymmetries mentioned earlier or to the source of the B5 spectrum. It is clear that any stable system will be symmetrical with respect to the plane through the components and the rotational axis. Hence, β Lyrae cannot be a stable system. The fact that in all probability the components have a common envelope may introduce an instability. The writer had examined this question in 1932 and had found that von Zeipel's theorem cannot be valid for a binary of unequal masses with a common envelope and that a stream of matter from A to B is likely to set in until equality of mass is attained. But even this stream from A to B does not seem to be sufficient for explaining the B5 spectrum. Accordingly, a second instability should be present, which will, indeed, arise if the envelope of A and B has such heights that it fills the largest equipotential surface inclosing the two components (cf. Figs. 2 and 3). Then, at point L (corresponding to the Lagrangian point L_2 of the *problème restreint*) instability will set in, and the matter will stream out, describing a free orbit, which may be found by integration of the equations of motion of the *problème restreint*. We shall see that this mechanism provides the elements of explaining the asymmetries of the light-curve, as well as the spectral features of β Lyrae.

Before giving the analytical discussions we note another type of instability which may arise in close binaries, consisting of one large, tenuous star and another, much denser and smaller one. Instability at point G (Fig. 3) will cause matter from the large star to envelope the small one in a manner discussed later. This type of instability seems of interest in interpreting such stars as CI Cygni, AX Persei, ϵ Aurigae, VV Cephei, and perhaps also ζ Aurigae.

2. INSTABILITY IN CONTACT BINARIES

Since most of the further discussions are concerned with binaries of which the components have a common envelope, we shall introduce the short term "contact binary" for such a system; it does not mean that mere contact exists, but a common envelope as well. For equipotential (or level) surfaces inside the common envelope we shall use the term "contact surfaces."

Von Zeipel has shown[31] that, if in a rotating mass of gas (which may be a contact binary) the angular velocity ω is constant and if, further, mechanical equilibrium obtains, the total pressure P, the density ρ, and the temperature T are constant on a level surface, ϕ = constant (ϕ includes the potential due to gravity as well as that due to the centrifugal force). The argument is simply that in equilibrium

$$dP = -\rho d\phi \,. \tag{1}$$

[30] The effect of the theorem $H \propto g$ on the derived ellipticities of separated components has been studied by Luyten (*M.N.*, **98**, 459, 1938) and Russell (*Ap. J.*, **90**, 653, 1939). When this paper was practically finished, Dr. Sitterly, at the Wellesley meeting of the American Astronomical Society (September, 1940), presented computations for components of equal mass in contact. The large effect on the empirically determined radii found by Dr. Sitterly makes it practically certain that the components of β Lyrae have a common envelope.

[31] *M.N.*, **84**, 665, 1924; Eddington, *The Internal Constitution of the Stars*, pp. 282–288.

On a level surface $d\phi = 0$; and hence $dP = 0$, or $P = P(\phi)$. Solving equation (1) for ρ, we find that ρ must be a function of ϕ only and must, therefore, be constant on a level surface. Finally, the same thing holds for T, found from

$$P = \frac{R\rho T}{\mu} + \tfrac{1}{3}aT^4 , \tag{2}$$

provided the composition (entering through μ) is constant over a level surface.

It can also be shown[31] that, under the same assumption, ω = constant, the surface brightness is given by $H \propto g$.

Consider now two components having a given mass ratio and the same composition. If the components are well separated, certain empirical relations between R, L, T_e, and M exist which will be of importance later. The significance of these relations is that they give central temperatures ($\propto M/R$) which lead to an energy generation equal to L, so that equilibrium will be maintained. We shall refer to these empirical quantities as the "physical" dimensions. We have, empirically,[32]

$$\frac{L}{\odot} = \left(\frac{M}{\odot}\right)^{4\frac{1}{2}}, \qquad \frac{R}{\odot} = \left(\frac{M}{\odot}\right)^{3/4}, \qquad \text{and hence} \qquad \left(\frac{T_e}{\odot}\right)^4 = \left(\frac{M}{\odot}\right)^3 , \tag{3}$$

valid for $\frac{1}{2} < M/\odot < 2\frac{1}{2}$; the third relation was verified by directly plotting T_e against M. For larger masses the exponents in the right-hand members decrease slowly as the mass increases, but their precise values become increasingly uncertain. For the interval $10 < M < 100$ we find the following approximate relations:

$$L \propto M^{2.3}; \qquad R \propto M^{0.6}, \qquad \text{and} \qquad T_e^4 \propto M^{1.1} . \tag{4}$$

On the basis of equations (3) and (4) we may compute the ratio and the sum of the radii of two components with constant average mass M_0 (to which corresponds the radius R_0). Table 2 shows the result. We note that the sum of the radii increases as the components approach equality. It is easily shown that this is generally the case whenever $R \propto M^n$, provided $0 < n < 1$.

TABLE 2

EMPIRICAL VALUES OF THE RATIO AND THE SUM OF THE RADII FOR SEPARATED COMPONENTS OF DIFFERENT MASS RATIO

M_A/M_B	R_A/R_B $\frac{1}{2}<M<2\frac{1}{2}$	$(R_A+R_B)/2R_0$ $\frac{1}{2}<M<2\frac{1}{2}$	R_A/R_B $10<M<100$	$(R_A+R_B)/2R_0$ $10<M<100$
1.0	1.00	1.000	1.00	1.000
1.5	1.36	0.996	1.28	0.995
2.0	1.68	0.989	1.52	0.986
2.5	1.99	0.982	1.73	0.977
3.0	2.28	0.975	1.93	0.968

If the two components are so close as to have a common envelope, the ratio of the radii is no longer free to adjust itself to the *physical* causes underlying equations (3) or (4) but is determined *mechanically* by the mass ratio. Strictly speaking, the ratio of the radii will depend not only on the mass ratio but also on the polytropic index of the com-

[32] *Ap. J.*, **88**, 472, 1938; 29 Canis Majoris was omitted.

ponents. Recent work[33] has empirically confirmed the older theoretical conclusion that the polytropic index of ordinary stars is close to 3. This being the case, the shape of the stars will deviate only slightly from the shape computed on the simple Roche model, as was shown by Chandrasekhar[34] for binaries with separated components. Chandrasekhar's result is obviously a consequence of the fact that for each component about 90 per cent of the mass is less than half the radius away from the center, in which region the equipotential surfaces are nearly spheres; hence, the attraction on an exterior point is very nearly the same as that valid for the Roche model. This situation is not materially changed when the components have a common envelope; hence, the approximation of the Roche model is good also in that case.

The equipotential surfaces of the Roche model are given by

$$-\Omega = \frac{1-\mu}{r_1} + \frac{\mu}{r_2} + \frac{x^2+y^2}{2}, \tag{5}$$

in which Ω is the (negative) potential and r_1 and r_2 are the distances of a point (x, y, z) to the mass centers, $M_1 = 1-\mu$ and $M_2 = \mu$; the co-ordinate system is rotating with the binary, the z-axis is the axis of rotation, the x-axis runs through the two mass centers, and the origin is at the center of gravity. The units are: the distance between the centers $= 1$; total mass $= 1$; angular velocity $= 1$ (or period $= 2\pi$).

With the aid of equation (5) we may now compute the ratio of the radii of the level surfaces; we shall call them "mechanical" radii. There are two limiting surfaces for each mass ratio, defined respectively by the Lagrangian points L_1 and L_2. L_1 gives the dimensions for the case in which the common envelope has zero height, whereas L_2 gives the maximum extent of the common envelope; if the extent should happen to be larger than defined by this limiting surface, the excess matter would stream off at L_2.

The co-ordinates of L_1 and L_2 are $y = z = 0$ and x determined by $\partial\Omega/\partial x = 0$. With the co-ordinates found, equation (5) gives the corresponding Ω_L, and then equation (5) is solved for the co-ordinates satisfying Ω_L just found. In this manner the principal axes a', a'', b, and c are found for each component and surface (a' refers to the outer dimension measured on the x-axis, and a'' to the inner dimension). Further, $b(L_1)$ and $c(L_1)$ are the y and z dimensions of the outer surface at L_1; they determine the maximum width of the bridge between the stars. As a unit we use the distance between the mass centers. On account of the pointed shape near L_1, we shall compute R from $R = \sqrt[3]{a'bc}$.

The results are found in Tables 3*a*–3*c* and are shown in Figure 2. The dots in Figure 2 mark the positions of the centers of gravity; the distance between the stellar centers was taken the same for each figure.

Before we can compare the "mechanical" dimensions of Table 3 with the "physical" dimensions of Table 2, we must know the change with changing mass ratio of the unit used in Table 3. We consider, therefore, a contact binary with total mass M = constant; with total orbital momentum $\mathcal{M}_0$ = constant, but with variable mass ratio. In considering $\mathcal{M}_0$ = constant we neglect possible variations in the rotational momentum of the two components. On the Roche model this rotational momentum would be zero, of course; actually, it is not zero but is probably small compared to the orbital momentum except when the companion has a very small mass compared to the primary. Its effect is studied below.

The total orbital momentum of the components with masses $(1-\mu)M$ and μM is, with respect to the center of gravity,

$$\mathcal{M}_0 = (1-\mu)M\mu^2a^2\omega + \mu M(1-\mu)^2a^2\omega = \mu(1-\mu)Ma^2\omega = \text{constant}.$$

[33] Cowling, *M.N.*, **98**, 734, 1938; Russell, *op. cit.*, p. 641.

[34] *M.N.*, **93**, 539, 1933 (cf. Fig. 9, p. 566, and pp. 569–571).

At any time ω is found from Kepler's third law, $\omega^2 a^3 = GM$. After elimination of ω we find

$$\mu^2(1 - \mu)^2 a = \text{constant}, \tag{6}$$

and for the period P

$$\mu^3(1 - \mu)^3 P = \text{constant}. \tag{7}$$

From equation (6) it follows that a has a minimum for $\mu = \frac{1}{2}$ and starts from infinity with $\mu = 0$. For very small μ-values, however, the rotational momentum of the primary will

TABLE 3*a*

PROPERTIES OF THE INNERMOST CONTACT SURFACE

M_A/M_B	μ	L_1	$\Omega(L_1)$	a_1'	a_1''	b_1	c_1	a_2'	a_2''	b_2	c_2
1.0	1/2	0.00000	2.0000	0.405	0.500	0.374	0.356	0.405	0.500	0.374	0.356
1.5	2/5	.14162	1.9905	.442	.542	.412	.390	.370	.458	.337	.323
2.0	1/3	.23742	1.9728	.468	.571	.440	.414	.346	.429	.313	.300
2.5	2/7	.30723	1.9537	.488	.593	.462	.433	.327	.407	.295	.283
3.0	1/4	0.36074	1.9353	0.505	0.611	0.480	0.448	0.313	0.389	0.280	0.269

TABLE 3*b*

PROPERTIES OF THE OUTERMOST CONTACT SURFACE

M_A/M_B	L_2	$\Omega(L_2)$	a_1'	b_1	c_1	$b(L_1)$	$c(L_1)$	a_2'	b_2	c_2
1.0	1.1984	1.7284	0.698	0.482	0.437	0.326	0.289	0.698	0.482	0.437
1.5	1.2308	1.7595	.589	.502	.456	.295	.265	.631	.427	.392
2.0	1.2490	1.7737	.583	.518	.471	.273	.246	.582	.390	.361
2.5	1.2597	1.7795	.586	.531	.481	.255	.231	.545	.363	.337
3.0	1.2659	1.7806	0.590	0.542	0.492	0.243	0.219	0.516	0.342	0.318

TABLE 3*c*

"RADII" OF THE INNER CONTACT SURFACES

M_A/M_B	R_A	R_B	R_A/R_B	R_A+R_B
1.0	0.378	0.378	1.00	0.756
1.5	.414	.343	1.21	.757
2.0	.440	.319	1.38	.759
2.5	.460	.301	1.53	.761
3.0	0.477	0.287	1.66	0.764

become of importance. The decrease of a with increasing μ is quite appreciable even for moderate values of μ; for instance, if we start with $M_A/M_B = 3$ and if later the masses have become equal, the distance of the centers will have decreased by the factor 9/16. By (7) the period of revolution will have decreased by 27/64. Assuming that at all times the periods of rotation are very nearly equal to the period of revolution, we find that, as the components approach equality, the rotational momentum increases; this is shown below. Hence, the orbital momentum decreases as $\mu \rightarrow \frac{1}{2}$, which proves that, in reality, the

distance between the components decreases even more rapidly than according to equation (6) and the period of revolution will decrease more rapidly than according to equation (7).

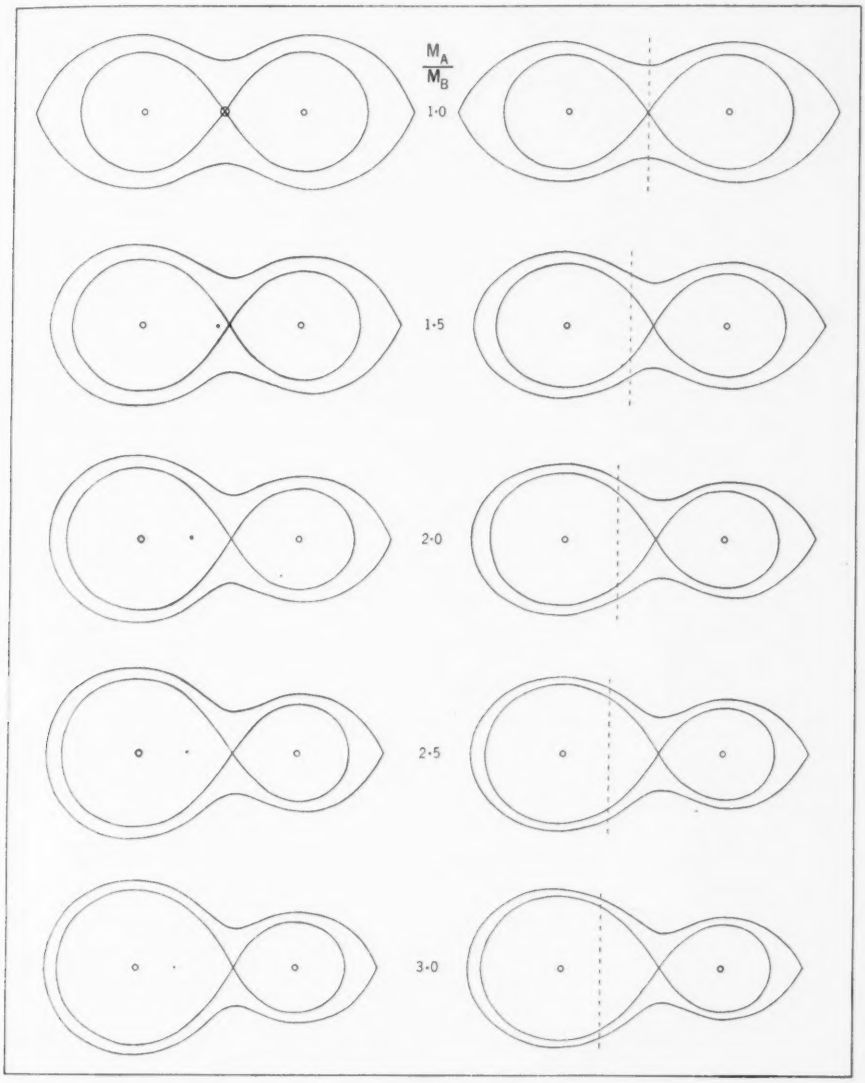

FIG. 2.—Inner and outer contact surfaces for different mass ratios. Sections in xy plane left, in xz plane right. Axes of rotation (through centers of gravity) shown as broken lines.

If γR is the radius of gyration of a star, its rotational momentum is $\gamma^2 R^2 M\omega$; the total rotational momentum of the components is $\gamma^2\omega[R_1^2 M_1 + R_2^2 M_2]$. Putting, as before, $R = M^n$ ($\frac{1}{2} < n < \frac{3}{4}$) and using equation (7), we find that the total rotational momentum is proportional to

$$\gamma^2\mu^3(1-\mu)^3\{(1-\mu)^{1+2n} + \mu^{1+2n}\} .$$

Evaluating this function for $\mu = \frac{1}{4}$ and for $\mu = \frac{1}{2}$, we find that in the latter case the rotational momentum is 1.90 or 1.62 times larger than in the former, depending upon whether we use the one or the other extreme value of n, $\frac{1}{2}$ or $\frac{3}{4}$. This proves the statement made above, at least if the approximation of ω = constant throughout the components is adequate. In view of the strong tidal forces, this approximation should be valid for the bulk of each star; the very central region, as well as the outermost parts (discussed below), may deviate, but their contribution to the momentum is slight.

In view of the considerable decrease in distance between the mass centers as the components approach equality and the comparatively small change in the sum of the "physical" radii shown in Table 2, it seems probable even at this stage that, if two unequal components once have a common envelope, they will continue to do so and that the envelope will become increasingly prominent. But, since the stars will be unable to retain their physical radii, we have to study the "adjustments" to the radii before certainty can be obtained as to the future of the envelope.

Consider, first, two separated components of masses M_1 and M_2, having "physical" radii R_1 and R_2, and internal energies $E_1(M_1, R_1)$ and $E_2(M_2, R_2)$. Compare this combination with a contact binary with the same masses but "adjusted" radii, $R_1 + h_1$ and $R_2 + h_2$. It seems probable that the adjustments in the radii will be made in such a way that the total energy of the system does not change. If this assumption is correct, we have

$$E_1(M_1, R_1 + h_1) + E_2(M_2, R_2 + h_2) = E_1(M_1, R_1) + E_2(M_2, R_2)\,. \tag{8}$$

After a Taylor expansion this reduces to (retaining only first-order terms)

$$h_1 E'(M_1, R_1) + h_2 E'(M_2, R_2) = 0\,, \tag{9}$$

in which the derivatives are taken with respect to the radius. The internal energy is proportional to M^2/R; the constant of proportionality will be the same for the two components if they have the same polytropic index and also the same ratio β between the gas pressure and the total pressure.[35] Equation (9) then becomes

$$h_1 \frac{M_1^2}{R_1^2} + h_2 \frac{M_2^2}{R_2^2} = 0\,. \tag{10}$$

It is of interest to note that one finds the same equation by considering the work done in displacing against gravity a small fraction, a, of each mass in opposite directions, the mean displacements being h_1 and h_2: $h_1 a M_1 g_1 + h_2 a M_2 g_2 = 0$, and $g \propto M/R^2$.

Equation (10) gives only the *ratio* of the increments of the radii. In order to obtain an indication of their absolute amount, we shall assume that the "mechanical" radii can be reached, starting from the "physical" radii, by the same adiabatic change (eq. [8]). Obviously, the radii adopted by the contact binary will be intermediate between the physical and the mechanical radii; we shall call them "compromise" radii.

Because of the ill-defined shape of the "compromise" binary, we shall examine the question of whether the common envelope will continue to exist by comparing the "physical" with the "mechanical" dimensions. Equation (10) plus the known ratio of the radii fixes the mechanical dimensions for each mass ratio,

$$\frac{(R_p + h)_1}{(R_p + h)_2} = \frac{(R_m)_1}{(R_m)_2} = \left(\frac{M_1}{M_2}\right)^m, \tag{11}$$

[35] Chandrasekhar, *Stellar Structure*, pp. 230–232, 1939.

in which R_p and R_m are the physical and mechanical radii, and the exponent m is found, from Table 3*c*, to be about 0.46. Using now in equations (10) and (11) the empirical relation $R_p = cM^n$ ($n = \frac{3}{4}$ for dwarfs, and about 0.6 for massive stars), we are able to solve for h_1 and h_2 in terms of M_1 and M_2. Then, putting $M_1 = M_0(1 + \delta)$ and $M_2 = M_0(1-\delta)$ we find, up to the second power of δ,

$$h_2 = R_0(n - m)\delta\{1 + 2(1 - n)\delta\}\ ; \qquad h_1 = -R_0(n - m)\delta\{1 - 2(1 - n)\delta\}\ , \quad (12)$$

in which R_0 is the physical radius corresponding to M_0 ($R_0 = cM_0^n$).

We consider first the change in the sum of the radii over the sum of the physical radii

$$\frac{h_1 + h_2}{2R_0} = 2(1 - n)(n - m)\delta^2\ . \quad (13)$$

If $\delta = \frac{1}{2}$, or $M_A/M_B = 3$, and $n = \frac{3}{4}$, the right-hand member of equation (13) is 0.036; if $n = 0.6$, the right-hand member is 0.028. If we add these figures to the sum of the physical radii found from Table 2 (0.975 and 0.968, respectively), we find 1.011 and 0.996 for dwarfs and massive stars, respectively. This shows that the sum of the "adjusted" mechanical radii (adjusted by means of eq. [10]) remains very nearly constant in comparison with R_0, i.e., in absolute measure, if the masses approach equality. Now we see from Table 3*c* that the sum of the mechanical radii remains very nearly constant if it is expressed in terms of the distance between the mass centers. Hence, if the degree of contact were to remain the same during the process of mass transfer, the distance of the mass centers would have to remain very nearly the same (more precisely: for dwarfs the change would have to be by the factor 0.999, and for massive stars by the factor 1.014, for a change of mass ratio from $A/B = 3$ to 1). Actually, as we have seen, the distance of the mass centers changes by a factor less than $9/16 = 0.562$. Hence, *the degree of contact increases very considerably during the process of mass transfer*—so much, in fact, that if the process should start with masses sufficiently different, instability on the outermost point of the companion would necessarily set in before equalization of masses would be attained (cf. Table 3, and Figure 2).

Since $n > m$, we see by equation (12) that the primary will be compressed and the companion expanded over the physical dimensions. The ratio h_2/h_1 is found to be

$$-\frac{h_2}{h_1} = 1 + 4(1 - n)\delta\ , \quad (14)$$

which may also be directly obtained from equation (10). It shows that the secondary always makes a larger adjustment to its radius than the primary. If $n = \frac{1}{2}$, we find from equation (10) that the changes in dimension are such that the total *volume* of the components remains the same; if $n = \frac{2}{3}$, the total *surface area* remains unchanged. If $n = 1$, the sum of the *radii* would remain unchanged; but n is never so large.

As was suggested before, the true dimensions of the components will be intermediate between the physical and mechanical dimensions. This appears inevitable because, first, the physical dimensions are ruled out, since they would not provide mechanical equilibrium, the outer surface not being an equipotential surface; this is a consequence of n being larger than m. But neither could an equipotential surface be the true boundary, because it would require such a contraction of A, and expansion of B, that the internal temperatures ($\propto 1/R$) would change materially, and even more so the energy generations ($\propto T^{18\pm}$). These changes would tend to restore, at least in part, the physical dimensions. Even after a long time the mechanical dimensions could not become equilibrium dimensions, because the empirical relations between L, R, and M would not exist. These em-

pirical relations are equivalent to such theoretical relations as are given by Gamow,[36] based on the carbon-nitrogen cycle of nuclear transmutations in stellar interiors. This shows that the true dimensions of the components must be intermediate between the two extremes considered.

This result leads at once to several important conclusions. The most important one is that on the outer equipotential surfaces the pressure could not be constant; in fact, some of these surfaces will be inside the envelope of A but already outside B. This result is contradictory to that derived on page 137 on the basis of constant angular velocity. Hence, ω cannot be constant throughout, particularly in the envelope where these contradictions occur. The pressure gradient along the level surfaces will cause matter to stream from A to B. Obviously, this current will be the more intense, the greater the disparity between the physical and the mechanical dimensions, or, in other words, the larger the mass ratio A/B. It will further depend on the extent of A beyond the lowest "contact surface."

Since the components assume compromise dimensions, R_A is smaller than normal; hence, the central temperature of A will be increased, and the energy generation will be considerably increased. Hence, L_A is increased, and also $T_e^4 \propto L/R^2$ (for two reasons). Opposite results follow for B. Hence, the magnitude difference, Δm, is increased considerably above the value normal for the mass ratio; also the ratio of the surface brightnesses and the difference in spectral type. All these results are of interest in connection with β Lyrae, where Δm is definitely too large for the mass ratio.

We shall now show that the greatest ratio between the pressures in A and B exists along the level surfaces in the outer parts of the common envelope; but the greatest pressure gradient, being determined by the difference in pressure, will be further down inside the envelope. Both statements follow from the fact that the pressure gradient is smaller in the envelope of A than in that of B. This results from the following:

We have shown that the effective temperatures of the components will differ more than according to the equilibrium relations (3) or (4). Hence, for components of unequal mass, $T_e(1) \gg T_e(2)$. Consider first isothermal atmospheres; we shall consider the pressure gradients along the "b"-axes, where the deviations from equilibrium will not be very large. Neglecting radiation pressure, we have

$$p = p_0 e^{-(\mu g h/RT)}, \tag{15}$$

in which μ is the mean molecular weight, g the surface gravity, and the co-ordinate h is measured in an outward direction from the level with pressure p_0. For the "compromise" radii $g_1 \cong g_2$; and a high value of T will result in a low value of μ, although, owing to the great abundance of hydrogen in stellar atmospheres, the variation in μ will not be great. The exponent in equation (15) is clearly less for the primary, having the higher temperature.

Now, extending the computations to greater depths, we have the standard equations

$$\frac{dP}{dh} = -g\rho, \tag{16}$$

$$P = \frac{R}{\mu}\rho T + \tfrac{1}{3}aT^4, \tag{17}$$

$$T^4 = T_0^4(1 + \tfrac{3}{2}\tau), \tag{18}$$

$$d\tau = -\frac{\kappa_0 \rho^2 dh}{T^{3.5+\Delta}}. \tag{19}$$

In equation (18) we have assumed that the layers considered are not so thick that the approximation of plane-parallel layers is invalid; then, also, g = constant. Furthermore,

[36] *Ap. J.*, **89**, 130, 1939.

equation (19) assumes that the hydrogen content of the two envelopes is the same;[37] the exponent Δ will take care of the principal deviations from Kramers' law in the envelope. The solution of these four equations is particularly simple if we assume a constant ratio β between the gas and the total pressure; equation (17) then becomes $\beta P = R\rho T/\mu$.

First we keep equation (18) and eliminate ρ; then we eliminate τ and get

$$\frac{dP}{P} = -B\frac{dh}{T} \qquad (20) \qquad \text{and} \qquad AT^{8.5+\Delta} \cdot dT = -P^2 \cdot dh\,, \quad (21)$$

in which

$$B = \frac{g\beta\mu}{R} \qquad \text{and} \qquad A = \frac{8}{3} \cdot \frac{R^2}{T_0^4 \kappa_0 \beta^2 \mu^2}\,. \qquad (22)$$

Now, eliminating dh from equations (20) and (21) and neglecting $T_0^{8.5+\Delta}$ in comparison with $T^{8.5+\Delta}$, we have

$$\frac{8.5+\Delta}{2} P^2 \cong ABT^{8.5+\Delta}\,, \qquad (23)$$

which is valid except at the very boundary. Putting, for brevity, $8.5 + \Delta = 2F$ (where $F \backsim 4$), we have by equations (20) and (23)

$$dT = -\frac{B}{F}dh \qquad (24') \qquad \text{or} \qquad T = T_* - \frac{B}{F}h\,, \qquad (24)$$

if $T_* = T(h = 0)$. By equation (23) we then have

$$P = \sqrt{\frac{AB}{F}}\left(T_* - \frac{B}{F}h\right)^F\,. \qquad (25)$$

Now compare the two components on the b-axes. Assuming Δ to be the same for the two stars, the pressure gradients given by equation (25) will depend on A and B. The values of g are almost identical. The value of μ need not be the same; but if hydrogen is as prominent in the outer parts as in the sun and in other stars (H : metals about 2000 by number), μ will be close to $\frac{1}{2}$ in either case because the ionization must soon be nearly complete. If, further, $\beta_1 \cong \beta_2$, $B_1 \cong B_2$. But $A \propto T_e^{-4}$.

Suppose, now, that the pressures of the two components were equal at the innermost "contact surface," where the densities are highest, and that we count h from this surface upward. Then by assumption $P_1^* = P_2^*$, and by equation (25) $A_1 T_{1*}^{2F} = A_2 T_{2*}^{2F}$; hence,

$$T_* \propto T_e^{2/F}\,. \qquad (26)$$

The value of T_* is, therefore, higher for A than for B, and by equation (24') this is true for any value of h in the envelope.[38] We obtain here another interesting contradiction to the results derived on page 137 on the assumption of ω = constant, quite independently from the previous discussion. Of course, this contradiction results from $T_e(1) \gg T_e(2)$, which, in connection with $g_1 \cong g_2$, is already in itself a contradiction of von Zeipel's theorems.

[37] Chandrasekhar, *Stellar Structure*, p. 293, 1939.

[38] Equal steps in h mean nearly equal steps in potential because $g_1 \cong g_2$.

Since $T_{1*} > T_{2*}$, it follows from equation (24) that the envelope of A extends to a greater height than B above the level for which by hypothesis $P_1 = P_2$; the ratio of the heights is $[T_e(1)/T_e(2)]^{2/F}$. Now, expressing h in terms of the height of B's envelope, we have by equations (25) and (26)

$$\frac{P_1}{P_2} = \left[\frac{1 - hf}{1 - h}\right]^F, \qquad \text{if} \qquad f = \left[\frac{T_e(2)}{T_e(1)}\right]^{2/F} < 1 . \tag{27}$$

This shows that in the whole envelope above the level where the pressures are equal, $(0 < h < 1)$, the pressure in A is larger than in B, so that matter must flow from A to B.

Summarizing the results of this section, we find:

1. If two components of unequal mass are so close as to have a common envelope, the angular velocity ω cannot be constant throughout the system, because, even if for some layer inside the common envelope the pressures were equal (as demanded by ω = constant), the pressure above that level would be larger in A than in B, causing a stream of matter to flow from A to B.

2. Owing to the fact that the equilibrium ("physical") radii of stars differ more than the "mechanical" radii of a contact binary, the true dimensions of the components will be intermediate between them. This causes A to be the larger, and B smaller, than the "average" level boundary surface. Hence, the pressures in the envelope will be larger in A than in B on the same level surface. This applies probably even to the deepest-level surface of the common envelope, so that the stream from A to B is probably more violent than that caused by the effect mentioned under 1.

3. Since A is smaller and B larger than their respective "physical" radii, the internal temperatures and luminosities of the components differ more than normal for their mass ratio; Δm and Δ(Sp.) are both abnormally large.

4. During the mass transfer from A to B the components draw closer together, increasing the extent of the common envelope. This may lead to an instability on the outside of B (at the Lagrangian point L_2). Obviously, the decrease in distance will not be quite as much as computed on dynamical grounds alone, because of the pressure at the interface.

The *origin* of a contact binary may be conceived in two ways:

a) The binary had so little initial angular momentum that it could not develop two separated components with radii appropriate for their masses and composition. This is no more mysterious than the formation of a binary with a larger angular momentum and consequent larger separation.

b) The process of stellar evolution (diminishing H content) may have caused an increase in the radii; this would cause the rotational momentum to increase and the orbital momentum to decrease, which would result in a decreased distance between mass centers. The two effects would be additive.

3. CURRENTS IN CONTACT BINARIES

We shall now try to find some properties of the motion of the matter streaming from A to B. Although the general problem is very complex, some results may easily be obtained.

It will be useful to have, first, more details about the shape of the equipotential surfaces because they show at once, for instance, the distribution of gravity. We have derived for one case, $M_A/M_B = 1.5$ (or $\mu = 0.4$), the cross-sections with the xy-plane of four crucial surfaces. The value of μ chosen is of no particular consequence, as all the significant features are also present for different mass ratios. The result of the computations is found in Tables 4*a* and 4*b* and is shown in Figure 3. In addition, data for the xz-plane are given in Table 4*c*.

We note that there are three points on the x-axis for which $\partial\Omega/\partial x = 0$; they are B, G, and L of Figure 3. They correspond to the Lagrangian straight-line solutions of the three-body problem; and equation (5), giving the equipotential surfaces, corresponds to the surfaces of zero velocity defined by Jacobi's integral. We shall make use of these circumstances in determining the motion of ejected matter.

TABLE 4*a*

VALUES OF x FOR CRUCIAL VALUES OF $-\Omega$

($M_A/M_B = 1.5$)

Point	$-\Omega$	x	Point	$-\Omega$	x
A	1.760	−1.370	G	1.990	+0.142
B	1.690	1.162	H	2.167	0.279
C	1.760	0.989	I	2.167	0.909
D	1.990	0.842	K	1.990	0.970
E	2.167	−0.781	L	1.760	+1.231
F	2.167	0.000			

TABLE 4*b*

VALUES OF $\pm y$ FOR GIVEN VALUES OF x AND $-\Omega$

($M_A/M_B = 1.5$)

x	$-\Omega$					
	2.167	1.990	1.760	1.690	1.690	1.760
−1.3						0.519
−1.2					0.444*	0.767
−1.1				0.138	0.763	0.932
−1.0				.285	0.928	1.056
−0.8		0.178	0.375	.450	1.143	1.236
−0.6	0.313	.371	.485	.530	1.280	1.358
−0.4	.365	.412	.502	.535	1.368	1.438
−0.2	.308	.362	.458	.496	1.418	1.485
0.0	.000	.202	.354	.404	1.436	1.501
+0.2		.087	.300	.355	1.422	1.488
+0.4	.222	.280	.380	.422	1.375	1.444
+0.6	.292	.337	.427	.466	1.290	1.366
+0.8	0.224	0.287	.406	.460	1.157	1.246
+1.0			.305	.415	0.941	1.065
+1.1			.211	0.425	0.759	0.938
+1.2			0.055			0.758
+1.27						0.545†

* Second value, 0.141. † Second value, 0.105.

The points B, G, and L have the x-co-ordinates given in Table 4*a;* the values of $-\Omega$ are 1.690, 1.990, and 1.760, respectively. At the center of gravity, F, $-\Omega = 2\frac{1}{6}$. The four surfaces defined by these values of the potential are those considered here.

The largest possible envelope of a contact binary will extend to the surface passing through L. If the system were larger, matter would flow off at L because, in the rotating frame of reference, gravity reverses itself there (or, in a stationary frame, the centrifugal force becomes larger than gravity).

Currents are defined as large-scale differential motions with respect to the condition ω = constant. If ω = constant, the level surfaces are also surfaces of constant P, ρ, and

T. In the preceding section we found several contradictions to these consequences of ω = constant, so that currents must exist.

On a "contact surface" the pressure is higher in A than in B. A stream of matter must therefore flow from A to B, although conceivably part of this stream may return; in that case the outgoing stream must be stronger than the returning stream. If gas and radia-

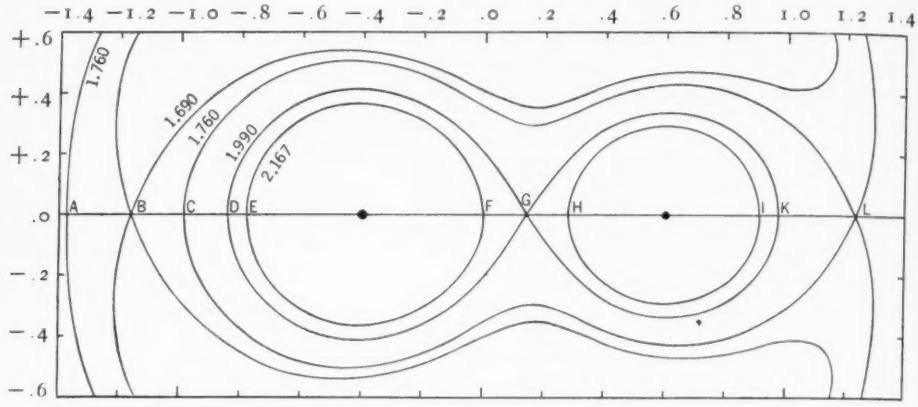

FIG. 3.—Four crucial equipotential curves in xy plane for μ=0.4

TABLE 4c

VALUES OF $\pm z$ FOR GIVEN VALUES OF x AND $-\Omega$

(M_A/M_B=1.5)

x	$-\Omega$			x	$-\Omega$		
	1.990	1.760	1.690		1.990	1.760	1.690
−1.6	.....	1.392	1.860	+0.3	0.194	0.308	0.344
1.5	.....	0.727	1.048	0.6	.323	0.391	0.418
1.45	.....	0.483	0.789	0.9	0.188	0.323	0.355
1.4	.....	0.252	0.583	1.1	.....	0.169	0.289
1.3	.....	.....	0.279	1.3	.....	0.121	0.384
1.0	.....	.....	0.213	1.4	.....	0.371	0.621
0.7	0.287	0.389	0.425	1.5	.....	0.749	1.052
−0.4	.390	0.456	0.480	+1.6	.....	1.389	1.852
0.0	0.196	0.319	0.358				

tion pressures were absent, and also viscous forces, the motion of the stream would be determined by the equations of motion of the *problème restreint*. These equations are[39]

$$\left.\begin{aligned} \ddot{x} &= 2\dot{y} + x - (1-\mu)\frac{x-x_1}{r_1^3} - \mu\frac{x-x_2}{r_2^3} \\ \ddot{y} &= -2\dot{x} + y - (1-\mu)\frac{y}{r_1^3} - \mu\frac{y}{r_2^3} \\ \ddot{z} &= -(1-\mu)\frac{z}{r_1^3} - \mu\frac{z}{r_2^3} \end{aligned}\right\} \quad \left(\begin{aligned} &\text{with} \\ &r_1^2 = (x-x_1)^2 + y^2 + z^2\,, \\ &r_2^2 = (x-x_2)^2 + y^2 + z^2 \end{aligned}\right). \qquad (28)$$

[39] E.g., Moulton, *Introduction to Celestial Mechanics* (2d ed.), p. 280, 1914.

If $z = 0$, $\ddot{z} = 0$; hence, if also $\dot{z} = 0$, the motion will remain in the xy-plane. If $z \neq 0$, we see that points symmetrical with respect to the xy-plane having symmetrical motions (i.e., the same $\dot{x}$ and $\dot{y}$; and $\dot{z}_1 = -\dot{z}_2$) will also have symmetrical accelerations. Hence, the motions will remain symmetrical with respect to the xy-plane. Adding, now, the effects of the pressure gradient and viscous forces, this symmetry will not be disturbed—not, at least, if we start with the reasonable assumption of initial symmetry in the distribution of matter. Hence, the principal current should be symmetrical with respect to the xy-plane.

Since two symmetrical currents in the z-direction would lead to a dissipation of energy not present in currents parallel to the xy-plane, it is very probable that the latter are the most important currents. We shall find their chief features by considering the motion in the xy-plane itself. Furthermore, in eclipsing binaries this is the plane in which observations may be made.

Consider the point G (Fig. 3), and assume that the pressure difference between the components gives rise to a current through G parallel to the x-axis ($\dot{x} = v$; $\dot{y} = 0$). Equation (28) now becomes

$$\ddot{x} = \text{finite}; \qquad \ddot{y} = -2v. \qquad (28')$$

The pressure gradient at G will have an x-component, but none in y, if we start from a symmetrical distribution of matter. Also, the viscous forces act only in the direction of the current, i.e., in x. Hence, these additional forces affect in equation (28′) only $\ddot{x}$. The current is going to be deflected in the $-y$-direction, owing to the well-known Coriolis force given by the second part of equation (28′).

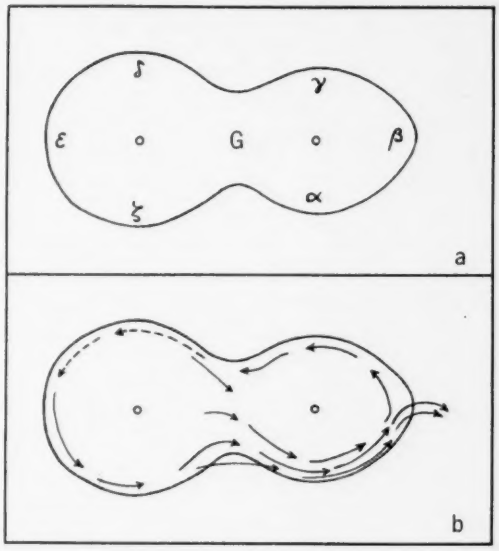

FIG. 4.—Currents in contact binaries; xy plane

The same conclusion can be reached for any point on the "interface" between the components. As this surface we may define the locus of points passing through G where the potential gradient is perpendicular to the x-axis. Consider two symmetrical points, $x_1 = x_2$; $y_1 = -y_2 = y$, and again $\dot{x} = v$, $\dot{y} = 0$. We now have $\ddot{x}_1 = \ddot{x}_2$; but $\ddot{y} = -2v \pm fy$, in which f is the same factor in the two cases. Starting again with a symmetrical distribution of matter with respect to the x-axis, there will be a component of the pressure gradient in both co-ordinates, being equal and of the same sign in the x-direction and equal but of opposite sign in the y-direction; its effect may be added to fy above. Hence, all currents passing the interface parallel to the x-axis are deflected in the $-y$-direction. The current from G (which will have a tendency to follow level surfaces) will therefore go principally in the direction of α (cf. Fig. 4, *a*) and not in the direction of γ.

Given a strong current near α in the $+x$-direction, what will its course be? Numerical integrations in section 7 show that, if the speed is below a certain value, the matter will go around the companion in the sense α, β, γ. If, however, the speed is large, the matter will fly off near β. The returning stream (in the $-x$-direction) will experience a Coriolis force in the $+y$-direction. Above G the returning stream meets the outgoing stream; but, owing to the opposite deflections in the y-direction, it is probable that part of the current

through γ survives and will go around the primary to join afterward the main stream near G.

The picture found is illustrated schematically in Figure 4, *b*. It is of great interest that Struve has actually identified these currents in β Lyrae.[40] The current near α has a velocity (in a stationary frame) of about 300 km/sec; this current is very prominent. Near γ a weaker returning current is observed with a speed of about 200 km/sec. Since the velocities were measured when these currents projected themselves on the primary, it is obvious that the figures quoted apply without alteration to the rotating frame in which these phenomena were considered here.

The true dimensions of the components are not represented by one level surface; hence the matter coming from the outer layers of A would practically find a vacuum over B. This is another reason why the current at α is more pronounced than that at γ.

The considerable velocities present in β Lyrae, in connection with the transverse effect of the Coriolis force, will make large departures possible from level surfaces, particularly where the potential gradient is low. This will be the case in the vicinity of point G as well as of L (cf. Fig. 3). In fact, the absorption due to the currents measured by Struve seems to be most prominent between G and α, and G and γ, respectively (Fig. 4, *a*); the discrepancy in the radii and the low effective gravity would combine to favor this region for the formation of extensive masses of gas of low density, as evidenced by the observed absorptions.

4. EJECTION OF MATTER FROM CLOSE BINARIES

In the introduction we noted two possible ways in which matter could be ejected from one of the components of a close binary; we shall refer to them as type A and type B of ejection. Type A takes place from the larger component (A), and AX Persei seems to be a good example; type B takes place on the outside of the smaller component (B) and is to be identified with β Lyrae. As is seen from Figure 3, type B arises when a contact binary "overflows" the level surface through L; type A arises if one of the components overflows the level surface through G and if the other component is much smaller than it would be according to this surface.

Some general remarks about the motion of the ejected material may readily be made on the basis of Jacobi's integral,[41]

$$\tfrac{1}{2}v^2 = \frac{1-\mu}{r_1} + \frac{\mu}{r_2} + \frac{x^2+y^2}{2} - C\,, \tag{29}$$

in which v is the velocity of the ejected particle in the rotating frame of reference. The unit of velocity is the relative orbital velocity in the binary; for β Lyrae, adopting $M_A/M_B = 1.5$, this is about $2.5 \times 183 = 460$ km/sec. For moderate velocities of ejection, v_0, the quantity $\frac{1}{2}v_0^2$ is therefore quite small. For instance, if in β Lyrae $v_0 \leqslant 50$ km/sec, $\frac{1}{2}v_0^2 \leqslant 0.006$, which is small compared to the constant C in (29); C equals 1.990 for point G of Figure 3, and 1.760 for L, if $v_0 = 0$ in both cases.

Now consider ejection either of type A or of type B. The value C_0 of C in (29) depends on v_0 but will be only slightly less than the value computed for $v_0 = 0$. Since always $v^2 > 0$, we have for the future co-ordinates of the ejected material the inequality

$$\frac{1-\mu}{r_1} + \frac{\mu}{r_2} + \frac{x^2+y^2}{2} > C_0\,, \tag{30}$$

which means that the matter has to remain on one side of the "surface of zero velocity" defined by equation (30) after making the inequality into an equality. These limiting

[40] Cf. p. 114.

[41] Easily derived from eqs. (28); cf. Moulton, *loc. cit.*

surfaces are illustrated in Figure 5; they are valid for small v_0. If v_0 should be large, the permitted regions will extend somewhat beyond the boundaries drawn, as is seen by comparison with Figure 3; the extensions are indicated by broken lines in Figure 5. The broken lines given for type B show the surface $-\Omega = 1.690$ and correspond therefore to $\frac{1}{2}v_0^2 = 1.760 - 1.690 = 0.070$, or $v_0 = 0.374$, i.e., about 170 km/sec in case of β Lyrae.

Ejection of type A appears to have the curious result that the large star ("M" star) makes a shell or ring around the small ("B") star. It is possible to derive from Jacobi's integral the approximate radius of the ring. If v_0 is not too large, the ejected particles start near their surface of zero velocity, and the orbit around B will therefore be eccentric. On account of the perturbations due to A, this orbit will have a rotation of the line of apsides; in addition the frame is rotating. Orbits of different particles will therefore intersect, and the result of collisions will be that a nearly circular ring will be formed with a radius determined by the available energy.

Let the radius of the final, common orbit be a, and assume a to be a small quantity of the first order (the unit is the distance AB). The mass of B being μ, the angular velocity in a fixed frame is found from Kepler's third law: $\omega^2 a^3 = \mu$. We shall see later that the motion around B is direct; hence the angular velocity in the rotating frame is $\omega_r = \omega - 1$. The left-hand term of equation (29) therefore equals

$$\tfrac{1}{2}v^2 = \tfrac{1}{2}a^2\omega_r^2 = \tfrac{1}{2}a^2(\mu^{1/2}a^{-3/2} - 1)^2 . \tag{31}$$

The right-hand member of equation (29) may be written as $U - C$, in which C is determined from the boundary condition of $\frac{1}{2}v_0^2 = U_0 - C$, and in our approximation

$$U = \frac{1-\mu}{1} + \frac{\mu}{a} + \frac{(1-\mu)^2}{2} . \tag{32}$$

Hence, a is found from

$$\tfrac{1}{2}a^2(\mu^{1/2}a^{-3/2} - 1)^2 = \frac{1-\mu}{1} + \frac{\mu}{a} + \frac{(1-\mu)^2}{2} - U_0 + \tfrac{1}{2}v_0^2 . \tag{33}$$

For $\mu = 0.4$ and $v_0 = 0$ we find $a = 0.21$; the value of a increases for increasing v_0 and is found to be 0.25 if $v_0 = 0.5$. These values of a are necessarily rough because of the approximations used. A precise result may be obtained by deriving the variational orbit around the companion having the Jacobian constant determined by the boundary conditions at the point of ejection. For the case of equal masses and small v_0 we find, by interpolation in a diagram by E. Strömgren,[42] that $a \cong 0.25$; while for the extreme case of $M_A/M_B = 10$, considered by G. H. Darwin,[43] we find that $a \cong 0.13$. The approximate result obtained above for $\mu = 0.4$ is hereby confirmed.

The correct order of magnitude for a is already obtained from the two-body problem, in which case the total energy in a circular orbit equals the potential energy at double the distance. According to this rule, the radius of the gaseous ring should be about half that of the curve of zero velocity, or about 0.2 for small v_0.

We may now take into account radiation pressure by a small, but hot, secondary. The example of the two-body problem would lead to the same radius of the ring as before if the radiation pressure does not exceed gravity; because, if α is the ratio between radiation pressure and gravity, the only effect will be to reduce the effective mass of the attracting star by the factor $(1-\alpha)$. In the three-body problem considered, the ring would

[42] *Bulletin astronomique*, **9**, 112, Fig. 23, 1935. The Jacobian constant is 16.

[43] *Scientific Papers*, **4**, 70, Pl. IV. The appropriate Jacobian constant is 40.1821.

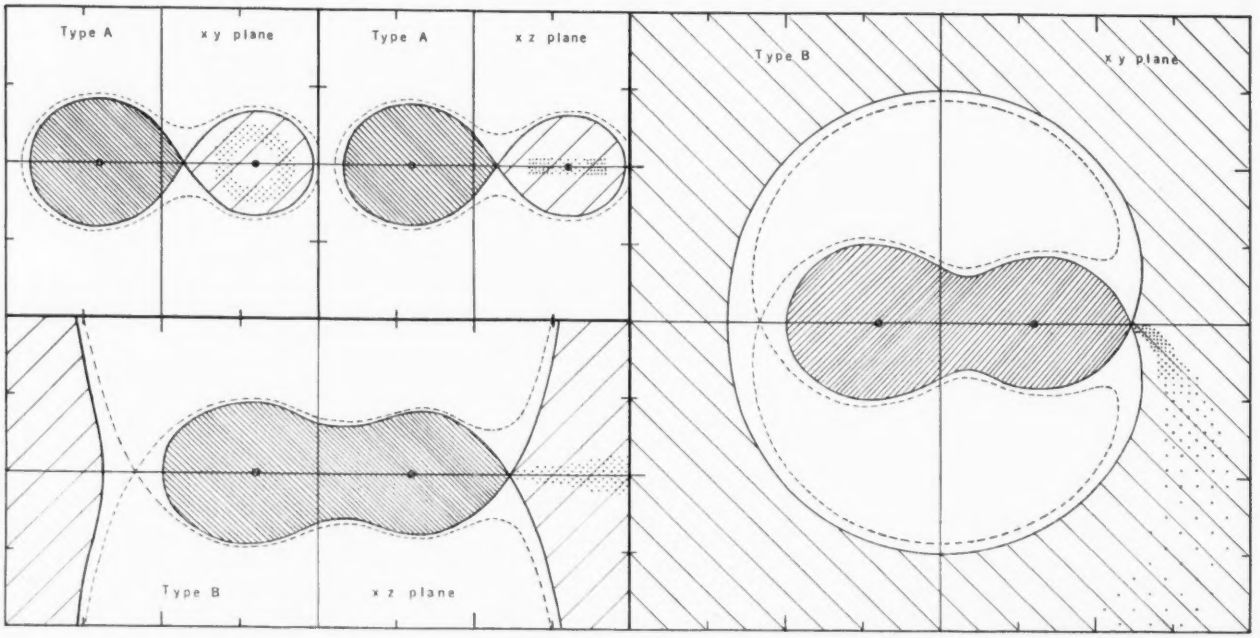

FIG. 5.—Surfaces of zero velocity and permitted regions (light shade) for ejection of types A and B. Small dots indicate actual positions of ejected particles. Stellar bodies are heavily shaded.

reduce in size, as is easily seen by multiplying, in equations (31)–(33), μ by $(1-\alpha)$ but leaving $(1-\mu)$ unchanged. Different results are obtained, however, if the ring should possess a considerable optical thickness in ultraviolet light, so that the stream falling toward the ring should experience little or no radiation pressure. Finally, the collisions active in rounding off the orbits will, if inelastic, tend to diminish the final radius.

Corresponding remarks may be made about ejection of type B. We see from Figure 5 that the ejected material cannot possibly form a *shell* around β Lyrae, as has often been assumed. The permitted region is shaded in Figure 5; but which part of this region is actually occupied can be found only from the equations of motion. If the velocity of ejection has a small z-component, the motion will be close to the xy-plane. It would again be possible to estimate the radius a of the ultimate orbit, by deriving the periodic orbit around the binary having the appropriate Jacobian constant,[44] if this periodic orbit were so stable that even the boundary conditions of the ejected particles would lead to an orbit not very different from the periodic orbit. This, however, is not the case, as will be seen later.

Further details about the orbits of the ejected particles can be obtained only by integration of equations (28). These equations being of the sixth order, the integration cannot be performed analytically except for small regions of space, where a first-order theory of small co-ordinate differences may be used. We shall therefore subdivide the discussion of equations (28) into two parts: (1) the motion near the points of ejection and (2) the motion farther away from these points. The first discussion can start from the standard theory of the motion near the Lagrangian points L_1 and L_2 (the unstable straight-line solutions); the second has to use numerical integrations.

5. THE MOTION NEAR THE POINTS OF EJECTION

The purpose of this section is to express the co-ordinates of the ejected material in terms of the initial conditions. Collisions and radiation pressure will be neglected; their effects are examined separately. The equations of motion are therefore equations (28). As initial conditions we assume that at $t = 0$ the particle has the co-ordinates of the libration point (L or G of Fig. 3) and the velocity components v_x, v_y, and v_z. We shall keep the mass ratio arbitrary except in the numerical work, where we shall use $M_A/M_B = 1.5$ (or $\mu = 0.4$). The discussion will be made to apply to ejection of either type A or type B. We shall use the same symbols as used in Moulton's textbook[45] and derive only such formulae as are not given there.[46]

If x', y', and z' are the co-ordinate differences in the rotating frame with respect to L or G and if these differences remain small ($\ll 0.1$), the motion in z' is periodic and is found to be

$$z = z' = \frac{v_z}{\sqrt{A}} \sin \sqrt{A}\, t\,. \tag{34}$$

The numerical values of A and other constants are found in Table 5 for both G and L; the period of the motion in z is $2\pi/\sqrt{A}$; its value, 4.77, for L, should be compared with 2π for the binary.

[44] The radius of the periodic orbit around AB, corresponding to $v_0 = 0$, is about 2.4; the radius is smaller for positive v_0.

[45] *Op. cit.*

[46] A review of the literature shows a vast amount of work carried out on the *problème restreint*, but few results are applicable to our problem which are not already contained in Moulton's book. The reason is that most of the numerical work (by G. H. Darwin, Thiele, Burrau, E. Strömgren, *et al.*) was done in search for periodic orbits, to which group the orbits discussed here do not belong.

The solutions for x' and y' are

$$x' = \sum_1^4 K_j e^{\lambda_j t} ; \qquad y' = \sum_1^4 L_j e^{\lambda_j t} , \tag{35}$$

in which the λ_j are the four roots of the equation

$$\lambda^2 = \frac{A - 2}{2} \pm \sqrt{2\tfrac{1}{4}A^2 - 2A} . \tag{36}$$

The values of A are such that the term under the square root in equation (36) is positive and that the values of λ^2 have opposite signs; the roots of equation (36) are, therefore, λ_1, $-\lambda_1$, $+i\sigma$, and $-i\sigma$, in which λ_1 and σ are positive, real numbers. Their values are given in Table 5.

TABLE 5

EJECTION CONSTANTS FOR $\mu = 0.4$

Constant	G (Type A)	L (Type B)	Constant	G (Type A)	L (Type B)
x	0.14162	1.2308	$-c_1 = +c_2$	0.3568	1.0748
A	7.92936	1.7320	c	4.3716	2.2973
z-period	2.2313	4.7742			
			h	0.089226	0.5516
λ_1	3.7646	1.2957	k	0.25007	0.5133
σ	2.8710	1.3953	l	0.020410	0.2401

The relation between the coefficients L_j and K_j, found by the introduction of equation (35) into the equations of motion, is

$$L_j = \frac{\lambda_j^2 - (1 + 2A)}{2\lambda_j} K_j = c_j K_j . \tag{37}$$

The constants c_j are also given in Table 5; $c_3 = -c_4$, is imaginary, $= ci$. If we now put

$$\left.\begin{aligned} K_1 + K_2 &= m ; & K_3 + K_4 &= n ; \\ K_1 - K_2 &= p ; & (K_3 - K_4)i &= q , \end{aligned}\right\} \tag{38}$$

we find, upon substitution of the boundary conditions in equation (35),

$$\left.\begin{aligned} 0 &= m + n ; & v_x &= \lambda_1 p + \sigma q ; \\ 0 &= -c_2 p + c q ; & v_y &= -c_2\lambda_1 m - c\sigma n . \end{aligned}\right\} \tag{39}$$

The solution is

$$\left.\begin{aligned} m = -n &= h v_y, \qquad \text{in which} \qquad h = \frac{1}{c\sigma - c_2\lambda_1} = \frac{2}{\lambda_1^2 + \sigma^2} , \\ p &= k v_x & k &= \frac{c}{c\lambda_1 + c_2\sigma} = \frac{h}{c_2} , \\ q &= l v_x & l &= \frac{c_2}{c\lambda_1 + c_2\sigma} = \frac{h}{c} . \end{aligned}\right\} \tag{40}$$

The numerical values of h, k, and l are found in Table 5. Equation (35) now becomes

$$\left.\begin{aligned} x' &= +m\cosh\lambda_1 t + p\sinh\lambda_1 t - m\cos\sigma t + q\sin\sigma t\,,\\ y' &= -c_2 m\sinh\lambda_1 t - c_2 p\cosh\lambda_1 t + cm\sin\sigma t + cq\cos\sigma t\,.\end{aligned}\right\} \tag{41}$$

It is noted that equation (41) is homogeneous in the initial velocity components and that the constants of Table 5 are all positive. For small t-values equation (41) reduces to a simple form due to certain relations between the different constants. Series development gives, up to the fourth order of t,

$$\left.\begin{aligned} x' &= v_x t + v_y t^2 + \frac{2A-3}{6}v_x t^3 + \frac{A-2}{12}v_y t^4 + \ldots\,,\\ y' &= v_y t - v_x t^2 - \frac{A+3}{6}v_y t^3 - \frac{A-2}{12}v_x t^4 + \ldots\,.\end{aligned}\right\} \tag{42}$$

Equation (42) gives fair accuracy for point L if $t < 1$ and for G if $t < \frac{1}{3}$. Considering only terms up to the second order, we find that, if the ejection takes place with a definite initial velocity, $v_0 = \sqrt{v_x^2 + v_y^2}$, but under all possible angles α, the trajectories are parabolae, equal in shape but of different orientation. They resemble the effect created by a pinwheel (cf. Fig. 6).

We return now to the case where t is not restricted. Again assuming v_0 to be constant but α arbitrary, we have

$$v_x = v_0\cos\alpha\,; \qquad v_y = v_0\sin\alpha\,, \tag{43}$$

and by equation (41)

$$\left.\begin{aligned} \frac{x'}{v_0} &= B\sin\alpha + C\cos\alpha\\ \frac{y'}{v_0} &= -D\sin\alpha - B\cos\alpha\end{aligned}\right\} \tag{44}$$

if

$$\left.\begin{aligned} B &= h(\cosh\lambda_1 t - \cos\sigma t)\\ C &= h\left(\frac{1}{c_2}\sinh\lambda_1 t + \frac{1}{c}\sin\sigma t\right)\\ D &= h(c_2\sinh\lambda_1 t - c\sin\sigma t)\end{aligned}\right\} \tag{45}$$

The quantities B, C, and D depend on constants (which, in turn, depend on the libration point selected and on μ) and on the time. Table 6 gives their values for point L and the interval $1 \leqslant t \leqslant 3$, which, together with equation (42), covers the range needed. With B, C, and D known, equation (44) gives the position of the ejected particle for any α. The structure of equation (44) proves at once the following theorem: *The locus of the particles ejected simultaneously with the same velocity, v_0, but in all possible directions, α, is an ellipse centered on the point of ejection; the scale of the ellipse at a given time is proportional to v_0; and the orientation of the ellipse changes with time.*

The theorem is here stated in its two-dimensional form. Since the motion in the z-coordinate and that in x and y are independent, the theorem also holds if v_0 means the projection of the velocity of ejection on the xy-plane. In either case the validity is restricted to the region around the point of ejection (within 0.1 from L).

The equation of the locus is found by eliminating α from equation (44):

$$x^2(B^2 + D^2) + y^2(B^2 + C^2) + 2xyB(C + D) = (B^2 - CD)^2\,. \tag{46}$$

The direction of the principal axes of this ellipse is found from

$$\tan 2\varphi = \frac{2B}{D - C}\,; \tag{47}$$

and their lengths, a_1 and a_2, from

$$a_{1,2}^2 = 2(B^2 - CD)^2 \left\{ 2B^2 + C^2 + D^2 \mp (C + D)\sqrt{(D - C)^2 + 4B^2} \right\}^{-1}. \tag{48}$$

The value of φ lying in the fourth quadrant is found in Table 6.

Figure 6 shows the orbits of particles ejected from L in various directions α; all multiples of 45° are shown, and the more important multiples of 15° as well. It follows from

TABLE 6

CONSTANTS FOR L IF μ=0.4

t	B	C	D	φ
1.0	+ 0.987	+ 1.100	− 0.247	−27° 51′
1.2	+ 1.419	+ 1.393	+ 0.079	−32 35
1.4	+ 1.938	+ 1.744	+ 0.590	−36 43
1.6	+ 2.559	+ 2.179	+ 1.313	−40 12
1.8	+ 3.30	+ 2.73	+ 2.27	−42 59
2.0	+ 4.20	+ 3.45	+ 3.48	−45 08
2.2	+ 5.30	+ 4.38	+ 5.00	−46 40
2.4	+ 6.68	+ 5.60	+ 6.86	−47 41
2.6	+ 8.42	+ 7.20	+ 9.14	−48 17
2.8	+10.66	+ 9.22	+11.95	−48 39
3.0	+13.55	+11.90	+15.43	−48 43

equation (44) that if v_0 is chosen as unit, one such diagram is sufficient; the validity of Figure 6 is limited only by the condition $\sqrt{x^2 + y^2} \ll 0.1$. Hence, if $v_0 = 0.01$ (or 4.6 km/sec for β Lyrae) the whole of Figure 6 will be valid; but if $v_0 = 0.1$, only the vicinity of the origin will be valid.

Some orbits will be physically impossible, either partly or wholly, because of interference by the body of the star. The boundary of the star near the point of ejection is found from equation (5); putting $x = L + x'$, $y = y'$, we find for the xy-plane up to the second order in x' and y':

$$-\Omega = -\Omega_L + \frac{2A + 1}{2}\,x'^2 - \frac{A - 1}{2}\,y'^2\,. \tag{49}$$

This is valid for either L or G (cf. Fig. 3). If we now put $\Omega = \Omega_L$, we find for the boundary of the star two straight lines through L (or G):

$$\left.\begin{aligned} y' = \pm\sqrt{\frac{2A + 1}{A - 1}}\,x' &= \pm 2.469x' \quad \text{for} \quad L \\ &= \pm 1.559x' \quad \text{for} \quad G\,. \end{aligned}\right\} \tag{50}$$

A higher approximation than equation (50) can be made only if the unit v_0 is specified numerically.

It is of interest to derive from equation (49) the equipotential curve equivalent to the "curve of zero velocity" specified by v_0. From equations (29) and (5) we find the Jacobian constant C by

$$\tfrac{1}{2}v_0^2 + C = -\Omega_L .$$

Hence, for any point

$$\tfrac{1}{2}v^2 = -\Omega - C = -\Omega + \Omega_L + \tfrac{1}{2}v_0^2 .$$

The curve of zero velocity in the xy-plane is therefore, by equation (49),

$$\frac{2A+1}{2}\,x'^2 - \frac{A-1}{2}\,y'^2 + \tfrac{1}{2}v_0^2 = 0 . \tag{51}$$

This is a hyperbola of fixed dimensions if x'/v_0 and y'/v_0 are used as co-ordinates, as in the case in Figure 6; the asymptotes are given by equation (50). Again, in a higher approximation the curve of zero velocity would depend on v_0.

The full-drawn orbits in Figure 6 are physically possible; they lie outside the star. Particles ejected in directions $\alpha = -45°$ and $-90°$ are seen to fall back into the star. Physically impossible orbits are indicated by broken lines. The heavy dots on the possible orbits are spaced by 0.2 in t; they show how the velocity varies along the path (in the rotating frame). Furthermore, the surface density of these dots (except near the origin where obviously some dots have been omitted) is proportional to the *density of matter* in the xy-plane.

The ellipses (eq. [46]) are also shown; the parts of physical interest are full-drawn, the other parts broken. It is interesting to note how these ellipses avoid crossing the curve of zero velocity.

Figure 6 suggests that the orbits emanating from the origin tend to become straight lines, either in the second or in the fourth quadrant.[47] From equation (41) it follows that for large values of t

$$x' \cong \tfrac{1}{2}(m+p)\cdot e^{\lambda_1 t}\,; \qquad \text{and} \qquad y' \cong -\tfrac{1}{2}c_2(m+p)\cdot e^{\lambda_1 t}\,, \tag{52}$$

so that the motion tends toward the straight line

$$y' = -c_2 x' . \tag{53}$$

Whether the asymptote is in the second quadrant or in the fourth appears to depend on the sign of $(m+p)$ or of the constant K_1 of (35). The limiting case, $(m+p) = K_1 = 0$, has curious properties. From equation (41) we then find, for any value of t,

$$\left.\begin{aligned} x' - me^{-\lambda_1 t} &= \sqrt{m^2+q^2}\,\sin(\sigma t - \psi) \\ y' - mc_2 e^{-\lambda_1 t} &= c\sqrt{m^2+q^2}\,\cos(\sigma t - \psi) \end{aligned}\right\}, \quad \text{if} \quad \left\{\begin{aligned} \frac{m}{\sqrt{m^2+q^2}} &= \sin\psi \\ \frac{q}{\sqrt{m^2+q^2}} &= \cos\psi \end{aligned}\right\}. \tag{54}$$

The right-hand side shows motion in an ellipse with eccentricity $e^2 = (c^2-1)/c^2$, having the major axis parallel to the y'-axis. These ellipses correspond to the well-known class of

[47] Cf. also S. S. Hough, in G. H. Darwin, *Scientific Papers*, 4, 118 ff., 1911

(unstable) periodic orbits around the libration points L_1, L_2, and L_3.[48] The curious fact is that the particle describes this orbit around a *displaced* center, given by the left-hand member of equation (54); the center of the orbit approaches the libration point asymptotically. The motion being *around* L or G, this limiting case, $(m + p) = 0$, is of no importance to the problem of ejection.

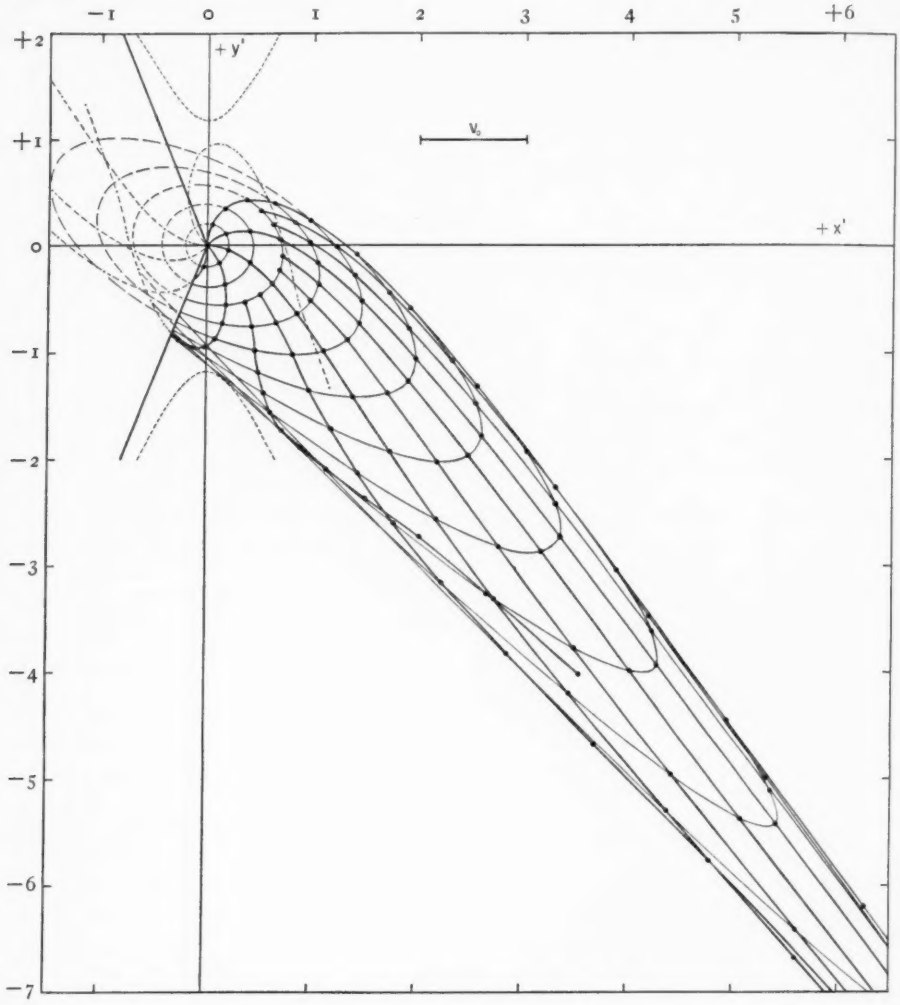

FIG. 6.—Ejection of type B in first-order theory; $\mu = 0.4$

For point L and $\mu = 0.4$ the values of a corresponding to this limiting case are $-42^\circ.94$ and $+137^\circ.06$. The latter value is of no practical importance, since it is inside the star. This shows that only material ejected between

$$-42^\circ.94 < a < +112^\circ.05 \qquad (55)$$

[48] Moulton, *op. cit.*, p. 304.

will leave the star permanently; the upper limit corresponds to the slope of the boundary of the star according to equation (50).

The previous discussion applies to ejection from point G as well as from point L if for each case the appropriate constants from Table 5 are used. It will therefore be sufficient to reproduce the result of the computations in Figure 7. The dots are here only 0.1 apart in t, against 0.2 in Figure 6. It is noted that the higher-order terms of equation (42) begin to become important much sooner than in Figure 6, so that the pinwheel effect has almost disappeared. Figure 7 may be taken to show orbits emanating from the more massive star toward the less massive star, or vice versa, the diagram being point-symmetrical in the first-order theory.

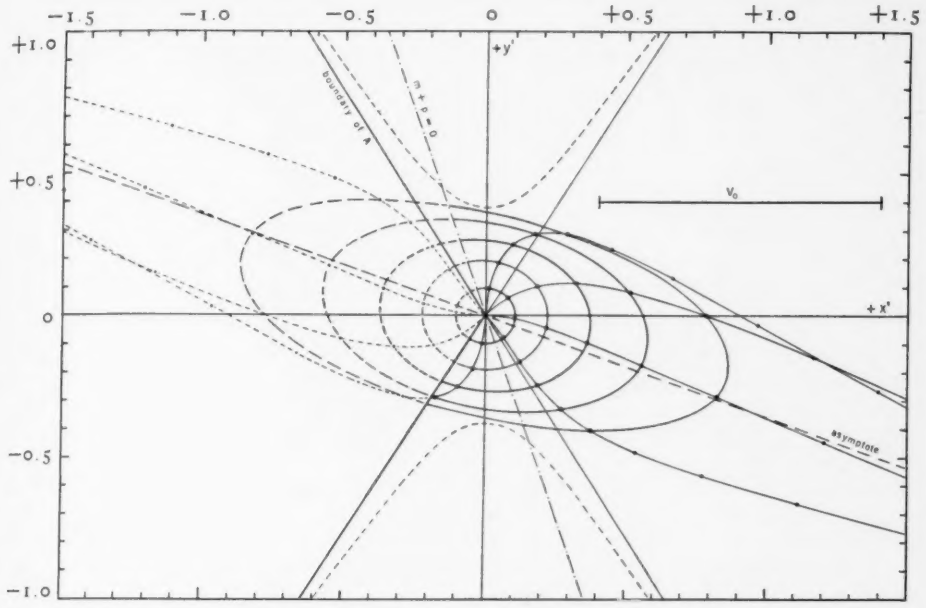

FIG 7.—Ejection of type A in first-order theory; $\mu=0.4$

The geometry of Figure 7 is such that all particles ejected in a whole hemisphere will leave the star permanently; the line of demarcation in the xy-plane, given as before by $(m + p) = 0$, is $109.^{\circ}64 \pm 180.^{\circ}$

Figures 6 and 7 show that for a given velocity of ejection, but for any value of α, the orbits of physical interest are quite similar for $t \gg 1$. But even the velocities at any point (x', y') of the common asymptotic orbit are the same, independently of v_0; for from equation (52) we find

$$\frac{dx'}{dt} = \lambda_1 x' \; ; \qquad \frac{dy'}{dt} = \lambda_1 y' \; , \tag{56}$$

in which λ_1 depends on the libration point and the mass ratio but not on v_0. In the frame of the first-order theory, therefore, *the motion of the ejected material is independent of the velocity and the angle of ejection except near the point of ejection itself.*

In the exact theory this invariance will be preserved *if* v_0 *is very small*, for then the motion of the ejected particle has already approached the asymptotic properties at the

time it leaves the region where the first-order theory applies. Figure 6 shows that this requires $v_0 \ll 0.01$.

This completes the discussion of the motion of the ejected material for the vicinity of the ejection points. Its application is the wider, the smaller the velocity of ejection is in terms of the relative orbital motion of the two stars. In the next two sections we trace the further course of the ejected matter by means of numerical integrations.

6. EJECTION OF TYPE A: ORBITS

The equations of motion are given by equation (28); we use, as before, $\mu = 0.4$. If $z \neq 0$, the acceleration $\ddot{z}$ will be of opposite sign to z; hence, excluding the improbable case of large initial $\dot{z}$, the values of z will always be small. The extension in the z-direction will probably be largely due to a pressure gradient in the accumulated gaseous body and is therefore not determined by equation (28). For these reasons we shall consider the plane problem based on equation (28).

The numerical integrations in this section and the next were carried out by using Taylor's formula up to the third derivative. If the time interval be δ, we have for x (and similarly for y)

$$\left.\begin{aligned} x(t+\delta) &= x(t) + \delta \cdot \dot{x}(t) + \frac{\delta^2}{2}\ddot{x}(t) + \frac{\delta^2}{6}\Delta\,, \\ \dot{x}(t+\delta) &= \dot{x}(t) + \delta \cdot \ddot{x}(t) + \frac{\delta}{2}\Delta\,, \end{aligned}\right\} \tag{57}$$

in which the third derivative is replaced by Δ/δ, and $\Delta = \ddot{x}(t+\delta) - \ddot{x}(t)$. At the boundary $x(t)$ and $\dot{x}(t)$ are given, and $\ddot{x}(t)$ is found from equation (28). The difference Δ has to be found from extrapolation once the integration is under way; if the value found in this way afterward appears to be too much in error, a new set of values for $x, \dot{x}, y, \dot{y}, r_1$, and r_2 has to be computed.

As each orbit requires several thousand numerical operations and as errors are cumulative, much work was carried out in duplicate, and numerous checks were made. All computations were made by the writer. A very useful check is found in Jacobi's constant (C of eq. [29]), the computation of which requires little additional work. Its deviations from constancy will not only reveal appreciable errors but will also show whether the series (57) is adequate.

Two orbits starting from the first libration point were computed, assuming $v_0 = 0.1$ and 0.5, respectively, the direction being along the positive x-axis in both cases. The results are found in Tables 7 and 8 and are shown in Figure 8. The interval δ was first taken as 0.1; but at $t = 0.7$ in Table 7 and at 0.3 in Table 8 the approximation (57) becomes too poor, as shown by the decrease in C, and smaller steps had to be taken. From then on, 0.01 was used, although not all steps are reproduced in the tables. The accuracy used in computing the increments, here as in the next section, was the nearest 0.00005 in x and y, 0.0001 in $\dot{x}$ and $\dot{y}$, and 0.001 or 0.01 in $\ddot{x}$ and $\ddot{y}$; but cumulative errors a few times larger than these values may be present apart from an error discussed below.

Near $t = 0.90$ (Table 7) and 0.49 (Table 8) a serious rise in C is noted which later practically disappears. This is due to the large arcs (up to 48°) covered in one step during the approach to B. The omission of the fourth derivative in equation (57) causes an error in the increment of x which is $\delta/4$ times that in $\dot{x}$; this ratio is 1/400 if $\delta = 0.01$. This shows that the change in C is almost entirely due to errors in the velocities. The co-ordinates would be affected appreciably only after several additional steps, whereas actually for only a few steps v is in error. Tables 7 and 8 show, in connection with the values of $\frac{1}{2}v^2$, also given, that the maximum errors in v are 4.3 and 2.0 per cent, respectively.

TABLE 7

t	x	y	$\dot{x}$	$\dot{y}$	$\frac{1}{2}v^2$	C
0.00	0.1416	0.0000	+0.100	0.000	0.005	1.986
.10	.1518	− .0010	+0.106	−0.020	0.006	1.986
.20	.1633	− .0041	+0.127	−0.042	0.009	1.985
.30	.1778	− .0095	+0.166	−0.066	0.016	1.985
.40	.1973	− .0175	+0.230	−0.095	0.031	1.985
.50	.2250	− .0287	+0.332	−0.131	0.064	1.985
.60	.2657	− .0441	+0.497	−0.176	0.139	1.982
.70	.3286	− .0639	+0.790	−0.219	0.336	1.975
.72	.3452	− .0683	+0.871	−0.225	0.405	1.974
.74	.3635	− .0728	+0.966	−0.227	0.493	1.974
.76	.3839	− .0773	+1.079	−0.223	0.607	1.975
.78	.4068	− .0814	+1.214	−0.208	0.759	1.975
.80	.4327	− .0854	+1.381	−0.174	0.969	1.974
.82	.4623	− .0882	+1.594	−0.104	1.275	1.974
.84	.4968	− .0890	+1.874	+0.042	1.756	1.972
.85	.5164	− .0880	+2.049	+0.172	2.114	1.973
.86	.5379	− .0854	+2.252	+0.372	2.605	1.971
.87	.5616	− .0801	+2.477	+0.698	3.311	1.971
.88	.5874	− .0706	+2.674	+1.258	4.366	1.994
.89	.6142	− .0536	+2.611	+2.216	5.864	2.124
.90	.6368	− .0257	+1.684	+3.376	7.116	2.594
.91	.6455	+ .0111	+0.045	+3.716	6.906	2.441
.92	.6391	+ .0454	−1.144	+3.087	5.418	2.042
.93	.6252	+ .0725	−1.564	+2.370	4.031	1.966
0.94	0.6089	+0.0935	−1.654	+1.856	3.090	1.952

TABLE 8

t	x	y	$\dot{x}$	$\dot{y}$	$\frac{1}{2}v^2$	C
0.00	0.1416	0.0000	+0.500	0.000	0.125	1.866
.10	.1929	− .0051	+0.535	−0.102	0.148	1.865
.20	.2515	− .0205	+0.655	−0.208	0.236	1.862
.30	.3290	− .0465	+0.930	−0.309	0.480	1.851
.32	.3484	− .0528	+1.013	−0.326	0.567	1.850
.34	.3697	− .0594	+1.114	−0.338	0.678	1.851
.36	.3931	− .0663	+1.237	−0.342	0.824	1.850
.38	.4193	− .0730	+1.391	−0.330	1.022	1.850
.40	.4490	− .0793	+1.588	−0.288	1.303	1.850
.42	.4833	− .0842	+1.849	−0.184	1.726	1.850
.44	.5236	− .0858	+2.200	+0.062	2.421	1.850
.45	.5466	− .0840	+2.411	+0.301	2.952	1.852
.46	.5718	− .0792	+2.623	+0.690	3.678	1.860
.47	.5988	− .0694	+2.745	+1.312	4.627	1.912
.48	.6256	− .0520	+2.524	+2.206	5.619	2.059
.49	.6473	− .0256	+1.701	+3.028	6.031	2.192
.50	.6586	+ .0066	+0.583	+3.272	5.523	2.041
.51	.6598	+ .0381	−0.259	+2.992	4.508	1.911
.52	.6547	+ .0660	−0.710	+2.579	3.577	1.875
.53	.6464	+ .0899	−0.925	+2.212	2.875	1.864
0.54	0.6366	+0.1105	−1.018	+1.919	2.359	1.862

The velocities in the rotating frame, $\dot{x}$ and $\dot{y}$, are added in Tables 7 and 8 because of their astrophysical importance. If X and Y are the velocities in a stationary frame having, at the moment considered, the same orientation as the rotating frame, we find X and Y from

$$X = \dot{x} - y\,; \qquad Y = \dot{y} + x\,. \tag{58}$$

These values determine the Doppler shifts of absorption and emission lines. (The unit of velocity is the relative velocity of A and B.)

As anticipated by the discussion of Figure 7, the orbits in Figure 8 are quite similar, and no further integrations seem necessary. The motion around B is direct, as was assumed in section 4 in the derivation of the radius of the ultimate mean orbit of the ejected gas.

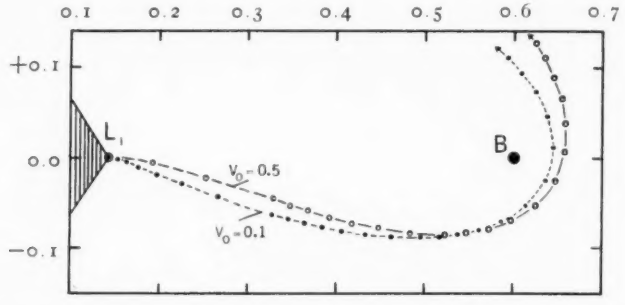

FIG. 8.—Orbits for ejection of type A; μ=0.4. Dots not equally spaced in time; they correspond to Tables 7 and 8.

The integrations may be easily extended to include radiation pressure by a hot component, B. We multiply in equation (28) the mass μ by $(1 - a)$ but leave $(1 - \mu)$ unchanged. The Coriolis force ($2\dot{y}$ or $-2\dot{x}$) remains the same, of course, and also the terms x and y, because the period of the binary is not affected by the radiation pressure. Because of varying optical thickness $(1 - a)$ will vary with position.

7. EJECTION OF TYPE B: ORBITS

We shall first investigate the fate of a stream of gas assumed to be parallel at some initial point near a of Figure 4, a, passing over the surface of B without friction. Struve found such a stream in β Lyrae having a velocity of about 300 km/sec. We shall adopt $v_0 = 0.55$, which corresponds to 250 km/sec for β Lyrae, if $M_A/M_B = 1.5$. This somewhat smaller value was chosen to compensate in part for neglected viscous forces.

For the initial x-co-ordinate we adopt $x = 0.40$; and for the velocity components of the parallel stream $\dot{x} = +0.44$, and $\dot{y} = -0.33$ ($v_0 = 0.55$), which means that for $y = -0.30$ the stream is directed away from the center of gravity (F of Fig. 3). We have made integrations for three initial values of y: -0.30, -0.34, and -0.38. The orbits are found in Tables 9–11 and are illustrated in Figure 9: for brevity 15 lines were omitted in Table 11.

As in Tables 7 and 8, the Jacobian constant is added as a check of the numerical work and of the approximation (57). In one instance an experiment was made by integrating with larger steps (0.5) as well as with those used in the tables (0.1). In this case it was found that 0.12 of the error in C was due to errors in the co-ordinates, and 0.88 to the velocities, confirming the general remarks made on page 160.

Figure 9 shows that the interior part of the stream will tend to swing around the sec-

ondary, whereas the outer part will fly off into space. These results were anticipated on page 149. The inner orbits, as computed, intersect with the star; but in reality the matter will, of course, more or less follow the stellar surface, the pressure gradient near that surface having been neglected in the integrations.

Figure 9 also shows the surface of zero velocity corresponding to the middle orbit ($C = 1.690$), taken from section 3. It shows that for the high velocity adopted here the outlet of B is, indeed, wide open. It would clarify the picture if additional integrations were made for $-y = 0.35$, 0.36, 0.37, 0.39, and 0.40. These would also show the *width* of the tail to be expected.

TABLE 9

t	x	y	$\dot{x}$	$\dot{y}$	$\frac{1}{2}v^2$	C
0.0	+0.4000	−0.3000	+0.440	−0.330	0.151	1.785
.1	+ .4475	− .3246	+ .512	−0.160	.144	1.785
.2	+ .5027	− .3317	+ .594	+0.021	.177	1.785
.3	+ .5666	− .3193	+ .683	+0.234	.260	1.786
.4	+ .6386	− .2827	+ .752	+0.513	.414	1.789
.5	+ .7134	− .2132	+ .719	+0.898	.662	1.800
0.6	+0.7720	−0.1013	+0.379	+1.337	0.966	1.850

TABLE 10

t	x	y	$\dot{x}$	$\dot{y}$	$\frac{1}{2}v^2$	C
0.0	+0.4000	−0.3400	+0.440	−0.330	0.151	1.691
0.1	+ .4457	− .3665	+ .475	−0.200	.132	1.691
0.2	+ .4952	− .3800	+ .516	−0.069	.136	1.691
0.3	+ .5492	− .3801	+ .565	+0.067	.162	1.691
0.4	+ .6082	− .3662	+ .614	+0.215	.212	1.691
0.5	+ .6717	− .3365	+ .652	+0.383	.286	1.693
0.6	+ .7375	− .2888	+ .655	+0.575	.380	1.695
0.7	+ .8005	− .2212	+ .592	+0.777	.477	1.699
0.8	+ .8530	− .1346	+ .442	+0.942	.542	1.703
0.9	+ .8871	− .0358	+ .236	+1.012	.540	1.703
1.0	+ .9006	+ .0642	+ .044	+0.971	.472	1.698
1.1	+ .8980	+ .1560	− .082	+0.857	.370	1.693
1.2	+ .8864	+ .2348	− .149	+0.720	.270	1.689
1.3	+0.8707	+0.3001	−0.160	+0.587	0.185	1.689

The fact that we have neglected viscous forces may, however, have led to a velocity of ejection at the libration point L_2 which is too high. This velocity is about 0.53, or some 245 km/sec for β Lyrae. Obviously, a test is provided by the measured velocity of the B5 absorption spectrum, which is roughly −70 km/sec, or −50 km/sec with respect to the center of gravity. This value gives the radial component along the line passing through A, measured in a fixed frame of reference. Accordingly, we have to continue the integration of Table 11 indefinitely. Fortunately, if we surpass a point about three times the distance AB from the center of gravity, we may approximate the problem by a two-body problem, having unit mass in the origin and an infinitesimal mass moving outward, with initial co-ordinates and velocity components given by Table 11, last line. From equation (58) we find X and Y; the energy integral

$$v^2 = X^2 + Y^2 = \frac{2}{r} - \frac{1}{a} \tag{59}$$

will then show whether the subsequent motion will be in an ellipse ($a > 0$) or a hyperbola ($a < 0$).

From the last line of Table 11 we find $-1/a = 0.3140$, showing that the matter will move out in a hyperbola with $a = 3.184$. Furthermore, equation (59) shows that for large r the asymptotic velocity is 0.5604, or about 260 km/sec for β Lyrae. The velocity nearer to the system will, by equation (59), be even larger, although without computation it is not certain that this also applies to the component measured in the radial velocity. We shall show below that this is the case and that a smaller velocity of ejection at L_2 is required. This makes it very probable that *viscous forces are slowing down appreciably the current around* B.

TABLE 11

t	x	y	$\dot{x}$	$\dot{y}$	$\frac{1}{2}v^2$	C
0.0	+0.4000	−0.3800	+0.440	−0.330	0.151	1.610
0.2	+0.4899	−0.4267	+0.463	−0.140	0.117	1.610
0.4	+0.5864	−0.4369	+0.506	+0.036	0.128	1.610
0.6	+0.6924	−0.4128	+0.553	+0.203	0.173	1.611
0.8	+0.8055	−0.3568	+0.571	+0.352	0.225	1.612
1.0	+0.9174	−0.2760	+0.542	+0.440	0.244	1.612
1.2	+1.0213	−0.1880	+0.500	+0.420	0.214	1.611
1.4	+1.1200	−0.1145	+0.495	+0.301	0.168	1.611
1.6	+1.2218	−0.0715	+0.528	+0.121	0.146	1.611
1.8	+1.3319	−0.0683	+0.573	−0.093	0.168	1.611
2.0	+1.4498	−0.1104	+0.602	−0.330	0.236	1.612
2.2	+1.5703	−0.2017	+0.596	−0.584	0.348	1.612
2.4	+1.6847	−0.3445	+0.538	−0.845	0.502	1.612
2.6	+1.7816	−0.5393	+0.420	−1.101	0.695	1.613
2.8	+1.8484	−0.7839	+0.236	−1.340	0.926	1.613
3.0	+1.8717	−1.0731	−0.014	−1.545	1.193	1.613
3.1	+1.8630	−1.2319	−0.163	−1.629	1.340	1.614
3.2	+1.8386	−1.3984	−0.327	−1.698	1.495	1.614
3.3	+1.7972	−1.5710	−0.504	−1.751	1.659	1.614
3.4	+1.7375	−1.7479	−0.692	−1.784	1.831	1.615
3.5	+1.6584	−1.9271	−0.891	−1.797	2.012	1.615
3.6	+1.5590	−2.1065	−1.097	−1.788	2.200	1.615
3.7	+1.4387	−2.2838	−1.309	−1.754	2.396	1.616
3.8	+1.2970	−2.4565	−1.524	−1.696	2.600	1.616
3.9	+1.1340	−2.6222	−1.738	−1.613	2.811	1.617
4.0	+0.9496	−2.7783	−1.949	−1.503	3.030	1.617
4.1	+0.7443	−2.9221	−2.155	−1.368	3.256	1.617

Instead of computing the elements of the hyperbola from the focus at the origin and from x, y, $\dot{x}$, $\dot{y}$, and then computing an ephemeris, it was found simpler to continue the numerical integrations in a nonrotating frame by means of the equations

$$\ddot{x} = -\frac{x}{r^3}; \qquad \ddot{y} = -\frac{y}{r^3}, \tag{60}$$

the accelerations being small; the interval used in equation (57) was now 0.5. The results are shown in Figure 10 for a nonrotating frame and in Figure 11 for a rotating frame; Figure 11 extends Figure 9. The velocity vectors computed for a stationary frame are also shown. The projections along radii drawn from A appear to be only slightly less than the space velocities themselves, or about 300–400 km/sec for β Lyrae, a value much higher than that observed.

From the Jacobian constant computed for the last point, $t = 9.6$, we find that the two-body approximation has introduced an error in the velocity (or co-ordinates) well under 1 per cent.

We now turn to smaller velocities of ejection. In order to avoid difficulties arising from viscosity, we start the following integrations at L_2 (or L in Fig. 3). The following discussion therefore extends the theory given in section 5 to large distances from the libration point.

Two velocities were adopted: $v_0 = 0.1$ and 0.01. Together with the orbit of Table 11 ($v_0 = 0.53$) they should suffice to determine the order of magnitude of v_0 responsible for the measured radial velocity of the B5 spectrum of β Lyrae.

The results are given in Tables 12 and 13 and are shown in Figure 12. For brevity, Table 12 shows for $0.0 < t < 3.2$ only half the steps used in the integrations,

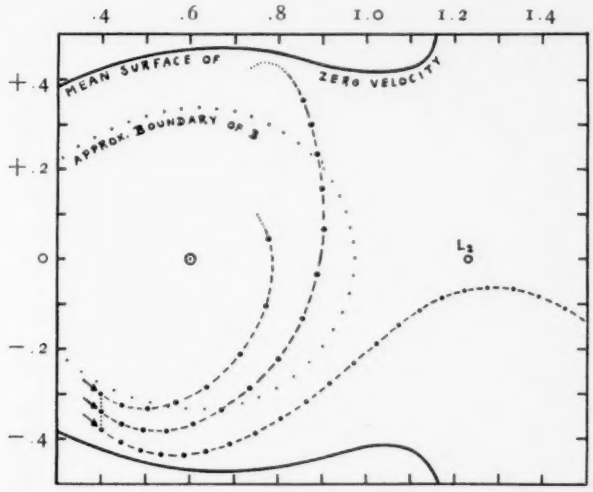

FIG. 9.—Orbits for ejection of type B; μ=0.4. Viscous forces neglected, and also presence of B's boundary.

and Table 13 shows only one-quarter. Since the amount of work done was already considerable, the integrations were not continued beyond the point where the radial-velocity test mentioned above could be applied.

The energy integral (eq. [59]) is valid only in the two-body problem; but we may test empirically the error made if we use equation (59) too close to the binary system. From the integration for $v_0 = 0.1$ we find the data of Table 14. In all three cases a positive value of $1/a$ is found, but the value has not yet reached its final value at $r < 3$. The asymptotic value for large r is probably still slightly above zero. The motion at $r \gg 3$ is therefore in a very long ellipse ($a \gg 100$) and, for practical purposes, in a parabola.

From the orbit with $v_0 = 0.01$ we find, at $t = 5.5$, that $r = 2.24$ and $1/a = -0.1275$. In view of the run of $1/a$ in Table 14 and the similarity between the two orbits, we may expect the true value of $1/a$ to be even somewhat smaller. Hence, the motion is in a hyperbola with $a < 7.8$; and $v_\infty > 0.357$, or > 164 km/sec for β Lyrae.

We have found the curious result that for v_0 small ($\sim$0.01, or 5 km/sec for β Lyrae), as well as large ($\sim$0.5, or 250 km/sec for β Lyrae), the ejected matter will recede from the binary with a large hyperbolic velocity, but that at an intermediate velocity of ejection ($\sim$0.1 or 50 km/sec for β Lyrae) the matter moves out in a roughly parabolic or even elliptic orbit. This shows that the observed velocity of recession, about 50 km/sec, is

within the range covered by our mechanism. It would be of interest to have additional integrations for $v_0 = 0.05$ and 0.2 and also to investigate the effect of the angle α of ejection.

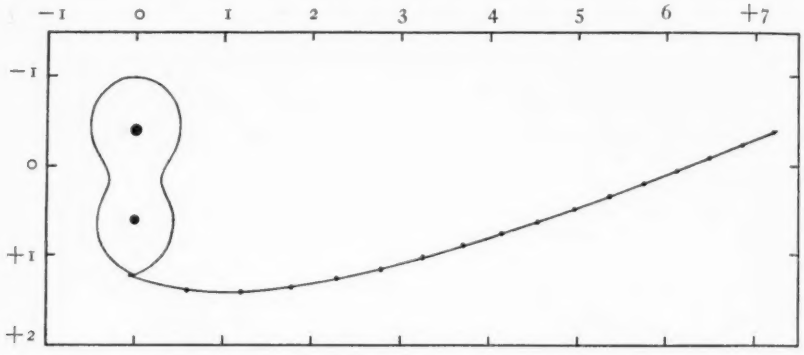

FIG. 10.—Ejection of type B; orbit in stationary frame. Position of binary given for moment of ejection. (Turned 90° with respect to other figures.)

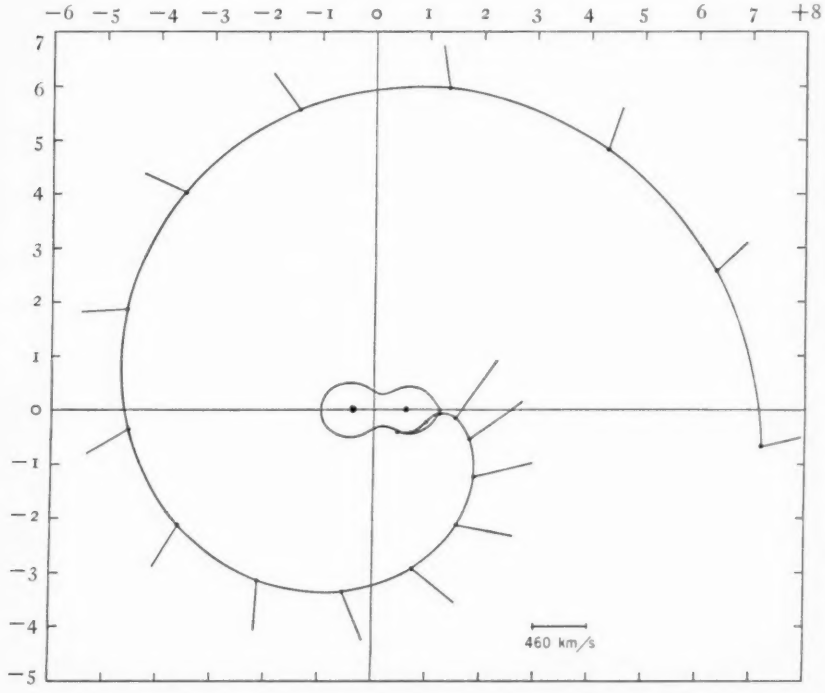

FIG. 11.—Extension of Fig. 9 for ejection orbit. Same orbit as in Fig. 10 but now in rotating frame. Dots are for $t = 0.1, \ldots, 9.6$, spaced by 0.5 (cf. Table 11). Velocity vectors, measured in a stationary frame, are indicated by short lines.

Radiation pressure may be introduced in the integration, as indicated earlier, but the complications due to eclipses and varying optical thickness will be serious. In view of the large velocities considered here, the effects of collisions on the x and y co-ordinates will

TABLE 12

t	x	y	$\dot{x}$	$\dot{y}$	$\frac{1}{2}v^2$	C
0.0	+1.2320	0.0000	+0.100	0.000	0.005	1.754
0.2	+1.2521	−0.0040	+0.101	−0.040	0.006	1.754
0.4	+1.2726	−0.0160	+0.104	−0.080	0.009	1.754
0.6	+1.2937	−0.0361	+0.107	−0.121	0.013	1.754
0.8	+1.3154	−0.0643	+0.110	−0.162	0.019	1.754
1.0	+1.3379	−0.1008	+0.114	−0.204	0.027	1.754
1.2	+1.3610	−0.1462	+0.117	−0.250	0.038	1.754
1.4	+1.3848	−0.2011	+0.120	−0.301	0.052	1.755
1.6	+1.4088	−0.2669	+0.120	−0.358	0.071	1.755
1.8	+1.4324	−0.3450	+0.115	−0.424	0.097	1.755
2.0	+1.4542	−0.4374	+0.102	−0.500	0.130	1.755
2.2	+1.4721	−0.5459	+0.076	−0.586	0.175	1.754
2.4	+1.4830	−0.6724	+0.031	−0.680	0.232	1.754
2.6	+1.4827	−0.8183	−0.037	−0.779	0.304	1.754
2.8	+1.4660	−0.9842	−0.134	−0.878	0.394	1.754
3.0	+1.4268	−1.1689	−0.263	−0.967	0.502	1.754
3.2	+1.3585	−1.3700	−0.426	−1.040	0.631	1.755
3.3	+1.3113	−1.4753	−0.519	−1.066	0.703	1.755
3.4	+1.2544	−1.5829	−0.620	−1.084	0.780	1.755
3.5	+1.1870	−1.6918	−0.729	−1.093	0.862	1.755
3.6	+1.1085	−1.8010	−0.843	−1.091	0.950	1.755
3.7	+1.0182	−1.9096	−0.963	−1.077	1.043	1.756
3.8	+0.9158	−2.0160	−1.087	−1.050	1.141	1.756
3.9	+0.8008	−2.1190	−1.213	−1.008	1.244	1.756
4.0	+0.6732	−2.2172	−1.341	−0.953	1.352	1.756
4.1	+0.5327	−2.3090	−1.468	−0.881	1.466	1.756
4.2	+0.3796	−2.3929	−1.593	−0.794	1.584	1.756
4.3	+0.2143	−2.4668	−1.713	−0.691	1.706	1.756
4.4	+0.0372	−2.5301	−1.828	−0.572	1.834	1.756
4.5	−0.1510	−2.5806	−1.934	−0.437	1.965	1.756
4.6	−0.3492	−2.6169	−2.030	−0.286	2.101	1.757
4.7	−0.5566	−2.6374	−2.114	−0.121	2.242	1.757
4.8	−0.7716	−2.6407	−2.184	+0.057	2.386	1.757
4.9	−0.9928	−2.6255	−2.238	+0.248	2.535	1.757

TABLE 13

t	x	y	$\dot{x}$	$\dot{y}$	$\frac{1}{2}v^2$	C
1.4*	+1.2494	−0.0194	−0.019	−0.028	0.001	1.760
1.8	+1.2588	−0.0326	+ .031	−0.042	0.001	1.760
2.2	+1.2738	−0.0523	+ .050	−0.064	0.003	1.760
2.6	+1.2975	−0.0831	+ .077	−0.102	0.008	1.759
3.0	+1.3331	−0.1327	+ .111	−0.166	0.020	1.759
3.4	+1.3833	−0.2129	+ .148	−0.267	0.047	1.760
3.8	+1.4467	−0.3408	+ .170	−0.419	0.102	1.760
4.2	+1.5127	−0.5381	+ .143	−0.628	0.208	1.761
4.6	+1.5548	−0.8265	+ .020	−0.881	0.388	1.761
5.0	+1.5276	−1.2172	− .248	−1.128	0.667	1.765
5.4	+1.3682	−1.6971	−0.683	−1.290	1.066	1.769

* The interval $0.0<t<1.4$ is obtained from the first-order theory in section 5.

probably be negligible except near the point of ejection itself. The effect on the z-co-ordinate will be to increase the vertical thickness of the tail over the dimensions determined by the z-velocities at the point of ejection.

8. APPLICATIONS

Applications to the problem of β Lyrae itself have been made throughout the paper. We may add that the asymmetrical light-curve (Fig. 1) can now be attributed to obscuration by the tail.

In section 5 we found the period for the motion in the z-co-ordinate to be 4.77, based on the first-order theory. If at the moment of ejection the amplitude is zero, the maximum amplitude will therefore be reached at $t = 1.19$; this is on the very edge where the first-order theory may be applied (cf. Table 12). This maximum semiamplitude according to equation (34) is $v_z/\sqrt{1.73}$. If v_z is of the order of the atomic velocities (about 0.01, compared to $v_0 = 0.1$), we find for the total extension in z only 0.015. This is small, compared to the dimension of the "outlet" of B as determined by the surface of zero velocity; for $v_0 = 0.1$ this dimension is about 0.2. We may therefore assume that the extension in z of the tail in the neighborhood of the binary is largely determined by the width of the outlet of B. This width is easily found from Jacobi's integral for any value of v_0.

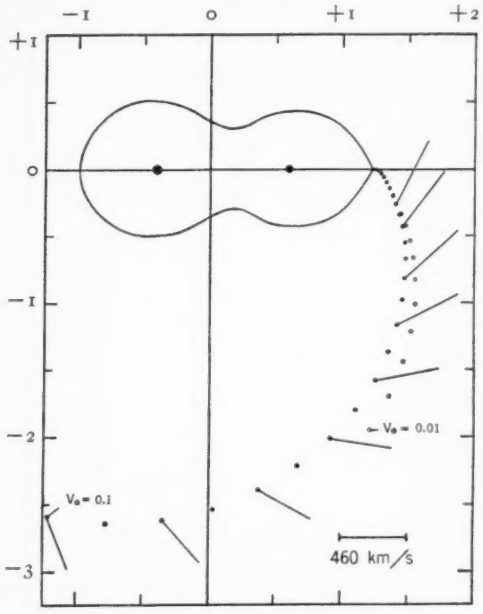

FIG. 12.—Ejection orbits of type B for v_0=0.1 and 0.01. Velocity vectors in stationary frame are indicated for v_0=0.1. Dots spaced 0.2 in t: cf. Tables 12 and 13.

The tail, therefore, does not cover the whole of A's disk when it emerges from eclipse after primary minimum but cuts out an equatorial strip roughly one-fifth of the diameter of the star. The rest of the disk is covered with the much more diluted gas of successive windings of the spiral which have acquired greater extension in z, owing to random initial velocities and to collisions.

The density measured per unit length along the tail (line density) falls off rapidly, as is seen from Tables 11–13 and from Figures 6, 11, and 12. The line density is obviously $\propto 1/v$, in which v is measured in the rotating frame. The space density falls off even more rapidly because of the increasing width of the tail in both co-ordinates perpendicular to its direction.

The gas streaming off from B must be comparatively cool, because (*a*) B is cool; (*b*) the region of ejection is the coolest part of B, gravity there being almost zero; (*c*) this region is eclipsed from radiation by A.

Some time after this cool gas has left B, it becomes exposed to radiation from A. If $v_0 = 0.1$, this happens between $t = 2.0$ and 2.5, or for β Lyrae between 4 and 5 days after ejection. It would be of interest to determine theoretically the time required for this gas to become mostly ionized by A. Without computation it may be said that the absorption lines of H and He I will be strong at first, if the B8 star is viewed through this cloud. This will account in part for the excessive strength of these lines shortly after

primary minimum, although other factors, mentioned below, enhance the effect. The spectral type, roughly B2–B5, must be a combined effect of the low density of matter and the somewhat diluted radiation by the B8 supergiant.

Proceeding along the first winding of the tail, we find (1) diminishing density—at first rapid, later more slowly; (2) increased extension in the z-direction; and (3) for the first 180° of the tail increasing ionization. Factors (1) and (3) will tend to diminish the strength of the absorption spectrum and (2) to increase it until the z-extension has reached the diameter of A. The observations show a pronounced decrease until after secondary minimum; then a slow increase takes place toward the next primary minimum. It seems possible that factor (3) reverses itself some time after secondary minimum, owing to the increasing distance from A and the fact that the side of A then visible may in part be covered by a cool returning current coming from B (cf. sec. 3).

At the completion of the first winding, the gas enters eclipse (cf. Fig. 11). The duration of this eclipse is of the order of a day, depending on v_0. The eclipse may well be

TABLE 14

t	r	$1/a$
3.5	2.067	+.0311
4.2	2.423	.0130
4.9	2.807	+.0078

total for the nearer windings. The effect will be a drop in the ionization; how much, only computation can show. This will result in a fresh absorption by the time the gas comes out of eclipse. At this time the z-extension is probably sufficient to cover most of A's disk; it is probable, therefore, that the effect of the second winding is even more important than the first one in producing a strong absorption after primary eclipse. Even the third and higher windings may have some effect, since the eclipse would affect them also.

There is an observational reason, as well, which suggests that the second and higher windings contribute considerably to the observed blend in absorption. The recessional velocity in the first quarter of the first winding is large, of the order of 0.6, or some 275 km/sec for β Lyrae. This value is much in excess of the observed 50 km/sec. It is true that we made integrations for only three values of v_0 (0.01, 0.1, and 0.53) and that a more favorable orbit could probably be found. But on dynamical grounds it seems certain that the recession of the first winding could not be brought below 200 km/sec (being about half the orbital velocity in the system AB). For the second and third windings the recessional velocity is much reduced, although perhaps not quite enough. If the ejection takes place in a highly elliptical orbit ($a \gg 10$), the velocity v is not much larger than the recessional velocity, as observed from A (cf. Fig. 9, drawn for hyperbolic motion). The latter being 50 km/sec, v could not exceed 100 km/sec at the distance r where the "mean" absorption takes place. The energy integral (59) gives, for $v = 0.2$ (92 km/sec) and for different a values, the following distances,[49] r:

a	r	a	r
10	14	100	40
20	22	∞	50
50	33		

[49] A more precise value of r giving $dr/dt = 50$ km/sec can be only found after the eccentricity or the parameter of the ellipse is specified. Our procedure underestimates r for large a.

This shows that the ejection has to be in a decidedly elliptical orbit in order that the mean distance shall not be excessive. Nevertheless it seems difficult to make the mean distance less than 10. This result is essentially due to the fact that β Lyrae is such a massive system and that orbital motion in its vicinity must be fast.

We conclude that the first winding is not of primary importance in producing the absorption spectrum, because the z-dimension of the tail is still insufficient to cover A's

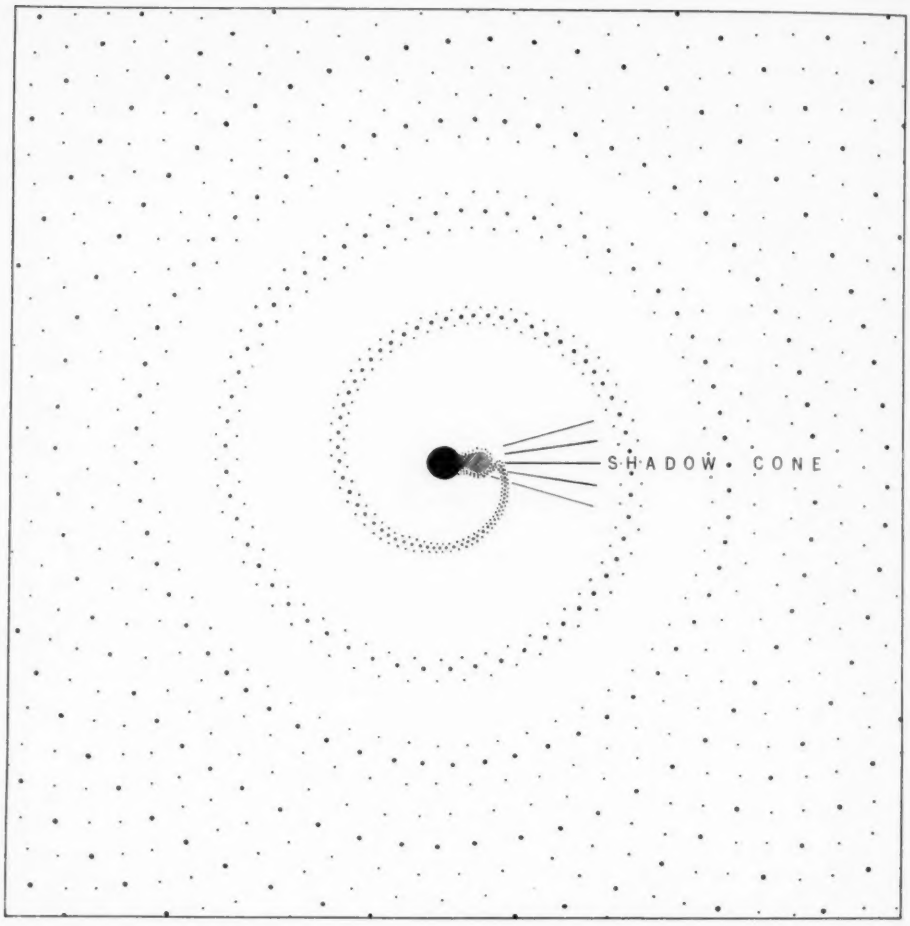

FIG. 13.—The system of β Lyrae in a frame rotating with the binary. Heavy dots indicate the central line of the spiral; light dots indicate schematically the width of the successive windings.

disk; that the next one or two windings are most effective in the absorption process; and that the still higher windings become of increasingly smaller importance. Further, the eclipse of the tail must play a major role in producing the fluctuations with phase of the line intensity. The picture developed is shown schematically in Figure 13. Since the ejection could not be perfectly regular, minor fluctuations in the line intensities and the radial velocities, as have been observed, should be expected. Finally, the inclination of the orbit must be quite close to 90° (within 2° or so).

The observed *emission* will obviously come from the whole visible part of the spiral,

with an intensity distribution depending on the density of matter and the degree of ionization. The problem is similar to that considered by B. Strömgren for interstellar matter surrounding hot stars.[50] The smoothness of the emission lines suggests that several windings of the spiral contribute to their formation. Their greatest width would be determined by the velocities of the inner winding; from Figure 12 we find about $2 \times 0.9 \times 460$ km/sec $\cong$ 800 km/sec, in good agreement with observation.

The irregularities in the light-curve at all phases are quite understandable on the basis of the picture developed.

One problem yet to be discussed is *the change in period of* β *Lyrae*. Various factors might be considered in this connection: (*a*) mass transfer from A to B, with constant total mass; (*b*) loss of mass and momentum by ejection of type B; (*c*) pressure at the interface between A and B.

Effect (*a*) was considered in section 2, with the result that a considerable *shortening* of the period should result from it.

The momentum per unit mass of the ejected matter is not constant as long as the three-body theory has to be applied; but as soon as the matter has receded far enough for the two-body approximation to become applicable, the momentum remains constant, because this constancy is identical with the validity of Kepler's law of areas. The momentum per unit mass of ejected gas may therefore be computed from the last line of Table 12, $v_0 = 0.1$ being the most probable ejection velocity obtained. The value so obtained may then be compared with the momentum per unit mass in the binary. Suppose the ratio between these momenta is Q. We shall show that, *if* $Q > 5/3$, *the period will decrease;* if $Q < 5/3$, the period of the binary will increase.

Taking as units the mass of the sun, the astronomical unit, and the year, we have

$$\frac{a^3}{P^2} = M \; ; \qquad v = \frac{2\pi a}{P} \; ; \qquad \text{and } \mathcal{M} = \mu(1-\mu)Mav \, , \tag{61}$$

in which M is the total mass and $\mathcal{M}$ the total momentum of the binary. Eliminating a and v, we have

$$\mathcal{M} = 2\pi\mu(1-\mu)M^{5/3}P^{1/3} \, . \tag{62}$$

Keeping the mass ratio constant, we obtain

$$\frac{d\mathcal{M}}{\mathcal{M}} = \frac{5}{3}\frac{dM}{M} + \frac{1}{3}\frac{dP}{P} \, . \tag{63}$$

By definition

$$\frac{-d\mathcal{M}}{-dM} : \frac{\mathcal{M}}{M} = Q \; ; \tag{64}$$

hence, by (63)

$$\frac{dP}{P} = 3(Q - \tfrac{5}{3})\frac{dM}{M} \, . \tag{65}$$

Since dM is negative, dP will be negative if $Q > 5/3$. The fact that we have kept μ constant is no restriction to our discussion, as the effect of a variable mass ratio is examined under (*a*) above.

[50] *Ap. J.*, **89**, 526, 1939.

From equation (58) we find the velocities X and Y valid for a nonrotating frame having the same instantaneous position as the rotating frame; X, Y, x, and y therefore determine the momentum per unit mass. We find 1.76 for the orbit with $v_0 = 0.1$, and 1.78 for the orbit with $v_0 = 0.53$. In the same units the orbital momentum in the binary is, per unit mass, $(1 - \mu)\,\mu^2 + \mu(1 - \mu)^2 = \mu(1 - \mu) = 0.24$ if $\mu = 0.4$. Hence, $Q \cong 7.4 \gg 5/3$. Hence the period should *decrease* as a result of the ejection.

As is well known, the period has been increasing during the interval of over a century covered by the observations. Of the three causes mentioned above only that under (*c*) might be able to produce such an increase. This question is examined in the addendum to this paper.

Other applications may be made to the W Ursae Majoris stars which seem to be contact binaries composed of two dwarf stars. The shallowness of the minima after correction for ellipticity apparently results from the great extent of the common envelope. The magnitude difference and the ratio in surface brightness should again be abnormally large for the difference in mass, so that from the near-equality of the components in several of these systems almost exact equality of masses must be concluded. The equalization of the masses, discussed in section 2, has in these stars reached, or nearly reached, its final stage. A closer spectroscopic study of the more unequal pairs of this class might show traces of currents around the components.

Ejection of type A seems to be fairly common, as more and more pairs become known which are composed of a large giant and a small hot component, the latter being surrounded by gas that might well have originated in the former, as described in section 4. We refer to such stars as WY Geminorum, W Cephei, Z Andromedae, T Coronae Borealis, and several others recently studied by Merrill[51] and by Swings and Struve.[52]

The case of Antares[53] is somewhat different, because, first, the primary does not nearly fill its first "contact surface" and, second, the orbital motion is probably very small (less than 8 km/sec, depending on the projection factor in the observed separation), not larger than the atomic velocities. Under these circumstances there is no longer a closed surface of zero velocity within which the atoms around B are trapped.

In conclusion, I wish to record my indebtedness to Dr. Struve for several discussions on the spectroscopic data concerning β Lyrae. These discussions have helped materially in finding the significant processes operating in this complex system.

YERKES OBSERVATORY
October 3, 1940

ADDENDUM

CHANGES OF PERIOD IN CONTACT BINARIES

In the preceding pages the influence on the orbital period of the pressure at the interface of the components was mentioned but was not examined numerically. A brief survey of the problem is made below.

1. *The numerical value of the pressure.*—In the dynamical problem to be considered later it is convenient to have the radial repulsive force, caused by the pressure at the interface, expressed in terms of the gravitational attraction between the components. We shall compute the repulsive force for the case of equal components, because in that case the large instabilities, present in unequal components, will be absent, so that von Zeipel's theorem on the distribution of pressure should give a good approximation.

[51] E.g., *Spectra of Long-Period Variable Stars*, chaps. vi and vii, 1940.

[52] *Ap. J.*, **91**, 546, 1940; *Pub. A.S.P.*, **52**, 199, 1940.

[53] *Ap. J.*, **92**, 316, 1940.

The procedure followed is this: By using the Roche model the variation of the potential is found in the yz-plane (the interface) and along the b-axis of one of the (equal) components. It is then assumed that the variation of pressure along the b-axis is the same as that along the radius of a single star having the same mass. Using the theoretical pressures for a polytrope of index 3, the pressure at the interface is computed in terms of the central pressure of the star, $P_c = 11.05\ (GM^2/R^4)$,[54] times an area, so that a comparison is possible with the gravitational attraction, GM^2/r^2, when R is fixed in terms of r. Different ratios of R/r are possible, between the extremes of binaries just in contact and those with envelopes of maximum possible height. Taking b as a good measure of R (cf. Table 3), we find from Table 3 that R/r (i.e., b/r) may vary from 0.374 to 0.482. The repulsive force will be zero in the former case and will have its maximum value in the latter case. Since in the process of mass transfer $\bar{R}$ is nearly constant in absolute measure, the variation of the repulsive force thus found will mean a variation with r; this is the relation needed in the dynamical problem.

TABLE 15

b/r	$-\Omega$	y/r	b/r	$-\Omega$	y/r
0.3740.....	2.0000	0.0000	0.4400.....	1.8158	0.2536
.3890.....	1.9804	.0756	.4600.....	1.7720	.2901
.4000.....	1.9192	.1583	0.4823.....	1.7284	0.3261
0.4200.....	1.8647	0.2112			

For small distances from the x-axis (i.e., in the region where the pressures are largest) the potential on the interface (the yz-plane) is given by

$$-\Omega = 2 - 3\tfrac{1}{2}y^2 - 4z^2 + \text{terms of fourth order, etc.} \qquad (66)$$

Near the x-axis the curves of constant potential are therefore ellipses with axes in the ratio

$$2 : \sqrt{3\tfrac{1}{2}} = 1 : 0.9354\,.$$

We shall make the computations for a circular distribution and afterward multiply by 0.935.

The variation of the potential along the y-axis of the interface and the b-axis of one of the components is given in Table 15. The first and the last lines correspond to the extreme cases of first contact and maximum envelope.

The pressure is now found as follows: Consider, e.g., the last line of Table 15. $R/r = 0.4823$ fixes r, needed in computing the gravitational attraction. The maximum value of P/P_c, found at $y = 0$, equals the value at radius $0.3740/0.4823 = 0.775$ of a single star of the same mass. From the *British Association Mathematical Tables, II*, we find that, for $n = 3$ and $x/x_0 = 0.775$, $P/P_c\ (= B) = 0.51 \cdot 10^{-4}$.

Similarly, the ratio P/P_c may be found for other points at the same interface and also for different values of R/r. Table 16 gives the results. The unit of P/P_c is 10^{-6}.

The total pressure (or repulsive force) at the interface is

$$F = 0.935\, P_c R^2 \int_0^\infty 2\pi \frac{y}{R} \cdot \frac{P}{P_c} \cdot d\left(\frac{y}{R}\right) = g \cdot R^2 P_c\,. \qquad (67)$$

[54] S. Chandrasekhar, *Stellar Structure*, p. 230.

The coefficients g are shown in Table 17; they were obtained by quadratures. The total pressure will be equal to the pressure at the center of the interface times a certain area. If this area is taken to be a circle, its radius, a/R, is found in Table 17. It shows that the central region becomes of increasing relative importance for a smaller degree of contact. Finally, F may now be expressed in terms of the gravitational attraction; if we denote the ratio by f (a dimensionless constant), we have $f = 11.05 \times g \times (r/R)^2$. The values of f are found in Table 17; the maximum is only 1/1800.

The results in Table 17 have been derived for the case of equal components; but we shall use them in the general case as well, since they will probably give a fair approxima-

TABLE 16

	R/r									
	0.4823		0.4600		0.4400		0.4200		0.4000	
y/r	y/R	P/P_c	y/R	P/P_c	y/R	P/P_c	y/R	P/P_c	y/R	P/P_c
0.0000.....	0.0000	51.0	0.0000	20.5	0.0000	7.1	0.0000	1.68	0.0000	0.17
.0756.....	.1567	38.6	.1643	14.4	.1718	4.6	.1800	0.90	.1890	.057
.1583.....	.3282	13.1	.3441	3.7	.3598	0.74	.3769	0.05	0.3958	0.000
.2112.....	.4379	3.5	.4591	0.61	.4800	0.04	0.5029	0.00	.....	.....
.2536.....	.5258	0.63	.5513	0.03	0.5764	0.00	.....	.....	.....	.....
.2901.....	.6015	0.04	0.6306	0.00	.....	.....	.....	.....	.....	.....
0.3261.....	0.6761	0.00	.....	.....	.....	.....	.....	.....	.....	.....

TABLE 17

R/r	$g \cdot 10^6$	a/R	$f \cdot 10^6$	r/R
0.4823.....	11.6	0.27	550	2.073
.4600.....	4.03	.25	210	2.174
.4400.....	1.24	.23	71	2.273
.4200.....	0.23	.21	14.3	2.381
.4000.....	0.014	.16	1.0	2.500
0.3740.....	0.000	0.00	0.00	2.674

tion and since no simple method seems available to determine the pressure between two unequal stars not in equilibrium.

2. *Secular changes of period.*—The first question to examine is whether the secular changes already considered (mass transfer from A to B and ejection), which were found to cause a *decrease* in period if the repulsive force at the interface is neglected, could produce an increase if this force is taken into account. Because of the smallness of the ratio f there seems little reason to expect this.

This expectation is confirmed by the following analysis. We are interested in secular changes of a nearly circular orbit, so that we put $\ddot{r} = 0$ in the equations of motion:

$$0 = r\omega^2 - \frac{M}{r^2}(1 - f), \qquad (68) \qquad \text{or} \qquad r^3\omega^2 = M(1 - f), \qquad (68')$$

and

$$\mu(1 - \mu)Mr^2\omega = \mathcal{M}. \qquad (69)$$

Here $M = M_1 + M_2 = (1 - \mu)M + \mu M$, and $\mathcal{M}_0$ is the total angular momentum of the binary. The first equation expresses the obvious fact that in the equilibrium orbit the sum of the centrifugal force and the repulsive force equals the gravitational attraction; equation (68′) gives the modified third law of Kepler. The second equation (eq. [69]), obtained after one integration, expresses the fact that only radial forces are operating; as the masses are variable, Kepler's law of areas has been replaced by the corresponding momentum integral. If ejection takes place, however, transverse forces will be present; they are automatically taken into account, if now, $\mathcal{M}_0$ is considered variable and $d\mathcal{M}_0/dM$ is taken from the theory of ejection. It is noted that the rotational momentum of the components has been neglected. Its effect is mentioned later.

We shall now compare the binary at two epochs, t_0 and t, far enough apart for changes of the first order to have taken place. We put

$$\left.\begin{aligned} \frac{r}{r_0} &= 1 + \delta\,, & \frac{M}{M_0} &= 1 + \beta,\\ \frac{\omega}{\omega_0} &= 1 + \epsilon\,, & \frac{\mathcal{M}_0}{\mathcal{M}_{00}} &= 1 + Q\beta\,,\\ \frac{\mu}{\mu_0} &= 1 + \lambda\,, & f &= f_0 + \varphi\,, \end{aligned}\right\} \tag{70}$$

in which the increments are proportional to the interval, $(t - t_0) = \Delta t$. (Hence, $\delta = [1/r_0]\,[dr/dt]\Delta t$, etc.) We know β to be negative or zero; its amount is known in principle. The ratio Q was defined on page 171 and was found to be about 7.4. Known in principle are also λ, governing the rate of mass transfer, and

$$\varphi = \frac{df}{dt}\Delta t = \frac{\partial f}{\partial r}\Delta r + \frac{\partial f}{\partial t}\Delta t = \frac{\partial f}{\partial r}\cdot r\cdot\delta + \frac{\partial f}{\partial t}\Delta t = h(-\delta + \gamma)\,,$$

because $(\partial f/\partial r)\Delta r$ is found from Table 17, and $(\partial f/\partial t)\Delta t$ is known, in principle, after the changes in the radii and masses have been allowed for. There remain the true unknowns, δ and ϵ; they are obtained by the introduction of equation (70) into equations (68) and (69). By differentiating equations (68′) and (69) logarithmically and multiplying by $\Delta t/dt$, we get

$$3\delta + 2\epsilon = \beta - \varphi\,, \tag{71}$$

$$\nu + \beta + 2\delta + \epsilon = Q\beta\,, \qquad \text{if} \qquad \nu = \lambda\frac{1 - 2\mu_0}{1 - \mu_0} \gtrless 0\,. \tag{72}$$

Solving equations (71) and (72) for δ and ϵ, we find

$$\left.\begin{aligned} \delta &= \frac{(2Q - 3)\beta - 2\nu + h\gamma}{1 + h}\,,\\ \epsilon &= \frac{-\{3Q - 5 - (Q - 1)h\}\beta + (3 - h)\nu - 2h\gamma}{1 + h}\,. \end{aligned}\right\} \tag{73}$$

The critical value of $Q = 5/3$ for the change of the period is confirmed by these general formulae; with $Q > 5/3$, ejection ($\beta < 0$) leads to a positive value of ϵ, as does mass transfer ($\nu > 0$). We found $Q \cong 7.4$.

The maximum value of h occurs in the first interval of Table 17; from $\Delta f = -h(\Delta r/r)$ we find for the mean value in this interval, $h = +0.0050$. For the four successive intervals the mean values are $+0.0031$, $+0.0012$, $+0.00027$, and $+0.000015$. The changes in the sum of the radii will in general be small compared to the change in distance between the components. The change of the repulsive force is, therefore, in general due chiefly to the latter cause; or $h\gamma \ll h\delta$ and may be entirely neglected in equation (73). Since $h \langle\langle\langle 3$ and $h \langle\langle\langle (3Q - 5)/(Q - 1) \cong 2.7$, we must conclude that *the period of a contact binary should secularly decrease despite the pressure at the interface.* The only escape from this conclusion provided by equation (73) is a rather sudden increase in the stellar diameter(s), causing a large value of γ during a limited interval. But such an increase in diameter would soon cause an increase in the rotational momentum of the stars (which was neglected in the derivation of eq. [73]), resulting in a decrease of the orbital period. In view of the weakness of the repulsive force, this opposite effect may well preponderate; so that a sudden *decrease* of the diameters might temporarily reverse the general trend of a decreasing period.

If the masses are very nearly equal ($\nu \leqq 0$) and if no ejection takes place ($\beta = 0$), as is probably the case for several W UMa stars, the period should remain secularly constant, unless changes occur in the stellar diameters.

3. *Periodic variations of period.*—Since we shall now consider fluctuations in r over shorter intervals, we have to retain $\ddot{r}$ in the equations of motion but may neglect the mass transfer and the ejection. The equations of motion are now (the second one after one integration):

$$\left.\begin{aligned} \ddot{r} &= r\dot{\theta}^2 - \frac{M}{r^2}(1 - f)\,, \\ r^2\dot{\theta} &= h\,. \end{aligned}\right\} \tag{74}$$

We eliminate $\dot{\theta}$ and obtain

$$\ddot{r} = \frac{h^2}{r^3} - \frac{M}{r^2} + \frac{MN}{r^2}\, e^{-sr/R}\,. \tag{75}$$

Here we have replaced f by an exponential relation found from Table 17: $\log f = 7.15 - 5(r/R)$, which represents the most important interval, $2.07 < r/R < 2.4$, quite well. We have, therefore, $N = 10^{7.15}$ and $s = (5/\mathrm{Mod}) = 11.5$.

The oscillations of r determined by equation (75) are most readily obtained by a perturbation method. If the orbit were circular, its radius would be found from equation (75) by putting $\ddot{r} = 0$ and $r = a$, the latter being the radius of the orbit. We shall refer to equation (75) in this form as equation (75′). Considering small oscillations, we put $r = a(1+\alpha)$; hence $\ddot{r} = a\ddot{\alpha}$, and from equation (75)

$$\ddot{\alpha} = -\alpha B^2\,, \qquad (76) \qquad \text{if} \qquad B^2 = 3\frac{h^2}{a^4} - 2\frac{M}{a^3} + \left(s\frac{a}{R} + 2\right)\frac{MN}{a^3}\, e^{-sa/R}\,. \qquad (77)$$

The solution of equation (76) is $\alpha = A \sin(Bt + \varphi)$, in which the semiamplitude, A, and the phase, φ, are arbitrary and the period of the oscillation is $2\pi/B$.

In order to see the relative importance of the terms in equation (77), we put first $N = 0$. From equation (75′) we then find $h^2/a^4 = M/a^3$, so that $B^2 = M/a^3$. Kepler's third law for the orbit gives $\omega^2 = M/a^3$. Hence, $B = \omega$, or the period of the oscillation

equals that of the period in the circular orbit. We obtain, therefore, motion in a stationary ellipse.

In the presence of the repulsive force equation (75′), or (74), gives as Kepler's third law:

$$\omega^2 = \frac{M}{a^3}(1 - f_0) ; \tag{78}$$

whereas from equations (77) and (75′) we find

$$B^2 = \frac{M}{a^3}\left[1 + \left(s\frac{a}{R} - 1\right)f_0\right] . \tag{79}$$

Here f_0 is the value of f at $r = a$, the mean radius of the orbit. Hence, if II is the period of the oscillation and P that of the circular orbit, we find

$$\frac{\text{II}}{P} = \frac{\omega}{B} = 1 - \frac{saf_0}{2R} . \tag{80}$$

For s we found 11.5; for a we may put the mean value $2.2R$; the coefficient of f_0 is therefore about -12.6. Since f_0 is, at most, about 0.00055 (cf. Table 17), we find that *the only effect of the repulsive force is a slow regression of the line of apsides.* The period P' of the rotation of the apse is

$$\frac{P'}{P} = \left(\frac{saf_0}{2R}\right)^{-1} \cong (12.6f_0)^{-1} > 152 . \tag{81}$$

The period P' is independent of the eccentricity of the orbit as long as e remains a quantity of the first order. (The ratio 152 is based on the correct limiting value of a, not on the mean value.) The effect (eq. [81]) will complicate the derivation of the density concentration from the rotation of the line of apsides whenever the components are in contact; and contact will exist if $R/r > 0.374$, in which R is the true (not necessarily the photometrically determined) radius.

Summary.—In the first section the repulsive force caused by the pressure at the interface of a contact binary is evaluated numerically for the case of equal components. The result is found in Table 17, in which f expresses the repulsive force, for different distances r/R, in terms of the gravitational attraction between the components. Next, secular changes of period are examined; it is found that the repulsive force does not materially change the rate of decrease of period caused by ejection of matter or mass transfer from A to B. Periodic changes are found to be limited to a rotation of the line of apsides, the period of which is given by equation (81). The conclusion is that only changes in the stellar radii can temporarily lead to an increase of the orbital period.

October 12, 1940

PHYSICAL PROCESSES IN GASEOUS NEBULAE

XI. STRENGTHS OF FORBIDDEN LINES IN p^2, p^3, AND p^4 AS A FUNCTION OF COUPLING

G. H. SHORTLEY, L. H. ALLER, J. G. BAKER, AND D. H. MENZEL

ABSTRACT

The coupling of configurations p^2, p^3, and p^4 is determined by a single parameter χ which ranges from 0 for *LS* to ∞ for *jj* coupling. This paper contains a tabulation of the magnetic-dipole strengths and the coefficient of the radial integral in the electric-quadrupole strengths for all the forbidden lines in these configurations for all values of χ. The transformation coefficients which express the actual eigenfunctions in terms of the *LS*-coupling eigenfunctions are also tabulated.

For a study of physical conditions in celestial objects, the night sky, and laboratory sources of "forbidden" radiation, it is necessary to have detailed theoretical information concerning the strengths of the lines. The first steps in this direction were made by Stevenson[1] and by Condon,[2] who considered certain lines of p^2 for *C* I, *N* II, and *O* III; of p^3 for *O* II and *S* II; and of p^4 for *O* I. But, since the properties of all possible coupling cases[3] for these configurations can be tabulated against a single parameter χ and since careful estimates of probable χ values for the various ions exist,[4] it seems desirable once and for all to tabulate the strengths of the lines as a function of χ with no approximations except the sometimes dubious one of using a pure configuration assignment. The parameter $\chi = \frac{1}{5}\zeta_p/F_2$ is essentially a measure of the departure from *LS* coupling, being 0 for pure *LS* coupling and ∞ for pure *jj* coupling.

The *absolute* values of the strengths of the magnetic-dipole lines are tabulated against χ; but for the quadrupole lines we may tabulate only the coefficients of the squares of the integrals

$$s_q = s_q(np, np) = \tfrac{2}{5}\epsilon \int_0^\infty r^2 R^2(np)\, dr\,, \qquad (1)$$

which involve the radial factor of the *p*-orbital and must be considered separately for each atom.[5] In atomic units ϵa^2, s_q is of the order of magnitude of unity. It will be noticed that we include the strengths of the very low-frequency "lines" connecting two levels of the same term. These values, which have been neglected in the past, are important in considerations of the populations of the levels in rarefied atmospheres. We also tabulate, for reference, the often needed transformation coefficients which express the intermediate-coupling eigenfunctions in terms of *LS*-coupling eigenfunctions.

[1] *Proc. Roy. Soc.*, Ser. A, **137**, 298, 1932.

[2] *Ap. J.*, **79**, 217, 1934. We disagree with certain of the formulas represented by equations (27), (31), (32), (41), (44), and (46) of this paper and, hence, with the numerical values obtained therefrom.

[3] See Condon and Shortley, *Theory of Atomic Spectra*, pp. 274–276, 300–301; and see, in particular, note 4 of this article.

[4] Robinson and Shortley, *Phys. Rev.*, **52**, 713, 1937, Tables V, VI, and VII. The $2p^3$ χ-values which are missing from Table VI may be obtained by interpolation in the data of Fig. 5 of this reference, which gives the following values for $\chi(2p^3)$: *N* I, 0.0086; *O* II, 0.0153; *F* III, 0.0251; *Ne* IV, 0.0365; *Na* V, 0.0549; *Mg* VI, 0.0772; *Al* VII, 0.103; *Si* VIII, 0.134; *P* IX, 0.168.

[5] This integral has been estimated by Condon[2] for certain cases, recently for many others by Pasternack, *Ap. J.*, **92**, 129, 1940.

In natural excitation the spontaneous-transition probability associated with the emission of *magnetic-dipole* radiation is given by

$$A_m(J, J') = 35{,}320 \frac{\sigma^3 S_m(J, J')}{2J + 1} \text{ sec}^{-1} . \tag{2}$$

Here J and J' are the quantum numbers of the upper and lower levels; σ is the wave-number of the line expressed in Rydbergs (1 Ryd. = 109,737 cm^{-1}); and $S_m(J, J')$ is the magnetic-dipole strength[6] in atomic units $e^2\hbar^2/4\mu^2c^2$, here given by Tables 1, 4, and 7.

The *electric-quadrupole* transition probability is

$$A_q(J, J') = 2648 \frac{\sigma^5 S_q(J, J')}{2J + 1} \text{ sec}^{-1} . \tag{3}$$

The quadrupole strength $S_q(J, J')$ is here to be expressed in atomic units $\epsilon^2 a^4$ (where a is the Bohr radius $\hbar^2/\mu\epsilon^2$). This strength may be written as the product of a numerical coefficient $C_q(J, J')$, which depends only on the coupling parameter χ, by the square of the integral in equation (1),

$$S_q(J, J') = C_q(J, J')\, s_q^2(np, np) . \tag{4}$$

It is the coefficient C_q which is given in Tables 2, 5, and 8.

THE CONFIGURATION p^2

The actual eigenfunctions for the levels of p^2 are functions of a parameter χ which ranges from 0 to ∞ as the coupling goes from extreme LS to extreme jj. If these functions (distinguished by primes) are expressed in terms of the pure Russell-Saunders functions (phases chosen as in n. 3) by

$$\left.\begin{aligned} \psi(^1D_2') &= a\psi(^1D_2) + b\psi(^3P_2) , \qquad \psi(^3P_0') = c\psi(^3P_0) + d\psi(^1S_0) , \\ \psi(^3P_2') &= a\psi(^3P_2) - b\psi(^1D_2) , \qquad \psi(^1S_0') = c\psi(^1S_0) - d\psi(^3P_0) , \\ &\psi(^3P_1') = \psi(^3P_1) , \end{aligned}\right\} \tag{5}$$

we find the following series for the coefficients near LS coupling, i.e., for small values of χ:

$$\left.\begin{aligned} a &= 1 - \tfrac{2}{14}\tfrac{5}{4}\chi^2 - \tfrac{1}{8}\tfrac{2}{6}\tfrac{5}{4}\chi^3 + \ldots . , \\ b &= \tfrac{5}{12}\sqrt{2}\,\chi(1 + \tfrac{5}{12}\chi - \tfrac{2}{7}\tfrac{5}{2}\chi^2 + \ldots .) , \\ c &= 1 - \tfrac{1}{9}\chi^2 + \tfrac{2}{27}\chi^3 + \ldots . , \\ d &= \tfrac{1}{3}\sqrt{2}\,\chi(1 - \tfrac{1}{3}\chi - \tfrac{2}{9}\chi^2 + \ldots .) . \end{aligned}\right\} \tag{6}$$

[6] See Shortley, *Phys. Rev.*, **57**, 225, 1940, for definitions. This reference contains the values of the magnetic-dipole and electric-quadrupole strengths in LS coupling and explains the method of transforming to intermediate coupling. We here give just the numerical values and the formulas from which they are obtained.

The magnetic-dipole strengths, in units $(-\epsilon h/4\pi\mu c)^2$, have, in general, the following values in terms of these coefficients and the following asymptotic expansions near *LS* coupling:[7]

$$\left.\begin{aligned}
&S_m(^1S_0', {}^1D_2') = 0\,,\\
&S_m(^1S_0', {}^3P_2') = 0\,,\\
&S_m(^1S_0', {}^3P_1) = (-)^2\, 2d^2 \quad = (-)^2\, \tfrac{4}{9}\chi^2(1 - \tfrac{2}{3}\chi - \tfrac{1}{3}\chi^2 + \ldots.)\,,\\
&S_m(^1S_0', {}^3P_0') = 0\,,\\
&S_m(^1D_2', {}^3P_2') = (+)^2\, \tfrac{1}{2}\tfrac{5}{5}a^2b^2 = (+)^2\, \tfrac{3}{14}\tfrac{7}{4}\tfrac{5}{4}\chi^2(1 + \tfrac{5}{6}\chi - \tfrac{1}{14}\tfrac{2}{4}\tfrac{5}{4}\chi^2 + \ldots.)\,,\\
&S_m(^1D_2', {}^3P_1) = (+)^2\, \tfrac{5}{2}b^2 \quad = (+)^2\, \tfrac{1}{14}\tfrac{2}{4}\tfrac{5}{4}\chi^2(1 + \tfrac{5}{6}\chi - \tfrac{2}{4}\tfrac{5}{8}\chi^2 + \ldots.)\,,\\
&S_m(^1D_2', {}^3P_0') = 0\,,\\
&S_m(^3P_2', {}^3P_1) = (+^2\, \tfrac{5}{2}a^2 \quad = (+)^2\, \tfrac{5}{2}(1 - \tfrac{3}{7}\tfrac{5}{2}\chi^2 + \ldots.)\,,\\
&S_m(^3P_2', {}^3P_0') = 0\,,\\
&S_m(^3P_1, {}^3P_0') = (+)^2\, 2c^2 \quad = (+)^2\, 2(1 - \tfrac{3}{8}\chi^2 + \ldots.)\,.
\end{aligned}\right\} \tag{7}$$

The electric-quadrupole strengths, in terms of the one-electron components in equation (9), are the following:

$$\left.\begin{aligned}
&S_q(^1S_0', {}^1D_2') = (+)^2\, \tfrac{5}{8}s_q^2(bd + 2ac)^2 = (+)^2\, \tfrac{2}{3}\tfrac{0}{5}s_q^2(1 - \tfrac{7}{2}\tfrac{7}{4}\chi^2 + \ldots.)\,,\\
&S_q(^1S_0', {}^3P_2') = (+)^2\, \tfrac{5}{8}s_q^2(ad - 2bc)^2 = (-)^2\, \tfrac{5}{6}s_q^2\chi^2(1 + \tfrac{1}{6}\tfrac{1}{5}\chi + \ldots.)\,,\\
&S_q(^1S_0', {}^3P_1) = 0\,,\\
&S_q(^1S_0', {}^3P_0') = 0\,,\\
&S_q(^1D_2', {}^3P_2') = (-)^2\, \tfrac{1}{4}\tfrac{0}{5}s_q^2a^2b^2 \quad = (-)^2\, \tfrac{8}{9}\tfrac{7}{6}\tfrac{5}{5}s_q^2\chi^2(1 + \tfrac{5}{6}\chi + \ldots.)\,,\\
&S_q(^1D_2', {}^3P_1) = (+)^2\, \tfrac{1}{4}\tfrac{5}{5}s_q^2b^2 \quad = (+)^2\, \tfrac{1}{9}\tfrac{2}{6}\tfrac{5}{5}s_q^2\chi^2(1 + \tfrac{5}{6}\chi + \ldots.)\,,\\
&S_q(^1D_2', {}^3P_0') = (+)^2\, \tfrac{5}{8}s_q^2(2ad - bc)^2 = (+)^2\, \tfrac{5}{24}s_q^2\chi^2(1 - \tfrac{1}{6}\tfrac{9}{}\chi + \ldots.)\,,\\
&S_q(^3P_2', {}^3P_1) = (+)^2\, \tfrac{1}{4}\tfrac{5}{5}s_q^2a^2 \quad = (+)^2\, \tfrac{1}{4}\tfrac{5}{5}s_q^2(1 - \tfrac{3}{7}\tfrac{5}{2}\chi^2 + \ldots.)\,,\\
&S_q(^3P_2', {}^3P_0') = (-)^2\, \tfrac{5}{8}s_q^2(2bd + ac)^2 = (-)^2\, \tfrac{5}{8}s_q^2(1 + \tfrac{1}{2}\tfrac{3}{4}\chi^2 + \ldots.)\,,\\
&S_q(^3P_1, {}^3P_0') = 0\,.
\end{aligned}\right\} \tag{8}$$

THE CONFIGURATION p^4

For the p^4 eigenfunctions we may conveniently use the same notation (eq. [5]) as for p^2. In this case the asymptotic values of a, b, c, and d may be obtained from equation (6) by writing $-\chi$ in place of χ.

The magnetic-dipole strengths are the same functions of a, b, c, d as for p^2, and their asymptotic forms are to be obtained from those of p^2 by reversing the sign of χ.

[7] The phases of $S^{1/2}$ to be used in transformations of coupling are noted for completeness. They are of no immediate significance (see n. 6 for details).

As shown in note 6, the quadrupole-moment matrix components in *LS* coupling are equal but of opposite sign for p^2 and p^4. Hence, the intermediate-coupling strengths are the same functions of a, b, c, and d in the two cases, and the asymptotic forms for p^4 are obtained from those of p^2 by reversing the sign of χ.

THE CONFIGURATION p^3

In this configuration we designate the eigenfunctions by

$$\left.\begin{aligned}
\psi(^2D'_{3/2}) &= a\psi(^2P_{3/2}) + b\psi(^4S_{3/2}) + c\psi(^2D_{3/2}) ,\\
\psi(^4S'_{3/2}) &= a'\psi(^2P_{3/2}) + b'\psi(^4S_{3/2}) + c'\psi(^2D_{3/2}) ,\\
\psi(^2P'_{3/2}) &= a''\psi(^2P_{3/2}) + b''\psi(^4S_{3/2}) + c''\psi(^2D_{3/2}) ,\\
\psi(^2P'_{1/2}) &= \psi(^2P_{1/2}) , \qquad \psi(^2D'_{5/2}) = \psi(^2D_{5/2}) .
\end{aligned}\right\} \tag{9}$$

We choose the phases of the Russell-Saunders eigenfunctions as in Condon and Shortley.[8] Near *LS* coupling these coefficients have the form

$$\left.\begin{aligned}
a &= -\tfrac{5}{12}\sqrt{5}\,\chi(1 - \tfrac{15}{864}\chi^2 + \dots.) , & a' &= -\tfrac{1}{3}\chi\,(1 + \tfrac{7}{108}\chi^2 + \dots.) ,\\
b &= -\tfrac{25}{108}\sqrt{5}\,\chi^2(1 - \tfrac{10}{864}\chi^2 + \dots.) , & b' &= 1 - \tfrac{1}{18}\chi^2 + \dots. ,\\
c &= 1 - \tfrac{13}{288}\chi^2 + \dots. , & c' &= \tfrac{5}{54}\sqrt{5}\,\chi^2(1 - \tfrac{13}{108}\chi^2 + \dots.) ,\\
& & a'' &= 1 - \tfrac{47}{96}\chi^2 + \dots. ,\\
& & b'' &= \tfrac{1}{3}\chi(1 - \tfrac{91}{96}\chi^2 + \dots.) ,\\
& & c'' &= \tfrac{5}{12}\sqrt{5}\,\chi(1 - \tfrac{157}{96}\chi^2 + \dots.) .
\end{aligned}\right\} \tag{10}$$

The magnetic-dipole strengths are

$$\left.\begin{aligned}
S_m(^2P'_{3/2}, {}^2P_{1/2}) &= (+)^2\,\tfrac{4}{3}a''^2 &&= (+)^2\,\tfrac{4}{3}(1 - \tfrac{47}{48}\chi^2 + \dots.) ,\\
S_m(^2P'_{3/2}, {}^2D_{5/2}) &= (+)^2\,\tfrac{1}{5}^2c''^2 &&= (+)^2\,\tfrac{25}{12}\chi^2(1 - \tfrac{157}{48}\chi^2 + \dots.) ,\\
S_m(^2P'_{3/2}, {}^2D'_{3/2}) &= (+)^2\,\tfrac{4}{15}(10aa'' + 15bb'' + 6cc'')^2 &&= (-)^2\,\tfrac{100}{27}\chi^2(1 - \tfrac{307}{108}\chi^2 + \dots.) ,\\
S_m(^2P_{1/2}, {}^2D_{5/2}) &= 0 ,\\
S_m(^2P_{1/2}, {}^2D'_{3/2}) &= (+)^2\,\tfrac{4}{3}a^2 &&= (-)^2\,\tfrac{125}{108}\chi^2(1 - \tfrac{1525}{432}\chi^2 + \dots.) ,\\
S_m(^2P'_{3/2}, {}^4S'_{3/2}) &= (+)^2\,\tfrac{4}{15}(10a'a'' + 15b'bb'' + 6c'c'')^2 &&= (+)^2\,\tfrac{30}{21}\chi^2(1 - \tfrac{1267}{432}\chi^2 + \dots.) ,\\
S_m(^2P_{1/2}, {}^4S'_{3/2}) &= (+)^2\,\tfrac{4}{3}a'^2 &&= (-)^2\,\tfrac{4}{27}\chi^2(1 + \tfrac{7}{54}\chi^2 + \dots.) ,\\
S_m(^2D_{5/2}, {}^2D'_{3/2}) &= (+)^2\,\tfrac{1}{5}^2c^2 &&= (+)^2\,\tfrac{1}{5}^2(1 - \tfrac{125}{144}\chi^2 + \dots.) ,\\
S_m(^2D_{5/2}, {}^4S'_{3/2}) &= (+)^2\,\tfrac{1}{5}^2c'^2 &&= (+)^2\,\tfrac{25}{243}\chi^4(1 - \tfrac{18}{54}\chi^2 + \dots.) ,\\
S_m(^2D'_{3/2}, {}^4S'_{3/2}) &= (+)^2\,\tfrac{4}{15}\,(10aa' + 15bb' + 6cc')^2 &&= (-)^2\,\tfrac{300}{972}\chi^4(1 - \tfrac{938}{432}\chi^2 + \dots.) .
\end{aligned}\right\} \tag{11}$$

[8] *Op. cit.*, pp. 225 and 268.

The quadrupole strengths are

$$\left.\begin{aligned}
S_q(^2P'_{3/2}, {}^2P_{1/2}) &= (-)^2\, 6s_q^2 c''^2 &&= (-)^2\, {}^{1\,2\,5}_{2\,4}\, s_q^2 \chi^2(1 - {}^{1\,5\,7}_{4\,8}\chi^2 + \dots.)\,,\\
S_q(^2P'_{3/2}, {}^2D_{5/2}) &= (-)^2\, 14 s_q^2 a''^2 &&= (-)^2\, 14 s_q^2(1 - {}^{4\,7}_{4\,8}\chi^2 + \dots.),\\
S_q(^2P'_{3/2}, {}^2D'_{3/2}) &= (-)^2\, 6s_q^2(a''c + ac'')^2 &&= (-)^2\, 6s_q^2(1 - {}^{4\,8}_{1\,2}\chi^2 + \dots.)\,,\\
S_q(^2P_{1/2}, {}^2D_{5/2}) &= (+)^2\, 4s_q^2\,, &&\\
S_q(^2P_{1/2}, {}^2D'_{3/2}) &= (-)^2\, 6s_q^2 c^2 &&= (-)^2\, 6s_q^2(1 - {}^{1\,2\,5}_{1\,4\,4}\chi^2 + \dots.)\,,\\
S_q(^2P'_{3/2}, {}^4S'_{3/2}) &= (-)^2\, 6s_q^2(a''c' + a'c'')^2 &&= (+)^2\, {}^{1\,2\,5}_{1\,9\,4\,4}\, s_q^2 \chi^4(1 - {}^{3\,0\,1\,7}_{4\,3\,2}\chi^2 + \dots.)\,,\\
S_q(^2P_{1/2}, {}^4S'_{3/2}) &= (-)^2\, 6s_q^2 c'^2 &&= (-)^2\, {}^{1\,2\,5}_{4\,8\,6}\, s_q^2 \chi^4(1 - {}^{1\,3}_{5\,4}\chi^2 + \dots.)\,,\\
S_q(^2D_{5/2}, {}^2D'_{3/2}) &= (-)^2\, 14 s_q^2 a^2 &&= (+)^2\, {}^{8\,7\,5}_{7\,2}\, s_q^2 \chi^2(1 - {}^{1\,5\,2\,5}_{4\,3\,2}\chi^2 + \dots.)\,,\\
S_q(^2D_{5/2}, {}^4S'_{3/2}) &= (-)^2\, 14 s_q^2 a'^2 &&= (+)^2\, {}^{1\,4}_{9}\, s_q^2 \chi^2(1 + {}^{7}_{5\,4}\chi^2 + \dots.)\,,\\
S_q(^2D'_{3/2}, {}^4S'_{3/2}) &= (-)^2\, 6s_q^2(ac' + a'c)^2 &&= (+)^2\, {}^{2}_{3} s_q^2 \chi^2(1 + {}^{1\,8\,1}_{4\,3\,2}\chi^2 + \dots.)\,.
\end{aligned}\right\} \quad (12)$$

NUMERICAL MAGNITUDES

We may add a few general remarks concerning orders of magnitude. If S is of the order of unity, as will be true if the line is permitted by all selection rules, and $\sigma \sim 0.2$ Ryd. (corresponding to $\lambda = 4580$ A), we find from equations (2), (3), and note 3 (p. 134),

$$\left.\begin{aligned}
A_p &\sim 2 \times 10^7 \text{ sec}^{-1}\,,\\
A_m &\sim 3 \times 10^2 \text{ sec}^{-1}\,,\\
A_q &\sim 8 \times 10^{-1} \text{ sec}^{-1}\,,
\end{aligned}\right\} \quad (13)$$

where A_p refers to the ordinary electric-dipole transition probability. Hence, other things being equal, the magnetic-dipole transitions will be of more importance than the electric-quadrupole.

However, all lines connecting different terms violate the magnetic-dipole selection rule which prohibits combinations between different terms; the multiplets p^2, p^4, $^1S \rightarrow {}^3P$, $^1D \rightarrow {}^3P$; p^3, $^2P \rightarrow {}^4S$, $^2D \rightarrow {}^4S$ violate the quadrupole prohibition of intersystem combinations. Such lines owe their existence to departure from Russell-Saunders coupling, and their strengths appear in the tables with order of magnitude χ^2 or χ^4, which, for example, have values for O III $2p^2$ of 1.4×10^{-4} and 2×10^{-8}, respectively. The transition probabilities are, hence, smaller than those of equation (13) by these factors. As one progresses in the periodic system, χ becomes of the order of unity, and we recover values of the order of equation (13).

For the transition between two levels of a term, with $\sigma \sim 109$ cm$^{-1} = 10^{-3}$ Ryd., as for the ground term of O III, we find

$$\left.\begin{aligned}
A_m &\sim 4 \times 10^{-5} \text{ sec}^{-1}\,,\\
A_q &\sim 2 \times 10^{-12} \text{ sec}^{-1}\,.
\end{aligned}\right\} \quad (14)$$

Although such transitions are rigorously forbidden for electric-dipole radiation, they are always allowed for magnetic-dipole for J changes of one unit. The quadrupole contributions, because of the σ^5 factor, are unimportant.

INTERFERENCE OF MAGNETIC-DIPOLE AND ELECTRIC-QUADRUPOLE RADIATION

In cases where the electric-quadrupole and magnetic-dipole transition probabilities are of comparable magnitude one must ask whether these *probabilities* are to be directly added to get the whole transition probability or whether *amplitudes* are to be added in some more complicated fashion.

This question may be answered by looking into the derivation of formulas (2) and (3) from the Dirac radiation theory. It turns out that the intensity of a line as a whole, which is of course isotropic and unpolarized in natural excitation, is the sum of the intensities of the quadrupole and magnetic-dipole radiation as separately computed, so that $A_m(J, J')$ *and* $A_q(J, J')$ *are to be directly added to obtain the total transition probability.* But the individual Zeeman components of the line interfere in a complicated fashion, which we sketch below.[9]

There is no interference among the Zeeman components except for spontaneous transitions of the type

$$J, M \rightarrow J', M \pm 1 ,$$

to which we confine attention.

We define a quantity $\mathscr{N}$ in such a way that $|\mathscr{N}|^2$ is the quadrupole strength $|(J, M|\mathfrak{R}'|J', M \pm 1)|^2$ of the component in question, and we take for the sign of $\mathscr{N}$ the sign of the coefficient of $\mathfrak{R}$ in formulas (3) of reference 6 for these strengths. Thus

$$\text{sign of } \mathscr{N} = \text{sign of } S_q^{1/2}(J, J') \times \text{sign of } \begin{cases} J \mp 2M & \text{if } J' = J + 1 \\ 2M \pm 1 & \text{if } J' = J \\ J \pm 2M + 1 & \text{if } J' = J - 1 . \end{cases}$$

We define a similar quantity $\mathscr{M}$ so that $|\mathscr{M}|^2$ is the magnetic-dipole strength $|(J, M|\boldsymbol{M}|J', M \pm 1)|^2$, with the sign given by the coefficient of $(\boldsymbol{i} \pm i\boldsymbol{j})$ in equation 9^311 (p. 63, in reference 3). Thus

$$\text{sign of } \mathscr{M} = \text{sign of } S_m^{1/2}(J, J') \times \begin{cases} \mp 1 & \text{if } J' = J + 1 , \\ +1 & \text{if } J' = J , \\ \pm 1 & \text{if } J' = J - 1 . \end{cases}$$

The signs of $S_q^{1/2}$ and $S_m^{1/2}$ needed for the above definitions are given for p^2 and p^3 (s_q is essentially positive) by equations (7), (8), (11), and (12). For p^4, the quadrupole signs are *opposite*, the magnetic-dipole signs the *same*, as for p^2 (cf. reference 6).

With this notation the intensity of radiation for $M \rightarrow M \pm 1$, at angle θ with the magnetic field, is proportional to

$$(\mathscr{N}\sigma\pi \cos 2\theta \pm \sqrt{2}\,\mathscr{M})^2 \text{ polarized in } \theta \text{ direction } (\pi)$$

$$(\pm\mathscr{N}\sigma\pi + \sqrt{2}\,\mathscr{M})^2 \cos^2\theta \text{ polarized in } \varphi \text{ direction } (\sigma) .$$

[9] Similar considerations have been independently made by E. Gerjuoy, as noted in the abstract of paper No. 16 presented at the Pasadena meeting of the American Physical Society, December 20, 1940, in connection with actual observations of the Zeeman effect of the $6p^2$ forbidden lines of *Pb* I.

That is, the two θ *amplitudes add* if the signs of $\mathcal{N}\cos 2\theta$ and $\mathcal{M}$ are the $\left\{\begin{matrix}\text{same}\\ \text{opposite}\end{matrix}\right\}$; they *subtract* otherwise. The two φ *amplitudes add* if the signs of $\mathcal{N}$ and $\mathcal{M}$ are the $\left\{\begin{matrix}\text{same}\\ \text{opposite}\end{matrix}\right\}$; they *subtract* otherwise.

The polarization is right elliptic if

$$\mathcal{N}\sigma\pi\cos 2\theta \pm \sqrt{2}\,\mathcal{M} \quad \text{and} \quad (\pm\mathcal{N}\sigma\pi + \sqrt{2}\,\mathcal{M})\cos\theta$$

have the same sign, left elliptic if they have opposite signs.

The *total intensity* of any Zeeman component, integrated over the sphere, is just the sum of the separate magnetic-dipole and electric-quadrupole intensities.

The authors wish to express their appreciation to Mrs. Martha E. Shapley for assistance in carrying out the calculations.

MENDENHALL LABORATORY OF PHYSICS
OHIO STATE UNIVERSITY
AND
HARVARD COLLEGE OBSERVATORY
April 1940

TABLE 1*

MAGNETIC DIPOLE STRENGTHS FOR p^2

	$S_m(^1D_2', ^3P_2')$	$S_m(^1D_2', ^3P_1)$	$S_m(^1S_0', ^3P_1)$	$S_m(^3P_2', ^3P_1)$	$S_m(^3P_1, ^3P_0')$
x 0.00	0.0000	0.0000	0.0000	2.5000	2.0000
.04	$0.^{1}0452$	$0.^{1}0151$	$0.^{2}0692$	2.4990	1.9996
.08	0.0177	$0.^{1}0590$	$0.^{1}0269$	2.4940	1.9976
.12	.0406	$0.^{1}1362$	$0.^{1}0588$	2.4860	1.9940
.16	.0735	0.0248	$0.^{1}1011$	2.4751	1.9896
.20	.1162	.0394	$0.^{1}1528$	2.4602	1.9848
.24	.1687	.0575	$0.^{1}2126$	2.4438	1.9784
.28	.2296	.0790	$0.^{1}2794$	2.4206	1.9721
.32	.2986	.1038	$0.^{1}3522$	2.3966	1.9646
.36	.3739	.1316	$0.^{1}4298$	2.3683	1.9570
.40	.4548	.1621	$0.^{1}5114$	2.3387	1.9491
.48	.6250	.2294	$0.^{1}6838$	2.2705	1.9314
.56	.7977	.3026	$0.^{1}8636$	2.1968	1.9137
.64	0.9641	.3787	0.1046	2.1215	1.8954
.72	1.1156	.4545	.1228	2.0453	1.8771
.80	1.2498	.5283	.1408	1.9714	1.8594
0.88	1.3657	.5985	.1583	1.9014	1.8417
x 1.00	1.5064	.6956	.1835	1.8046	1.8164
1/x 0.95	1.5563	.7347	.1941	1.7653	1.8061
.90	1.6055	.7759	.2056	1.7243	1.7944
.85	1.6506	.8182	.2179	1.6810	1.7823
.80	1.6952	.8632	.2312	1.6366	1.7687
.75	1.7366	.9099	.2457	1.5904	1.7544
.70	1.7727	0.9579	.2612	1.5421	1.7387
.65	1.8045	1.0074	.2783	1.4927	1.7220
.60	1.8307	1.0579	.2965	1.4421	1.7035
.55	1.8515	1.1096	.3163	1.3905	1.6836
.50	1.8661	1.1621	.3377	1.3381	1.6620
.45	1.8742	1.2149	.3609	1.2856	1.6391
.40	1.8747	1.2677	.3861	1.2324	1.6139
.35	1.8688	1.3206	.4131	1.1792	1.5867
.30	1.8569	1.3731	.4424	1.1269	1.5576
.25	1.8376	1.4247	.4739	1.0749	1.5260
.20	1.8134	1.4757	.5076	1.0240	1.4923
.15	1.7844	1.5261	.5437	0.9744	1.4562
.10	1.7489	1.5749	.5823	0.9254	1.4176
.05	1.7098	1.6213	.6234	0.8788	1.3768
1/x 0.00	1.6664	1.6668	0.6666	0.8332	1.3333

*In this and the succeeding tables the exponent following the decimal indicates the number of ciphers actually omitted. Thus: $0.^{1}2454$ signifies 0.02454; $0.^{2}0692$ signifies 0.000692, etc.

TABLE 2. ELECTRIC QUADRUPOLE STRENGTHS FOR p^2 (cf. Eq. 4)

	$C_q(^1S_0', ^1D_2')$	$C_q(^1S_0', ^3P_2')$	$C_q(^1D_2', ^3P_2')$	$C_q(^1D_2', ^3P_1)$	$C_q(^1D_2', ^3P_0')$	$C_q(^3P_2', ^3P_1)$	$C_q(^3P_2', ^3P_0')$
x 0.00	6.6666	0.0000	0.0000	0.0000	0.0000	3.7500	1.6666
.04	6.6657	$0.^{2}1548$	$0.^{1}1580$	$0.^{1}0226$	$0.^{3}2668$	3.7485	1.6687
.08	6.6545	$0.^{2}6095$	$0.^{1}6182$	$0.^{2}8854$	$0.^{2}1020$	3.7410	1.6726
.12	6.6360	$0.^{1}1453$	0.1422	$0.^{1}2043$	$0.^{2}1972$	3.7290	1.6790
.16	6.6126	$0.^{1}2720$	0.2573	$0.^{1}3713$	$0.^{2}2973$	3.7126	1.6886
.20	6.5827	$0.^{1}4447$	0.4069	$0.^{1}5906$	$0.^{2}3902$	3.6902	1.7006
.24	6.5501	$0.^{1}6655$	0.5906	$0.^{1}8630$	$0.^{2}4678$	3.6657	1.7160
.28	6.5025	$0.^{1}9353$	0.8035	0.1185	$0.^{2}5227$	3.6010	1.7311
.32	6.4540	0.1252	1.0453	.1558	$0.^{2}5568$	3.5949	1.7493
.36	6.3976	.1613	1.3086	.1973	$0.^{2}5703$	3.5524	1.7684
.40	6.3395	.2017	1.5918	.2431	$0.^{2}5627$	3.5081	1.7896
.48	6.2018	.2929	2.1872	.3441	$0.^{2}4987$	3.4058	1.8323
.56	6.0566	.3933	2.8442	.4539	$0.^{2}4050$	3.2952	1.8782
.64	5.9070	.4988	3.3742	.5681	$0.^{2}3010$	3.1823	1.9254
.72	5.7560	.6058	3.9113	.6831	$0.^{2}2007$	3.0680	1.9722
.80	5.6084	.7058	4.3751	.7925	$0.^{2}1307$	2.9570	2.0174
0.88	5.4686	.8020	4.7801	0.8978	$0.^{2}0742$	2.8521	2.0613
x 1.00	5.2759	.9328	5.2710	1.0435	$0.^{2}0662$	2.7068	2.1255
1/x 0.95	5.1973	0.9845	5.4469	1.1020	$0.^{2}0118$	2.6479	2.1523
.90	5.1147	1.0378	5.6191	1.1639	$0.^{2}0040$	2.5865	2.1805
.85	5.0287	1.0922	5.7776	1.2274	$0.^{3}0028$	2.5215	2.2111
.80	4.9398	1.1485	5.9325	1.2948	$0.^{3}0097$	2.4549	2.2446
.75	4.8479	1.2058	6.0769	1.3649	$0.^{3}0580$	2.3856	2.2815
.70	4.7506	1.2632	6.2055	1.4369	$0.^{3}1537$	2.3132	2.3195
.65	4.6526	1.3195	6.3158	1.5111	$0.^{3}2646$	2.2390	2.3626
.60	4.5496	1.3747	6.4076	1.5868	$0.^{3}4005$	2.1632	2.4068
.55	4.4472	1.4285	6.4811	1.6643	$0.^{3}5400$	2.0858	2.4567
.50	4.3417	1.4802	6.5310	1.7432	$0.^{3}6868$	2.0072	2.5105
.45	4.2373	1.5283	6.5599	1.8223	$0.^{3}7993$	1.9284	2.5689
.40	4.1307	1.5710	6.5625	1.9016	$0.^{3}8588$	1.8485	2.6313
.35	4.0233	1.6092	6.5415	1.9809	$0.^{3}8817$	1.7688	2.6979
.30	3.9194	1.6408	6.4995	2.0596	$0.^{3}8363$	1.6904	2.7714
.25	3.8158	1.6653	6.4312	2.1370	$0.^{3}7350$	1.6123	2.8506
.20	3.7137	1.6833	6.3472	2.2136	$0.^{3}5953$	1.5360	2.9349
.15	3.6152	1.6932	6.2449	2.2891	$0.^{3}4108$	1.4616	3.0263
.10	3.5172	1.6938	6.1215	2.3624	$0.^{3}2243$	1.3881	3.1227
.05	3.4243	1.6847	5.9850	2.4319	$0.^{3}0640$	1.3182	3.2253
1/x 0.00	3.3333	1.6667	5.8328	2.5000	$0.^{3}0000$	1.2500	3.3333

TABLE 3

TRANSFORMATION COEFFICIENTS FOR p^2 (cf. Eq. 5)

	a	b	c	d
x 0.00	1.0000	0.0000	1.0000	0.0000
.04	0.9998	$0._{1}2454$	0.9999	.0186
.08	.9988	$0._{1}4859$	.9994	.0367
.12	.9972	$0._{1}7382$	.9985	.0542
.16	.9950	$0._{1}9950$	.9974	.0711
.20	.9920	0.1255	.9962	.0874
.24	.9887	.1517	.9946	.1031
.28	.9840	.1778	.9930	.1182
.32	.9791	.2038	.9911	.1327
.36	.9733	.2294	.9892	.1466
.40	.9672	.2546	.9872	.1599
.48	.9530	.3029	.9827	.1849
.56	.9374	.3479	.9782	.2078
.64	.9212	.3892	.9735	.2287
.72	.9045	.4264	.9688	.2478
.80	.8880	.4597	.9642	.2653
0.88	.8721	.4893	.9596	.2813
x 1.00	.8496	.5275	.9530	.3029
1/x 0.95	.8403	.5421	.9503	.3115
.90	.8305	.5571	.9472	.3206
.85	.8200	.5721	.9440	.3301
.80	.8091	.5876	.9404	.3400
.75	.7976	.6033	.9366	.3505
.70	.7854	.6190	.9324	.3614
.65	.7727	.6348	.9279	.3730
.60	.7595	.6505	.9229	.3850
.55	.7458	.6662	.9175	.3977
.50	.7316	.6818	.9116	.4109
.45	.7171	.6971	.9053	.4248
.40	.7021	.7121	.8983	.4394
.35	.6868	.7268	.8907	.4545
.30	.6714	.7411	.8825	.4703
.25	.6557	.7549	.8735	.4868
.20	.6400	.7683	.8638	.5038
.15	.6243	.7813	.8533	.5214
.10	.6084	.7937	.8419	.5396
.05	.5929	.8053	.8297	.5583
1/x 0.00	0.5773	0.8165	0.8165	0.5773

TABLE 4. MAGNETIC DIPOLE STRENGTHS FOR p^3

	$S_m(^2P_{\frac{1}{2}}, {}^4S_{\frac{1}{2}}')$	$S_m(^2P_{\frac{1}{2}}', {}^2P_{\frac{1}{2}})$	$S_m(^2P_{\frac{1}{2}}, {}^2D_{\frac{1}{2}}')$	$S_m(^2D_{\frac{1}{2}}, {}^4S_{\frac{1}{2}}')$	$S_m(^2P_{\frac{1}{2}}', {}^2D_{\frac{1}{2}})$	$S_m(^2D_{\frac{1}{2}}, {}^2D_{\frac{1}{2}}')$	$S_m(^2P_{\frac{1}{2}}', {}^2D_{\frac{1}{2}}')$	$S_m(^2P_{\frac{1}{2}}', {}^4S_{\frac{1}{2}}')$	$S_m(^2D_{\frac{1}{2}}', {}^4S_{\frac{1}{2}}')$
x 0.00	0.0000	1.3333	0.0000	0.0000	0.0000	2.4000	0.0000	0.0000	0.0000
.05	$0.^{3}3705$	1.3301	$0.^{2}2868$	$0.^{6}6426$	$0.^{2}5166$	2.3948	$0.^{2}9175$	$0.^{2}1838$	$0.^{4}1935$
.10	$0.^{2}1483$	1.3207	$0.^{1}1118$	$0.^{4}1026$	$0.^{1}2017$	2.3798	$0.^{1}3573$	$0.^{2}7196$	$0.^{3}3047$
.15	$0.^{2}3343$	1.3059	$0.^{1}2412$	$0.^{4}5180$	$0.^{1}4368$	2.3563	$0.^{1}7703$	$0.^{1}1563$	$0.^{2}1504$
.20	$0.^{2}5955$	1.2968	$0.^{1}4055$	$0.^{3}1630$	$0.^{1}7377$	2.3261	0.1295	$0.^{1}2651$	$0.^{2}4596$
.25	$0.^{2}9329$	1.2648	$0.^{1}5919$	$0.^{3}3956$	0.1083	2.2913	0.1892	$0.^{1}3907$	$0.^{1}1078$
.30	$0.^{1}1347$	1.2410	$0.^{1}7884$	$0.^{3}8144$	.1454	2.2537	.2530	$0.^{1}5259$	$0.^{1}2134$
.35	$0.^{1}1839$	1.2164	$0.^{1}9849$	$0.^{2}1495$	.1834	2.2151	.3181	$0.^{1}6636$	$0.^{1}3759$
.40	$0.^{1}2410$	1.1919	0.1174	$0.^{2}2524$	.2209	2.1765	.3831	$0.^{1}7980$	$0.^{1}6082$
.45	$0.^{1}3060$	1.1679	.1348	$0.^{2}3991$	.2572	2.1387	.4461	$0.^{1}9244$	$0.^{1}9204$
.50	$0.^{1}3789$	1.1449	.1506	$0.^{2}5994$	.2915	2.1026	.5073	0.1039	0.1323
.55	$0.^{1}4596$	1.1230	.1644	$0.^{2}8627$	.3237	2.0677	.5665	.1139	.1823
.60	$0.^{1}5479$	1.1024	.1762	$0.^{1}1198$	.3535	2.0345	.6228	.1225	.2428
.65	$0.^{1}6438$	1.0831	.1859	$0.^{1}1614$	.3810	2.0028	.6773	.1293	.3138
.70	$0.^{1}7466$	1.0651	.1936	$0.^{1}2118$	.4062	1.9726	.7299	.1343	.3953
.75	$0.^{1}8562$	1.0483	.1995	$0.^{1}2716$	.4293	1.9436	.7808	.1377	.4872
.80	$0.^{1}9718$	1.0337	.2035	$0.^{1}3410$	.4503	1.9156	.8314	.1391	.5887
.85	0.1093	1.0181	.2059	$0.^{1}4201$	.4695	1.8882	.8777	.1398	.6992
.90	.1219	1.0046	.2070	$0.^{1}5091$	.4870	1.8619	.9250	.1389	.8169
0.95	.1349	0.9920	.2066	$0.^{1}6074$	.5034	1.8362	0.9686	.1368	0.9410
x 1.00	.1481	.9802	.2051	$0.^{1}7147$	.5175	1.8111	1.0139	0.1336	1.0695
1/x 0.90	.1783	.9567	.1983	$0.^{1}9808$	.5455	1.7564	1.3638	1.1067	0.1239
.80	.2161	.9318	.1854	0.1354	.5735	1.6912	1.7267	1.2147	0.1085
.70	.2626	.9054	.1654	.1863	.6008	1.6129	2.1458	1.3390	$0.^{1}8783$
.60	.3178	.8774	.1382	.2526	.6268	1.5206	2.5786	1.4796	$0.^{1}6354$
.55	.3481	.8628	.1224	.2912	.6390	1.4699	2.7772	1.5560	$0.^{1}5109$
.50	.3797	.8499	0.1058	.3326	.6520	1.4170	2.9502	1.6400	$0.^{1}3936$
.45	.4121	.8324	$0.^{1}8884$	.3759	.6608	1.3633	3.0863	1.7196	$0.^{1}2859$
.40	.4447	.8164	$0.^{1}7219$	.4199	.6700	1.3101	3.1798	1.8070	$0.^{1}1954$
.35	.4769	.8000	$0.^{1}5640$	.4631	.6779	1.2590	3.2227	1.8977	$0.^{1}1236$
.30	.5082	.7831	$0.^{1}4201$	.5044	.6840	1.2116	3.2283	1.9928	$0.^{2}7109$
.25	.5383	.7656	$0.^{1}2942$	.5425	.6882	1.1694	3.1901	2.0924	$0.^{2}3599$
.20	.5670	.7475	$0.^{1}1892$	.5766	.6900	1.1334	3.1188	2.1971	$0.^{2}1537$
.15	.5941	.7286	$0.^{1}1066$	.6062	.6892	1.1046	3.0232	2.3072	$0.^{2}0499$
.10	.6200	.7089	$0.^{2}4741$	.6314	.6853	1.0836	2.9132	2.4228	$0.^{3}1007$
.05	.6438	.6883	$0.^{2}1185$	.6512	.6779	1.0709	2.7826	2.5370	$0.^{4}0637$
1/x 0.00	0.6667	0.6667	0.0000	0.6666	0.6666	1.0667	2.6667	2.6667	0.0000

TABLE 5. ELECTRIC QUADRUPOLE STRENGTHS FOR p^3 (cf. Eq. 4)

TABLE 5. ELECTRIC QUADRUPOLE STRENGTHS FOR p^3 (cf. Eq. 4)

	$C_q(^2P_{\frac{3}{2}}, ^2P_{\frac{1}{2}})$	$C_q(^2P_{\frac{3}{2}}, ^2D'_{\frac{3}{2}})$	$C_q(^2P'_{\frac{1}{2}}, ^2D'_{\frac{3}{2}})$	$C_q(^2P_{\frac{1}{2}}, ^2D'_{\frac{3}{2}})$	$C_q(^2P_{\frac{3}{2}}, ^4S'_{\frac{3}{2}})$	$C_q(^2P_{\frac{1}{2}}, ^4S'_{\frac{3}{2}})$	$C_q(^2D_{\frac{5}{2}}, ^2D'_{\frac{3}{2}})$	$C_q(^2D_{\frac{3}{2}}, ^4S'_{\frac{3}{2}})$	$C_q(^2D'_{\frac{3}{2}}, ^4S'_{\frac{3}{2}})$
x 0.00	0.0000	14.0000	6.0000	6.0000	0.0000	0.0000	0.0000	0.0000	0.0000
.05	$0.^{1}1291$	13.9660	5.9468	5.9871	$0.^{6}3949$	$0.^{5}1606$	$0.^{1}3012$	$0.^{2}3890$	$0.^{2}1668$
.10	$0.^{1}5044$	13.8670	5.7936	5.9495	$0.^{5}6001$	$0.^{4}2566$	0.1174	$0.^{1}1557$	$0.^{2}6695$
.15	0.1092	13.7116	5.5578	5.8907	$0.^{4}2793$	$0.^{3}1295$	.2533	$0.^{1}3510$	$0.^{1}1514$
.20	.1844	13.5117	5.2531	5.8152	$0.^{4}7866$	$0.^{3}4075$	.4258	$0.^{1}6253$	$0.^{1}2712$
.25	.2709	13.2805	4.9346	5.7281	$0.^{3}1664$	$0.^{3}9890$	.6215	$0.^{1}9795$	$0.^{1}4277$
.30	.3636	13.0307	4.5952	5.6344	$0.^{3}2918$	$0.^{2}2036$	0.8279	0.1415	$0.^{1}6229$
.35	.4585	12.7727	4.2589	5.5378	$0.^{3}4466$	$0.^{2}3738$	1.0341	.1931	$0.^{1}8586$
.40	.5523	12.5150	3.9401	5.4413	$0.^{3}6156$	$0.^{2}6309$	1.2324	.2531	0.1137
.45	.6429	12.2633	3.6450	5.3468	$0.^{3}7830$	$0.^{2}9979$	1.4157	.3213	.1460
.50	.7288	12.0212	3.3769	5.2566	$0.^{3}9288$	$0.^{1}1498$	1.5814	.3978	.1829
.55	.8092	11.7915	3.1353	5.1694	$0.^{2}1039$	$0.^{1}2157$	1.7268	.4826	.2244
.60	.8837	11.5753	2.9206	5.0861	$0.^{2}1102$	$0.^{1}2996$	1.8498	.5753	.2705
.65	0.9524	11.3725	2.7302	5.0069	$0.^{2}1113$	$0.^{1}4036$	1.9520	.6759	.3211
.70	1.0155	11.1833	2.5624	4.9315	$0.^{2}1075$	$0.^{1}5296$	2.0334	.7840	.3760
.75	1.0732	11.0068	2.4142	4.8589	$0.^{3}9918$	$0.^{1}6739$	2.0945	0.8990	.4348
.80	1.1258	10.8535	2.2870	4.7890	$0.^{3}8640$	$0.^{1}8524$	2.1371	1.0204	.4969
.85	1.1738	10.6901	2.1692	4.7206	$0.^{3}7272$	0.1050	2.1623	1.1476	.5617
.90	1.2175	10.5479	2.0677	4.6549	$0.^{3}5736$	.1273	2.1734	1.2797	.6286
0.95	1.2586	10.4154	1.9781	4.5906	$0.^{3}4274$	.1519	2.1689	1.4160	.6969
x 1.00	1.2938	10.2918	1.8997	4.5278	$0.^{3}2799$	.1787	2.1535	1.5554	.7657
1/x 0.90	1.3637	10.0456	1.7548	4.3911	$0.^{3}0577$	.2452	2.0822	1.8721	0.9163
.80	1.4336	9.7840	1.6191	4.2280	$0.^{3}0182$	.3384	1.9468	2.2691	1.0915
.70	1.5021	9.5066	1.4960	4.0322	$0.^{3}3384$	.4657	1.7361	2.7574	1.2803
.60	1.5671	9.2128	1.3894	3.8015	$0.^{2}1118$	.6314	1.4505	3.3366	1.4584
.55	1.5975	9.0597	1.3436	3.6747	$0.^{2}1642$	.7279	1.2852	3.6551	1.5326
.50	1.6299	8.9237	1.3066	3.5425	$0.^{2}2177$	.8315	1.1107	3.9872	1.5908
.45	1.6519	8.7398	1.2696	3.4083	$0.^{2}2641$	0.9398	0.9328	4.3263	1.6298
.40	1.6750	8.5728	1.2434	3.2753	$0.^{2}2947$	1.0496	.7580	4.6693	1.6475
.35	1.6946	8.4006	1.2245	3.1476	$0.^{2}3024$	1.1578	.5922	5.0072	1.6444
.30	1.7101	8.2228	1.2136	3.0291	$0.^{2}2833$	1.2609	.4411	5.3360	1.6226
.25	1.7204	8.0391	1.2117	2.9234	$0.^{2}2405$	1.3561	.3089	5.6521	1.5860
.20	1.7251	7.8484	1.2185	2.8334	$0.^{2}1804$	1.4415	.1986	5.9529	1.5391
.15	1.7230	7.6503	1.2344	2.7615	$0.^{2}1146$	1.5155	0.1119	6.2378	1.4867
.10	1.7132	7.4437	1.2592	2.7091	$0.^{2}0555$	1.5785	$0.^{1}4978$	6.5100	1.4336
.05	1.6948	7.2274	1.2924	2.6773	$0.^{3}1453$	1.6279	$0.^{1}1244$	6.7605	1.3808
1/x 0.00	1.6667	7.0000	1.3333	2.6667	0.0000	1.6666	0.0000	7.0000	1.3333

TABLE 6. TRANSFORMATION COEFFICIENTS FOR p^3 (cf. Eq. 9)

	a	b	c	a'	b'	c'	a"	b"	c"
x 0.00	-0.0000	-0.0000	1.0000	-0.0000	1.0000	0.0000	1.0000	0.0000	0.0000
.05	$0._{1}4638$	$0._{2}1290$	0.9989	$0._{1}1667$	0.9999	$0._{3}5174$	0.9988	$0._{1}1663$	$0._{1}4640$
.10	$0._{1}9157$	$0._{2}5116$	.9958	$0._{1}3335$	.9994	$0._{2}2068$	.9952	$0._{1}3302$	$0._{1}9169$
.15	0.1345	$0._{1}1135$	.9908	$0._{1}5007$	.9987	$0._{2}4645$	.9896	$0._{1}4899$	0.1349
.20	.1744	$0._{1}1981$	.9845	$0._{1}6683$	.9977	$0._{2}8241$	.9824	$0._{1}6436$	.1753
.25	.2107	$0._{1}3028$	.9771	$0._{1}8365$	.9964	$0._{1}1284$	.9740	$0._{1}7902$	.2124
.30	.2432	$0._{1}4252$	.9690	0.1005	.9948	$0._{1}1842$	.9648	$0._{1}9293$	.2462
.35	.2718	$0._{1}5631$	.9607	.1174	.9928	$0._{1}2496$	.9552	0.1061	.2764
.40	.2967	$0._{1}7147$	.9523	.1344	.9904	$0._{1}3243$	.9455	.1184	.3034
.45	.3180	$0._{1}8777$	.9440	.1515	.9876	$0._{1}4078$	.9359	.1300	.3273
.50	.3361	0.1051	.9360	.16857	.9844	$0._{1}4998$	.9266	.1410	.3485
.55	.3512	.1232	.9282	.18566	.9808	$0._{1}5996$	.9177	.1513	.3672
.60	.3634	.1421	.9207	.2027	.9767	$0._{1}7066$	.9093	.1610	.3838
.65	.3734	.1615	.9135	.2197	.9721	$0._{1}8202$	.9013	.1701	.3984
.70	.3811	.1813	.9066	.2366	.9670	$0._{1}9395$	.8938	.1787	.4114
.75	.3868	.2015	.8999	.2534	.9615	0.1064	.8867	.1869	.4229
.80	.3907	.2218	.8934	.2700	.9555	.1192	.8805	.1946	.4332
.85	.3930	.2423	.8870	.2863	.9490	.1323	.8738	.2020	.4423
.90	.3940	.2626	.8808	.3023	.9420	.1456	.8680	.2089	.4505
0.95	.3936	.2828	.8747	.3180	.9396	.1591	.8625	.2156	.4580
x 1.00	.3922	.3028	.8687	.3333	.9269	.1726	.8574	.2219	.4644
½x 0.90	.3857	.3456	.8555	.3657	.9085	.2021	.8471	.2349	.4767
.80	.3729	.3953	.8394	.4026	.8840	.2375	.8360	.2494	.4888
.70	.3521	.4516	.8198	.4438	.8517	.2786	.8240	.2657	.5004
.60	.3219	.5126	.7960	.4882	.8102	.3244	.8112	.2842	.5111
.55	.3030	.5438	.7826	.5110	.7859	.3483	.8044	.2943	.5160
.50	.2817	.5747	.7684	.5337	.7594	.3723	.7984	.3056	.5212
.45	.2581	.6044	.7537	.5560	.7309	.3958	.7901	.3169	.5247
.40	.2327	.6324	.7388	.5775	.7011	.4183	.7825	.3294	.5284
.35	.2057	.6581	.7243	.5980	.6704	.4393	.7746	.3428	.5315
.30	.1775	.6809	.7105	.6174	.6393	.4584	.7664	.3573	.5339
.25	.1485	.7005	.6980	.6354	.6085	.4754	.7578	.3729	.5355
.20	0.1191	.7166	.6872	.6521	.5784	.4901	.7487	.3897	.5362
.15	$0._{1}8942$	.7292	.6784	.6675	.5494	.5026	.7392	.4079	.5359
.10	$0._{1}5963$	.7382	.6720	.6819	.5220	.5129	.7292	.4275	.5344
.05	$0._{1}2981$	.7436	.6680	.6949	.4958	.5209	.7185	.4487	.5315
½x 0.00	-0.0000	-0.7454	0.6667	-0.7071	0.4714	0.5270	0.7071	0.4714	0.5270

TABLE 7

MAGNETIC DIPOLE STRENGTHS FOR p^4

	$S_m(^1D_2', ^3P_2')$	$S_m(^1D_2', ^3P_1)$	$S_m(^1S_0', ^3P_1)$	$S_m(^3P_2', ^3P_1)$	$S_m(^3P_1, ^3P_0')$
x 0.00	0.0000	0.0000	0.0000	2.5000	2.0000
.04	$0.^{1}0402$	$0.^{1}0134$	$0.^{1}0730$	2.4975	1.9992
.08	$0.^{1}1547$	$0.^{1}0517$	$0.^{1}0299$	2.4935	1.9968
.12	$0.^{1}3340$	$0.^{1}1119$	$0.^{1}0687$	2.4885	1.9928
.16	$0.^{1}5681$	$0.^{1}1908$	$0.^{1}1246$	2.4805	1.9876
.20	$0.^{1}8470$	$0.^{1}2857$	$0.^{1}1980$	2.4706	1.9800
.24	0.1162	$0.^{1}3938$	$0.^{1}2894$	2.4602	1.9713
.28	.1507	$0.^{1}5127$	$0.^{1}3987$	2.4498	1.9602
.32	.1868	$0.^{1}6392$	$0.^{1}5257$	2.4357	1.9468
.36	.2246	$0.^{1}7726$	$0.^{1}6699$	2.4226	1.9326
.40	.2630	$0.^{1}9101$	$0.^{1}8305$	2.4084	1.9173
.48	.3410	0.1194	0.1196	2.3810	1.8806
.56	.4174	.1479	.1612	2.3532	1.8382
.64	.4907	.1760	.2065	2.3237	1.7940
.72	.5600	.2032	.2542	2.2963	1.7458
.80	.6250	.2294	.3029	2.2705	1.6972
.88	.6852	.2542	.3516	2.2458	1.6486
x 1.00	.7666	.2890	.4226	2.2104	1.5774
1/x 0.95	.8000	.3035	.4526	2.1968	1.5470
.90	.8340	.3186	.4848	2.1814	1.5148
.85	.8702	.3349	.5194	2.1655	1.4802
.80	.9076	.3521	.5564	2.1479	1.4433
.75	.9469	.3706	.5958	2.1294	1.4042
.70	0.9879	.3903	.6375	2.1096	1.3626
.65	1.0310	.4113	.6815	2.0889	1.3187
.60	1.0747	.4335	.7279	2.0662	1.2723
.55	1.1212	.4573	.7761	2.0430	1.2237
.50	1.1677	.4825	.8259	2.0169	1.1741
.45	1.2165	.5094	.8772	1.9901	1.1229
.40	1.2664	.5380	.9294	1.9616	1.0705
.35	1.3171	.5683	0.9833	1.9312	1.0179
.30	1.3694	.6007	1.0354	1.8997	0.9644
.25	1.4204	.6345	1.0882	1.8654	.9118
.20	1.4723	.6706	1.1400	1.8297	.8599
.15	1.5231	.7084	1.1908	1.7918	.8092
.10	1.5721	.7480	1.2403	1.7514	.7597
.05	1.6207	.7899	1.2879	1.7098	.7119
1/x 0.00	1.6660	0.8333	1.3333	1.6663	0.6666

TABLE 8. ELECTRIC QUADRUPOLE STRENGTHS FOR p^4 (cf. Eq. 4)

	$C_q(^1S_0', ^1D_2')$	$C_q(^1S_0', ^3P_2')$	$C_q(^1D_2', ^3P_2')$	$C_q(^1D_2', ^3P_1')$	$C_q(^1D_2', ^3P_0')$	$C_q(^3P_2', ^3P_1')$	$C_q(^3P_2', ^3P_0')$
x 0.00	6.6666	0.0000	0.0000	0.0000	0.0000	3.7500	1.6666
.04	6.6600	$0.^{2}1235$	$0.^{1}1407$	$0.^{2}2012$	$0.^{3}3765$	3.7463	1.6673
.08	6.6507	$0.^{2}4552$	$0.^{1}5413$	$0.^{2}7751$	$0.^{2}1684$	3.7403	1.6714
.12	6.6380	$0.^{2}9390$	0.1169	$0.^{1}1678$	$0.^{2}4200$	3.7328	1.6792
.16	6.6195	$0.^{1}1523$	.1988	$0.^{1}2863$	$0.^{2}8200$	3.7208	1.6893
.20	6.5922	$0.^{1}2159$	.2966	$0.^{1}4286$	$0.^{1}1395$	3.7058	1.7015
.24	6.5663	$0.^{1}2811$	.4069	$0.^{1}5906$	$0.^{1}2169$	5.6904	1.7173
.28	6.5335	$0.^{1}3445$	.5276	$0.^{1}7691$	$0.^{1}3163$	3.6746	1.7353
.32	6.4912	$0.^{1}4032$	.6539	$0.^{1}9589$	$0.^{1}4387$	3.6532	1.7532
.36	6.4523	$0.^{1}4563$	.7862	0.1159	$0.^{1}5859$	3.6338	1.7750
.40	6.4085	$0.^{1}5023$	0.9203	.1365	$0.^{1}7580$	3.6124	1.7985
.48	6.3115	$0.^{1}5708$	1.1936	.1790	0.1175	3.5715	1.8487
.56	6.2005	$0.^{1}6077$	1.4608	.2218	.1681	3.5284	1.9010
.64	6.0897	$0.^{1}6188$	1.7173	.2639	.2263	3.4856	1.9570
.72	5.9687	$0.^{1}6085$	1.9598	.3048	.2898	3.4444	2.0115
.80	5.8513	$0.^{1}5838$	2.1874	.3441	.3570	3.4058	2.0672
.88	5.7332	$0.^{1}5500$	2.3982	.3814	.4255	3.3686	2.1203
x 1.00	5.5602	$0.^{1}4910$	2.6830	.4335	.5275	3.3158	2.1953
½x 0.95	5.4650	$0.^{1}4643$	2.8001	.4552	.5712	3.2951	2.1973
.90	5.4102	$0.^{1}4350$	2.9180	.4778	.6182	3.2719	2.2597
.85	5.3277	$0.^{1}4028$	3.0468	.5025	.6693	3.2483	2.2960
.80	5.2375	$0.^{1}3692$	3.1762	.5282	.7234	3.2216	2.3337
.75	5.1433	$0.^{1}3335$	3.3138	.5558	.7817	3.1939	2.3743
.70	5.0432	$0.^{1}2975$	3.4576	.5854	.8429	3.1642	2.4172
.65	4.9375	$0.^{1}2606$	3.6083	.6169	.9076	3.1335	2.4637
.60	4.8247	$0.^{1}2234$	3.7622	.6502	0.9748	3.0994	2.5113
.55	4.7073	$0.^{1}1873$	3.9241	.6860	1.0443	3.0645	2.5623
.50	4.5855	$0.^{1}1536$	4.0871	.7237	1.1147	3.0255	2.6158
.45	4.4608	$0.^{1}1220$	4.2575	.7641	1.1862	2.9850	2.6730
.40	4.3330	$0.^{2}9358$	4.4323	.8070	1.2565	2.9422	2.7332
.35	4.2035	$0.^{2}6905$	4.6045	.8524	1.3252	2.8969	2.7963
.30	4.0732	$0.^{2}4787$	4.7932	.9011	1.3923	2.8496	2.8632
.25	3.9423	$0.^{2}3110$	4.9718	0.9518	1.4542	2.7982	2.9322
.20	3.8153	$0.^{2}1857$	5.1529	1.0058	1.5105	2.7446	2.1770
.15	3.6888	$0.^{2}0957$	5.3288	1.0624	1.5613	2.6876	3.0822
.10	3.5643	$0.^{2}0380$	5.5020	1.1220	1.6046	2.6272	3.1620
.05	3.4455	$0.^{3}0845$	5.6726	1.1850	1.6395	2.5646	3.2457
½x 0.00	3.3333	0.0000	5.8328	1.2500	1.6667	2.5000	3.3333

TABLE 9

TRANSFORMATION COEFFICIENTS FOR p^4 (cf. Eq. 5)

	a	b	c	d
x 0.00	+1.0000	-0.0000	+1.0000	-0.0000
.04	0.9995	$0._{1}2316$	0.9998	$0._{1}1910$
.08	.9990	$0._{1}4547$	.9992	$0._{1}3866$	
.12	.9977	$0._{1}6689$	.9982	$0._{1}5862$	
.16	.9961	$0._{1}8737$	.9969	$0._{1}7893$	
.20	.9941	0.1069	.9950	$0._{1}9951$	
.24	.9920	.1255	.9928	0.1203	
.28	.9899	.1432	.9900	.1412	
.32	.9870	.1599	.9866	.1621	
.36	.9844	.1758	.9830	.1830	
.40	.9815	.1908	.9791	.2038	
.48	.9759	.2185	.9697	.2446	
.56	.9700	.2432	.9587	.2839	
.64	.9641	.2653	.9471	.3214	
.72	.9584	.2851	.9343	.3565	
.80	.9530	.3029	.9212	.3892	
.88	.9478	.3189	.9079	.4193	
x 1.00	.9403	.3400	.8881	.4597	
½x 0.95	.9374	.3484	.8795	.4757	
.90	.9341	.3570	.8703	.4923	
.85	.9307	.3660	.8603	.5096	
.80	.9269	.3753	.8495	.5274	
.75	.9229	.3850	.8379	.5458	
.70	.9186	.3951	.8254	.5646	
.65	.9141	.4056	.8120	.5838	
.60	.9091	.4164	.7976	.6033	
.55	.9040	.4277	.7822	.6229	
.50	.8982	.4393	.7662	.6426	
.45	.8922	.4514	.7943	.6623	
.40	.8858	.4639	.7316	.6817	
.35	.8789	.4768	.7134	.7008	
.30	.8717	.4902	.6944	.7195	
.25	.8638	.5038	.6752	.7376	
.20	.8555	.5179	.6557	.7549	
.15	.8466	.5323	.6361	.7716	
.10	.8370	.5470	.6163	.7875	
.05	.8270	.5621	.5966	.8024	
½x 0.00	+0.8164	+0.5773	+0.5773	-0.8165	

PHYSICAL PROCESSES IN GASEOUS NEBULAE

XII. THE ELECTRON DENSITIES OF SOME BRIGHT PLANETARY NEBULAE

DONALD H. MENZEL AND LAWRENCE H. ALLER

ABSTRACT

The electron densities of some typical, bright, planetary nebulae have been estimated from the intensity of the continuous emission beyond the limit of the Balmer series. The densities so obtained are of the order of 10^4 electrons/cm^3 for the objects studied and are probably somewhat lower in the fainter planetaries.

Before the predictions in theories of gaseous nebulae can be compared with the observations, one must first determine the values of two fundamental parameters: the electron density and the electron temperature. In this paper we shall show how the electron density may be estimated from the intensity of the emission beyond the limit of the Balmer series, and in the next paper of this series estimates of the electron temperatures will be derived from a comparison of the green nebular lines of *O* III (λ 4959 and λ 5007) with the λ 4363 line of the same ion. The electron density was derived some time ago by one of us[1] by a similar method, but it is now possible to make closer estimates because of more accurate observational data. The earlier determinations gave the correct order of magnitude.

From equation (23) of the first paper of this series[2] we find that the emission at the head of the Balmer series, $n' = 2$ and $\nu = R/4$, per unit volume in the frequency interval $d\nu$, is

$$E_{\kappa n} d\nu = N_i N_e \frac{K}{T_e^{3/2}} \frac{g}{8} h d\nu \,. \tag{1}$$

For convenience, we re-write this formula in terms of a wave-length interval rather than a frequency interval, $d\nu = (c/\lambda^2)d\lambda$, where $c = 3\times 10^{10}$ cm/sec and $\lambda = 3.65\times 10^{-5}$ cm at the Balmer limit. If $\Delta\lambda$ is expressed in angstrom units, $d\nu = 2.25\times 10^{11}\Delta\lambda$. From (I, 6)[2] we have $Kh = 6.99\times 10^{-33}$; also $g = 0.88$ at the Balmer limit. Therefore,

$$E_{\kappa n} d\nu = N_i N_e \frac{1.73 \times 10^{-22}}{T_e^{3/2}} \Delta\lambda \,. \tag{2}$$

For the observational data used in the present paper, an interval of 20 A at the Balmer limit was employed. Our equation then becomes

$$E_{\kappa n} \Delta\nu = 3.46 \times 10^{-21} \frac{N_i N_e}{T_e^{3/2}} \,. \tag{3}$$

In a homogeneous spherical nebula the total emission will be

$$\tfrac{4}{3}\pi E_{\kappa n} \Delta\nu A^3$$

[1] Menzel, *Pub. A.S.P.*, **43**, 337, 1931.

[2] Menzel, *Ap. J.*, **85**, 330, 1937. The Roman numeral refers to the number of the paper in the series, the Arabic number to the number of the equation. In the original (I, 6) the *h* was inadvertently omitted.

and in a homogeneous shell of thickness d and outer radius A, the total emission will be

$$\tfrac{4}{3}\pi E_{\kappa n}\Delta\nu[3A^2d - 3Ad^2 + d^3] ,$$

or

$$4\pi E_{\kappa n}\Delta\nu A^2 d ,$$

when d is much smaller than A. The surface through which this energy must flow has an area $4\pi A^2$, so that the average surface brightness, S_n, for this 20 A range of Balmer continuum will be, for the three separate cases

$$S_n = \tfrac{1}{3}E_{\kappa n}\Delta\nu A = \frac{1.15 \times 10^{-21}}{T_e^{3/2}} N_i N_e A \qquad \text{(homogeneous sphere)} , \tag{4}$$

$$S_n = E_{\kappa n}\Delta\nu d = \frac{3.46 \times 10^{-21}}{T_e^{3/2}} N_i N_e d \qquad \text{(thin homogeneous shell)} , \tag{5}$$

$$\left.\begin{aligned} S_n = \frac{1.15 \times 10^{-21} N_i N_e}{T_e^{3/2}} 3d\left[1 - \frac{d}{A} + \frac{d^2}{3A^2}\right] = \frac{1.15 \times 10^{-21}}{T_e^{3/2}} N_i N_e D , \\ \text{(thick homogeneous shell)} , \end{aligned}\right\} \tag{6}$$

where

$$D = 3d\left[1 - \frac{d}{A} + \frac{d^2}{3A^2}\right] . \tag{7}$$

The photometrically determined surface brightness of a planetary is usually expressed in magnitudes per square minute of arc. Our next problem is to convert the surface brightness of the nebula at the Balmer limit, as measured in magnitudes, to the physical units of brightness in ergs emitted per square centimeter. Since surface brightness is independent of distance, no knowledge of the parallax is required.

To effect the conversion we find it convenient to employ the sun as a reference standard. According to Kuiper,[3] the apparent bolometric magnitude of the sun is -26.95. The surface area of the sun is 806 square minutes of arc. Therefore, the surface brightness in magnitudes per square minute of arc is

$$H_\odot = -19.68 . \tag{8}$$

The amount of solar energy $S_\odot$ radiated per second[4] is 6.25×10^{10} erg/cm^{-2}. Let H_n denote the surface brightness of the nebula at the Balmer limit, in terms of magnitudes per square minute of arc. Then we easily obtain the elementary conversion formula

$$\log S_\odot - \log S_n = 0.4 \log (H_n - H_\odot)$$

$$S_n = 0.840 \times 10^3 (2.512)^{-H_n} \qquad \text{in ergs sec}^{-1}\,\text{cm}^{-2} . \tag{9}$$

We assume that the number of hydrogen ions is equal to the number of electrons, which is equivalent to assuming that hydrogen is the predominant element. This assumption

[3] *Ap. J.*, **88**, 438, 1938.

[4] Russell, Dugan, and Stewart, *Astronomy*, **2**, 534.

leads to a minimum value for N_e and a maximum for N_i. If we put $N_i = N_e$ we obtain from equation (4)

$$N_e = 2.94 \times \frac{10^{10} T_e^{3/4} S_n^{1/2}}{A^{1/2}} = 8.54 \times 10^{11} \frac{T_e^{3/4} (2.512)^{-H_n/2}}{A^{1/2}}, \qquad (10)$$

and a similar equation in which A is replaced by D as defined above. Equation (10) suffices to determine N_e when A, H_n, and T_e are known.

The radius of a planetary may be determined from its apparent size if the distance is known. The distances here considered were taken from the data of Berman;[5] the angular sizes, from the estimates of H. D. Curtis;[6] and the apparent photographic magnitudes from the work of Vorontsov-Velyaminov and Parenago and Hubble as tabulated by Louis Berman.[5]

The remaining necessary data are, of course, the intensity of the Balmer continuum at the series limit and the electron temperature. The latter, as will be discussed in the next paper of this series, is evaluated from the relative intensities of λλ 5007, 4959, and 4363 or *O* III. For the planetaries in question, the electron temperatures lie between 6000° K and 10,000° K. The intensity of the continuum must be obtained from spectrophotometric observations. Fortunately, the results are insensitive to the exact temperature.

A spectrophotometric study of a number of the brighter and more interesting planetaries has been undertaken by one of us. The plates were secured with the quartz slitless spectrograph attached to the Crossley reflector of the Lick Observatory. Although a detailed account of this investigation is to be reported in a subsequent paper of the series, it seems worth while to summarize here the portion of the study relating to the intensity of the Balmer continuum at the series limit.

Of the eleven planetary nebulae observed during the summers of 1938 and 1939, suitable plates for a study of the Balmer continuum were obtained of the following objects: NGC 6543, 6572, 6826, 7009, 7027, 7662, and IC 418. In addition, plates of NGC 1535 taken by Mr. R. H. Stoy were kindly made available for this photometric study. Standards were impressed by means of a tube sensitometer. For the region of the Balmer continuum, a Wratten 18A filter was utilized; in the visual region, a 50 filter. The star π_1 Cygni was employed as the comparison star. The energy distribution for this star was that assumed by Popper[7] in his study of Nova Lacertae and depends ultimately on the spectrophotometric studies by Barbier and his colleagues.[8]

The spectrograms were measured with the microdensitometer of the Harvard Observatory, by a method similar to that employed by Berman;[9] that is, successive tracings were made parallel to the dispersion until the total surface of the planetary had been covered.

For all these objects there seemed to be a general continuum in addition to that of the Balmer series. In some cases it was rather difficult to estimate this continuum because of the numerous overlapping images of the faint lines; near the Balmer limit the faint lines on slitless spectra overlap, and, in consequence, the intensity of the general continuum has to be estimated upon the basis of some likely wave-length variation. In practice, the intensity of the general continuum in the neighborhood of the Balmer limit was estimated by eye from the reduced tracings. Thus, the estimates of the intensity of the Balmer continuum may be systematically in error because of unknown variations in the intensity of the general continuum. The values tabulated here are, consequently,

[5] *Lick Obs. Bull.*, **18**, 73, 1937.

[6] *Lick Obs. Pub.*, **13**, 55, 1918.

[7] *Ap. J.*, **92**, 262, 1940.

[8] Barbier *et al.*, *J. d. obs.*, **19**, 149, 1936; *C.R.*, **210**, 99, 1940.

[9] *Lick Obs. Bull.*, **15**, 86, 1930.

to be considered as tentative estimates which may easily be in error by as much as 25 per cent or perhaps even 40 per cent. The order of magnitude of the calculated electron densities is insensitive, however, to errors of this sort.

It may be remarked in passing that in the case of NGC 7662, which is a particularly suitable object for such a study because of the small amount of space absorption in this region of the sky, the wave-length variation of the intensity of the Balmer continuum was investigated in an effort to estimate the electron temperature, but no satisfactory value could be found. Photometric difficulties, the effect of space absorption, and the unknown wave-length variation of the general continuum render this method of estimating the electron temperature uncertain.

The intensity of the 20 A interval of the Balmer continuum was estimated from the reduced tracings. With the intensity of $H\beta$ taken as 10, we obtain the results shown in the accompanying table. The means of two plates were used for each of these objects except for NGC 1535, for which only one suitable plate was available.

NGC 7027	0.27	IC 418	0.69
6572	0.68	NGC 7662	0.62
6826	0.75	7009	0.86
6543	0.84	1535	1.57

We have yet to reduce these intensities to the apparent-magnitude scale in order to be able to use our formulae. The determination of the magnitudes of gaseous nebulae is very different from the determination of stellar magnitudes, since in the former practically all the light is concentrated within a few bright lines. The strongest lines in most of the gaseous nebulae are the green lines of O III, but the plate sensitivity of most blue-sensitive emulsions is low in their neighborhood. For a tentative estimate of the magnitude of the planetaries at the Balmer limit the following procedure was adopted. It was assumed that the magnitude scale taken from Berman's paper[5] corresponded to a plate-*plus*-instrument sensitivity combination similar to that found by Yü[10] for a Seed 23 plate and a silver-coated mirror. The relative intensities of all the strong nebular lines (on the scale $H\beta = 10$) were then multiplied by this plate-*plus*-instrument sensitivity factor and added together. The intensity of the Balmer continuum at the series head was then compared with this sum to give the amount by which the nebular magnitude had to be corrected to give the magnitude of the 20 A interval of Balmer continuum.

The details of the calculation are summarized in Table 1. Successive columns give the designations of the nebula according to its NGC or IC number, the magnitude of the planetary as quoted by Berman,[5] the dimensions in seconds of arc as derived from the data by Curtis,[11] and the value of r in parsecs according to Berman. The columns labeled A'' and A (see Table 1) give, respectively, the assumed radii of these planetaries in seconds of arc and in centimeters. Uncertainties introduced in estimating these radii provide a fundamental limitation upon the accuracy of our results. As soon as the area in seconds of arc has been calculated, we may compute the mean surface brightness of the planetary in terms of magnitudes per square minute of arc. The latter quantity is then corrected for the ratio of brightness of the continuum at the Balmer limit to the brightness of the whole nebula multiplied by the assumed plate-*plus*-instrument sensitivity. The column labeled ΔH_n gives the amount by which the tabulated magnitude m_n is to be corrected to reduce it to the surface brightness of the nebula in magnitudes, in terms of a 20 A interval at the Balmer limit. The choice of this wave-length interval, as previously explained, depended upon convenience. We could have expressed the bright-

[10] *Lick Obs. Bull.*, **12**, 104, 1926. [11] *Op. cit.*

ness in terms of unit-frequency interval, but there seemed to be little point in multiplying by a large factor and dividing by it again. The quantity S_n may be immediately computed. For each planetary a value of T_e was assumed on the basis of calculations which are yet to be described. With these data we may compute N_e by means of equation (10).

For the ring nebulae, which are apparently shell structures, estimates of the thickness, d, of the shell were taken from the paper by Curtis and the corresponding corrections to the densities were evaluated.

The electron densities of these brighter planetaries seem to range from about 9×10^3 electrons/cm^3 for NGC 1535 to about 4×10^4 electrons/cm^3 for NGC 7009. It is to be

TABLE 1

ELECTRON DENSITIES FROM INTENSITY OF BALMER CONTINUUM

NEBULA	m_n	Dimensions	r (Parsecs)	d/A	A''	$A \times 10^{-17}$ (Cm)	Δm/Sq. Min.
NGC 7027	9.8	12″×8″	2130	1.0	5	1.59	−3.94
6572	9.2	15 ×11	1230	1.0	7	1.29	3.35
6826	9.2	27 ×24	1050	1.0	13	2.04	1.85
6543	8.7	22 ×16	1080	0.2	10	1.61	2.52
IC 418	10.6	14 ×11	1800	0.2	6	1.61	3.42
NGC 7662	8.7	17 ×14*	1200	0.2	8	1.43	2.95
7009	7.9	25 ×12*	930	0.3	9	1.25	2.70
1535	9.9	20 ×17	1720	0.3	9	2.32	−2.56

NEBULA	Δm (Balmer Continuum)	ΔH_n	H_n	$\sqrt{D} \times 10^{-8}$	T_e	N_e
NGC 7027	+5.85	+1.91	+11.71	4.10	9,500	9.3×10^3
6572	4.71	1.36	10.56	3.59	9,200	17
6826	4.39	2.54	11.74	4.52	7,200	7
6543	4.16	1.64	10.34	2.80	6,000	18
IC 418	4.17	0.75	11.35	2.80	6,800	12
NGC 7662	5.27	2.32	11.04	2.64	10,300	20
7009	4.52	1.82	9.72	2.87	9,500	33
1535	+3.82	+1.26	+11.16	3.91	10,000	13

* These are the dimensions of the inner and brighter shell of the planetary.

kept in mind that these quantities are only orders of magnitude, as the irregular structures of the planetaries preclude the specification of more accurate values. More accurate parallaxes and magnitudes would improve these mean values. It is to be remarked that the electron densities of the fainter planetaries may be somewhat lower.

We next examine the possibility of estimating nebular densities from the intensities of the hydrogen lines, in particular $H\beta$. This method should prove useful when the continuum is too weak to be measured with any degree of certainty. The intensity of any line of the Balmer series may be written down from (I, 9) as

$$E_{n2} = N_i N_e \frac{6.99 \times 10^{-33}}{T_e^{3/2}} b_n Z^4 \frac{g}{8} \frac{2RZ^2}{n^3} e^{X_n} \qquad \left(X_n = \frac{hRZ^2}{n^2 k T_e}\right). \quad (11)$$

For $H\beta$ we have, since $g = 0.822$,

$$E_{H\beta} = 7.37 \times 10^{-20} \frac{N_i N_e}{T_e^{3/2}} b_4 e^{X_4} . \tag{12}$$

Therefore,

$$S_4 = \frac{2.46 \times 10^{-20}}{T_e^{3/2}} b_4 N_i N_e D e^{X_4} , \tag{13}$$

and, by setting $N_i = N_e$ as before, we obtain

$$N_e = 1.84 \times 10^{11} \frac{T_e^{3/4} e^{-X_4/2}}{\sqrt{D b_4}} (2.512)^{-H_n/2} , \tag{14}$$

where H_n is now taken to mean the brightness of $H\beta$ in terms of magnitudes per square minute of arc. When T_e is adopted from other data, as before, we may work out the

TABLE 2

b_4 FOR TYPICAL PLANETARIES

	$\Delta m(H\beta)$	$H(H\beta)$	e^{X_n}	$N_e\sqrt{b_4}$	b_4*
NGC 7027	+1.95	+7.80	2.79	7.2×10^3	0.61
6572	1.80	7.65	2.91	8.3	.23
6826	1.57	8.92	3.87	2.7	.16
6543	1.46	7.64	5.14	5.9	.11
IC 418	1.27	8.45	4.23	4.8	.15
NGC 7662	1.24	7.00	2.59	17.3	.75
7009	1.86	7.05	2.79	14.2	.19
1535	+1.84	+9.18	2.66	4.2	0.11

* Mean value of b_4 (excluding NGC 7662 and 7027) is 0.16 ± 0.01.

TABLE 3

ELECTRON DENSITY FROM INTENSITY OF $H\beta$

	m_n	Dimensions	A''	r (Parsecs)	$A\times10^{17}$ (Cm)	d/A	Δm/Sq.Min. ($H\beta$)
NGC 40	9.5	38″×35″	18	1220	3.29	0.2	−1.08
NGC 2022	12.4	22 ×17	10	4570	6.84	0.2	−2.46

	$m(H\beta)$	$H(H\beta)$	T_e(Adopted)	$\sqrt{D}\times10^{-8}$	$N_e\sqrt{b_4}$	N_e
NGC 40	0.96	9.4	6,000	4.01	1.84×10^3	5×10^3
NGC 2022	2.03	12.0	10,000	5.78	0.78	2×10^3

values of $N_e\sqrt{b_4}$ (see Table 2). We obtain the values of b_4 from a comparison of $N_e\sqrt{b_4}$ with the previous values of N_e. Except for NGC 7027 and NGC 7662 the values of b_4 are remarkably constant from one nebula to another. It seems fairly safe, therefore, to

assume $b_4 \sim 0.16$, and to use the observed intensities of $H\beta$ to deduce the densities of nebulae for which the Balmer continuum is too faint to be observed.

We may apply this method to NGC 40 and NGC 2022, both of which have low surface brightnesses. The relevant data are given in Table 3. To estimate N_e, we assumed that $b_4 = 0.16$. The electron temperature of NGC 40 is assumed to be 6000°, that of NGC 2022, 10,000°. Both nebulae are assumed to possess shell structures. If the adopted value of b_4 is approximately correct, it is apparent that the density of the electrons is somewhat lower in these objects than in the others, as one would expect on the basis of their lower surface brightnesses.

On the strength of these results, we shall adopt electron densities of the order of 10^4 electrons/cm^3 in future theoretical studies of the planetary nebulae. This value seems to be about correct for the brighter planetaries. For the fainter objects, values of the order of 2×10^3 electrons/cm^3 may be assumed. In the next paper of this series we shall show how the electron temperature may be derived.

HARVARD COLLEGE OBSERVATORY
June 8, 1940

THE ABSOLUTE DIMENSIONS OF A WOLF-RAYET ECLIPSING BINARY: HV 11111 = BD+38°4010 = HD 193576

SERGEI GAPOSCHKIN

ABSTRACT

The Wolf-Rayet star BD+38°4010 is shown to be an eclipsing binary with the period of $4^d.21238$, and with ranges $8^m.39$–$8^m.70$ and $8^m.39$–$8^m.53$. The star has received the Harvard Variable number 11111.

A light-curve has been derived from 1084 photographic observations made on Harvard patrol plates. A straightforward interpretation of the light-curve as that of an eclipsing binary, leads to the derivation of the following elements: $L_1 = 0.151$, $L_2 = 0.849$, $r_1 = 0.160$ A, $r_2 = 0.266$ A. Thus, the ratio of the radii is 0.60, and that of the surface brightnesses is 0.493. The subscript 1 refers to that component which is in front during primary minimum—that is, to the Wolf-Rayet component.

The most probable absolute dimensions, with the use of the spectroscopic results of O. C. Wilson, are: $R_1 = 5.8\ \odot$, $R_2 = 9.7\ \odot$, $\mu_1 = 10.2\ \odot$, $\mu_2 = 25.9\ \odot$, $\rho_1 = 0.05\ \odot$, $\rho_2 = 0.03\ \odot$, $M_{vis} = -1.64$, $M_{vis.2} = -3.53$, $i = 80°.3$, and the computed gravitational red shift at the surface of the Wolf-Rayet component is only 1 km/sec. An effective temperature derived in the usual manner from the observed depths of the minima appears to be not more than 13,000° for the Wolf-Rayet component, in glaring contrast to the excitation temperature.

General remarks.—Out of about eighty known Wolf-Rayet stars[1] none has hitherto been included among the established variables. There has, indeed, been a general impression that these stars are remarkably constant in brightness. This is the more remarkable since Martin and Plummer,[2] as long ago as 1919, stated, on the basis of their photographic observations, that "the majority of the Wolf-Rayet stars are variable within narrow limits." A Wolf-Rayet variable star, which certainly deserves further attention, was announced by Miss Anger[3] in 1933. There are, moreover, a number of stars of class O with Wolf-Rayet characteristics (such as UW = 29 Canis Majoris) which are spectroscopic binaries, and the star just mentioned is a variable star with well-defined minima.

History of HV 11111.—The star became well known when, in 1939, O. C. Wilson published a short note[4] in which he announced it to be a spectroscopic binary. In 1940 he published a detailed list of spectroscopic observations and his results concerning the masses of the components.[5]

Interested by Wilson's notes, the author obtained several hundred observations of the star on the Harvard patrol plates. It was soon evident that the star was variable, though with a small range; and, since it is a spectroscopic binary, he inferred that it is an eclipsing system. Meanwhile, he was unaware of the fact that Martin and Plummer had obtained 24 photographic observations of the star in 1916 and 1917 and had found for it an average deviation of $\pm 0^m.062$ as compared with ± 0.03 for other stars and that they had obtained on two nights, separated by a year and one day, the magnitudes 8.28 and 8.49, respectively. Martin and Plummer concluded that the star is definitely variable, but they published no range and assigned no type to it. The star was, therefore, not included among accepted variable stars, but it was included in the catalogue of suspected variables published by Zinner.[6]

[1] See Payne, *Harvard Obs. Mono.*, No. 3, 1931; Vorontsov-Velyaminov, *New Stars and Galactic Nebulae*, 1935.

[2] *M.N.*, **79**, 196, 1919.

[3] *Harvard Bull.*, No. 891, p. 8, 1933.

[4] *Pub. A.S.P.*, **51**, 55, 1939.

[5] *Ap. J.*, **91**, 379, 1940; **91**, 394, 1940.

[6] *Astr. Abhandl.*, **8**, Part I, 1929.

Photographic observations.—The star under discussion is of the eighth magnitude and is situated in a rather dense portion of a bright star cloud, not far from P Cygni; in the same region there are about ten other O stars. The selected comparison stars are shown in Table 1. Star b, on account of its redness, was avoided as much as possible. Star c is slightly variable. Stars a and d have faint companions which introduce difficulties on plates of small scale. We have, therefore, limited the discussion to measures made with the $1\frac{1}{2}$-inch Cooke lens (AC), although an almost equal number of estimates were made on other plates, such as those of series AI, RH, BM, FA, and CA.

The magnitudes of the comparison stars, which proved somewhat difficult to determine in the absence of good, near-by standards, are based on Harvard Standard Region B7.

The range of variation.—The mean maximum brightness of the variable, derived from 740 observations outside the minima, is $8^m.39$. This value is derived from AC plates; from RH plates the maximum appears to be about 0.03 mag. brighter. The depths of the minima are $8^m.70$ and $8^m.53$, so that the ranges are $0^m.31$ and $0^m.14$, respectively. The

TABLE 1

COMPARISON STARS

Designation	BD	HD	Magnitudes		Color Index	Spectrum
			IPg	HPv		
a	+38j 4019	193681	$8^m.26 \pm 0^m.04$	.....	$0^m.0$:	A0
b	+38 4003	193469	8.2:	$6^m.35$	+1.8:	K2
c	+38 3980	193032	8.45 0.06	.....	+0.3:	B2
d	+38 4026	.....	8.72 0.05	.....	0.0:	B9
f	+38 4012	193595	8.8:	.....	.....	B
Var	+38 4010	193576	8.39–8.70	8.02	+0.37	(Ob) B1, WN5

secondary minimum gives a larger scatter than the primary and conveys the impression of varying somewhat in depth.

The color index.—A simple inspection of red and yellow plates shows that the variable has a positive color index. The apparent redness may result partly from spectral peculiarities and partly from interstellar absorption. The investigation of the star in light of different colors will be of importance in its future study.

The period and the light-curve.—Eighty-four times of observed minima, from JD 2414600 on, were used in checking Wilson's spectroscopic period. No correction to the period was found, and there was no indication of variability in period.

The light-curve shown in Figure 1 and summarized in Table 2 was formed from 1084 photographic observations. The phases are computed from JD 2400000.000.

Comparison with spectroscopic observations.—The comparison between our light-curve and Wilson's velocity-curve (his normal points are used) is shown in Figure 1. The observed phases of minima coincide with the intersections of both orbital velocity-curves with the corresponding lines for the center of gravity. It will be shown later that our results leave no place for the gravitational red shift derived by Wilson. It should be noted that this conclusion does not affect the value of the minimum masses obtained by Wilson.

Three solutions for uniform brightness.—The results which can be derived from a light-curve with such shallow minima are rather indeterminate. Formally speaking, there are many possible solutions in a wide range for the ratio of radii ($k = 0.53$ and $k = 2.46$);

we shall give three solutions and later show which seems to us to be the most probable. One limiting solution (*a*) is obtained by assuming that the first component is the larger one. The component in front at the primary eclipse is denoted as the first; in the present case the first is the Wolf-Rayet component. In solution (*a*) the primary eclipse is then at the limit of totality. The other limiting solution (*c*) is obtained by assuming that the

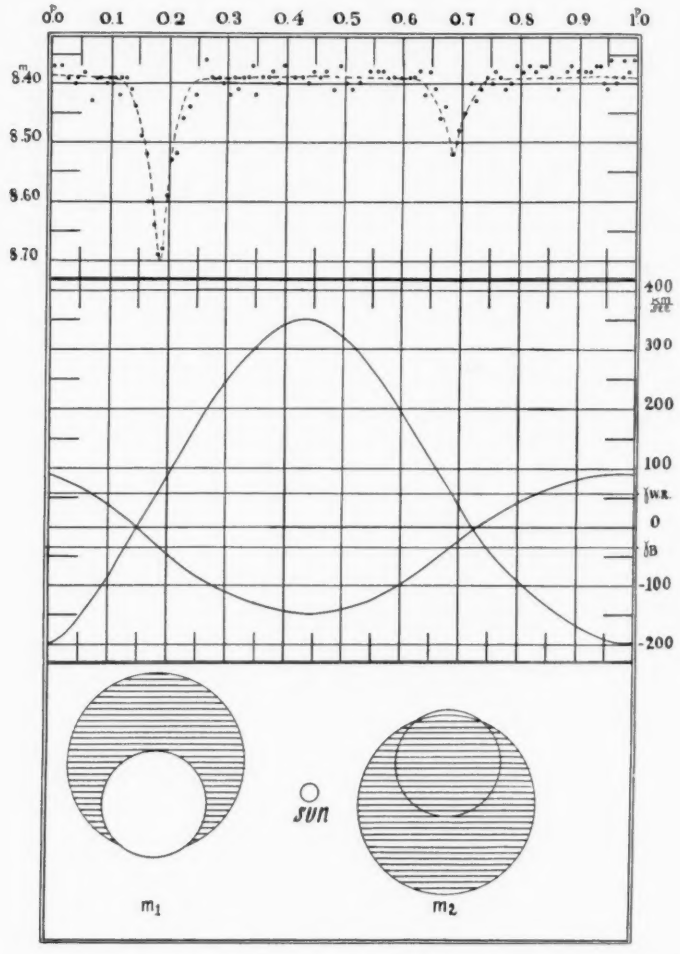

FIG. 1.—The system of HV 11111. Light-curve (*above*), phase against photographic magnitude; radial velocity-curve (*middle*), phase against radial velocity; sizes and positions of components during minima (*bottom*), primary (m_1) and secondary (m_2). The smaller star is the Wolf-Rayet component.

Wolf-Rayet component is the smaller. The primary eclipse is then at the limit of annularity. A third solution (*b*) is given for the case of equal radii. The three sets of results are shown in Table 3.

The three last lines of Table 3 were computed on the assumption[7] that the temperature of the B1 component is 19,950°.

[7] S. Gaposchkin, *Proc. Amer. Phil. Soc.*, **82**, No. 3, 1940.

TABLE 2

MEAN LIGHT-CURVE

(10-Point Means)

Phase	IPg Mag.	Phase	IPg Mag.	Phase	IPg Mag.
0P0031	8m37 ± 0m02	0P3111	8m39 ± 0m01	0P6815	8m52 ± 0m03
0.0159	8.37 0.01	0.3194	8.41 0.02	0.6907	8.50 0.02
0.0284	8.39 0.02	0.3280	8.39 0.02	0.6972	8.48 0.03
0.0393	8.40 0.02	0.3371	8.39 0.02	0.7072	8.45 0.02
0.0420	8.39 0.02	0.3416	8.37 0.02	0.7168	8.40 0.02
0.0565	8.38 0.02	0.3492	8.42 0.02	0.7249	8.43 0.01
0.0694	8.43 0.02	0.3597	8.39 0.02	0.7325	8.41 0.02
0.0768	8.39 0.01	0.3705	8.39 0.01	0.7439	8.39 0.02
0.0815	8.39 0.01	0.3782	8.38 0.02	0.7520	8.40 0.02
0.0928	8.40 0.01	0.3873	8.40 0.02	0.7581	8.38 0.02
0.0989	8.39 0.02	0.3979	8.37 0.02	0.7655	8.39 0.02
0.1038	8.40 0.02	0.4150	8.39 0.02	0.7750	8.41 0.02
0.1094	8.39 0.02	0.4288	8.39 0.02	0.7826	8.40 0.02
0.1166	8.42 0.02	0.4377	8.40 0.02	0.7941	8.37 0.03
0.1189	8.39 0.01	0.4476	8.38 0.03	0.8054	8.38 0.02
0.1285	8.39 0.01	0.4589	8.39 0.02	0.8163	8.37 0.02
0.1359	8.41 0.01	0.4692	8.38 0.01	0.8267	8.38 0.03
0.1434	8.44 0.01	0.4806	8.41 0.01	0.8358	8.37 0.02
0.1529	8.49 0.01	0.4928	8.37 0.03	0.8441	8.37 0.01
0.1617	8.52 0.02	0.5029	8.40 0.02	0.8542	8.39 0.02
0.1664	8.60 0.02	0.5138	8.41 0.02	0.8651	8.41 0.02
0.1715	8.60 0.02	0.5269	8.40 0.02	0.8799	8.38 0.03
0.1764	8.64 0.02	0.5443	8.38 0.01	0.8867	8.37 0.02
0.1828	8.69 0.02	0.5574	8.38 0.02	0.8990	8.38 0.02
0.1904	8.68 0.02	0.5660	8.38 0.02	0.9112	8.38 0.04
0.1972	8.59 0.01	0.5758	8.39 0.02	0.9214	8.38 0.01
0.2053	8.53 0.01	0.5852	8.39 0.01	0.9296	8.37 0.02
0.2131	8.52 0.02	0.5972	8.39 0.01	0.9359	8.37 0.03
0.2258	8.46 0.02	0.6109	8.39 0.03	0.9432	8.40 0.01
0.2356	8.44 0.02	0.6176	8.39 0.02	0.9483	8.41 0.02
0.2463	8.42 0.01	0.6285	8.38 0.03	0.9554	8.36 0.03
0.2635	8.36 0.02	0.6377	8.42 0.03	0.9647	8.40 0.03
0.2743	8.39 0.02	0.6473	8.38 0.02	0.9748	8.39 0.02
0.2857	8.39 0.01	0.6549	8.41 0.02	0.9785	8.36 0.02
0.2915	8.40 0.02	0.6622	8.46 0.02	0.9867	8.38 0.03
0.3041	8.42 ± 0.01	0.6722	8.44 ± 0.02	0.9948	8.36 ± 0.03

TABLE 3

LIMITING SOLUTIONS FOR HV 11111

	Solution (*a*)	Solution (*b*)	Solution (*c*)		Solution (*a*)	Solution (*b*)	Solution (*c*)
$k_{1/2}$	2.463	1.000	0.533	μ_2	25.96 ⊙	26.58 ⊙	25.38 ⊙
$\eta_{1/2}$	2.994	0.493	0.141	M_{vis} (Wolf-Rayet)	−2m88	−2m42	−1m43
$\gamma_{1/2}$	0.493	0.493	0.493	M_{vis} (B star)	−1m68	−3m19	−3m57
r_1	0.293 A	0.226 A	0.144 A	Effective temperature (Wolf-Rayet)	12,600°	13,000°	13,200°
r_2	0.119 A	0.226 A	0.270 A				
i	80°.0	76°.7	82°.8				
R_1	10.65 ⊙	8.28 ⊙	5.20 ⊙				
R_2	4.32 ⊙	8.28 ⊙	9.74 ⊙				
μ_1	10.19 ⊙	10.44 ⊙	9.97 ⊙				

The adopted solution.—It appears to the writer that solution (*c*) is nearest to the truth. Solution (*a*), in which the B star is wholly eclipsed, may be ruled out on the basis of Wilson's observation that the spectrum of the B star never disappears during the minimum. Solution (*c*) is preferred because it gives for the second component values which are normal for a star of class B1. The author has found, from a statistical study based upon eclipsing stars,[8] an average absolute visual magnitude of -3.51 ± 0.23 for stars of class B1.0. The value derived by Stebbins, Huffer, and Whitford[9] for stars of spectral class B1 is -3.6. These two values agree very closely with the value -3.57 given by solution (*c*), though the value of solution (*b*) does not differ very greatly.

TABLE 4

ADOPTED SOLUTION

Ratio of radii	0.60	Distance between centers	36.32 ⊙
Ratio of surface brightnesses	0.493	Mass, Wolf-Rayet component	10.17 ⊙
Ratio of total brightnesses	0.177	Mass, B component	25.90 ⊙
Total brightness, Wolf-Rayet component	0.151	Density, Wolf-Rayet component	0.05 ⊙
Total brightness, B component	0.849	Density, B component	0.03 ⊙
Difference of luminosities	$1^m.887$	Temperature, B component (adopted)	19,950[b]
Relative radius, Wolf-Rayet component	0.160 A	Absolute visual magnitude (Wolf-Rayet)	$-1^m.64$
Relative radius, B component	0.266 A	Absolute visual magnitude (B)	$-3^m.53$
Ellipticity of components	0.986	Effective temperature (Wolf-Rayet)	13,070°
Radius, Wolf-Rayet component (mean)	5.81 ⊙	Red (gravitational) shift, Wolf-Rayet comp	1.11 km/sec.
Radius, B component (mean)	9.68 ⊙		

A similar conclusion may be reached concerning the mass of the B1 component. If we reverse the usual procedure and, having the absolute radius of the B component deduced from the relation[10]

$$\log_{10} R = 0.82 \log_{10} \mu,$$

we deduce the ratio of the radii, we find a value of the latter not greater than 0.2. Thus, this line of reasoning leads to a value for the ratio of radii even more extreme than that required by solution (*c*).

We conclude, therefore, that both methods indicate that solution (*c*) is the most probable. In order not to deal with a limiting case we shall adopt for the final elements the value of 0.6 for the ratio of the radii.

Concluding remarks.—Our treatment of the light-curve of HV 11111 has been of a straightforward kind. We have made simple geometrical solutions of the kind made for ordinary eclipsing stars and have not considered limb darkening, which ordinarily gives nearly the same dimensions. However, some general conclusions can be drawn from our results.

Perhaps the most startling of our conclusions is the low "effective temperature" of 13,000°, which was derived in the usual manner from the surface brightness of the Wolf-Rayet star. This temperature is in striking contrast to the excitation temperature of about 80,000°, which is suggested by the bright lines in the spectrum. It is here, how-

[8] *Ibid.*, **82**, 321, 1940. [9] *Ap. J.*, **90**, 215, 1939.

[10] S. Gaposchkin, *Proc. Amer. Phil. Soc.*, **82**, 319, 1940; *J.R. Acad. Sci. Canada*, **33**, 238, 1939.

ever, that the simple geometrical picture breaks down, and when we try to replace it by an explicit picture of the structure of a Wolf-Rayet star we have little to go upon. This problem will be more fully discussed elsewhere.

It is noteworthy that the size of the Wolf-Rayet star, which is deduced without uncertainty from the light-curve, is considerably greater than that of the sun and quite different from the small dimensions pictured by Wilson. The large radius, as may be seen from Table 4, leads to a gravitational red shift which would be inappreciable and requires that the *observed* red shift be interpreted in other terms.

The combination of the evidence furnished by the present investigation that the Wolf-Rayet component has a large, stellar disk several times the size of the sun and the evidence furnished by the symmetrically widened bright lines in its spectrum lead us to the conclusion that the current picture of the nature of Wolf-Rayet stars is inadequate.

HARVARD COLLEGE OBSERVATORY
November 1940

NOTES

USE OF THE HALE SPECTROHELIOSCOPE FOR THE OBSERVATION OF SPECTRA OF CHROMOSPHERIC ERUPTIONS

The Hale spectrohelioscope has proved its value in the study of many types of solar activity. It is possible to observe in detail many features of the spectra of solar eruptions. The spectrum in the spectrohelioscope is usually produced by a reflection grating with about 15,000 lines per inch. The sun is viewed in the light of one line, usually $H\alpha$, of one of the first-order spectra. The other spectra ordinarily go to waste. If, however, a two- or three-inch portable refracting telescope is placed close to the grating, in such a position that it intercepts the light in the *other* first-order spectrum, it is possible to examine the highly dispersed spectrum of the portion of the sun incident on the first slit of the spectrohelioscope.

If an eruption is seen on the disk, its spectrum may be observed by stopping the mechanical rotation of the Anderson prisms and moving the prisms slowly by hand until the image of the eruption is placed exactly on the first slit of the spectrohelioscope. This position can be determined by watching the appearance of $H\alpha$ emission in either the second slit of the spectrohelioscope or through the telescope. If the spectrohelioscope has only a simple lens, it is necessary to refocus the image of the sun on the first slit for the wave-length region to be studied. For certain problems, a long-focus camera could be advantageously substituted for the telescope, since by visual observations alone it is difficult to determine the lines in which the emission is made manifest only by the weakening of the absorption lines.

The Mount Wilson, Zürich, and Canberra studies[1] of eruption spectra agree in describing them as bright-line spectra without accompanying changes in the intensity of the continuous spectrum. These reports, however, are not completely accordant as to the number and intensity of the lines observed. The most interesting lack of agreement is in the reported behavior of helium. The singlets λ 4388 and λ 6678 and the triplets $\lambda\lambda$ 4471, 5876, and 10830 have all been observed as affected during an eruption. These lines sometimes appeared as emission lines, sometimes as absorption lines, and sometimes they were not observed at all. It is probable that the behavior of the helium lines varies from eruption to eruption. Comparative studies of the observable hydrogen and helium lines for each eruption would yield valuable information about the important but unobservable ultraviolet radiations associated with them.

With a 60-mm refracting telescope having a magnifying power of 42, used in conjunction with the Hale spectrohelioscope at the Whitin Observatory, we saw the line λ 5876 of helium in absorption in the spectrum of the eruption which occurred on November 9, 1940, at 15^h30^m GCT in heliographic latitude $+10°$ and longitude 320°. The line appeared very broad, of intensity about 7 on the Rowland scale, and showed variations in intensity and structure within the line. By using similar small auxiliary telescopes, observers with Hale spectrohelioscopes can supply information regarding the presence or absence of the helium lines λ 5876 and λ 6678 almost as easily as they can indicate the occurrence of the eruption. Such data might provide further clues to the nature of these solar phenomena.

HELEN W. DODSON

WHITIN OBSERVATORY
WELLESLEY, MASSACHUSETTS
December 1940

[1] *Ap. J.*, **89**, 347, 1939; **91**, 334, 1940; *Naturwissenschaften*, **24**, 638, 1936; *M.N.*, **100**, 635, 1940.

FREDERICK EUGENE FOWLE

1869–1940